Universidade do Minho
Escola de Ciências

UNIVERSIDAD
DE GRANADA

Maria Pestana da Luz Pereira Ramos

The interplay between collider and astrophysical probes of non-minimal composite Higgs models

September, 2021

The interplay between collider and astrophysical probes of non-minimal composite Higgs models

Maria Pestana da Luz Pereira Ramos

UMinho | 2021

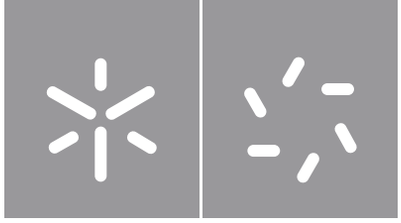

Universidade do Minho
Escola de Ciências

UNIVERSIDAD
DE GRANADA

Maria Pestana da Luz Pereira Ramos

The interplay between collider and astrophysical probes of non-minimal composite Higgs models

Doctoral Thesis
Programa de Doctorado en Física y Ciencias del Espacio

Work supervised by
Nuno Filipe da Silva Fernandes de Castro
Mikael Rodriguez Chala

September, 2021

Editor: Universidad de Granada. Tesis Doctorales
Autor: Maria Pestana da Luz Pereira Ramos
ISBN: 978-84-1117-229-5
URI: http://hdl.handle.net/10481/72877

DECLARATION

To the women who paved the way, showing that this is not a "singularly unfeminine profession"

Acknowledgements

I thank first and foremost to my advisors, Nuno Castro and Mikael Chala, for their daily encouragement and support. I start by thanking Nuno for having always time to answer my doubts and for his patience. Our conversations gave me different perspectives on several problems that shaped the purposes of this thesis. From Miki, I learned not only the most exciting physics, but how to prepare talks, how to collaborate in a productive way, how to think with clarity, how to be a caring and effective mentor and how to enjoy the best aspects of the academic life. I thank him for his everyday dedication, for including me in several interesting projects and mostly for being a scientific reference for me. It goes without saying that without you both this thesis would not be possible.

I would like to thank LIP for supporting my work, as well as Ana, Emanuel, Henrique and Tiago, who were always available to help. I owe a great debt to Michael Spannowsky for hosting me in Durham and for his golden advices. I also thank Arsenii, Jakub, Nuno, Silvia, Matheus, Andreas and Gurpreet for our memorable game nights together. I am immensely grateful to José Santiago, who made me feel so welcome in Granada, and from whom I learned a lot through our discussions in the blackboard. I thank Jorge, Adrian and Pawel, for the good moments over coffee and all the discussions we had. I also thank José María, Dani and Alejandro, for being great office mates, as well as Fran, Pablo and António, with whom I shared some of the best moments of my PhD. I am thankful to my friends from Cargese and Trieste, Kin, Yann, Adrien, Alfredo, Alejo, Rupert, Ulserik, Petar, Janak, Amitayus, Javier and Yong, that made my time there so much better. I finally thank Xabier Vidal for the opportunities he provided to share my work.

Above all, I thank my mom for her example, her strength and her joy everyday. I admire you beyond what I could write in one page. I am specially thankful to my dad, my sister and my grandmother Isabel, for their generosity and patience. I thank also Vofina, Ricardo and Berta for being a great presence in my life. I would like to thank Simão, João G., Carlos, Maurício and João P., for all the laughing and musical moments, as well as Bea, Joana and Teresa, for the strong friendship we have been sharing over the years.

Last but not least, I would like to thank my favourite collaborator and the love of my life, Guilherme. Thanks for revising this work and for the constant support along the last years. (I have been looking at you through rose-colored glasses and I am so glad that all the flags are just flags.)

This work is supported by the projects POCI-01-0145-FEDER-007334 and CERN/FIS-PAR/0024/2019, and my MAP-Fis grant PD/BD/142773/2018, financed by Fundação para a Ciência e a Tecnologia.

Abstract

The Higgs boson is the most recently discovered particle in the Standard Model of particle physics. While its presence is compatible with the fundamental principles of our description of Nature, such scalar, if elementary, seems to make our Universe incredibly unnatural.

A plausible explanation to restore a natural Universe is therefore that the Higgs is composite, made out of new fermions bound together by a new strong force. Composite Higgs models provide a consistent way to incorporate this idea, while justifying why the new sector may have eluded the numerous searches for these models conducted at particle experiments. Such searches can lose sensitivity to non-oversimplified (non-minimal) composite Higgs models in which new electroweak particles arise along with the Higgs boson but have not been searched for in conjunction with the latter.

Using such non-minimal realizations, we aim to answer the following questions: *Can compositeness, one of our traditional solutions for naturalness in the Higgs sector, still fulfill its purpose while shedding light on other problems in particle physics? If so, where can the most interesting aspects of the phenomenology arise?*

Driven by these questions, we will construct several composite Higgs models with candidates to solve long-standing questions, from the generation of the baryon asymmetry to the nature of dark matter, and study their viability by collecting collider and astrophysical probes. On a complementary approach, we will also build non-minimal effective field theories, independent of the details of the physics at the ultraviolet, to explore new signatures of the lightest composite particles, as well as to compute the energy evolution of the parameters in the theory, required for a meaningful interpretation of the bounds collected by different experiments across several energy scales.

Resumo

O bosão de Higgs é a partícula mais recentemente descoberta no Modelo Padrão da física de partículas. Embora a sua existência seja compatível com os princípios fundamentais da nossa descrição da Natureza, este escalar, sendo elementar, parece fazer do nosso Universo um lugar extraordinariamente antinatural.

Uma explicação plausível para restaurar um Universo natural é, portanto, que o Higgs seja uma partícula composta, constituída por fermiões ainda desconhecidos, de um novo sector de interações fortes. Os modelos de Higgs composto providenciam uma maneira consistente de incorporar esta ideia justificando, ao mesmo tempo, por que razão este sector poderia ter iludido as várias pesquisas experimentais, conduzidas no intuito de descobrir estes modelos, em aceleradores de partículas. Estas pesquisas podem perder sensibilidade a modelos de Higgs composto complexos (não-mínimos), em que, para além do bosão de Higgs, surgem novas partículas à escala eletrofraca, que não foram procuradas em conjunto com o primeiro.

Usando estas realizações não-mínimas, pretendemos responder às seguintes questões: *Podem ainda estas teorias compostas, sendo uma das nossas soluções tradicionais para a naturalidade no sector do Higgs, atingir os seus objetivos, bem como oferecer soluções para outros problemas da física de partículas? Se sim, onde poderão ser esperados os aspetos mais interessantes da fenomenologia destes modelos?*

Motivados por estas questões, construiremos vários modelos de Higgs composto com candidatos para resolver questões colocadas há várias decadas, desde a geração da assimetria entre bariões e anti-bariões até à natureza da matéria escura, estudando a sua viabilidade através da recolha de dados de experiências astrofísicas e em colisionadores. Numa abordagem complementar, construiremos também teorias efetivas não-mínimas, independentes dos detalhes da física no ultravioleta, com os objetivos de investigar novas assinaturas das partículas compostas mais leves e calcular a evolução dos parâmetros da teoria com a energia, o que é necessário para uma interpretação correta dos constrangimentos experimentais recolhidos por diferentes experiências a diversas escalas de energia.

Resumen

El bosón de Higgs es la partícula del modelo estándar descubierta más recientemente. Aunque su existencia es compatible con los principios fundamentales de nuestra descripción de la naturaleza, este escalar, si es elemental, parece hacer de nuestro Universo un lugar extraordinariamente antinatural.

Una explicación plausible para restaurar un Universo natural es, por tanto, que el Higgs sea una partícula compuesta, formada por fermiones aún desconocidos, de un nuevo sector de interacciones fuertes. Los modelos de Higgs compuesto proporcionan una forma consistente de incorporar esta idea, al tiempo que justifican por qué este sector podría haber eludido las diversas búsquedas experimentales realizadas para descubrir las nuevas partículas en aceleradores. Estas búsquedas pueden perder sensibilidad a modelos de Higgs compuesto complejos (no mínimos), en los que, además del Higgs, emergen nuevas partículas a la escala electrodébil, pero que no se han buscado junto con el primero.

Utilizando estos modelos no mínimos, tenemos la intención de responder las siguientes preguntas: *¿Pueden estas teorías de Higgs compuesto, siendo parte de nuestras soluciones tradicionales para la naturalidad en el sector de Higgs, aún lograr sus objetivos, así como brindar soluciones a otros problemas en la física de partículas? Si es así, ¿dónde cabe buscar los aspectos más interesantes de la fenomenología de estos modelos?*

Motivados por estas preguntas, construiremos varios modelos de Higgs compuesto con candidatos para resolver misterios cuyo origen se remonta décadas atrás, desde la generación de asimetría entre bariones y antibariones hasta la naturaleza de la materia oscura, estudiando su viabilidad mediante la recopilación de datos de experimentos astrofísicos y en colisionadores. En un enfoque complementario, también construiremos teorías efectivas no mínimas, independientes de los detalles de la física en el ultravioleta, con el fin de investigar nuevas señales de las partículas compuestas más ligeras y de calcular la evolución de los parametros de las teorías según cambia la energía, lo cual es necesario para una correcta interpretación de los datos experimentales recopilados por diferentes experimentos a distintas escalas.

Contents

List of Figures

List of Tables

Acronyms

C	charge conjugation
CP	charge conjugation and parity
CPT	charge conjugation, parity and time reversal
P	parity
T	time reversal
$d.o.f.$	degrees of freedom
pp	proton-proton
1PI	one-particle irreducible
1S1C	one-scale one-coupling
ALP	axion-like particle
BF	background field
BFM	background field method
BP	benchmark point
c.m.e.	center of mass energy
CC	charged current
CCWZ	Callan-Coleman-Wess-Zumino
CHM	composite Higgs model
CKM	Cabibbo-Kobayashi-Maskawa
CL	confidence level

DM dark matter

EDM electric dipole moment
EFT effective field theory
EOM equation of motion
EW electroweak
EWPD electroweak precision data
EWPO electroweak precision observable
EWSB electroweak symmetry breaking

FCCC flavour-changing charged current
FCNC flavour-changing neutral current

GC galactic center
GIM Glashow, Iliopoulos and Maiani
GW gravitational wave

HL high luminosity
HP hierarchy problem

IBP integration by parts
IR infrared

l.h.s. left-hand side
LEFT low-energy effective field theory
LFU lepton flavour universality
LH left-handed

LHC	Large Hadron Collider
LISA	Laser Interferometer Space Antenna
LO	leading order
MC	Monte Carlo
MCHM	minimal composite Higgs model
MET	missing transverse energy
MFV	Minimal Flavour Violation
NC	neutral current
NGB	Nambu-Goldstone boson
NLO	next-to-leading order
NMCHM	non-minimal composite Higgs model
PC	power-counting
pNGB	pseudo Nambu-Goldstone boson
PT	phase transition
QCD	quantum chromodynamics
QED	quantum electrodynamics
QFT	quantum field theory
r.h.s.	right-hand side
RegI	Regime I
RegII	Regime II
RGE	renormalization group equation
RH	right-handed

SI	spin-independent
SIMP	strongly-interacting massive particle
SM	Standard Model
SMEFT	Standard Model effective field theory
SUSY	supersymmetry
UV	ultraviolet
VEV	vacuum expectation value
VLL	vector-like lepton
VLQ	vector-like quark
WFR	wave function renormalization
WIMP	weakly-interacting massive particle
WZW	Wess-Zumino-Witten

Chapter 1

Introduction

In his letter to students at the start of their scientific careers, Prof. Steven Weinberg advises them to "aim for rough water", that is to pursue an area in which the path forward is not clear and where creative work can still be done. This is the defining paradigm of particle physics today. However, when the Large Hadron Collider (LHC) started operating, more than a decade ago, it was not expected that waters would not have calmed by now.

By that time, hopes abounded that a plethora of new particles would be discovered, leading the way into a new Golden Age. Instead, only the Higgs boson was found in 2012, establishing that our current theory of fundamental particles and their interactions, the Standard Model (SM), is mathematically consistent up to very high energies. Since then, all data being produced in countless experiments across several energy scales seem to agree with the SM predictions.

While the possibility that future experiments will only further confirm the SM seems nothing like "rough water", some scientists have referred to this situation as the *nightmare* scenario. This stems from the lack of explanations to several observations in the Universe, such as the existence of dark matter (DM) (whose first evidence dates back from 1933 [1]) and the absence of a symmetry between matter and antimatter (which requires three conditions already proposed in 1967 [2]). These, together with other unexplained phenomena, show that the SM cannot be the ultimate theory.

Not only must there be extra ingredients that we do not know how to add to the SM, but theoretical calculations in the current theory indicate that the existence of the Higgs boson, while very well compatible with fundamental principles, makes the Universe extremely unnatural.

Such puzzling situation is not itself the *nightmare*, because the existence of problems is the ground zero for new solutions and the path into a more fundamental theory. What makes this period so critical is that all efforts to replace the SM have been persistently ruled out by data, and we have no clear theoretical

indication (like the one which anticipated the Higgs discovery) that new physics should show up anytime soon.

In this regard, the problem related to the Higgs boson is particularly interesting since the most compelling solutions to it require new physics close to the energy we can currently probe. It all lies on the Higgs mass: unlike the other particles we know, the scalar Higgs boson could have *any* mass, but we have measured it to be very small in comparison to the largest scale up until which the SM is valid (which, to the best of our knowledge, could be close to the Planck scale). So, although this hierarchy problem (HP) does not make the theory inconsistent in such a way that would demand the existence of new physics, it makes us unable to understand the nature of the Higgs scalar.

While it might seem there is less motivation to build new models and experiments today, because no new physics *needs* to pop up at twice (or ten, or hundred times) the energy we have access to, the urge to understand the Higgs particle demands that such energies are crossed. That provides a way to test if the Higgs interactions to itself and other particles are point-like and, consequently, find out if there exists indeed an elementary scalar in Nature.

Together with supersymmetry (SUSY), compositeness is one of the most popular solutions to the problem affecting the Higgs mass. The former postulates that all bosons have a fermionic partner which can cancel large corrections to their masses; while the latter proposes that the Higgs is made out of new fermions bound together by a new strong force. While SUSY could be realized in Nature, compositeness has been already observed in the strong sector of the SM. These two solutions are the most searched for at particle experiments and therefore the ones subject to more constraints.

Compositeness would show in deviations from the SM couplings of the Higgs boson, together with the presence of new composite particles, which have been probed at current accelerators. The data collected so far seem to point out that, if the Higgs is indeed composite, it must be lighter than the corresponding compositeness scale. In turn, the idea of the Higgs boson being a pseudo Nambu-Goldstone boson (pNGB) of an extended symmetry, that is spontaneously broken at low-energy, has become more and more popular in recent years. This is the basis of composite Higgs models (CHMs), which we will study thoroughly in this work.

In the first part of the thesis, we will choose particular realizations of these models and study their low-energy consequences. This is the so-called *top-down* approach, which is suitable to probe new physics assuming that it manifests close to the energies we can currently probe. In such approach, the particles predicted by a model can be produced and decay at colliders and therefore be searched for directly. If instead the scale of the unknown physics is much larger than the electroweak (EW) scale, this new physics can be integrated out, giving rise to an expansion in effective operators. By measuring the corresponding coefficients, we could therefore obtain indirect information about the underlying ultraviolet (UV) theory. This is the so-called *bottom-up* approach. Following this approach, in the second part of the thesis, we will build non-minimal effective field theories (EFTs) by extending the SM with new degrees of freedom

($d.o.f.$) which are expected to be the lightest composite states and which have gathered strong theoretical evidence.

Altogether, we aim to use the richness of CHMs to motivate new regions of signal which are compatible with the experimental data but might be hidden in the vast region of phase space. A subsequent goal is to propose the experimental strategies which could probe such regions and hopefully be part of the process of preparing the next generation experiments.

Our theoretical and experimental goals can be summed up in two questions, which will drive the development of this work:

1: *Can CHMs, one of our traditional solutions to the HP, still fulfill their purpose while shedding light on other problems in particle physics?*

2: *If so, where can the most interesting aspects of the phenomenology arise?*

To put the ideas into context and set the basis for these questions, we start with a brief overview of the SM and some of its shortcomings in chapter 2. We assume that the reader is comfortable with the essential ideas and tools of quantum field theory (QFT), such as Feynman diagrams, loop calculations, renormalization and group theory. In chapter 3, we give a short introduction to collider physics, defining the most typical collider objects and observables. We use this chapter to set the stage of the experimental analyses performed in subsequent chapters, describing the computational tools we use to simulate a virtual collider. In these first chapters, we do not aim to write a careful review of the topics, but rather focus on the key aspects which are more relevant to the discussion that follows. On the other hand, in chapter 4, we funnel the discussion into the focus of this thesis, by introducing in detail the features of CHMs and discussing their experimental constraints.

The novel works published in the development of this thesis [3–8] are presented in chapters 5 and 6. In chapter 5, we follow the *top-down* approach and construct several non-minimal CHMs. Based on these setups, we study particular aspects of their phenomenology, from flavour physics to DM, assessing the interplay between collider and astrophysical probes. On the other hand, in chapter 6, we adopt the *bottom-up* approach and construct two different EFTs of the SM, one extended with a vector-like fermion, the other with a pseudoscalar singlet. Such particles are common to a variety of CHMs and therefore the top-down and bottom-up approaches are very complementary to one another.

While we present individual conclusions for each of the independent works cited above, in chapter 7 we discuss the overarching goals of the thesis and the answers to the two questions posed above. Note that several appendices are presented after the conclusions, providing auxiliary material and detailed calculations, as well as extending the topics which are discussed more straightforwardly in the main text.

Chapter 2

A brief description of the Standard Model

The SM of particle physics is the theory of fundamental particles and their interactions. The SM Lagrangian, $\mathcal{L}_{\text{SM}}$, is fixed by principles of symmetry, the field content and its representations, the requirement of renormalizability and the pattern of spontaneous symmetry breaking. We describe briefly each of these building blocks below.

To begin with, the SM must respect the symmetries of spacetime, so all operators in the Lagrangian are Lorentz invariant. Furthermore, gauge symmetry, albeit non-physical, is an important tool to have a local description of massless vector fields. The SM is built on the gauge group

$$SU(3)_c \otimes SU(2)_L \otimes U(1)_Y \,. \tag{1}$$

The first is called the color group and describes the theory of the strong interactions, quantum chromodynamics (QCD), while the second and the third define the EW group $\mathcal{G}_{\text{EW}} \equiv SU(2)_L \times U(1)_Y$, a unified description of the weak and the hypercharge (Y) interactions. The corresponding gauge bosons, transforming in the adjoint representations of each group, are the gluon G^A_μ ($A = 1, \ldots, 8$), the W^I_μ ($I = 1, 2, 3$) and the B_μ, respectively. They mediate the interactions between matter fields: the quarks, which carry color, and the leptons, which are colorless. In what concerns $SU(2)_L$, the subscript itself indicates that only the left-handed (LH) components of the matter fields transform non-trivially. Hence, it is useful to project their chiralities[1] and write $\mathcal{L}_{\text{SM}}$ in terms of Weyl spinors:

$$l_L = \begin{pmatrix} \nu_{eL} \\ e^-_L \end{pmatrix}, \quad q_L = \begin{pmatrix} u_L \\ d_L \end{pmatrix}, \quad u_R\,, \quad d_R\,, \quad e^-_R\,; \tag{2}$$

the first two transforming in the $(1/2, 0)$ representation of the Lorentz group, and the last three on the $(0, 1/2)$. The corresponding charges under the SM gauge group are defined in table 1; note that there is

[1] We denote the corresponding chirality projectors by P_L (for LH fields) and P_R (for the right-handed (RH) ones).

	Field	$SU(3)_c$	$SU(2)_L$	$U(1)_Y$
Gauge (spin 1)	G_μ^A	**8**	**1**	0
	W_μ^I	**1**	**3**	0
	B_μ	**1**	**1**	0
Quarks (spin 1/2)	q_L	**3**	**2**	1/6
	u_R	**3**	**1**	2/3
	d_R	**3**	**1**	−1/3
Leptons (spin 1/2)	l_L	**1**	**2**	−1/2
	e_R	**1**	**1**	−1
Higgs (spin 0)	H	**1**	**2**	1/2

Table 1: The SM field representations under the gauge group.

no RH neutrino field. There are three replicas of each fermion family, only distinguishable by the mass; see table 2. The different fermions with equal gauge charges are said to be of different flavour.

Given this content, there is an infinite number of symmetry invariants that we could build. Imposing renormalizability, that is, the requirement that all divergences generated at any order in perturbation theory can be absorbed by a finite set of parameters, only operators with mass dimension ≤ 4 are however included in $\mathcal{L}_{\text{SM}}$. Together with the previous symmetries, this greatly restricts the form of the Lagrangian.

The last ingredient that characterizes the SM is the spontaneous breaking $\mathcal{G}_{\text{EW}} \to U(1)_{\text{em}}$, the last being the electromagnetic group. It explains why we do not observe the full EW symmetry, but only electromagnetism with a massless photon and massive fermions, plus three heavy gauge bosons. This is achieved by the vacuum expectation value (VEV) of a colorless spin-0 doublet, the Higgs boson (see table 1):

$$H = \begin{pmatrix} h^+ \\ h_0 \end{pmatrix}. \tag{3}$$

Its conjugate is $\widetilde{H} = \epsilon H^* = \mathrm{i}\sigma_2 H^*$, with σ_I being the Pauli matrices.

Gathering all these features, the most generic Lagrangian that we can write is

$$\begin{aligned} \mathcal{L}_{\text{SM}} = & -\frac{1}{4} G^A_{\mu\nu} G_A^{\mu\nu} - \frac{1}{4} W^a_{\mu\nu} W_a^{\mu\nu} - \frac{1}{4} B_{\mu\nu} B^{\mu\nu} + \theta \widetilde{G}^A_{\mu\nu} G_A^{\mu\nu} \\ & + \overline{q_L^\alpha} \mathrm{i} \not{D} q_L^\alpha + \overline{l_L^\alpha} \mathrm{i} \not{D} l_L^\alpha + \overline{u_R^\alpha} \mathrm{i} \not{D} u_R^\alpha + \overline{d_R^\alpha} \mathrm{i} \not{D} d_R^\alpha + \overline{e_R^\alpha} \mathrm{i} \not{D} e_R^\alpha \\ & + \left(D_\mu H\right)^\dagger \left(D^\mu H\right) - \mu_H^2 |H|^2 - \lambda_H |H|^4 - \left[y^u_{\alpha\beta} \overline{q_L^\alpha} \widetilde{H} u_R^\beta + y^d_{\alpha\beta} \overline{q_L^\alpha} H d_R^\beta + y^e_{\alpha\beta} \overline{l_L^\alpha} H e_R^\beta + \text{h.c.} \right], \end{aligned} \tag{4}$$

$(\psi_\uparrow,\ \psi_\downarrow)$	$(\nu_e,\ e^-)$	$(\nu_\mu,\ \mu^-)$	$(\nu_\tau,\ \tau^-)$	$(u,\ d)$	$(c,\ s)$	$(t,\ b)$
m_ψ [GeV]	$(0,\ 0.0005)$	$(0,\ 0.1)$	$(0,\ 1.8)$	$(0.002,\ 0.005)$	$(1.3,\ 0.009)$	$(173,\ 4.2)$

Table 2: The three generations of leptons and quarks and the approximate value of their masses [9]. Particles in the same cell belong to the same EW doublet. From left to right, they are called the electron-neutrino and the electron; the muon-neutrino and the muon; the tau-neutrino and the tau-lepton; the up-quark and the down-quark; the charm and the strange; and finally the top and the bottom quarks.

where α and β are flavour indices. The different field strength tensors are given by $B_{\mu\nu} = \partial_\mu B_\nu - \partial_\nu B_\mu$, $W^I_{\mu\nu} = \partial_\mu W^I_\nu - \partial_\nu W^I_\mu + g_2 \epsilon^I_{JK} W^J_\mu W^K_\nu$ and $G^A_{\mu\nu} = \partial_\mu G^A_\nu - \partial_\nu G^A_\mu + g_3 f^A_{BC} G^B_\mu G^C_\nu$. We have also defined $\not{D} \equiv \gamma^\mu D_\mu$ and

$$D_\mu = \partial_\mu - \mathrm{i} g_3 \frac{\lambda_A}{2} G^A_\mu - \mathrm{i} g_2 \tau^I W^I_\mu - \mathrm{i} g_1 Y B_\mu \,, \tag{5}$$

λ^A being the Gell-Mann matrices and $\tau^I = \sigma^I/2$.

Finally, note the presence of the last term in the first line of $\mathcal{L}_{\mathrm{SM}}$, the so-called QCD θ-term, where $\widetilde{G}^A_{\mu\nu} \equiv \epsilon_{\mu\nu\sigma\rho} G^{A\sigma\rho}/2$ and $\epsilon_{\mu\nu\sigma\rho}$ is the totally antisymmetric Levi-Civita tensor. In spite of being a total derivative, this term is topological (characterizing the non-trivial homotopic map between the gauge and coordinate spaces) and therefore cannot be consistently set to zero.

2.1 Higgs-bosonic interactions

Let us focus on the Higgs sector. Following the last line in equation 4, we find that the Higgs potential has a non-trivial minimum for $\mu_H^2 < 0$. By performing a suitable rotation, we can choose to align this VEV along the real direction of the neutral component of the doublet, so that

$$H = \frac{1}{\sqrt{2}} \begin{pmatrix} 0 \\ h + v \end{pmatrix}, \quad \text{with} \quad v = \sqrt{\frac{-\mu_H^2}{\lambda_H}}, \tag{6}$$

in the unitary gauge. The other $d.o.f.$ in the Higgs doublet, corresponding to $h^\pm$ and the imaginary component of h_0, are the Nambu-Goldstone bosons (NGBs) associated with the electroweak symmetry breaking (EWSB). They endow the W^I_μ and the B_μ with a longitudinal polarization that characterizes massive vector fields [10–12].

To obtain such masses, we must expand the Higgs covariant derivative. Reading off the v^2 term, we find that the B_μ and the W^3_μ actually mix; therefore, the physical fields of the theory after EWSB are not those present in equation 5 but linear combinations of the latter:

$$Z_\mu = c_\omega W^3_\mu - s_\omega B_\mu \quad \text{and} \quad A_\mu = s_\omega W^3_\mu + c_\omega B_\mu \,, \tag{7}$$

together with

$$W_\mu^\pm = \frac{1}{\sqrt{2}}\left(W_\mu^1 \mp \mathrm{i}W_\mu^2\right) . \tag{8}$$

In the equations above, s_ω and c_ω stand for the sine and cosine of the rotation angle, the so-called Weinberg angle $\theta_\omega = \tan^{-1}(g_1/g_2)$. In turn, the EW covariant derivative in equation 5 can be rewritten as

$$D_\mu = \partial_\mu - \mathrm{i}g_2\tau^\pm W_\mu^\pm - \mathrm{i}\frac{g_1}{c_\omega}\left[\tau^3 - s_\omega^2 Q\right]Z_\mu - \mathrm{i}g_1 s_\omega Q A_\mu , \tag{9}$$

with $\tau^\pm = (\tau^1 \pm \mathrm{i}\tau^2)/\sqrt{2}$ and $Q = \tau^3 + Y$.

After rotating to the mass basis and in the unitary gauge, we find at last:

$$(D_\mu\phi)^\dagger(D^\mu\phi) = \frac{1}{2}\partial_\mu h\partial^\mu h + \frac{g_2}{4}v^2\left(1 + 2\frac{h}{v} + \frac{h^2}{v^2}\right)\left[W_\mu^+ W^{\mu-} + \frac{1}{2c_\omega^2}Z_\mu Z^\mu\right] . \tag{10}$$

Hence, the masses of the physical gauge bosons read $m_W = g_2 v/2$ and $m_Z = g_2 v/(2c_\omega)$. On the other hand, A_μ remains massless and can be identified with the photon field; consequently, Q is the electric charge and $e \equiv g_1 s_\omega = g_2 c_\omega$ the electromagnetic coupling strength.

The Higgs mechanism also predicts that

$$\rho \equiv \frac{m_W^2}{m_Z^2 c_\omega^2} = 1 . \tag{11}$$

This is a remnant of **custodial symmetry**. Neglecting the hypercharge and the Yukawa interactions, the Higgs Lagrangian is invariant under a larger global $SO(4)$ rotation, under which the Higgs field transforms as a fourplet. After EWSB, only the custodial group $SO(3)_V$ is preserved. Such symmetry protects the gauge boson masses and explains that $\rho = 1 + \Delta\rho_{\mathrm{SM}} \approx 1$, where $\Delta\rho_{\mathrm{SM}}$ comes from hypercharge and Yukawa corrections [13]. We will turn to this topic in section 4.5.1.

2.2 Flavour structure and additional symmetries

After the Higgs develops a VEV, the different fermion flavors mix:

$$\mathcal{L}_{\mathrm{SM}} \supset -\frac{1}{\sqrt{2}}(v+h)\left[y^u_{\alpha\beta}\overline{u^\alpha_L}u^\beta_R + y^d_{\alpha\beta}\overline{d^\alpha_L}d^\beta_R + y^e_{\alpha\beta}\overline{e^\alpha_L}e^\beta_R + \mathrm{h.c.}\right] . \tag{12}$$

To turn to the physical basis, we have to diagonalize the Yukawa matrices y^ψ. With this aim, we rotate independently the chiral fermions, $\psi^\alpha_L \to (V_{\psi L})^\alpha_\sigma \psi^\sigma_L$ and $\psi^\alpha_R \to (V_{\psi R})^\alpha_\sigma \psi^\sigma_R$, so that $V^\dagger_{\psi L} y^\psi V_{\psi R}$ becomes a diagonal matrix in flavour space, with real and positive entries, y_ψ. The mass of each fermion is therefore determined by the strength of its couplings to the Higgs boson, $m_\psi = v/\sqrt{2}y_\psi$. This is another crucial prediction of the Higgs mechanism.

The rotations into the mass basis change the gauge interactions with the W boson,

$$\mathcal{L}_{\text{kin}} \supset \frac{g_2}{\sqrt{2}} \overline{u_L} \gamma^\mu d_L W_\mu^+ + \text{h.c.} \to \frac{g_2}{\sqrt{2}} \overline{u_L} \gamma^\mu \left[{V_{uL}}^\dagger V_{dL} \right] d_L W_\mu^+ + \text{h.c.}\,, \tag{13}$$

where the matrix within the brackets is the unitary Cabibbo-Kobayashi-Maskawa (CKM) matrix:

$$V_{\text{CKM}} \equiv \begin{pmatrix} V_{ud} & V_{us} & V_{ub} \\ V_{cd} & V_{cs} & V_{cb} \\ V_{td} & V_{ts} & V_{tb} \end{pmatrix} = \begin{pmatrix} 1 - \lambda^2/2 & \lambda & A\lambda^3(\rho - \mathrm{i}\eta) \\ -\lambda & 1 - \lambda^2/2 & A\lambda^2 \\ A\lambda^3(1 - \rho - \mathrm{i}\eta) & -A\lambda^2 & 1 \end{pmatrix} + \mathcal{O}(\lambda^4)\,. \tag{14}$$

In the second equality, we have used the Wolfenstein parameterization [14], where the four physical parameters of the CKM (three mixing angles plus a phase) are explicit. The interactions in equation 13 therefore induce flavour-changing charged currents (FCCCs). They are unsuppressed in the quark sector of the SM[2].

On the contrary, flavour-changing neutral currents (FCNCs) are extremely suppressed. They are absent at tree level, because all neutral bosons in the SM couple diagonally in the mass basis. Indeed, the Higgs couplings are automatically aligned with the mass matrices, while the photon and the gluon couple universally, as required by gauge invariance. There are also no FCNCs mediated by the Z boson, since it couples to each type of fermions with strength $\propto {V_{\psi L}}^\dagger V_{\psi L} = 1$ (similarly for ψ_R).

At the loop level, FCNC processes are also suppressed. The corresponding one-loop amplitudes are parametrically of the form $\mathcal{M}_{\text{1-loop}} \propto (V_{\text{CKM}})^*_{ia} (V_{\text{CKM}})_{ib} f(m_i^2/m_W^2)/(4\pi)^2$ [15], where the sum over internal quarks i is implicit and a, b are external quarks, *e.g.* s and d in the case of $K_S^0 \to \mu^+\mu^-$. (Note that if the only flavour dependence of the amplitude were the CKM factors, it would vanish due to unitarity.) The mass suppression in the amplitude is the so-called Glashow, Iliopoulos and Maiani (GIM) factor [16], which was proposed to control the quadratic divergences found in different FCNC amplitudes [17]. This led to the prediction of the charm quark mass, four years later [18]. At present, the impressive limits set on these rare processes, $\mathcal{B}(K_S^0 \to \mu^+\mu^-) < 10^{-9}$ versus the unsuppressed $\mathcal{B}(K^+ \to \mu^+\nu) = 0.64$ [13], are an outstanding probe of the SM.

Let us also remark that, as illustrated in equation 13, the W boson couples only to the LH fermions; since a parity (P) transformation takes $P_L \leftrightarrow P_R$, this symmetry is violated maximally by the weak interactions. The Z boson also distinguishes between LH and RH fermions through their weak isospin; see equation 9. Hence, its couplings also violate this discrete symmetry. On the other hand, fermions are vector-like with respect to electromagnetism, which therefore preserves P.

Charge conjugation and parity (CP) or time reversal (T) violation is related to the presence of complex phases in the Lagrangian. Due to the presence of η in equation 14, $V^*_{\text{CKM}} \neq V_{\text{CKM}}$ in general. Up to date fits for the CKM parameters[3] give $A \approx 0.83$, $\rho \approx 0.15$, $\eta \approx 0.36$ and $\lambda \approx 0.22$. This proves that CP is

[2] There are no FCCCs in the lepton sector. Since neutrinos are massless in the SM, we can choose $V_{\nu L} = V_{e_L}$ such that the equivalent to interaction 13 in the lepton sector becomes diagonal.

[3] See http://www.utfit.org/UTfit/.

violated in the quark sector. Furthermore, in the Wolfenstein parameterization, λ works as an expansion parameter that demonstrates the CKM hierarchical structure: at zero order in λ, it is just a diagonal matrix; only at next-to-leading order (NLO), the first two generations communicate with the third.

Another CP violating phase exists in the strong sector of the SM, due to the presence of the θ-angle. This term violates both P and T symmetries, which implies by the CPT theorem [19] that θ also breaks CP. We could try to rotate away this term by making axial rotations on the fermion fields, $\psi \longrightarrow e^{-\mathrm{i}\alpha_5\gamma^5}\psi$. Given the axial symmetry anomaly [20], such changes produce a variation in the quarks Lagrangian which is of the same form as the θ-term [21],

$$\delta\mathcal{L}_{\mathrm{QCD}} = \alpha_5\partial_\mu J^{\mu 5} = -\frac{n_G g_3^2}{16\pi^2}\alpha_5 \widetilde{G}^A_{\mu\nu}G_A^{\mu\nu} + 2\mathrm{i}\alpha_5\overline{q}m_q\gamma_5 q\,, \tag{15}$$

with n_G the number of fermion generations involved and $J^{\mu 5} \equiv \overline{\psi}\gamma^\mu\gamma_5\psi$. For non-zero quark masses, the axial symmetry is also explicitly broken at tree level leading to the second term in the equation above. Therefore, by performing this change of basis, we would only accomplish to transfer θ to the quarks mass matrix. The QCD θ-angle is consequently physical. The non-observation of CP-violating interactions in QCD sets however a stringent limit on $|\theta| < 10^{-11}$ [22].

More generically, in any four-dimensional Yang-Mills theory based on a symmetry G with a non-trivial homotopy group $\pi_3(G)$, additional vacuum angles are expected [23]. In particular, a weak θ-angle can arise too in the SM which could provide additional sources of CP violation. This term can be analogously adjusted if there are currents sensitive to $W\widetilde{W}$ which are classically conserved but broken at the quantum level. In this case, we can perform vector $U(1)$ rotations, $q \longrightarrow e^{-\mathrm{i}\alpha_B/3}q$ and $l \longrightarrow e^{-\mathrm{i}\alpha_L}l$, leading to [24]

$$\delta\mathcal{L}_{\mathrm{EW}} = \alpha_B\partial_\mu J_B^\mu + \alpha_L\partial_\mu J_L^\mu = -\frac{n_G g_2^2}{32\pi^2}(\alpha_B+\alpha_L)\widetilde{W}^I_{\mu\nu}W_I^{\mu\nu}\,, \tag{16}$$

with $J^\mu \equiv \overline{\psi}\gamma^\mu\psi$. Therefore, we can choose the rotation phases in order to cancel entirely the contribution from the $SU(2)$ θ-term, that is consequently non-physical.

Finally, let us note that, turning off the Yukawa interactions, the SM Lagrangian enjoys a larger (flavour) symmetry $G_{\mathrm{flavour}} = U(3)^5$, since the gauge interactions are flavour blind [15]. The Yukawa term breaks $G_{\mathrm{flavour}} \longrightarrow U(1)_{L_e}\otimes U(1)_{L_\mu}\otimes U(1)_{L_\tau}\otimes U(1)_{\mathrm{B}}$, with $U(1)_L$ being the lepton number and $U(1)_B$ the baryon number symmetries that were used above. The charge assignement is by convention $q_B = 1/3$ for baryons and $q_L = 1$ for each family of leptons, all other particles being uncharged. Such symmetries do not arise from first principles, but are accidental features of the tree level Lagrangian. The $B+L$ combination is in fact anomalous, as demonstrated by equation 16; it is however known that the effects sourced by the anomaly are of non-perturbative nature [25]. The $B-L$ current is, on the other hand, exactly preserved.

2.3 Reasons to go beyond the Standard Model

To sum up, there are nineteen physical parameters in the SM: three gauge couplings; three real parameters from the lepton Yukawa sector (the charged lepton masses); nine real parameters from the quark Yukawa sector (the quark masses and mixing angles) plus one complex phase; the θ-angle; the Higgs mass and its VEV. This small set of parameters has been over-constrained by countless experiments, probing different processes over a wide range of energies[4].

While we do not aim to exhaust the huge experimental scrutiny the SM has been under, we would like to highlight some important probes of the Higgs mechanism, the last piece needed to render the SM as a self-consistent QFT. In particular, the linear dependence of the Yukawa couplings on the fermion masses has been checked in several channels, including the rare $h \longrightarrow \mu^+\mu^-$ [26]. Knowing the masses of fermions (see table 2), we can readily check that such measurements are consistent with the Higgs VEV $v \sim 246$ GeV. In conjunction with the measured Higgs mass $m_H \sim 125$ GeV, such VEV implies a Higgs self-coupling $\lambda_H \approx 0.13$ [9] which is compatible with measurements from direct searches, namely in multi-Higgs production (the corresponding cross sections are however too small to allow a precise measurement; significantly improved prospects are expected at the next luminosity phase of the LHC [27, 28]). Plugging in the Weinberg angle and the weak coupling constant, we can verify that the predictions for the gauge boson masses in equation 10 are also in perfect agreement with the experimental values, $m_W \approx 80.4$ GeV and $m_Z \approx 91.2$ GeV [9]. The Higgs-vector couplings present in this equation have all been tested as well, for instance through vector boson fusion production or the Higgs decay into VV^*[5]. Finally, the ρ-parameter has been also measured with high precision, $\rho = 1.00039 \pm 0.00019$ at the 95% confidence level (CL) [9], in agreement with equation 11.

With the current experimental accuracy, other theory calculations have been also pushed to several loops. For example, the magnetic dipole moment of the electron is known up to five loops in quantum electrodynamics (QED) [29], showing an agreement with the experimental result up to nine significant digits. The fight gets harder but the SM seems to keep winning on all fronts.

Nevertheless, there are some (long-lasting) observations that cannot be accounted by the SM $d.o.f.$ alone, therefore showing that it cannot be the ultimate theory[6]:

1. In the presence of an UV scale, the Higgs boson mass receives large quantum corrections; therefore, we would naively expect it to be as large as the UV scale itself, contrarily to what we have found experimentally. This is the essence of the EW HP.

[4] For a summary plot of LHC measurements, see https://atlas.web.cern.ch/Atlas/GROUPS/PHYSICS/CombinedSummaryPlots/SM/ATLAS_c_SMSummary_TotalXsect_rotated/ATLAS_c_SMSummary_TotalXsect_rotated.png.

[5] Hereafter, we use V to denote the W or Z bosons. The star refers to off-shell particles.

[6] We leave aside other SM problems which are less relevant for this thesis, such as the absence of a candidate for inflation, dark energy, or the huge mismatch between the theoretical and observed values associated to the cosmological constant.

2. We have no explanation for the hierarchy of fermion masses, which expand around six orders of magnitude.

3. There is very strong evidence of DM, a stable and electrically neutral component that makes $\sim 27\%$ of the energy density in the Universe [9], which cannot be accounted for by any of the SM particles.

4. The observed matter in the Universe is dominantly baryons, with only a tiny amount of antibaryons being observed in cosmic ray data [30]. Although the SM discriminates between particles and antiparticles due to CP violating interactions, such breaking is not sufficient to explain the asymmetry that we observe [31].

5. Neutrino oscillations have been observed, which implies that neutrinos are massive [7] [9]. However, there is no mechanism to generate their masses in the SM.

6. We have no explanation either for the smallness of the QCD θ-angle, which leads to the so-called strong CP problem.

7. The SM does not incorporate a complete description of gravity.

We start by noting that the last item in this list implies that the SM cannot give predictions above the Planck scale M_P. Indeed, the Einstein-Hilbert action admits a perturbative expansion around a flat space in powers of $1/M_P$ [32]; above this scale, we cannot estimate the effects of new physics nor rely on the SM predictions. Hence, the SM is at most valid up to $\Lambda_{\text{SM}} \leq M_P$ and it can be therefore regarded as an EFT.

The basic idea of EFTs is that any interaction mediated by internal propagating $d.o.f.$, at much lower energies E than the scale of the virtual particles M, can be described by a contact interaction that is independent of the physics model in the UV. Therefore, we can rely on a systematic expansion in (E/M) of *all* allowed operators, constructed with the relevant $d.o.f.$, to describe low-energy phenomena. As an example, the Fermi theory, obtained by integrating out the heavy gauge bosons in $\mathcal{L}_{\text{SM}}$, can perfectly account for the muon decay [33].

Such EFT approach is furthermore remarkably efficient [34] since *(1)* it can be applicable to any theory; *(2)* it provides the broadest and an unbiased view on the nature of new physics; *(3)* it greatly simplifies the calculations by allowing us to deal with one scale at a time; *(4)* it allows us to break large logarithms, which can spoil a perturbative analysis, and to sum them using renormalization group equations (RGEs); *(5)* it keeps power-counting manifest (with an *appropriate* choice for the regulator of the theory). In particular, the last point allows us to systematically improve the accuracy of any EFT computation, by including additional terms in the (E/M) expansion.

[7] This consequently implies that there can be also FCCCs in the leptonic sector, where the analogous to the CKM is called the Pontecorvo-Maki-Nakagawa-Sakata matrix. In this case, seven new parameters are introduced in the theory, assuming neutrinos are Dirac fermions.

Extending this approach to the SM itself leads to the Standard Model effective field theory (SMEFT) Lagrangian:

$$\mathcal{L}_{\text{SMEFT}} = \mathcal{L}^{(d=4)} + \frac{c_5}{\Lambda_{\text{SM}}}\mathcal{L}^{(d=5)} + \frac{c_6}{\Lambda_{\text{SM}}^2}\mathcal{L}^{(d=6)} + \dots\,, \tag{17}$$

where the dots encode operators with mass dimension $d > 6$. Such parameterization has become one of the most preferred tools to describe particle physics at current energies [35], given the absence of direct discoveries in the last years and our lack of knowledge about the UV. So far, the independent bases of operators in the SMEFT are available up to dimension $d = 9$ [36–42]. The corresponding Wilson coefficients are unknown[8].

From observations, we can however set limits on these coefficients and therefore on the size of the cut-off scale. The SM-only picture is recovered by taking $\Lambda_{\text{SM}} \to \infty$. In this way, the renormalizable part of the SMEFT Lagrangian basically accounts for everything we observe, besides the open questions enumerated above. Let us then explore whether they could be explained by the non-renormalizable interactions.

There is only one five-dimensional operator in the SMEFT, the Weinberg operator (with $\Delta L = 2$) [36]:

$$\mathcal{L}_W = \frac{c_5}{\Lambda_{\text{SM}}}(\bar{\ell}_L\widetilde{H})(C\ell_L\widetilde{H})\,, \tag{18}$$

where $C = \mathrm{i}\gamma^2\gamma^0$ is the charge conjugation matrix. This operator gives Majorana neutrinos masses of required size $m_\nu \sim c_5 v^2/\Lambda_{\text{SM}} \lesssim 0.1$ eV [44] for $\Lambda_{\text{SM}} \sim 10^{15}$ GeV and $c_5 \sim \mathcal{O}(1)$.

At dimension six, other operators of the form $qqq\ell$ ($\Delta B = \Delta L = \pm 1$) can mediate proton decay $p \to M\ell$, M denoting a meson. The corresponding decay width is naively given by

$$\frac{\Gamma\,(p \to M\ell)}{m_p} \sim \frac{c_6^2 f_p^2}{(2\pi)^2}\left(\frac{m_p}{\Lambda_{\text{SM}}}\right)^4 < 10^{-66}\,, \tag{19}$$

where m_p is the proton mass, $(2\pi)^2$ is a phase space factor and f_p is a form factor encoding the $p \to M$ transition. On the right-hand side (r.h.s.), we have used the bound on the proton lifetime $\tau_p > 10^{34}$ yrs from $p \to e^+\pi^0$ searches [45]. Assuming $c_6 f_p \sim \mathcal{O}(0.01)$, it may even be that the same cutoff scale for which neutrino masses can be explained is compatible with this bound, which would hint towards a promising unification of the new physics.

Six- and eight-dimensional pure Higgs operators can, on the other hand, lead to a strong first order phase transition (PT) at the EW scale [46, 47]. Such PT occurs out-of-equilibrium, which provides one of the necessary conditions for baryogenesis; see appendix D.

This SMEFT picture makes it very plausible that new physics could be encountered only at very large energies (if other issues, such as dark matter, do not introduce a new scale below Λ_{SM}). The glaring problem that challenges this picture is encoded in operators of the Lagrangian with mass dimension $d < 4$.

[8] Interestingly, some LHC datasets seem to favor non-vanishing values of these Wilson coefficients [43]; additional data is however required to make a precise claim.

Had we continued the EFT analysis for such operators, the Higgs mass term would expectedly be $c_2\Lambda_{\rm SM}^2 H^\dagger H$. The huge mismatch between this expectation and the observed value of the Higgs mass makes it very *unlikely* that $\Lambda_{\rm SM} \gtrsim 10^{15}$ GeV. Instead, we are led to expect new physics[9] to lie close to the EW scale.

Let us suppose we knew a more fundamental theory comprising a heavy fermion Ψ, with Lagrangian

$$\mathcal{L}_{\rm UV} \supset \mathcal{L}_{\rm SM} + \overline{\Psi}\left(M_\Psi - i\not{\partial}\right)\Psi + Y_\Psi \overline{\Psi} H \Psi \,. \tag{20}$$

Upon integrating the heavy fermion out, the Higgs mass would receive the following correction at one-loop:

$$(\delta\mu_H^2)_{\rm UV} \sim \frac{3Y_\Psi^2}{16\pi^2} M_\Psi^2 \,. \tag{21}$$

Matching the UV and the infrared (IR) theories, we would therefore obtain:

$$(\mu_H^2)_{\rm IR} = (\mu_H^2)^0_{\rm UV} + (\delta\mu_H^2)_{\rm UV} \,; \tag{22}$$

with the left-hand side (l.h.s.) corresponding to the Higgs mass parameter that we have measured. The r.h.s. shows that, in the presence of very heavy new physics, we would have to find in the UV a bare value $(\mu_H^2)^0_{\rm UV} \approx -(\delta\mu_H^2)_{\rm UV}$. The HP is therefore a fine-tuning problem. The amount of fine-tuning can be, in turn, characterized by [49]

$$\Delta \equiv \left|\frac{\partial \log \mathcal{O}}{\partial \log x}\right| = \left|\frac{x}{\mathcal{O}}\frac{\partial \mathcal{O}}{\partial x}\right| \sim \frac{3Y_\Psi^2}{16\pi^2}\left(\frac{M_\Psi}{m_H}\right)^2 , \tag{23}$$

which encodes the sensitivity of the measured observable $\mathcal{O} = m_H^2$ to variations in the UV parameter $x = M_\Psi^2$, related to any heavy physics coupled to the Higgs boson. This formula also gives a quantitative meaning to the HP: if indeed there was an equation like 22 and the UV parameters were huge, their difference would still be of the same order unless the two numbers were equal up to several significant digits. Such terms would have to be measured with incredible accuracy, which might be beyond the capacity of any of our experimental tools. In this sense, a large fine-tuning could become a predictability issue as well.

Why should, however, Nature care about our predictability issues? Or the fact that we do not like fine-tuning? Indeed, naturalness can be an important guide into new physics, but the limitations in following this approach should be clarified.

First, note that if there is no x, there is no HP. Indeed, if the SMEFT describes only the EW scale, all particles in the theory must have a mass $\lesssim v$; otherwise, the construction of such EFT would be

[9] In this work, we will assume that the new physics corresponds to a high-energy sector where new particles should be encountered. Another interesting approach is to consider that the new physics scale is associated with field values rather than new particles, in analogy with Fermi's findings that $G_F \sim 1/v^2$. In this case, new particles could appear only at much larger energies than those of current experiments [48].

invalid. Nevertheless, we know that the Higgs boson interacts at least gravitationally. At one-loop, scattering processes involving the *graviton* are expected to scale as [50]

$$\mathcal{M}_{2\to 2} \sim \frac{N}{(4\pi)^2}\frac{E^2}{M_P^2}, \tag{24}$$

with N denoting the number of particles in the loop. Consequently, we expect some new behavior to be manifest at $E \sim 4\pi M_P/\sqrt{N}$. In order not to introduce another scale, we should match $E \sim v$, which requires the presence of a huge number N in the UV. Since these new particles presumably couple to the Higgs boson, we end up reintroducing the HP.

Second, we argued that two huge parameters in the UV are unlikely to give a small value in the IR; how likely that is depends however on the prior distribution functions we assume for those parameters. Naturalness assumes priors peaked at $\mathcal{O}(1)$, with no fundamental reason. Given our ignorance about the UV, that is *an* assumption we can make, although we should not use it to undermine theories with are viable beyond naturalness. Such assumption allows us to search for an underlying theory for the Higgs mass and has been very useful in the past, namely anticipating the discoveries of the ρ-meson and the charm quark [51]. (Even not allowing us to predict exact values, naturalness has been a good indicator of where to expect qualitatively new phenomena.) It is also worth noting that our best theories to solve the HP also offer some of the most compelling candidates for other unexplained observations, such as DM [52, 53].

Third, we should note that even if our naive assumption on the priors was true, Nature could just be fine-tuned. Although possible, this is like any other explanation for a given data which brings more complexity and input parameters than the theory we have actually accepted. Therefore, even if such hypothesis were true, this should not stop our attempts for a simpler theory from which the Higgs mass emerges as an *output*.

Altogether, we aim to argue that the moderate naturalness position [54] is the most useful, which is based on the idea that theories should be natural, without however rejecting regions of the parameter space where the level of tuning is large, *"just as the rare case of a B-meson decaying to a strange meson does not eliminate the understanding that a B-meson decays much more often to a charm meson"*.

To define which level of tuning is or is not acceptable, we are again led to some subjectivity. Not only in the final numbers, but in the measure of fine-tuning itself. For instance, if we want to evaluate equation 23 in a non-renormalizable UV theory, we should be aware that different parameterizations are possible. Consequently, a value of x which is sizable in a given basis of operators can vanish in another one, which would lead to an artificial large Δ. Furthermore, this measure quantifies the fine-tuning at a single point. Under the Barbieri-Guidice criteria, a model which can explain certain phenomena throughout the entire parameter space is thus considered as favorable as another which does it at a single point, with all others already ruled out by data. Other measures have been suggested in the literature to surpass this limitation [55].

In this work, we assume the form of equation 23 and focus on models leading to $\Delta \lesssim 10^3$, as it is *conventionally* accepted. These values are not too narrow, but sufficiently small to assume that the Higgs mass could be predicted from the UV theory. More importantly, the existence of such *natural* theory is falsifiable. By exploring the SM in the multi-TeV range, we will eventually have access to the region in the phase space where the fine-tuning becomes too large, in which case new approaches beyond naturalness should be considered. For now, there are still motivated and natural (non-minimal) theories that remain untested and large amounts of data to test their viability.

Before ending this chapter, it is also worth clarifying why the HP is connected to the Higgs boson and no other elementary particle in the SM. We understand that the other particles are light, because in the limit of $m \longrightarrow 0$ the SM recovers a symmetry (chiral or gauge symmetries, in the case of massless fermions or gauge bosons). Any physical parameter satisfying this (t'Hooft) criteria is *technically natural* [56]; and the Higgs mass is not. Since quantum corrections respect the symmetries of the QFT, they must be proportional to the symmetry violation parameter, in this case the mass. Therefore, provided m is small, these effects are small as well. While in this Higgs case, there is nothing special about $\mu_H = 0$.

The last statement holds for any scalar. Therefore, we might wonder why the other spin-0 bosons we have previously observed in Nature, the QCD hadrons, did not stir up a similar interest. The answer is that their masses are generated dynamically by confinement, which in turn arises from the renormalization group evolution of the strong coupling constant:

$$\frac{\partial \alpha_3}{\partial \log \mu} = -\frac{7}{2\pi}\alpha_3^2, \tag{25}$$

at one-loop (see, for example, equation 142 in Ref. [8]). We define $\alpha = g^2/(4\pi)$. Using the coupling strength value at M_P as the boundary condition on this RGE, we can run it down to some lower scale μ, obtaining:

$$\frac{1}{\alpha_3(\mu)} = \frac{1}{\alpha_3(M_P)} - \frac{7}{2\pi}\log\left(\frac{M_P}{\mu}\right), \tag{26}$$

which eventually diverges in the IR. At this point, it is rather a dimensionfull parameter that characterizes the QCD interactions, Λ_{QCD}, which is found by setting the r.h.s. of this equation to zero:

$$\Lambda_{\text{QCD}} = M_P e^{-\frac{2\pi}{7}\frac{1}{\alpha_3(M_P)}}. \tag{27}$$

The exponential suppression in this result gives an explanation for the huge separation between the proton mass and the fundamental scale. Furthermore, it is clear that no HP arises because QCD has no scales in the UV; instead, a natural strong coupling can generate the proton mass due to this mechanism of *dimensional transmutation*.

Chapter 3

Collider physics and statistical tools

A common prediction of models targeting the HP is the presence of new heavy particles in the spectrum. They can be produced and decay at high-energy colliders which in turn provide a powerful way to test these scenarios.

We therefore dedicate this chapter to describe the general features of the detectors where the physics we want to probe takes place, namely at the LHC; see section 3.1. We define the main collider objects and observables in section 3.2.

To understand the evolution of the parton collision up to the formation of stable detector objects, we have to rely on evolved computational programs, which have been developed by experts over several decades. These programs are based on Monte Carlo (MC) simulations, which reproduce the events we are interested in according to their probability to occur in Nature. The different stages of these simulations are discussed in section 3.3.

Finally, in section 3.4, we present the statistical tools we use to determine if a given model signal is compatible with the data (and how sure we are that it in fact is).

3.1 The Large Hadron Collider

The LHC [57–59], located at CERN (Geneva, Switzerland), is the most energetic and largest collider ever built. This experiment collides beams of protons at nearly the speed of light, with a center of mass energy (c.m.e.) $\sqrt{s} = 13$ TeV. This energy is then converted into mass, therefore forming the SM and possibly beyond the SM particles.

There are four big detectors located in different collision points at the LHC: ATLAS [60, 61], CMS [62, 63], LHCb [64, 65] and ALICE [66]. The first two are multipurpose detectors, designed to study physics

from the Higgs boson to SUSY scenarios, capturing particles that fly in all directions from the collision point. The last two detectors above are, on the other hand, specialized to test particular phenomena. LHCb is a forward detector whose main goal is to study the properties of heavy flavour particles, containing a b or a c quark. Finally, ALICE is dedicated to explore heavy-ion physics, to provide insight on the properties of the QCD plasma at extreme conditions; it is outside the scope of this thesis.

While ATLAS and CMS are particularly suitable for searching new heavy particles, LHCb is dedicated to explore the precision frontier where light and long-lived particles might lie. To tag the heavy flavour mesons (which typically fly a few cm), this detector is specially designed to select forward displaced decays with soft final states. The unique particle identification ability and the outstanding mass resolution of the detector are furthermore key features to search for the hidden particles with masses and lifetimes similar to those of the heavy mesons. Other B-factories around the world perform complementary studies on stealth physics, namely Belle [67] (at SuperKEKB, Japan) and BaBar [68] (at SLAC, USA).

Moreover, the results from previously active facilities can constrain large regions of the parameter space of new physics models, two of the most iconic being the Tevatron [69] (Fermilab, USA) and LEP [70] (CERN, Geneva). Tevatron was the highest energy particle collider before the LHC; it was where the top quark was discovered [71, 72]. It reached $\sqrt{s} \sim 1$ TeV in proton-proton (pp) collisions and collected more than 10 fb^{-1} of data. LEP, on the other hand, was a circular e^+e^- collider that reached $\sqrt{s} = 209$ GeV; its tunnel was reused to build later on the LHC.

3.2 Colliders language and geometry

The number of collisions at the detector, that is, the number of events N is given by the cross section σ times the *integrated* luminosity L. The latter is obtained by integrating over time the *instantaneous* luminosity $\sim 10^{34}\text{cm}^{-2}\text{s}^{-1}$ up to date, at the LHC. Multiplying by the pp cross section $\sigma_{pp} \sim \pi(1\text{ fm})^2 \sim \mathcal{O}(10)$ mb, this corresponds to $\sim 10^8$ collisions per second, which is obviously a huge number of events to record.

This number can be further reduced with a triggering system, which gives the necessary conditions for an event to be recorded. This system is usually comprised by a hardware and a software trigger: the former can demand, for instance, a minimum momentum for all tracks; while the latter handles more complex requirements and can process the full event with detail, being able to use tracking information to keep events with specific numbers of electrons or muons.

To be able to test particular models, specific data analyses need to be designed, in order to keep the majority of signal events while losing large portions of the background, that is all the other SM processes not contributing to the interaction we want to probe. This is very challenging in two ways: first, the interactions of interest are usually very rare; second, they look similar to the backgrounds which are much more common.

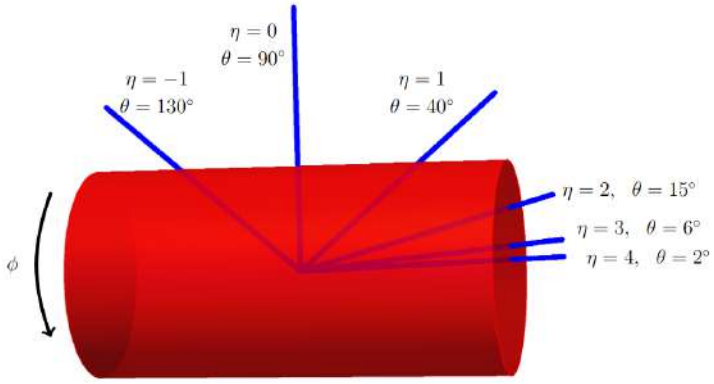

Figure 1: The geometry of a detector (taken from Ref. [73]). The pseudorapidity is a function of the polar angle: it goes from $\eta \longrightarrow -\infty$ ($\theta = \pi$) to $\eta \longrightarrow +\infty$ ($\theta = 0$) along the beam line, that we define as the z-axis. The azimuthal angle ϕ goes around the beam, with $\phi = 0$ corresponding to the x-axis. Note that particles with $|\eta| \gtrsim 4$ are already very close to the beam line.

For these reasons, we study different selection cuts on collider observables which can optimize the chance to see the signal at particular regions of the phase space. These observables are functions of the four-momentum $p^\mu = (E, p_x, p_y, p_z)$ of the particles that reach the detector. In first approximation, p^μ can be reconstructed from the deposits of energy in the calorimeters and their flight directions, parameterized by the polar and azimuthal angles $(\theta,\ \phi)$ that describe the cylinder centered around the beam line; see figure 1. Some of the typical kinematic observables at colliders are:

- The rapidity, $y \equiv \frac{1}{2} \ln \frac{E+p_z}{E-p_z}$;
- The pseudorapidity, $\eta \equiv \ln \cot \frac{\theta}{2} \approx \frac{\pi}{2} - \theta$, which coincides with the rapidity in the limit of massless particles;
- The angular separation between two tracks, $\Delta R \equiv \sqrt{(\Delta\phi)^2 + (\Delta y)^2}$;
- The missing transverse momentum, $\left(p_T^{\text{miss}}\right)^\mu \equiv -\sum_i \left(p_T^\mu\right)^i$, where i runs over all visible tracks and $p_T = \sqrt{p_x^2 + p_y^2}$;
- The missing transverse energy (MET), $E_T^{\text{miss}} = \left|p_T^{\text{miss}}\right|$;
- The invariant mass of n objects, $m^2 \equiv \left|\sum_{i=1}^n p_i^\mu\right|^2$;
- The transverse mass, $m_T^2 \equiv \left|\sum_{i=1}^n {p_T}_i^\mu\right|^2$, which is particularly relevant when the longitudinal momentum of a particle is unknown.

The ATLAS and CMS detectors have a coverage as close to 4π as possible over the collision point and typically identify charged particles in a pseudorapidity volume $|\eta| < 2.5$. On the other hand, the LHCb detector is designed to cover the interval $2.0 < \eta < 5.0$.

Inside the detector, the heavy particles typically decay promptly so we can never actually see them. Instead, we find indications of their existence by looking into the subsequent products of their decay. These final particles can be identified as they leave specific signatures in different layers of the detector.

The innermost layer measures the tracks of charged particles. Their trajectories are bent by magnetic fields, the radius and orientation of the curvature allowing the extraction of the particle momentum and electric charge. Electrons, as well as photons (producing e^+e^- pairs), lose all their energy in the electromagnetic calorimeter, while hadrons get into the subsequent layer, the hadronic calorimeter. Muons, on the other hand, reach the farthest regions of the detector, the small curvatures of the most energetic muon tracks being one of the reasons the detector needs to be so big. Neutrinos leave the detector having rarely interacted at all, typically leading to events with large MET. Their existence can be inferred from the fact that the total momentum in an event is conserved.

Quarks and gluons, on the other hand, can only be found inside of hadrons[1]. Therefore, at the detector level, it makes no sense to talk about these particles, but to define a collection of closed objects that originate from short-distance quarks and gluons, that is a *jet* [74].

Jet definitions are ambiguous, but typical clustering algorithms operate iteratively by calculating the distance d_{ij} between any two protojets i and j and their distance to the beam d_{iB}. If the smallest of these distances is d_{ij}, i and j are merged; if it is d_{iB} instead, i is removed from the list of objects and it is called a jet; this goes on until there are no other protojet pairs within a cone of arbitrary radius $R = \sqrt{(\Delta\theta)^2 + (\Delta\phi)^2}$. (Objects in this cone can be hadrons, but also *e.g.* electrons which are surrounded by a large hadronic activity.) In all works described in this thesis, we will use the anti-k_T algorithm [75], in which

$$d_{ij} = \min\left(\frac{1}{p_{T_i}^2}, \frac{1}{p_{T_j}^2}\right)\frac{(\Delta R)^2}{R^2} \quad \text{and} \quad d_{iB} = \frac{1}{p_{T_i}^2}\,. \tag{28}$$

Furthermore, algorithms have been also developed to discriminate the jet flavour, namely to distinguish jets produced by a b-quark[2]. B-tagging relies on the defined flight distance of the B-meson, $c\tau \sim 0.5\gamma$ mm (where $\gamma \sim p/m$ represents the boost factor), and involves typically three steps: *(1)* searching for a displaced vertex a few mm away from the primary interaction point; *(2)* constructing the invariant mass of the particles emerging from such vertex; *(3)* selecting the candidates whose invariant mass is closest to the B- meson mass. Current algorithms, also relying on maching learning to construct higher-level observables, typically achieve b-tagging efficiencies around 70%. (The mis-tagging probability to wrongly identify a c- or a light-flavour jet as a b-jet is typically $\mathcal{O}(1/10)$ and $\mathcal{O}(1/100)$, respectively [76].)

[1] With the exception of the top quark, whose lifetime is so small that it decays before hadronization.

[2] The identification of a b-jet can be subsequently used to tag the top, since the branching ratio $\mathcal{B}(t \to Wb) \approx 1$ [13].

3.3 Event generation

In order to study the collider phenomenology of a theoretical model, we resort to MC simulators. This proceeds in three main steps.

First, we obtain the parton-level particles resulting from the pp (or other) collision. They include leptons, photons, gluons or quarks. The calculations at this level involve matrix elements evaluated up to a certain order in the SM or the new physics coupling. In all works described in this thesis, the parton-level events are produced with `MadGraph` [77]. This step is model dependent and requires the implementation of the Lagrangian in an UFO model, that we generate with `FeynRules` [78].

Second, we must describe the showering and hadronization of the partons. This involves mainly QCD calculations and is model-independent. However, matrix elements involving the emission of gluons show both collinear and soft divergences; furthermore, a large number of particles can be radiated which makes these calculations computationally expensive. To complement this approach, we rely on parton showering algorithms, such as those implemented in `Pythia` [79], which takes into account the successive splitting of partons. Still, for hard processes with well separated objects, matrix elements give the most reliable predictions. Therefore, the two approaches are combined in `MadGraph` to generate multi-jet processes, each description being assumed in different regions of the phase space. In order to avoid overlapping and consequently double-counting of jets, we need to find the optimized scale to switch between the approaches, the so-called matching scale. This scale can in turn be found by studying the smoothness of the differential jet rate distributions[3]. The objects resulting from the showering must be subsequently collected into hadrons due to QCD confinement. This hadronization process is also simulated with `Pythia`.

The last step is to simulate the detector response. With this aim, we can follow standard experimental analyses, assuming the typical momenta thresholds to detect the particles, as well as average values for the reconstruction efficiencies. However, to include the largest available set of real detector effects, we rely on `Delphes` [80]. This tool includes parameterizations of the effects of the detector geometry, as for example momenta smearing due to the calorimeter response. The efficiencies to reconstruct and identify the tracks in `Delphes` are functions of kinematic variables, typically (p_T, η), that reproduce the experimental probability of a particular configuration, as seen in the actual detector. The same for heavy flavour tagging efficiencies, as well as the trigger simulation. Note, however, that when proposing new analyses for future collider runs, the first approach described is a good approximation, since we do not actually know the improvements on the trigger or tracking performance at future facilities.

[3] See `https://indico.cern.ch/event/656211/attachments/1498666/2333189/TASI_feynrules_madgraph_tutorial.pdf`

3.4 Data analysis and statistical tools

After generating the detector objects, we can perform an analysis. The output from `Delphes` can be read by `ROOT` [81], which provides tools for combining variables, histogramming, fitting and computing limits, among others. That is our ultimate goal: to understand if the signal we are interested in is or *could be* excluded by experiments, and inherently quantify the potential to discover new physics.

To turn to this point, let us suppose we make an N-bin experiment (or equivalently N independent counting experiments). The distribution of the number of selected events per bin n_i is well modeled by a Poissonian distribution with an expected number of events: $s+b$, in the presence of signal plus background; or b, for background only. The basis of the CL_s method [82], that we use in the following to compute limits, is the ratio

$$Q \equiv \frac{L_{s+b}(n)}{L_b(n)} = \Pi_{i=1}^{N} \frac{(s_i+b_i)^{n_i} e^{-(s_i+b_i)}}{{b_i}^{n_i} e^{-b_i}}\,, \tag{29}$$

where the likelihood function $L_x(n) \equiv P(n|x)$ is defined as the conditional probability for the observed data n, given that a set of model parameters x occurred (in this case, the expectation value).

Such Q is used to distinguish between the hypothesis $s+b$ or b: it takes large values if the former is true; or small values if the latter is true instead. To evaluate which of these hypotheses is more compatible with the data, we define the probability, in each *ansatz*, that the test statistic is at least as probable as the actual measurement Q_{obs}:

$$\mathrm{CL}_{s+b} \equiv P_{s+b}\left(Q \leq Q_{\mathrm{obs}}\right) \quad \text{and} \quad \mathrm{CL}_b \equiv P_b\left(Q \leq Q_{\mathrm{obs}}\right)\,. \tag{30}$$

In this way, if $\mathrm{CL}_{s+b} \leq \alpha = 0.05$, the signal is excluded at a CL $= 1-\alpha = 95\%$. Given a model, we can therefore find a maximum number of expected signal events, s_{max}, such that cross sections above $\sigma_{\mathrm{max}} \equiv \epsilon s_{\mathrm{max}} L$, ϵ being the selection efficiency and L the collected luminosity, are excluded at this CL.

It is however well known that using CL_{s+b} to derive upper limits is problematic when the two distributions P_{s+b} and P_b almost overlap, that is, when $s \ll b$. In this limit, the method can artificially exclude models it has no sensitivity to. To avoid this case, in the CL_s method, we normalize CL_{s+b} by a quantity that increases as the $s+b$ hypothesis becomes less plausible, therefore penalizing CL_{s+b}; such quantity can be CL_b itself. In this modified approach [83], a signal is considered excluded if:

$$\mathrm{CL}_s \equiv \frac{\mathrm{CL}_{s+b}}{\mathrm{CL}_b} \leq \alpha = 0.05\,. \tag{31}$$

For a single-bin experiment, equation 29 reads:

$$Q = e^{-s}\left[1+\frac{s}{b}\right]^n\,. \tag{32}$$

or equivalently,

$$\ln Q = -s + n \ln\left[1+\frac{s}{b}\right]\,. \tag{33}$$

The test variable has therefore the same distribution as n. In this limit, equation 31 becomes:

$$\mathrm{CL}_s = \frac{P_{s+b}(n \leq n_{\mathrm{obs}})}{P_b(n \leq n_{\mathrm{obs}})} = \frac{\sum_{n=0}^{n_{\mathrm{obs}}} (s+b)^n e^{-(s+b)}}{\sum_{n=0}^{n_{\mathrm{obs}}} b^n e^{-b}} \,. \tag{34}$$

If zero background events are expected and zero events are observed, we can consequently exclude models predicting

$$\mathrm{CL}_s = e^{-s_{\mathrm{max}}} < 0.05 \rightarrow s_{\mathrm{max}} \gtrsim 2.99 \,. \tag{35}$$

For more elaborate multi-bin analyses, we can use automatized tools to compute the expected upper limits. Given the signal, background and observed yields, as well as the systematic uncertainties under which they are allowed to fluctuate, the `TLimit` class in `ROOT` runs a set of pseudo-experiments in order to compute the CL parameters. Alternatively, we can pass the distribution of a discriminant variable to `OpTHyLiC` [84] which outputs an expected upper limit on the signal strength $\sigma_{\mathrm{max}}/\sigma_{\mathrm{th}}$, assuming Poissonian statistical uncertainties. The signal cross section σ_{th} is computed with `MadGraph`.

Finally, we remark that the expected background CL can be converted into an expected Gaussian significance $Z\sigma$, by finding a Z such that

$$\mathrm{CL}_b = \int_Z^{+\infty} \frac{1}{\sqrt{2\pi}} e^{-x^2/2} dx \,. \tag{36}$$

If no signal events are observed, all the theoretical points leading to $Z \geq 2$ can be excluded at 95% CL. If, instead, an excess is observed relatively to the SM predictions, it is claimed as *evidence* if $Z \geq 3$ (corresponding to a 3σ deviation from the expected limit); or a *discovery* if $Z \geq 5$ (5σ deviation)[4]. In the last case, the data would have less than 10^{-7} probability to occur if the background only hypothesis was true [87].

Considering a single bin, the statistical significance is given by [88]:

$$Z = \sqrt{2\left[(s+b)\ln\left(1+\frac{s}{b}\right) - s\right]} \approx \frac{s}{\sqrt{b}}\left[1 + \mathcal{O}\left(\frac{s}{b}\right)\right] . \tag{37}$$

This formula provides a straightforward way to evaluate the experimental sensitivity to a given model. It is obtained in the limit where $\tau \equiv \mathcal{L}_{\mathrm{MC}}/\mathcal{L}_{\mathrm{data}} \rightarrow \infty$, with $\mathcal{L}_{\mathrm{MC}}$ ($\mathcal{L}_{\mathrm{data}}$) referring to the generated (actual) luminosity. This is difficult to attain in a simulation; however, it is known [89] that for $\tau > 5$ the improvement in the sensitivity is only slight.

[4] These requirements were agreed upon as conventions, in particular to avoid the "look-elsewhere effect". This describes phenomena where an apparent statistically significant observation is actually the result of random and flat data (if, for instance, the data sample is not sufficiently large). It was not long ago when ATLAS [85] and CMS [86] observed the famous 750 GeV di-photon excess, with a local significance of 3.8 and 3.4σ, respectively. When more data was collected, the anomaly went away and was eventually considered just a statistical fluctuation.

Chapter 4

The composite Higgs idea

Compositeness is, in some way, the most plausible strategy to address the HP as it is one trick we already know Nature has. Indeed, in the strong sector of the SM, we find composite scalar particles which are protected from large quantum corrections due to their finite size; they are just not at the same scale as the Higgs boson.

CHMs therefore propose a new strongly interacting sector that confines at $m_* \gtrsim v$, in order to generate a *natural* Higgs mass. Such theories were first proposed in early attempts to parameterize EWSB in the 80's [90–92], but have received increased attention in recent years [53, 93–110] in light of the theoretical progress on the construction of realist UV completions and, to some extent, the null results of substantial searches for SUSY[1].

Since they introduce another scale, plenty of other resonances are also expected to arise from these models which have been searched for at colliders. In particular, the bounds covered so far for exotic spin-1 and spin-$1/2$ particles have pushed $m_* \gtrsim$ few TeV which is already quite large in comparison to the Higgs scale. The little hierarchy $m_H \ll m_*$ can be however explained if the Higgs is a NGB associated with the spontaneous breaking of an extended global symmetry of the strong sector, at a scale $f \lesssim m_*$. This same mechanism explains why the mass of the pion is $m_\pi \sim 140 \ll m_\rho \sim 775$ MeV [9]: since it is massless in the limit where the (chiral) symmetry is exact, the pion can be *naturally* lighter than other QCD resonances, such as the ρ-meson.

Unlike previous theories of Technicolor [111], CHMs provide also a mechanism by which the elementary Higgs is recovered, that is, a way to make the Higgs couplings very close to the SM values. This is achieved through the vacuum misalignment, a mechanism that we start exploring in section 4.1.

[1] See https://atlas.web.cern.ch/Atlas/GROUPS/PHYSICS/PUBNOTES/ATL-PHYS-PUB-2021-019/fig_23.pdf and https://twiki.cern.ch/twiki/pub/CMSPublic/PhysicsResultsSUS/barplot_Squark.png for some examples.

Although the presence of a strong coupling signals our inability to compute at low energies, the dynamics of the NGB Higgs can be described by an EFT completely determined by the symmetry group of the new sector. To construct such theory, we employ the Callan-Coleman-Wess-Zumino (CCWZ) formalism that is described in section 4.2. We therefore need a rule of power-counting (PC) to systematically rank the size of the effective operators, as well as to estimate the size of the interactions among the heavy sector of the theory; see section 4.3.

The rest of the SM is assumed to be elementary. However, since the composite sector must necessarily carry EW charges (as the Higgs does), the two sectors are coupled by gauging:

$$\mathcal{L}_{\not{\mathcal{G}}} \supset g_e B_\mu J_C^\mu \,, \tag{38}$$

with g_e being an elementary charge and J_C^μ a global current of the composite sector. Through this interaction, the Higgs boson can develop radiatively a mass and become a pNGB.

Moreover, some hypothesis must be taken on how the elementary fermions communicate with the composite sector. This is inevitable to generate the Yukawa couplings to the Higgs boson. Furthermore, this is the main source of explicit symmetry breaking in generic models, due to the large Yukawa coupling of the top quark. In CHMs, the hypothesis of partial compositeness is taken, under which the physical fermions are a superposition of composite and elementary states. We explore the predictions of this mechanism in section 4.4.

Finally, in section 4.5, we construct the minimal composite Higgs model (MCHM) and review the current experimental constraints on its parameter space.

4.1 Vacuum misalignment

Let us consider the spontaneous symmetry breaking pattern of $\mathcal{G} \to \mathcal{H}$. We split the generators of the global group in terms of unbroken T^a and broken X^a generators:

$$T^A = \left\{T^a, X^a\right\} \,, \tag{39}$$

the first (second) of which span $\mathcal{H}$ ($\mathcal{G}/\mathcal{H}$). The generators of the EW group are part of the first set,

$$T_{\text{EW}} = c_a T^a \,. \tag{40}$$

We also define a reference vacuum Σ_0 that leaves the EW group unchanged, that is

$$T^a \Sigma_0 = 0 \quad \text{while} \quad X^a \Sigma_0 \neq 0 \,. \tag{41}$$

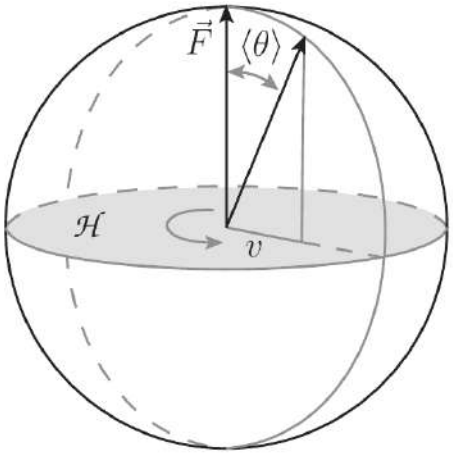

Figure 2: Illustration of the mechanism of vacuum misalignment (taken from Ref. [112]), in the case of $\mathcal{G} = SO(3)$ and $\mathcal{H} = SO(2)$. We identify $\vec{F} = \vec{\Sigma}_0$ and $\theta = \Pi$.

We can now act on the reference vacuum with a symmetry transformation to obtain a different field configuration,

$$\Sigma = e^{-\mathrm{i}\frac{\sqrt{2}}{f}\Pi_a(x)X^a}\Sigma_0\,, \tag{42}$$

where Π_a are the NGB modes. In the absence of an explicit breaking of the global symmetry, any non-vanishing $\langle\Pi\rangle$ can be set to zero, by using the defining shift-symmetry of the Goldstones. In this case, the vacuum of the Σ-field becomes aligned with Σ_0 and no EWSB occurs (because Σ_0 only breaks the generators which are orthogonal to the EW group). It is only when the NGBs acquire a potential, in particular a physical VEV, that the EW group is broken; hence, $\overrightarrow{\Pi}$ behaves exactly as the Higgs boson of the SM.

This physical misalignment defines the true vacuum of the theory, $v = f\sin\left(\langle\Pi\rangle/f\right)$. It corresponds to the projection of the reference vacuum onto the $\mathcal{H}$-plane; see figure 2. Therefore, the amount of breaking is not fixed, but depends on the free parameter

$$\xi \equiv \frac{v^2}{f^2} = \sin^2\frac{\langle\Pi\rangle}{f}\,. \tag{43}$$

For $\xi = 1$, this breaking is maximal. It corresponds to the scenario in which $\mathcal{G} \longrightarrow \mathcal{G}_{\mathrm{EW}}$ directly, as enforced in Technicolor theories [111]. For $\xi \longrightarrow 0$, on the other hand, the "SM only" picture is attained, since the new physics becomes too heavy.

In CHMs, the interesting case is when there is some gap between v and f, such that $\xi \neq 0 \ll 1$. In any successful beyond the SM extension (given the precise agreement of the SM with experimental data), the EW couplings need to be as in the SM, up to small corrections:

$$g_{\mathrm{CHM}} = g_{\mathrm{SM}}\Big[1 + O(\xi)\Big]\,. \tag{44}$$

4.2 Callan-Coleman-Wess-Zumino formalism

In equation 42, the exponential of the Goldstone fields is called the Goldstone matrix:

$$U[\Pi] \equiv e^{-\mathrm{i}\frac{\sqrt{2}}{f}\Pi_a(x)X^a}\,. \tag{45}$$

Using this parameterization, the spontaneously broken symmetry acting on the Σ-field becomes non-linearly realized on the Goldstone modes. We can find this transformation implicitly, by considering [112]

$$\Pi(x) \to \Pi^{(g)(x)} \quad \text{is such that} \quad U[\Pi^{(g)}] = g \cdot U[\Pi] \cdot h^{-1}[\Pi; g]\,, \tag{46}$$

where g and h are, respectively, elements of the broken and unbroken symmetry groups. Indeed, by acting with this transformation on the fundamental field, we find:

$$\Sigma \to g \cdot U[\Pi] \cdot h^{-1} \cdot \Sigma_0 = g \cdot \Sigma\,, \tag{47}$$

leaving the theory invariant.

The simple action of the global group on the Goldstone matrix is the reason why the latter is the building block to construct symmetry invariants, according to the CCWZ formalism [113, 114]. Taking the Maurer-Cartan one-form,

$$\omega_\mu \equiv \mathrm{i}U^\dagger \cdot \partial_\mu U = d^a_\mu(\Pi)X_a + e^a_\mu(\Pi)T_a \equiv d_\mu + e_\mu\,, \tag{48}$$

which we have decomposed along the group generators as any other element of the Lie algebra, we find that

$$\mathrm{i}U^\dagger \cdot \partial_\mu U \to h \cdot (\mathrm{i}U^\dagger \cdot \partial_\mu U) \cdot h^{-1} + \mathrm{i}h \cdot \partial_\mu h^{-1}\,, \tag{49}$$

under a local $\mathcal{G}$-transformation. (Note that h depends on spacetime coordinates through the Goldstone fields.) The second term in the equation above is a Maurer-Cartan form of the $\mathcal{H}$-group itself and therefore does not have components along the broken generators. This shows that the d_μ-symbol transforms only into the first term, and hence linearly in $\mathcal{H}$:

$$d_\mu \to h \cdot d_\mu \cdot h^{-1}\,. \tag{50}$$

On the other hand, e_μ transforms like a gauge field of the local unbroken symmetry. As such, it can be employed to construct the covariant derivatives of the composite fields.

Moreover, equation 49 implies that, using the Maurer-Cartan form, we just need to find $\mathcal{H}$-invariants to build our EFT, from which the full $\mathcal{G}$-invariance follows automatically. At the level of two derivatives in Goldstone fields, the shift-symmetric Lagrangian is therefore given by:

$$\mathcal{L}_{\text{kin}} = \frac{f^2}{4}\mathrm{Tr}[d_\mu d^\mu] \approx \frac{1}{2}\left(\partial_\mu \Pi_a\right)^2 + \dots \tag{51}$$

The couplings to the gauge fields are obtained by replacing $\partial_\mu \to D_\mu$ in equation 48.

4.3 Power-counting

CHMs are assumed to be one-scale one-coupling (1S1C) theories, which can be described completely in terms of the typical composite resonance mass m_* and its coupling $g_* \geq 1$. Therefore, the Lagrangian of the composite theory can be parameterized as [115]

$$\mathcal{L} = \frac{m_*^4}{g_*^2}\mathcal{L}'\left[\frac{\partial}{m_*}, \frac{g_*\Pi}{m_*}, \frac{g_*\sigma}{m_*}\right], \tag{52}$$

where we use σ to denote generically any heavy composite resonance. To check the consistency of this hypothesis, let us work out the EFT of the NGBs from integrating σ out:

$$\mathcal{L}_{\text{EFT}}(\Pi) = \mathcal{L}^{(2)} + \mathcal{L}^{(4)} + \mathcal{L}^{(6)} + \dots, \tag{53}$$

where the superscript denotes the number of derivatives in each term. In particular, $\mathcal{L}^{(2)}$ includes the term in equation 51. The σ resonance can couple to the NGBs via such term, producing an operator in $\mathcal{L}^{(4)}$. Using equation 52, we can estimate the size of this term, $\mathcal{L}^{(4)} \sim g_*^2/m_*^4[\mathcal{L}^{(2)}]^2 = (g_*^2/m_*^4)(m_*^8/g_*^4)\mathcal{L}'$ (where one power of m_*^2 comes from a heavy propagator), which remains consistent with PC rule. Similar arguments could be carried out for the higher derivative terms in the NGBs EFT.

The places where g_* arises in the PC formula can be understood from dimensional analysis, plugging in $\hbar \neq 1$. Since $\hbar$ has the same dimensions as the action $S = \int d^4x\mathcal{L}$, then $[\mathcal{L}] = [\hbar]/L^4$. Consequently, the canonical spin-0 (Π), spin-$1/2$ (ψ) and spin-1 (A) fields have mass dimensions $[\Pi] = [A_\mu] = [\hbar]^{1/2}/L$ and $[\psi] = [\hbar]^{1/2}/L^{3/2}$. Computing, for example, a gauge interaction involving two fermions (elementary or composite), we find that $[g_e] = [g_*] = [\hbar]^{-1/2}$; similarly, $[m_*] = L^{-1}$. Therefore, the prefactor in equation 52 gives correctly the dimensions of a Lagrangian. All terms within parenthesis are in turn adimensional.

Operators that arise at the loop level carry an extra adimensional factor $\hbar g_*^2/(4\pi)^2$ [112]. Including such operators, together with the composite fermions Ψ, and restoring natural units, we obtain the complete EFT Lagrangian:

$$\begin{aligned}\mathcal{L}_{\text{EFT}} = &\frac{m_*^4}{g_*^2}\mathcal{L}'_{\text{tree}}\left[\frac{\partial}{m_*}, \frac{g_*\Pi}{m_*}, \frac{g_*\sigma}{m_*}, \frac{g_*\Psi}{m_*^{3/2}}, \frac{g_eA_\mu}{m_*}, \frac{\lambda_\psi\psi}{m_*^{3/2}}\right] \\ &+ \frac{g_*^2}{(4\pi)^2}\frac{m_*^4}{g_*^2}\mathcal{L}'_{\text{1-loop}}\left[\frac{\partial}{m_*}, \frac{g_*\Pi}{m_*}, \frac{g_*\sigma}{m_*}, \frac{g_*\Psi}{m_*^{3/2}}, \frac{g_eA_\mu}{m_*}, \frac{\lambda_\psi\psi}{m_*^{3/2}}\right].\end{aligned} \tag{54}$$

This formula is valid in the regime of perturbativity, *i.e.* for $g_* \lesssim 4\pi$; otherwise, we cannot distinguish between tree and loop level operators. (Note that g_eA and ∂ are multiplied by the same dimensionfull factor, as required by the structure of the covariant derivative.)

Importantly, the PC rule also allows us to identify the scale of spontaneous symmetry breaking with the 1S1C parameters. Noting that the Goldstone fields enter in the Lagrangian only through the Goldstone

matrix $U[\Pi/f]$, we find by comparing with the equation above that

$$m_* = g_* f \ . \tag{55}$$

Having checked that PC remains consistent upon integrating the composite resonances out, it remains to be seen that integrating out the elementary fields does not spoil this consistency. Furthermore, the scalar potential is generated at the loop level by one-particle irreducible (1PI) mixed diagrams where both composite and elementary particles run internally. (Otherwise, the Higgs shift-symmetry would not be broken.)

Since the potential is one term in the one-loop Lagrangian, the prefactor in equation 54 gives us already the correct mass dimensions. Consequently, the presence of an elementary coupling must be balanced by another object with the same dimensions which, in the 1S1C hypothesis, can only be g_*. Therefore, in natural units, the potential takes the following form:

$$V = \frac{N_C m_*^4}{(4\pi)^2} V'\left[\left(\frac{g_e}{g_*}\right)^2 \frac{h^2}{f^2}\right], \tag{56}$$

where we have included the color factor for quarks running in the loops.

4.4 Partial Compositeness

In this section, we describe the hypothesis of partial compositeness, sourcing the main contributions to equation 56. According to this hypothesis, the fermions of the elementary and composite sectors couple linearly [116]:

$$\mathcal{L}_{\text{int}} = \frac{\lambda_{t_L}}{\Lambda_{\text{UV}}^{d_L-\frac{5}{2}}} \overline{q_L} O_F^{t_L} + \frac{\lambda_{t_R}}{\Lambda_{\text{UV}}^{d_R-\frac{5}{2}}} \overline{t_R} O_F^{t_R} \,, \tag{57}$$

where λ_{t_L,t_R} are the unknown UV couplings and the corresponding composite operators O_F have mass dimensions $d_{L,R}$. Furthermore, it is assumed that, above the confining scale, the strong sector approaches a fixed point, such that the Wilson coefficients λ run just because of the different normalizations of the operators in the IR, which are set by m_* rather than the UV cutoff. In this case, the evolution of the coupling is given by [112]:

$$\lambda_t(m_*) = \left(\frac{m_*}{\Lambda_{\text{UV}}}\right)^{d_L-\frac{5}{2}} \lambda_t(\Lambda_{\text{UV}}) \,. \tag{58}$$

Such fixed point can be regarded as a free theory of techniquarks — the new fermions that constitute the Higgs and other composite particles in the model. These techniquarks are not in the strongly-coupled EFT and their interactions emerge in a more fundamental theory $\Lambda_{\text{UV}} \gg m_*$. Given this hierarchy of scales, to reproduce the sizable Yukawa coupling of the top quark, fermionic operators with $d_L \approx 5/2$ are required.

Note that, unlike other hypotheses, there is no risk of reintroducing the HP in partial compositeness[2], since the mass dimensions of the fermionic operators squared are $[\mathcal{O}_F^2] > 4$.

Unlike bilinear interactions to elementary quarks, where the color index could be contracted among the elementary species, partial compositeness implies the existence of colored composite resonances. Hence, the composite symmetry group should be extended to $\mathcal{G} \times SU(3)_C$ (with the color group being considered unbroken).

Furthermore, each elementary quark i can couple to the composite sector through its own set of operators, with $d^i_{L,R} \neq d^j_{L,R}$. According to equation 58, these can lead to different fermion masses at low-energy, even if there is no coupling hierarchy present in the UV. The partial compositeness scenario therefore sheds some light on the flavour puzzle. Nevertheless, the construction of a realist UV theory for CHMs providing these features is challenging and still a work on progress [117].

Once the strong sector confines, each operator $\mathcal{O}_F$ is expected to excite a heavy SM partner from the vacuum with the same quantum numbers as the SM fermion present in the effective interaction. Such composite partners have a Dirac mass before EWSB, so the two chiralities transform equally under the SM gauge group. This feature has important consequences both at the theoretical and experimental levels: being vector-like, their contributions to quantum anomalies are exactly canceled, so the gauge symmetry is not spoiled; furthermore, other (fourth generation) fermions that only gain mass after EWSB have been already excluded by Higgs precision data [118].

For example, an operator coupled to q_L can excite from the vacuum a vector-like quark (VLQ) transforming in the fundamental representations of $SU(2)_L \times SU(3)_C$, $Q \sim (\mathbf{2}_{1/6}, \mathbf{3})$, with the following Lagrangian:

$$\mathcal{L}_Q = (\overline{q_L}\ \overline{Q_L}) \begin{pmatrix} 0 & \lambda_{t_L} f \\ 0 & m_* \end{pmatrix} \begin{pmatrix} q_R \\ Q_R \end{pmatrix} + \text{h.c.} \tag{59}$$

After diagonalizing the mass matrix, we find that the physical states are *partially composite*:

$$\left|q'_L\right\rangle = \cos\theta_L \left|q_L\right\rangle + \sin\theta_L \left|Q_L\right\rangle \ , \ \text{where} \ \sin\theta_L = \frac{\lambda_{t_L}}{g_*} \, . \tag{60}$$

The elementary fermions therefore couple to the composite sector, namely to the Higgs boson, only by mixing with the fermionic resonances Q and T (the latter being the partner of the RH top). Consequently, the Yukawa interactions in CHMs are generated at tree level with strength proportional to the mixing angles,

$$y_t \sim g_* \sin\theta_L \sin\theta_R \approx \frac{1}{g_*} \lambda_{t_L} \lambda_{t_R} \, ; \tag{61}$$

see the left panel of figure 3. In particular, due to its large Yukawa coupling, the top quark is the most composite fermion and thus the main source of explicit symmetry breaking. For completeness, we represent

[2] This would not hold, for instance, in the case of bilinear couplings of the form $\frac{\lambda_t}{\Lambda_{\text{UV}}^{[\mathcal{O}_s]-1}} \overline{q_L} \mathcal{O}_s t_R$, in which the composite operator has the same quantum numbers as the Higgs boson. Even if $[\mathcal{O}_s] = 1+\epsilon$ to reproduce the large top Yukawa coupling, $[\mathcal{O}_s^2] = 2 + \mathcal{O}(\epsilon)$ would reintroduce the HP.

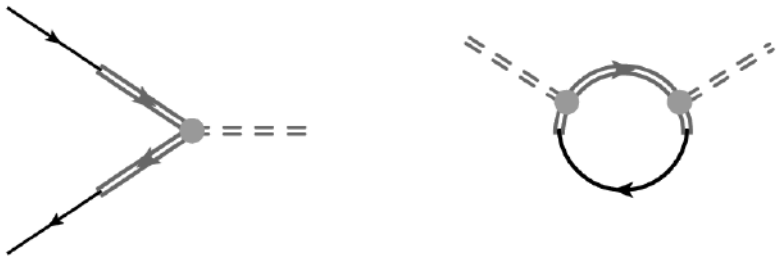

Figure 3: (Left) Generation of the Higgs boson Yukawa interactions in partial compositeness. Double lines represent composite objects: either the vector-like fermions (straight line) or the Higgs boson (dashed line). The gray dot illustrates a strong coupling. (Right) Generation of the NGB Higgs potential at one-loop. The same notation is taken.

in the right panel of the same figure a contribution to the Higgs potential, that is generated analogously but at the loop level.

4.5 The minimal composite Higgs model

Altogether, the previous considerations set the basis to construct the MCHM [93]. It is based on the coset $\mathcal{G}/\mathcal{H} = SO(5)/SO(4)$ which produces exactly four NGBs to be identified with the Higgs doublet $d.o.f.$ (the adjoint representation of $\mathcal{G}$ decomposes as $\mathbf{10} = \mathbf{6} \oplus \mathbf{4}$ under $\mathcal{H}$, the latter being the representation where the broken generators, and thus the NGBs fields, transform). Importantly, $\mathcal{H}$ not only contains $\mathcal{G}_{\text{EW}}$, but also a residual custodial symmetry $SO(4)$. As we explore in the next section, this requirement is necessary to make the model experimentally viable.

4.5.1 Embedding the SM gauge group

Consider an arbitrary field in the fundamental representation of the chiral group, $\Sigma \in (\mathbf{2}, \mathbf{2})$. It transforms as

$$\Sigma \to g_L \cdot \Sigma \cdot g_R^\dagger \,, \tag{62}$$

where g_L and g_R are, respectively, $SU(2)_L$ and $SU(2)_R$ transformations. Adopting the following parameterization

$$\Sigma = \frac{1}{\sqrt{2}} \left(\mathrm{i}\sigma_I \Pi^I + \Pi^4 \right) \,, \tag{63}$$

and using that $\text{Tr}\left[\sigma_I \sigma_J\right] = 2\delta_{IJ}$, we further obtain the trace

$$\text{Tr}[\Sigma^\dagger \Sigma] = |\overrightarrow{\Pi}|^2 \,, \tag{64}$$

which is preserved by the chiral transformations. Hence, the norm of $\overrightarrow{\Pi}$ is identically preserved. Since $SO(4)$ is the most general group of norm-preserving transformations that act on the fourplet, this result

implies that $SO(4) \supset SU(2)_L \times SU(2)_R$. The two groups have in fact the same number of generators and the same algebra, so they are locally isomorphic (see the appendix 2.A in Ref. [112]). The generators of $SO(4)$ can be therefore split into two subsets, $T^a = \{T_L^I,\ T_R^I\}$ $(I = 1, 2, 3)$, that span each of the $SU(2)$ algebras. In this way, we can identify the generators of the SM gauge group $SU(2)_L$ with T_L^α, and choose one of the others, *e.g.* $T_R^3 = e^{i\sigma_3/2}$, as the SM hypercharge generator.

Having figured out the embedding of the SM gauge group, we can study the quantum numbers of the composite fermions that couple to the SM directly. They arise at a scale well above the one at which the explicit breaking of the Goldstone symmetry occurs; therefore, they transform in complete representations of $SO(5)$. For the fundamental and spinorial representations, we have the following decomposition branching rules:

$$\begin{aligned}
\mathbf{5}_{2/3} &\xrightarrow{SU(2)\times SU(2)} (\mathbf{2},\mathbf{2}) \oplus (\mathbf{1},\mathbf{1}) \xrightarrow{\mathcal{G}_{\text{EW}}} \mathbf{2}_{1/2\color{gray}{+2/3}} \oplus \mathbf{2}_{-1/2\color{gray}{+2/3}} \oplus \mathbf{1}_{0\color{gray}{+2/3}}\,; \\
\mathbf{4}_{1/6} &\xrightarrow{SU(2)\times SU(2)} (\mathbf{2},\mathbf{1}) \oplus (\mathbf{1},\mathbf{2}) \xrightarrow{\mathcal{G}_{\text{EW}}} \mathbf{2}_{0\color{gray}{+1/6}} \oplus \mathbf{1}_{1/2\color{gray}{+1/6}} \oplus \mathbf{1}_{-1/2\color{gray}{+1/6}}\,.
\end{aligned}$$

Neither of these cases can therefore account for the quantum numbers of the SM quarks. One solution to this problem is simply extending the global group to $SO(5) \times U(1)_X \to SO(4) \times U(1)_X$. Correspondingly, the hypercharge is redefined as

$$Y = T_R^3 + X\,, \tag{65}$$

leading to the charges in gray in the decomposition rules above. With this extension, we do find the quantum numbers of the fermionic resonances that couple to the q_L and t_R fields. (In particular, the spinorial representation could also accommodate the resonance coupling to b_R.)

On the contrary, the Higgs field is not charged under $U(1)_X$. This is because the $\mathbf{4} = (\mathbf{2},\mathbf{2})$ representation of $SO(4)$ includes already the $\mathbf{2}_{1/2}$. Equivalently, any real fourplet, or chiral bi-doublet, can be rewritten in terms of a complex doublet with the same quantum numbers as the Higgs boson[3]:

$$\Sigma = \left(\widetilde{H},\ H\right)\,. \tag{66}$$

After EWSB and in the unitary gauge,

$$\Sigma \to \frac{v}{\sqrt{2}}\mathbb{1}\,, \tag{67}$$

which is preserved by transformations in the vector subgroup, with $g_L = g_R \equiv g_V$. This corresponds to the custodial symmetry $SU(2)_V \approx SO(3)_C$.

The important remark to make is that the couplings of the W boson do not break this symmetry, since it transforms as a triplet of $SO(3)_C$. This can be seen by setting $g_1 \to 0$ in the mass Lagrangian,

$$\mathcal{L}_{W^2} = f^2 A(\xi)\left[g_2^2\left(W_\mu^1\right)^2 + g_2^2\left(W_\mu^2\right)^2 + \left(g_2 W_\mu^3 - g_1 B_\mu\right)^2\right]; \tag{68}$$

[3]Note that the transformation in equation 62 leads to $H \leftrightarrow \widetilde{H}$, matching the expected transformation in $\mathcal{G}_{\text{EW}}$.

the compositeness function $A(\xi)$ is determined later on, in equation 75. Rotating to the physical basis,

$$\mathcal{L}_{W^2} = f^2 A'(\xi) g_2^2 \left[|W|^2 + \frac{1}{2c_\omega^2} Z^2 \right] . \tag{69}$$

Custodial symmetry therefore requires that $m_W^2/m_Z^2 = 1$. Turning on the hypercharge interactions, we obtain $\rho = 1$ exactly, at tree level, in the MCHM.

The choice of an unbroken group $\mathcal{H} \supset SO(3)_C$ is therefore of extreme importance to make the model compatible with electroweak precision data (EWPD) constraints. As a counterexample, working out the $SU(3) \to SU(2) \times U(1)$ breaking pattern, which gives rise to the same number of NGB fields, we obtain $\rho = 1 + \xi + \mathcal{O}(\xi^2)$. The precise measurement of this parameter sets a lower bound on $f \gtrsim 10$ TeV, which results in a large fine-tuning in the theory of the order of $\Delta \gtrsim 10^3$.

4.5.2 Scalar interactions

We use the following representation for the $SO(5)$ generators:

$$\begin{aligned} T^{mn}_{ij} &= -\frac{\mathrm{i}}{\sqrt{2}} \left(\delta^m_i \delta^n_j - \delta^n_i \delta^m_j \right) , \quad m < n \in [1,4] ; \\ X^{m5}_{ij} &= -\frac{\mathrm{i}}{\sqrt{2}} \left(\delta^m_i \delta^5_j - \delta^5_i \delta^m_j \right) , \quad m \in [1,4] . \end{aligned} \tag{70}$$

According to the discussion of the last section, we identify the generators of $\mathcal{G}_{\text{EW}}$ with

$$T^1_L = \frac{1}{\sqrt{2}}(T^{14} + T^{23}) , \quad T^2_L = \frac{1}{\sqrt{2}}(T^{24} - T^{13}) , \quad T^3_L = \frac{1}{\sqrt{2}}(T^{12} + T^{34}) \tag{71}$$

and

$$T^3_R = \frac{1}{\sqrt{2}}(T^{12} - T^{34}) . \tag{72}$$

In the unitary gauge, it is always possible to align the physical Higgs field along X^{35}, so that the Goldstone matrix reads:

$$U = e^{-\mathrm{i}\sqrt{2}\frac{h}{f}X^{45}} = \begin{pmatrix} 1 & 0 & 0 & 0 & 0 \\ 0 & 1 & 0 & 0 & 0 \\ 0 & 0 & \cos\frac{h}{f} & 0 & -\sin\frac{h}{f} \\ 0 & 0 & 0 & 1 & 0 \\ 0 & 0 & \sin\frac{h}{f} & 0 & \cos\frac{h}{f} \end{pmatrix} . \tag{73}$$

Using this parameterization in equation 51, we obtain the kinetic interactions:

$$\begin{aligned} \mathcal{L}_{\text{kin}} &= \frac{f^2}{4} \text{Tr} \left[(U^\dagger D_\mu U)_X (U^\dagger D^\mu U)^\dagger_X \right] + \mathcal{O}(\partial^4) \\ &= \frac{1}{2} (\partial_\mu h)^2 + \frac{f^2}{8} \sin^2 \frac{h}{f} \left[g_2^2 \left(W^1_\mu \right)^2 + g_2^2 \left(W^2_\mu \right)^2 + \left(g_2 W^3_\mu - g_1 B_\mu \right)^2 \right] , \end{aligned} \tag{74}$$

where the notation $()_X$ refers to the projection along the broken generators. After EWSB, this Lagrangian becomes

$$\mathcal{L}_{\text{kin}} = \frac{1}{2}\left(\partial_\mu h\right)^2 + \frac{f^2}{4}\sin^2\frac{h+V}{f} g_2^2 \left[W_\mu^+ W_\mu^- + \frac{1}{2c_\omega^2} Z_\mu^2\right]. \tag{75}$$

It is apparent that in the absence of gauge interactions the VEV produces no effect. In this shift-symmetry preserving limit, we only obtain the kinetic term for the Higgs, with no source to generate its mass. Otherwise, the gauge fields also develop a mass, given by

$$m_W \sim g f \sin\frac{V}{f} \equiv g v\,, \tag{76}$$

to make the analogy with the SM. The argument of the sine is thus the misalignment angle; see figure 2. Expanding around $h = 0$ in the vector mass term, we can check that the composite Higgs corrections are indeed all $O(\xi)$:

$$\mathcal{L}_{\text{kin}} \supset \frac{g_2^2}{4} v^2 \left(1 + 2k_V \frac{h}{v} + c_V \frac{h^2}{v^2} + \dots\right)\left[W_\mu^+ W_\mu^- + \frac{1}{2c_\omega^2} Z_\mu^2\right], \tag{77}$$

where

$$k_V \equiv \frac{g^{\text{CH}}_{VVh}}{g^{\text{SM}}_{VVh}} = \sqrt{1-\xi} \quad \text{and} \quad c_V = (1-2\xi)\,. \tag{78}$$

The composite nature is encoded in these multiplication factors, which are equal to 1 in the SM; check equation 10.

Let us now compute the Yukawa interactions, by embedding the SM fields in equation 57 into fiveplets of $SO(5)$:

$$\mathcal{L}_{\text{int}} = \lambda_{t_L} \overline{Q^i_{t_L}} O^{t_L}_{Fi} + \lambda_{t_R} \overline{T_R}^i O^{t_R}_{Fi}\,, \tag{79}$$

where

$$Q_L = \frac{1}{\sqrt{2}}\left(b_L,\ -\mathrm{i}b_L,\ t_L,\ \mathrm{i}t_L,\ 0\right)^T \quad \text{and} \quad T_R = \frac{1}{\sqrt{2}}\left(0,\ 0,\ 0,\ 0,\ t_R\right)^T. \tag{80}$$

Since not all components in the embeddings above transform under the global group, the linear interaction with O_F breaks explicitly the global symmetry. However, in order to calculate an amplitude with several SM fermions and Higgs fields, we can uplift Q and T to spurions that transform fully in the $\mathcal{G}$-group, that is

$$Q \to g \cdot Q \quad \text{and} \quad T \to g \cdot T\,, \tag{81}$$

and use their physical values only after the computation (assuming that the original spurions take some VEV). To employ the CCWZ method, we then dress these spurions with the Goldstone matrix:

$$Q_{L,D} \equiv U^{-1} Q_L \to h \cdot U^{-1} \cdot g^{-1} \cdot g \cdot Q_{t_L} = h \cdot \left(U^{-1} Q_{t_L}\right), \tag{82}$$

so that an index transforming with g is turned into one transforming with h. In this way, we can form $\mathcal{H}$-invariants by simply contracting the objects in equation 82.

With that aim, it is useful to decompose the dressed spurions into components that transform in irreducible representations of $SO(4)$:

$$U^{-1}Q_L = \begin{bmatrix} Q^{\mathbf{4}}_{L,D} \\ Q^{\mathbf{1}}_{L,D} \end{bmatrix} . \tag{83}$$

To compute the Yukawa interactions, two invariants could be build *a priori* by contracting the singlet in this vector with the other from T_R ($\mathbf{1}_L \times \mathbf{1}_R$), as well as the fourplets ($\mathbf{4}_L \times \mathbf{4}_R$). However, the two are not independent, since their combination gives a full $SO(5)$ singlet [112]. At zero order in derivatives, the generalized Yukawa Lagrangian of two fermions and several Higgs fields is therefore:

$$\begin{aligned} \mathcal{L}^t_{\text{yuk}} &= -c_t \frac{\lambda_{t_L}\lambda_{t_R}}{g_*^2} m_* \overline{Q^{\mathbf{1}}_{L,D}} T^{\mathbf{1}}_{R,D} + \text{h.c.} \\ &= -c_t \frac{\lambda_{t_L}\lambda_{t_R}}{g_*^2} m_* \frac{1}{2\sqrt{2}} \sin\left[\frac{2h}{f}\right] \overline{t_L} t_R + \text{h.c.}\,, \end{aligned} \tag{84}$$

where the coefficient shows the source of each field and is determined by PC, and $c_t \sim \mathcal{O}(1)$ is an unknown UV coefficient. After the Higgs takes a VEV, we can subsequently identify the top quark mass as

$$m_t = c^t \frac{\lambda_{t_L}\lambda_{t_R}}{g_*^2} m_* \frac{\sqrt{\xi(1-\xi)}}{\sqrt{2}} . \tag{85}$$

Writing the Lagrangian in terms of this parameter and expanding around $h = 0$, we obtain:

$$\mathcal{L}^t_{\text{yuk}} = -m_t \overline{t_L} t_R \left[1 + k_t \frac{h}{v} + c_2 \frac{h^2}{v^2} + \dots\right], \tag{86}$$

where

$$k_t^5 \equiv \frac{g^{\text{CH}}_{htt}}{g^{\text{SM}}_{htt}} = \frac{1-2\xi}{\sqrt{1-\xi}} \quad \text{and} \quad c_2^5 = -2\xi\,, \tag{87}$$

the superscript denoting the $SO(5)$ representation where the SM fermions are embedded. The interactions with the lighter fermions are obtained analogously.

The dressed spurions can be similarly employed in the CCWZ construction of the potential; we just have to factorize out the SM fermions to obtain constant spurion fields, Λ_R and $(\Lambda_L)^I$, where $I = t, b$ originates from the unfolding of Q_L in equation 80. As the spurions of the SM fermions are accompanied by the mixing coefficients $\lambda_{L,R}$, the latter can take the role of an expansion parameter in this analysis. At leading order (LO), two $\mathcal{H}$-invariant terms can be built, such that

$$\begin{aligned} V^{\mathbf{5}\oplus\mathbf{5}}(h) &= \lambda_L^2 f^4 \left(\Lambda^{\mathbf{1}*}_{L,D}\right)^I \left(\Lambda^{\mathbf{1}}_{L,D}\right)_I + \lambda_R^2 f^4 \left(\Lambda^{\mathbf{1}*}_{R,D}\right)\left(\Lambda^{\mathbf{1}}_{R,D}\right) \\ &= c_1 f^4 \sin^2\left[\frac{h}{f}\right] + c_2 f^4 \cos^2\left[\frac{h}{f}\right] . \end{aligned} \tag{88}$$

Therefore, the potential in the fundamental representation cannot account for EWSB; to realize it, NLO terms are mandatory.

If, instead, we embed the SM fermions in larger representations of the global group, EWSB can be successfully described. For example, let us assume that the LH top transforms in the symmetric representation, while the RH top is a full singlet of the global group, that is $\overline{q_L} \oplus t_R = \mathbf{14} \oplus \mathbf{1}$. In this case:

$$Q_L = \frac{1}{2}\begin{pmatrix} 0_{4\times 4} & \mathbf{v}^T \\ \mathbf{v} & 0 \end{pmatrix}, \tag{89}$$

where $\mathbf{v} = (\mathrm{i}b_L, b_L, \mathrm{i}t_L, -t_L)$. Note that the $\mathbf{14} = \mathbf{9} \oplus \mathbf{4} \oplus \mathbf{1}$ under the unbroken group, so there are now two independent LH invariants arising in the potential:

$$\begin{aligned} V^{\mathbf{14}\oplus\mathbf{1}}(h) &= \lambda_L^{(1)^2} f^4 \left[\left(\Lambda^{*\mathbf{1}}_{L,D}\right)^I \left(\Lambda^{\mathbf{1}}_{L,D}\right)_I \right] + \lambda_L^{(2)^2} f^4 \left[\left(\Lambda^{\mathbf{4}*}_{L,D}\right)^I_m \left(\Lambda^{\mathbf{4}}_{L,D}\right)^m_I \right] \\ &= c_1 f^4 \sin^2\left[\frac{h}{f}\right] + c_2 f^4 \sin^4\left[\frac{h}{f}\right], \end{aligned} \tag{90}$$

where m sums over the generators transforming in the representation $\mathbf{4}$. In this case, EWSB can indeed be achieved at LO. In particular, the two unknown constants in the potential can be traded by two EW parameters, such as the Higgs mass and its VEV.

4.5.3 Heavy fermion interactions

In the previous sections, we have showed how the linear coupling between heavy-light fermions triggers the Higgs potential and Yukawa interactions, and how the choice for the embeddings of the SM fermions determines their structure. This choice has important consequences too for the VLQ phenomenology; it determines, in particular, which composite resonances are expected to be the lightest and their branching ratios.

To see an example, we focus on a multiplet of VLQs transforming in the representation $\mathbf{5}_{X=2/3}$ of $SO(5)$,

$$\Psi = \frac{1}{\sqrt{2}}\left(B - X_{5/3},\ -\mathrm{i}(B + X_{5/3}),\ T + \mathrm{i}X_{2/3},\ X_{2/3} + \mathrm{i}T,\ \sqrt{2}\widetilde{T}\right)^T \equiv \left(\Psi_{\mathbf{4}},\ \Psi_{\mathbf{1}}\right)^T, \tag{91}$$

which contains two $SU(2)_L$ doublets, $Q = (T, B)^T$ and $X = (X_{5/3},\ X_{2/3})^T$, plus a singlet $\widetilde{T}$. Since Q and $\widetilde{T}$ have the same quantum numbers as the SM quarks (see table 3), they naturally mix. The complete Lagrangian of the fermion sector is therefore

$$\begin{aligned} \mathcal{L}_\Psi = {} & \mathrm{i}\overline{\Psi}\not{D}\Psi + \mathrm{i}\bar{q}_L\not{D}q_L + \mathrm{i}\bar{t}_R\not{D}t_R - \left[M_\Psi \overline{\Psi}_L \Psi_R + y_\Psi f \left(\overline{\Psi}_L \Sigma\right)\left(\Sigma^T \Psi_R\right) + \text{h.c.}\right] \\ & - \lambda_L \overline{Q}_L \Psi_R - \lambda_R \overline{\Psi}_L T_R + \text{h.c.}\,, \end{aligned} \tag{92}$$

Ψ_i	T_L^3	T_R^3	Y	Q
$X_{5/3}$	$\frac{1}{2}$	$\frac{1}{2}$	$\frac{7}{6}$	$\frac{5}{3}$
$X_{2/3}$	$-\frac{1}{2}$	$\frac{1}{2}$	$\frac{7}{6}$	$\frac{2}{3}$
T	$\frac{1}{2}$	$-\frac{1}{2}$	$\frac{1}{6}$	$\frac{2}{3}$
B	$-\frac{1}{2}$	$-\frac{1}{2}$	$\frac{1}{6}$	$-\frac{1}{3}$
$\widetilde{T}$	0	0	$\frac{2}{6}$	$\frac{2}{3}$

Table 3: The SM quantum numbers of the fields in the Ψ-multiplet defined in equation 91. The explicit expressions of the $SU(2)$ generators are written in equations 71 and 72. The third and forth columns refer to the generalized hyper- and electric charges.

where the first line includes the proto-Yukawa interactions of the VLQs with the NGBs, which arise in the composite sector. Equivalently, we can make a field redefinition $\Psi_{L,R} \to U\Psi_{L,R}$, so that the VLQ interactions become:

$$\begin{aligned}\mathcal{L}_\Psi \to\ & \mathrm{i}\overline{\Psi}\left(\not{D} - \mathrm{i}\gamma^\mu e_\mu\right)\Psi - \left[M_\Psi \overline{\Psi}_L \Psi_R + y_\Psi f \left(\overline{\Psi}_L \Sigma_0\right)\left(\Sigma_0^T \Psi_R\right) + \text{h.c.}\right] \\ & - \lambda_L \overline{Q}_L U \Psi_R - \lambda_R \overline{\Psi}_L U^\dagger T_R + \text{h.c.}\end{aligned} \tag{93}$$

Such Lagrangian is more commonly found in the literature [119]. Here, the pNGB nature of the Higgs boson is explicit: for $\lambda_{L,R} = 0$, the latter has only derivative interactions with the VLQs (encoded in the first term).

The mass terms in this Lagrangian become diagonal after rotating the LH and the RH fields:

$$q_L \to c_L q_L + s_L Q_L \quad \text{and} \quad Q_L \to -s_L q_L + c_L Q_L\,; \tag{94}$$

$$t_R \to c_R t_R + s_R \widetilde{T}_R \quad \text{and} \quad \widetilde{T}_R \to -s_R t_R + c_R \widetilde{T}_R\,, \tag{95}$$

with $\tan\phi_{t_L} \equiv s_L/c_L = \lambda_L/M_\Psi$ and $\tan\phi_{t_R} \equiv s_R/c_R = \lambda_R/(M_\Psi + f y_\Psi)$. Accordingly, the VLQ physical masses in the unbroken phase read:

$$m_Q = \frac{m_X}{c_L}, \quad m_X = M_\Psi \quad \text{and} \quad m_{\widetilde{T}} = \frac{M_\Psi + f y_\Psi}{c_R}\,, \tag{96}$$

while the SM top remains massless. In this representation, the exotic doublet is therefore expected to be lighter than Q. After EWSB, all these parameters get corrections of $\mathcal{O}(\sqrt{\xi})$; in particular, the components in the EW doublets get split, but not sufficiently to decay into one another plus a SM boson.

To depict the top partner phenomenology at energies $E \gg v$, we can make use of the Equivalence Theorem [120]. The longitudinal components of the $W^\pm$ and Z bosons are then well approximated by the NGBs in the Higgs doublet. (On the other hand, the interactions with their transverse components can be

typically neglected [121]. They are determined by the covariant derivative, hence they are suppressed by the gauge coupling $g \ll y_\Psi$. Furthermore, such interactions are flavour-diagonal, so they cannot mediate flavour-changing interactions at zero order in ξ.) Computing the proto-Yukawa interaction in equation 92, with[4]

$$\Sigma = \left(\frac{h^+ + h^-}{\sqrt{2}f},\ \mathrm{i}\frac{h^+ - h^-}{\sqrt{2}f},\ \frac{h}{f},\ \frac{h_0}{f},\ 1 \right)^T , \tag{97}$$

we can therefore obtain the physical top partner couplings to a SM fermion and a SM boson:

$$\begin{aligned} \mathcal{L}_\Psi \supset\ & \frac{y_\Psi}{\sqrt{2}} c_L s_R \overline{T}_L (h - \mathrm{i}h_0) t_R + y_\Psi c_L s_R \overline{B}_L h^- t_R \\ & - \frac{y_\Psi}{\sqrt{2}} s_R \overline{X_{2/3}}_L (\mathrm{i}h - h_0) t_R - y_\Psi s_R \overline{X_{5/3}}_L h^+ t_R \\ & + y_\Psi s_L c_R \overline{\widetilde{T}}_R \left[\frac{1}{\sqrt{2}} (h + \mathrm{i}h_0) t_L + h^+ b_L \right] + \text{h.c.} \end{aligned} \tag{98}$$

The corresponding branching ratios are:

$$\mathcal{B}(T \to ht) = \mathcal{B}(T \to Zt) = 0.5\,; \quad \mathcal{B}(B \to Wt) = 1.0\,; \tag{99}$$

$$\mathcal{B}(X_{5/3} \to Wb) = 1.0\,; \quad \mathcal{B}(X_{2/3} \to ht) = \mathcal{B}(X_{2/3} \to Zt) = 0.5\,; \tag{100}$$

$$\mathcal{B}(\widetilde{T} \to ht) = \mathcal{B}(\widetilde{T} \to Zt) = \frac{1}{2}\mathcal{B}(\widetilde{T} \to Wb) = 0.5\,, \tag{101}$$

in agreement with Refs. [112, 122].

4.5.4 Heavy vector interactions

As in the case of fermions, the interaction in equation 38 implies that the elementary and composite vector bosons mix and therefore the physical states are partially composite; the SM gauge bosons being identified with the massless eigenstates. Since each elementary gauge boson mixes with a composite resonance, we expect a set of spin-1 resonances transforming in the adjoint representation of the global group:

$$\mathbf{10} \xrightarrow{SU(2)\times SU(2)} (\mathbf{3},\ \mathbf{1}) \oplus (\mathbf{1},\ \mathbf{3}) \oplus (\mathbf{2},\ \mathbf{2})\,. \tag{102}$$

Furthermore, a singlet vector resonance associated with the $U(1)_X$ symmetry, as well as new heavy gluons, are expected to be part of the composite spectrum. These cannot couple directly to the NGBs, since they are not charged under $SO(4)$.

To learn the phenomenological implications, let us focus on a vector field in the $(\mathbf{3},\ \mathbf{1})$ representation and with zero hypercharge, $\rho^\mu \equiv \rho^\mu_a T^a_L$. PC dictates that this vector has a mass $m_\rho \sim m_*$, as well as the overall strength of the operators in the relevant Lagrangian

$$\mathcal{L}_\rho = -\frac{1}{4}\rho^a_{\mu\nu}\rho^{a\mu\nu} + \frac{1}{2}\frac{m_*^2}{g_*^2}\left(g_*\rho^\mu - g_e W_e^\mu\right) + |D_\mu H|^2 + \overline{Q}_L \left(\mathrm{i}\not{\partial} + g_*\not{\rho} - M_Q\right) Q_L\,, \tag{103}$$

[4] With a slight abuse of notation, we identify $h_0 = h + \mathrm{i}h_0$, h being the physical Higgs particle.

where $\rho^a_{\mu\nu} = \partial_\mu \rho^a_\nu - \partial_\nu \rho^a_\mu + \epsilon^{abc} \rho^b_\mu \rho^c_\nu$ and $D_\mu H = \left(\partial_\mu - \mathrm{i} g_* \rho_\mu + \dots\right) H$. As before, this Lagrangian can alternatively be set by employing the e_μ symbol [112]:

$$\mathcal{L}_\rho = -\frac{1}{4}\rho^a_{\mu\nu}\rho^{a\mu\nu} + \frac{m_*^2}{2g_*^2}\left(g_*\rho^a_\mu - e^a_\mu\right)^2 + \overline{\Psi}_{\mathbf{4}}\gamma^\mu\left(g_*\rho^a_\mu - e^a_\mu\right)T^a_L\Psi_{\mathbf{4}}\,, \tag{104}$$

where $\Psi_{\mathbf{4}}$ is made out of the first four components in equation 91. Note that the combination $(g_*\rho_\mu - e_\mu)$ appears as one single field, since both vectors transform exactly in the same way; see equation 49. Given that $e_\mu \equiv \mathrm{Tr}[\omega_\mu \cdot X^a] \approx \mathrm{Tr}[\mathrm{i}D_\mu \mathbb{1} \cdot X^a]$, the mass term induces the mixing that is explicitly shown in equation 104.

The physical vector states are found by rotating $\rho^\mu \to c_\theta \rho^\mu + s_\theta W_e^\mu$ and $W_e^\mu \to -s_\theta \rho^\mu + c_\theta W_e^\mu$. After diagonalizing both bosonic and fermionic interactions, the Lagrangian takes the following form:

$$\begin{aligned}\mathcal{L}_\rho \supset & \frac{1}{2}\frac{m_*^2}{c_\theta^2}\rho_\mu\rho^\mu - g_2\cot\theta\,\rho_\mu H^\dagger \mathrm{i}\overleftrightarrow{\partial^\mu} H + \overline{Q}\left(\mathrm{i}\not{\partial} - \frac{M_Q}{c_L}\right)Q - g_2\left[\overline{q_L}\left(\frac{s_L c_L}{s_\theta c_\theta}\right)\not{\rho} Q_L + \mathrm{h.c.}\right] \\ & - g_2\left[\overline{q_L}\left(s_L^2\cot\theta - c_L^2\tan\theta\right)\not{\rho} q_L + \overline{Q_L}\left(c_L^2\cot\theta - s_L^2\tan\theta\right)\not{\rho} Q_L + \mathrm{h.c.}\right] + \dots\,,\end{aligned} \tag{105}$$

where

$$\tan\theta = \frac{g_e}{g_*}\,, \quad g_2 = g_e c_\theta = g_* s_\theta\,, \tag{106}$$

and s_L, c_L are the mixing angles obtained after equations 94-95. Similar results can be derived for other fermions.

In the expected limit $g_* \gg g_e$, the mixing between the composite and elementary vectors is small; hence, $\cot\theta$ is large. Since the largest $\tan\phi_{t_L}$ corresponds to the heaviest fermions, we can draw the following conclusions: *(1)* the exotic vector coupling to first generation fermions is $g_{uu} \sim g_2\tan\theta \sim g_e^2/g_*$, which is suppressed by a factor of g_e/g_* relatively to the coupling of an elementary ρ; *(2)* the coupling to quarks of the third generation is in turn large, $g_{tt} \sim g_2\cot\theta s_L^2 = g_* s_L^2$; *(3)* the coupling to the Higgs (and similarly to the gauge bosons, by virtue of the Equivalence Theorem) is identically large, $g_{hh} \sim g_2 g_*/g_e \sim g_*$.

Concerning point *(3)*, plugging all the Higgs doublet $d.o.f.$ in the Goldstone matrix, and trading for the charged vector components, $\rho^1 = (\rho^+ + \rho^-)/\sqrt{2}$, $\rho^- = \mathrm{i}(\rho^- - \rho^+)/\sqrt{2}$ and $\rho^0 = \rho^3$, we explicitly obtain:

$$\mathcal{L}_{\rho,h,W,Z} = g\cot\theta\,\rho^0_\mu\left[W_L^+\mathrm{i}\overleftrightarrow{\partial^\mu}W_L^- - h\partial^\mu Z_L + Z_L\partial^\mu h\right] + g\cot\theta\,\rho^+_\mu\left(h - \mathrm{i}Z_L\right)\mathrm{i}\overleftrightarrow{\partial^\mu}W_L^- + \mathrm{h.c.} \tag{107}$$

Therefore, ρ^0 decays mostly into W^+W^-, Zh and $t\bar{t}$; while the charged component has the largest branching fractions into $t\bar{b}$, ZW^+ and hW^+ (or the conjugated) final states. These conclusions agree with Ref. [112].

4.6 Experimental constraints

Having studied the predictions of the MCHM, we dedicate this section to discuss how they are constrained by experiment.

4.6.1 Collider phenomenology

4.6.1.1 Higgs couplings

The pNGB nature of the Higgs boson modifies its couplings to the SM, as we have found in equations 78 and 87. In particular, the Higgs couplings to the gauge bosons, arising from the CCWZ kinetic term, are generic to all CHMs (with the same coset structure) and the corresponding bound on k_V is therefore universal. The latter is directly constrained by measurements of the Higgs production cross section; for example, the following vector boson fusion channel $pp \to qqH,\ H \to VV^*$ is sensitive to k_V^4.

Contrarily, the corrections to the Higgs Yukawa couplings depend on the $\mathcal{G}$-representation under which the SM fermions transform. We have found that, if $q_L \oplus t_R = \mathbf{5} \oplus \mathbf{5}$, then $k_t^5 \approx 1 - 3\xi/2 \equiv k_F^A$. However, if *e.g.* $q_L \oplus t_R = \mathbf{10} \oplus \mathbf{5}$ instead, we obtain $k_t^{10} = \sqrt{1-\xi} \approx 1 - \xi/2 \equiv k_F^B$. The couplings to lighter fermions are generated in a complete analogous way and, in full generality, the SM fermions can be embedded into different multiplets of the global group. Consequently, the bounds on k_F can, with enough precision, flavour some CHMs over others.

Furthermore, composite couplings to gluons k_g and photons k_γ can be induced at loop level as a function of $(k_t,\ k_b,\ k_V)$. Therefore, LHC searches sensitive to these couplings, such as $pp \to Htt$, $H \to \gamma\gamma$, can be also used to constrain the CHM.

Taking the structures of the Higgs couplings from different CHMs into account, Ref. [123] performed a global fit to the Run 1 (at $\sqrt{s} = 7$ and 8 TeV) and Run 2 (at $\sqrt{s} = 13$ TeV) LHC data released by the ATLAS and CMS collaborations. The most constrained model is the one with $k_t = k_F^A$ and $k_b = k_\tau = k_F^B$. The combined analysis sets an upper bound on $\xi \lesssim 0.17$ at the 95% CL (an improvement of around 30% relatively to Run 1 results). This corresponds to a lower bound on the new physics scale of around $f \gtrsim 600$ GeV.

4.6.1.2 Vector-like quarks

On top of these effects, CHMs predict a large spectrum of new particles around the TeV scale. In particular, the vector-like fermions have a determinant role if they are pushed by experiment to very large scales, the pNGB Higgs cannot get a natural mass.

The VLQs can be pair or singly produced in pp collisions. Most searches up to date have, however, focused on pair-production of top partners, since the dominant (QCD) contribution is model-independent, as well as decays into third generation quarks. Regarding this last assumption, it should be noted that,

as the largest mixings $s_L \sim \lambda_L/M$ correspond to the heaviest SM quarks in partial compositeness, their partners are indeed expected to be the lightest. Moreover, the experimental analyses typically assume that the VLQ branching ratios into the SM bosons all add to one, which makes different searches [124–128] complementary to one another.

To discuss an example, we focus on the $Ht + X$ topology, namely the search presented in Ref. [125], where the $H \to \bar{b}b$ channel is explored. The final state is expected to comprise at least a boosted isolated lepton (from a W decay) or large MET (from non-reconstructed leptons or the decay of a Z) , plus multiple jets. This search is therefore also sensitive to $T\overline{T} \to Zt+X$, $Z \to \bar{\nu}\nu$. Only events passing a single-lepton or MET trigger are considered. Among the most important cuts in the 1- (0-)lepton channel, at least 5 (6) jets are required, among which at least 2 must be b-tagged, and the MET is required to be $E_T^{\text{miss}} > 20\ (200)$ GeV. After this selection, the effective mass of the total system is used as discriminating variable between signal and background (mostly from $\bar{t}t$+jets production), to set exclusion limits. Using 36.1 fb^{-1} of data at $\sqrt{s} = 13$ TeV, VLQ masses below 1.43 TeV and 1.17 TeV have been excluded at the 95% CL assuming that $\mathcal{B}(T \to Ht) = 1$ and $\mathcal{B}(T \to Zt) = 1$, respectively. If the assumption is made, instead, on the weak-isospin nature of the top partner, these limits are at $1.31\ (1.19)$ TeV for doublets (singlets).

Recently, the ATLAS collaboration has presented a combined analysis of VLQ searches in different final states [129], being able to exclude slightly larger masses, $m_T \lesssim 1.37\ (1.31)$ TeV, for a weak doublet (singlet) top partner. In comparison, masses $m_B \gtrsim 1.22$ TeV are allowed for a singlet bottom partner. By naively rescaling these limits with the luminosity, we can expect that in the next high luminosity (HL)-phase of the LHC, with a collected luminosity of 3 ab^{-1}, masses as large as ~ 4 TeV could be probed.

For such large values of the mass, pair-production of top partners becomes however phase space suppressed and single-production through the EW interaction starts dominating. This brings the additional complication of the VLQ couplings to EW gauge bosons being dependent on the mixing angles and subject to indirect constraints.

The singly produced top partner typically yields cleaner topologies, characterized by the presence of one large-R jet, J, and at least one forward jet [130–136]. As an example, the monotop analysis presented in Ref. [133] constrains top partners that decay into Zt, with $Z \to \bar{\nu}\nu$. Among the most important selection cuts, it is required that the $p_T(J) > 250$ GeV and $E_T^{\text{miss}} > 200$ GeV; the presence of at least one b-tagged jet; and that $\Delta\Phi(E_T^{\text{miss}},\ J) > \pi/2$, since signal events are likely to be produced back-to-back. The transverse mass $m_T(E_T^{\text{miss}},\ J)$ is finally used as the discriminating variable between signal and background (mostly from $\bar{t}t$ production). The 95% CL lower limit on the top partner mass, obtained with a collected luminosity of 36.1 fb^{-1}, is ~ 1.5 TeV for mixing angles $s_L \gtrsim 0.5$.

4.6.1.3 Vector-like leptons

Direct searches for vector-like leptons (VLLs) have been carried out too at the LHC [137–141], mostly in pair-production and assuming VLL decays into SM gauge bosons only. (A recast of current searches to

probe decays into an exotic stable particle is presented in Ref. [142].) In comparison to the case of VLQs, the smaller production cross section of the VLLs, mostly via Drell-Yann, makes the sensitivity reach of the experimental analyses quite limited.

For example, Ref. [139] presented a search for multi-lepton signals of a VLL $E \longrightarrow Z\ell$ at $\sqrt{s} = 8$ TeV. Among the most important selection cuts, two opposite sign same flavour leptons are required to reconstruct a Z boson, as well as a third one to be found within an angular separation $\Delta R < 3$ relatively to the Z boson candidate. Several signal regions are defined regarding the presence of additional leptons and di-jet pairs. The mass difference $\Delta m \equiv m_{3\ell} - m_{\ell^+\ell^-}$, obtained by subtracting the invariant mass of the two leptons that reconstruct the Z from the trilepton invariant mass, is used as the discriminating variable between the signal and the dominant backgrounds (ZZ and WZ) to set upper limits on the VLL mass. Using 20.3 fb^{-1} of data, VLL masses below $\lesssim 170$ GeV (in either the muon or the electron channels) are correspondingly excluded, assuming the branching ratios of an EW singlet.

On the other hand, VLLs charged under $SU(2)$ have a larger production cross section and are in turn subject to more stringent bounds. In the case of a doublet, the search presented in Ref. [140] at $\sqrt{s} = 13$ TeV and using 77.4 fb^{-1} of data excludes VLL masses below ~ 790 GeV at the 95% CL, considering couplings to third generation leptons only.

4.6.1.4 Vector resonances

Among the spin-1 resonances, EW singlet states V with sizable couplings to the SM leptons are specially motivated since they can explain the apparent anomalies observed in lepton flavour universality (LFU) tests; we discuss this later on, in section 5.3.2. As these vectors have a small coupling to the lightest quarks (see equation 105), Drell-Yann production is very suppressed, being mostly triggered by b quarks. This coupling is, moreover, strongly constrained by $B^0 - \overline{B}^0$ mixing, implying that $g_{qq} \lesssim \mathcal{O}(0.05)$ for $m_V < 6$ TeV [143].

Such V can subsequently decay into the SM leptons. Ref. [106] recast the ATLAS search based on 36.1 fb^{-1} of $\sqrt{s} = 13$ TeV data presented in Ref. [144] which, although sensitive to this scenario, was designed to probe SUSY models. The authors show that vector masses $m_V \lesssim 1.8$ TeV are excluded at the 95% CL in the muon channel. However, when kinematically allowed, the composite V can also decay into ℓE, the corresponding decay width being a factor of g_e/g_* larger than $\Gamma(V \longrightarrow \ell\ell)$. In such case, the aforementioned limit gets reduced by $\sim 30\%$. Therefore, in Ref. [106], a new dedicated analysis is proposed to test this composite channel which could reach $m_V \sim 3$ TeV at the HL-LHC.

Other uncolored resonances, such as the EW triplet considered in equation 107, can couple directly to the Higgs and to the longitudinal components of the gauge bosons. Since all these particles are composite, these channels easily dominate the vector decay width. Furthermore, vector boson fusion processes could potentially dominate the production cross section of the vector triplets, as well; they are however suppressed by the EW gauge couplings that arise along with the virtual gauge bosons. The production cross section of

the EW resonances at pp colliders is therefore small. The most stringent limits are, as expected, obtained in channels involving the SM gauge bosons and exclude $m_\rho \lesssim 3.7$ TeV at the 95% CL, using $\sqrt{s} = 13$ TeV LHC data and a luminosity of 137 fb^{-1} [145].

Finally, let us also comment the prospects regarding gluon partners, whose production cross section is mediated by the strong, rather than the weak, coupling and can therefore give rise to significant effects at colliders. The current lower bounds from LHC searches using Run 1 data on the mass of these resonances lie close to 2–3 TeV [146–151]. No dedicated search up to date has however probed the composite gluon in final states with top partners. In Ref. [152], the authors study the implications of this decay on heavy gluon searches, by recasting the ATLAS results presented in Ref. [151] and exploring the reach of the corresponding analysis at $\sqrt{s} = 14$ TeV. The authors find that the expected upper limits on the mass of the composite gluon, ~ 6 TeV in the absence of decays into top partners and for a luminosity of 300 fb^{-1}, could be weakened by more than 1 TeV if such decays are instead prominent. Similar prospects assuming a broader decay width of the composite gluon are discussed in Ref. [153]. The complementary approach, that is, the implications of heavy gluon production on top partner searches, was considered for example in Ref. [154].

4.6.2 EW precision tests

Loops of fermionic resonances contribute to electroweak precision observables (EWPOs), such as the Peskin and Takeuchi (S and T) parameters [155], which measure the corrections to the EW gauge boson propagators, and the $Z\bar{b}b$ effective vertex, both being severely constrained by LEP. The corresponding limits can be significantly stronger than those from direct searches [156] if the model is not protected by additional symmetries; however, they cannot be taken at face value since they always require important assumptions about the UV.

The MCHM, by incorporating custodial symmetry, can protect the T-parameter from large tree level corrections. Furthermore, by embedding $q_L = \mathbf{4}_{2/3} \sim (\mathbf{2},\, \mathbf{2})_{2/3}$, the theory becomes invariant under a $L \leftrightarrow R$ symmetry that protects the model against tree level corrections to the $Z\bar{b}b$ coupling [157]. For this reason, the spinorial representation is disfavored by experimental data; in turn, the exotic doublet X in equation 92 becomes strongly motivated. As shown in equation 100, X can only decay into Wt. Under this assumption, the CMS search for $pp \to X_{5/3}X_{5/3} \to WtWt$ [158], using 35.9 fb^{-1} of data at $\sqrt{s} = 13$ TeV, has excluded masses $m_X \lesssim 1.3$ TeV.

In Ref. [159], a detailed analysis of the corrections to EWPOs in the MCHM was presented, taking into account the interplay between the most low-lying spin-$1/2$ and spin-1 resonances (and assuming the decoupling of heavier new physics). The authors report that the contribution of a fermionic fourplet alone implies a 95% CL lower limit on $f \gtrsim 1700$ GeV. However, other contributions arise which can cancel the large one-loop contributions from heavy top partners: *(1)* the non-linear dynamics of the pNGB

Higgs boson modifies the scalar–vectors coupling, resulting in shifts to the EWPOs; *(2)* composite vector resonances lead to additional tree level (through mass mixing with the elementary gauge bosons) and one-loop effects. Taking all these contributions into consideration, by performing matching at the scale of the heavy resonances followed by the RGE evolution to the weak scale, the authors show that compositeness scales as small as $f \sim 500$ GeV can still be compatible with the data. For purposes of comparison, the contribution from *(1)* alone excludes $f \lesssim 900$ GeV at the 95% CL.

4.6.3 Flavour bounds

Another important requirement for new TeV physics is that it complies with the most stringent flavour bounds [160]. In the case of CHMs, partial compositeness is an important ingredient to face this challenge, as it implies that the flavour structure at low-energy is identical to that of the SM, therefore evading many of the constraints.

In section 4.4, we discussed the scenario in which the strong sector is assumed to be anarchic, such that the different masses and mixing of the SM fermions arise from the mixings with the composite operators, all assumed to be $\mathcal{O}(1)$ in the UV. Due to the renormalization group running, the hierarchical Yukawa couplings at low-energy can be generated, provided that the different fermions couple to different sets of composite operators with different mass dimensions. This scenario naturally suppresses Higgs FCNCs, because in the low-energy theory the only sources of flavour violation are the SM Yukawa matrices[5]. In this way, partial compositeness moderately incorporates Minimal Flavour Violation (MFV) [161].

Still, higher-order operators involving the Higgs boson can be generated which could mediate these rare processes[6]. Similarly, four-fermion operators with generic flavour structure can be triggered upon integrating out the heavy resonances of the composite sector. However, since any elementary insertion must be weighted by the corresponding degree of compositeness, operators involving light quarks (which are the most constrained experimentally [162]) can only induce very small flavour-violating effects.

In spite of this efficient suppression, the constraints on flavour observables are so severe that a small tension with the data might be unavoidable. Furthermore, the anarchic scenario faces strong constraints from electric dipole moments (EDMs) because new $\mathcal{O}(1)$ complex phases are expected to arise [112]. An additional problem is that FCNCs in the Z sector are usually unprotected.

A common approach to protect the model against these flavour-breaking effects is to rather assume that the strong sector is flavour symmetric. Different symmetries to accomplish MFV have been considered in the literature, sharing the prediction that at least some of the light quarks must have a large degree of compositeness, being related by the flavour symmetry with that of the top quark. Consequently, composite

[5] Departures from this scenario can arise if, for example, more than one zero-momentum invariant is present in equation 84.

[6] An example being $\mathcal{O} \sim \frac{v}{f^2}(\partial_\mu h)\overline{u_R}\widetilde{\kappa}\gamma^\mu u_R$ + h.c. [112] which, upon the use of integration by parts (IBP) and the u_R equation of motion (EOM), gives $\mathcal{O} \sim \frac{v}{f^2} h\overline{u_R}(y^{u\dagger}\widetilde{\kappa})u_R$ + h.c. Since the $\widetilde{\kappa}$ flavour matrix does not need to be aligned with y^u, these interactions can give rise to FCNCs.

MFV is strongly constrained by EWPD except in the case of RH compositeness [163]. Together with the requirement of minimal CP violation, which can be attained if the leading breaking originates from the mixing with third generation quarks (which are also the least constrained by the EDM bounds [112]), or that the strong sector is CP invariant, such scenario can assure flavour protection in generic CHMs.

Chapter 5

Non-minimal composite Higgs models

As we have seen, there is no evidence of the MCHM *yet*, and if no new physics shows up with more data, the minimal model will eventually become too fine-tuned to give a *natural* explanation for the Higgs mass.

The requirement of minimality though, in spite of being a good starting point to establish the experimental searches for the model, has no intrinsic value. We do not know what the breaking structure is, so all CHMs are on equal footing (restricting the discussion to custodial symmetric groups); besides, larger coset spaces do not necessarily imply more free parameters in the theory. There are furthermore compelling reasons to explore non-minimal composite Higgs models (NMCHMs):

1. They are more common: there are infinite possibilities in which the Higgs plus other NGBs arise, but only one where exactly 4 $d.o.f.$ are produced.

2. They can evade more easily the experimental constraints [102, 103, 164]: for example, new decay channels open for the heavy resonances of the composite sector, therefore reducing their branching ratios into the SM. This possibility is completely unprobed and could render the bounds from current collider searches significantly weaker, still allowing top partner masses as light as ~ 400 GeV [165]. The implications for naturalness are obvious.

3. They can admit four-dimensional UV completions, one example being the $SU(5)/SO(5)$ NMCHM [166].

4. They can be anomalous [96]: since the anomaly coefficients depend on the fermionic content of the UV theory, there is the possibility of measuring them in some LHC process and obtain qualitative information about the underlying UV theory.

5. They produce additional pNGBs which can help addressing the long-standing problems in particle

physics, providing a protected DM candidate [53, 101, 104, 107–110, 167–179], the necessary conditions for EW baryogenesis [98, 105], *etc.*

6. They lead to new signatures at several experiments, with significant implications for Higgs and flavour physics, as will be demonstrated in the following discussion.

We remark that the non-minimality of CHMs can refer either to the dimension of the global symmetry group or to the number of NGBs that arise. Under the first criteria only, $SO(6)/SO(4)$ and $SO(6)/SO(5)$ are identical, but the latter produces the H plus one extra NGB, so $4+1$ $d.o.f.$; while the former leads to $4+5$. Other cosets, such as $SO(7)/SO(6)$, $SO(8)/SO(7)$ and $SO(7)/G_2$, produce an even smaller number of NGBs. The features of the most common coset groups explored in the literature are summarized in Ref. [103].

Let us denote the pNGBs emerging from a NMCHM by $\varphi = \{h_i,\ \kappa_j,\ \eta\}$, where j runs over all extra singlets on top of η or the components of a new weak-isospin multiplet. After performing the replacements in Ref. [96] to make the physical parameters easier to read, the Goldstone matrix becomes a two-block matrix:

$$U = \begin{bmatrix} \mathbb{1}_{3\times3} & & & & & \\ & 1-h^2/(f^2+\Xi) & -h\eta/(f^2+\Xi) & -h\kappa_1/(f^2+\Xi) & -h\kappa_2/(f^2+\Xi) & \dots & h/f \\ & -h\eta/(f^2+\Xi) & 1-\eta^2/(f^2+\Xi) & -\eta\kappa_1/(f^2+\Xi) & -\eta\kappa_2/(f^2+\Xi) & \dots & \eta/f \\ & -h\kappa_1/(f^2+\Xi) & -\eta\kappa_1/(f^2+\Xi) & 1-\kappa_1^2/(f^2+\Xi) & -\kappa_1\kappa_2/(f^2+\Xi) & \dots & \kappa_1/f \\ & \dots & \dots & \dots & \dots & \dots & \dots \\ & -h/f & -\eta/f & -\kappa_1/f & -\kappa_2/f & \dots & \Xi/f^2 \end{bmatrix}, \tag{108}$$

with $\Xi = f^2(1-h^2/f^2-\eta^2/f^2-\kappa_i^2/f^2)^{1/2}$ and h the rotated field that sets the EWSB (the sine factor has been absorbed in its definition).

The shift-symmetric Lagrangian, obtained from the CCWZ prescription, is

$$\begin{aligned} \mathcal{L}_{\text{kin}} &= \frac{1}{2}\partial_\mu\varphi^i\partial^\mu\varphi_i + \frac{(\varphi_i\partial_\mu\varphi^i)(\varphi_i\partial^\mu\varphi^i)}{2(f^2-\varphi_i\varphi^i)} \\ &= \frac{1}{2}\partial_\mu h^i\partial^\mu h_i + \frac{1}{2}\partial_\mu\kappa^i\partial^\mu\kappa_i + \frac{1}{2}\partial_\mu\eta\partial^\mu\eta + \frac{1}{f^2}\left[(\eta\partial^\mu\eta)(h_i\partial_\mu h^i + \kappa_i\partial_\mu\kappa^i)\right] + \dots, \end{aligned} \tag{109}$$

where the ellipsis stand for interactions not involving η at an order smaller than $\mathcal{O}(1/f^2)$.

On the other hand, the shift-breaking part is sourced by the Yukawa couplings of the SM fermions which generate an effective one-loop potential for the NGBs. This potential can be further expanded in

powers of λ_ψ/g_*, according to equation 56:

$$V(h_i,\kappa_i,\ \eta) = m_*^4\frac{N_c}{(4\pi)^2}\left\{\left(\frac{\lambda_\psi}{g_*}\right)^2\mathcal{V}_{(2)}\left[\frac{h_i}{f},\frac{\kappa_j}{f},\frac{\eta}{f}\right]+\left(\frac{\lambda_\psi}{g_*}\right)^4\mathcal{V}_{(4)}\left[\frac{h_i}{f},\frac{\kappa_j}{f},\frac{\eta}{f}\right]+\cdots\right\} \tag{110}$$

$$= g_*^2\lambda_\psi^2\frac{N_c}{(4\pi)^2}f^4\left[\alpha_{h^2}\frac{h_i^2}{f^2}+\alpha_{\kappa^2}\frac{\kappa_i^2}{f^2}+\alpha_{\eta^2}\frac{\eta^2}{f^2}+\beta_{h\kappa h}\frac{(h\kappa)_i h^i}{f^2}+\beta_{h^2\eta}h_i^2\eta+\beta_{\kappa^2\eta}\kappa_i^2\eta\right.$$

$$\left.+\beta_{\eta^3}\eta^3+\beta_{h^2\eta^2}\frac{h_i^2\eta^2}{f^4}+\beta_{h^2\kappa^2}\frac{h_i^2\kappa_j^2}{f^4}+\beta_{\eta^2\kappa^2}\frac{\kappa_i^2\eta^2}{f^4}+\beta_{h^4}\frac{h_i^4}{f^4}+\beta_{\eta^4}\frac{\eta^4}{f^4}+\beta_{\kappa^4}\frac{\kappa^4}{f^4}+\cdots\right],$$

where the dots encode interactions not determinant for the following discussion as well as higher-dimensional terms. The α and β couplings are $O(1)$ coefficients. Their particular values depend on how the SM fermions are embedded in $\mathcal{G}$. Moreover, $\beta_{h\kappa h}\neq 0$ only if $\overrightarrow{\kappa}$ transforms in a representation x of $SU(2)_L$ such that $x\otimes\mathbf{2}\otimes\mathbf{2}$ contains a group singlet; this is trivially obtained if $\kappa_i=\kappa$ is one-component. (We have not included tadpole terms, which can be removed via field redefinitions.)

The integration of the composite fermions triggers also the Yukawa interactions. In the unitary gauge, and after EWSB, they read:

$$\mathcal{L}_{\text{yuk}} = -\frac{1}{\sqrt{2}}\overline{\psi_L}h\left[y-c_\eta\frac{\eta}{f}-c_\kappa\frac{\kappa}{f}+c_{\eta^2}\frac{\eta^2}{2f^2}+\ldots\right]\psi_R+\text{h.c.}\,, \tag{111}$$

where the coefficients are matrices in flavour space[1]. Both c_η and c_κ take real (imaginary) values for scalars with CP-even (-odd) charges.

Finally, the non-minimal scalar spectrum implies also non-minimal interactions with the heavy resonances of the composite sector, such as the VLQs and vector states. They can be parameterized as:

$$\mathcal{L}_{\text{heavy}} = -g_*\left[\overline{\Psi_L}h\left(1-C_\eta\frac{\eta}{f}-C_\kappa\frac{\kappa}{f}+C_{\eta^2}\frac{\eta^2}{2f^2}+\ldots\right)t_R+\text{h.c.}\right]-g_*\frac{C_V}{\sqrt{2}}V_\mu\eta\partial^\mu\eta+\ldots\,, \tag{112}$$

where only the singlet components of V_μ couple to η directly; otherwise, the coupling is suppressed by additional ξ factors. Interactions with other flavours arise analogously.

Using this generic parameterization, we can anticipate the phenomenological signatures that are expected to arise from different models; see table 4 for a summary. We focus our analysis in next-to-minimal models, in particular those based on the $SO(6)$ and $SO(7)$ groups.

We start by noting that equation 111 can give rise to FCNCs mediated by the exotic particles. Since they are so suppressed in the SM, these processes are an ideal place to search for new physics, as we explore in section 5.1.

However, if each SM fermion mixes with a single composite resonance, the Yukawa-like couplings become $c_i\propto y$, such that the exotic pNGBs couple to the SM fermions with Higgs-like strength. Furthermore, for pseudoscalars, the renormalizable interactions with the Higgs boson, *e.g.* $\beta_{h\kappa h}$, are strongly

[1] We have dropped the $SU(2)$ indices, for simplicity.

$\mathcal{G}/\mathcal{H}$	$\mathbf{r}_{SU(2)\times SU(2)}$	μ [GeV]	$q_L \oplus t_R$	couplings	signals
$SO(6)/SO(5)$	$S \sim (1,1)$	100	$\mathbf{6} \oplus (\mathbf{6} \oplus \mathbf{15})$	c_η	top FCNCs 5.1
$SO(7)/G_2$	$\Phi \sim (1,3)$	100	$\mathbf{35} \oplus \mathbf{1}$	β_{κ^4}, c_κ^q	collider and GWs 5.2
$SO(7)/SO(6)$	$a_1, a_2 \sim (1,1)$	1	$\mathbf{27} \oplus \mathbf{1}$	$\beta_{\kappa^2\eta}$, $c_{\eta,\kappa}^\ell$, C_V	B-decays 5.3
	$\eta, \kappa \sim (1,1)$	100	$\mathbf{6} \oplus \mathbf{6}$	$\beta_{\eta^2\kappa^2}$, c_κ, C_κ	dark sector 5.4
			$\mathbf{27} \oplus \mathbf{1}$	$\beta_{h^2\eta^2}$, c_κ, C_κ	

Table 4: Summary of the non-minimal setups that will be discussed in this work. From the left to the right column, we present *(1)* the coset groups under study; *(2)* the nomenclature adopted in each section, as well as the quantum numbers of the exotic pNGBs under the chiral group; *(3)* the scale μ at which the new phenomenology is expected; *(4)* the different embeddings for the SM fermions which are considered; *(5)* the most relevant couplings triggering the phenomenology we are interested in probing (the superscript in c_i refers to lepto- or hadro-philic regimes); and finally *(6)* the section in which each case is discussed. The mass terms for each field (α_{η^2} and α_{κ^2}) are implicitly assumed in the fifth column.

constrained by EDM measurements [180, 181]; therefore, the corresponding phenomenology is mainly driven by the effective interactions. These facts together strongly motivate searches for EW scalars decaying into third generation quarks,that we study in section 5.2 assuming that κ is an $SU(2)_L$ triplet. Moreover, extended scalar sectors can modify the EW PT. In particular, first order PTs are characterized by a stochastic spectrum of gravitational waves (GWs) that could be detected by future space-based observatories. We study the interplay between collider and GW probes of the triplet model also in this section.

On another front, the coupling between light and heavy resonances of the strong sector, in particular C_V, triggers rare decays of mesons into the exotic particles, in the low scalar mass regime. We propose dedicated analyses to study these channels at the LHCb in section 5.3.

Finally, in section 5.4, we explore the scenario in which one of the pNGBs is stable and a potential DM candidate (for instance η, provided that $\beta_{h^2\eta} = \beta_{\kappa^2\eta} = \beta_{\eta^3} = c_\eta = C_\eta = 0$). Composite scalar DM is strongly motivated by several reasons: *(1)* it can be naturally at the EW scale, in agreement with the weakly-interacting massive particle (WIMP) paradigm (see appendix E); *(2)* it becomes automatically protected from the HP; *(3)* the portal coupling $\beta_{h^2\eta^2}$ can be small, as required by current low-energy constraints, while the derivative interactions in equation 109 are $\mathcal{O}(m_\eta^2/f^2)$ at the annihilation scale. These interactions can therefore accommodate the DM relic density *per se*, which sets an important difference between the composite and elementary DM scenarios, as in the latter the requirement $\beta_{h^2\eta^2} \ll 1$ is typically in tension with a thermal η being all the DM we observe.

Furthermore, if there are additional pNGB below the DM scale, the DM phenomenology can be drastically different. To probe this case, bounds from DM experiments need to be rescaled and reinterpreted accordingly. Likewise, it is not sufficient to study VLQ decays into the DM particle, triggered by C_η, but searches for $\Psi \longrightarrow \kappa_i \psi$, triggered by C_κ instead, are mandatory to establish the non-minimality of the model. Thereofore, in section 5.4, we perform a sensitivity study of such decay in $\overline{\Psi}\Psi$ production at a future circular collider reaching energies of $\sqrt{s} = 100$ TeV.

5.1 Flavour-changing neutral currents in the top sector

5.1.1 The SO(6)/SO(5) model

The $SO(6)/SO(5)$ symmetry breaking pattern of the strong sector can be achieved by the VEV of a fundamental field transforming in the representation $\mathbf{6}$ of $SO(6) \approx SU(4)$ [96]. The model construction and the embedding of the SM are obtained in complete analogy with the MCHM. (This holds for any $SO(n+1)/SO(n)$ construction.) This particular breaking produces five NGBs transforming as a $\mathbf{5}$ of $SO(5)$, which decomposes as $\mathbf{1} \oplus \mathbf{4} = (\mathbf{1},\mathbf{1}) \oplus (\mathbf{2},\mathbf{2})$ under $SO(4) \approx SU(2)_L \times SU(2)_R$. The chiral bi-doublet is therefore identified with the Higgs boson while the extra singlet is denoted by S.

The exact values of the parameters in the shift-breaking Lagrangian depend on the representations under which q_L and t_R transform. Among others, there are the $\mathbf{6} \oplus \mathbf{6}$, $\mathbf{6} \oplus \mathbf{15}$, $\mathbf{15} \oplus \mathbf{15}$ or the $\mathbf{20} \oplus \mathbf{1}$. In the first case, both quarks break the global symmetry. The fundamental representation decomposes as $\mathbf{6} = \mathbf{5} \oplus \mathbf{1} = \mathbf{4} \oplus \mathbf{1} \oplus \mathbf{1}$, under $SO(5)$ and $SO(4)$, respectively. Therefore, the RH quark can couple to the two singlets in this decomposition and equation 80 should be generalized to

$$T_R = \left(0\,,0\,,0\,,0\,,\mathrm{i}\gamma t_R,\ t_R\right)^T\ ; \tag{113}$$

with γ being a free parameter. By contracting the LH and RH singlet components, $\mathbf{1}_L \times \mathbf{1}_R$, we obtain the Yukawa Lagrangian in equation 111, with $c_\eta = \mathrm{i}\gamma y$. Two interesting limits are worth mentioning: *(1)* if $\gamma \longrightarrow 0$, the singlet becomes stable; *(2)* if $\gamma \longrightarrow 1$, its shift-symmetry remains unbroken (it is an exact NGB).

On the other hand, the LO potential is obtained by combining two $\mathcal{H}$-invariants, $\mathbf{1}_{L,R} \times \mathbf{1}_{L,R}$. As in the MCHM, this potential has a minimum at $h = 0$ and therefore NLO terms are mandatory to achieve the form of $V(H)$, which increases the number of the UV parameters, not allowing us to make precise predictions. The same holds for the other representations smaller than the $\mathbf{20}$. When $t_R \sim \mathbf{15}$, the shift symmetry of the singlet remains furthermore unbroken.

Nevertheless, we can use PC to estimate the singlet mass. Following equation 110,

$$m_S^2 \sim N_c \frac{y_\psi^2 m_*^2}{(4\pi)^2}\,, \tag{114}$$

where we have traded λ_ψ by the Yukawa coupling that is subsequently generated at low-energy. Therefore, S can be naturally at or below the Higgs scale, depending on which type of quarks breaks its shift-symmetry. For instance, if all SM fermions but the top (bottom) quark are embedded in a representation with $\gamma = 1$, the singlet can be heavier (lighter, with $m_S \sim O(10)$ GeV) than the Higgs boson. This scenario can be actually predicted if the fermions transform in the $\mathbf{20}$ representation of the global group, leading to $m_S^2 \sim \lambda_H f^2 \left[1 + O(\xi)\right]$.

Note also that, in spite of being imposed classically by forcing $\gamma = 0$, the stability limit cannot be assured at the quantum level, since the global group $SO(6)$ is anomalous. A Wess-Zumino-Witten (WZW) term can therefore arise in the Lagrangian [96],

$$\mathcal{L} \supset \frac{c_W}{(4\pi)^2} S \left(g_2^2 W^A_{\mu\nu} \widetilde{W}^{A\mu\nu} - g_1^2 B_{\mu\nu} \widetilde{B}^{\mu\nu} \right) , \tag{115}$$

where n_W is an integer that is fixed by the UV content of the CHM completion.

In order to avoid this term, we can extend the symmetry to $O(6)/O(5)$, so that the parity transformation

$$P_{\text{DM}} = \text{diag}(1, 1, 1, 1, -1, 1) \in O(5) , \tag{116}$$

leading to $P_{\text{DM}}^{-1} U(h, S) P_{\text{DM}} = U(h, -S)$, is respected at all orders in derivatives.

This model therefore provides a potential DM candidate at the EW scale. The corresponding composite phenomenology was first explored in Ref. [53]; current bounds from DM experiments have already excluded $m_S \lesssim 500$ GeV considering the (most predictive) $\mathbf{20} \oplus \mathbf{1}$ model.

Dropping the requirement of stability, many other phenomenological consequences arise, particularly in the case of a CP-odd singlet, for which $\gamma \in \mathbb{R}$ in equation 113. For example, such particle can be an *axion* of the Peccei-Quinn solution for the strong CP problem [182, 183]. Instead of trying to explain an extremely small value for the QCD θ-term, this model considers a dynamical field coupled to $G\widetilde{G}$ whose VEV could precisely cancel an *a priori* sizable θ. This requires in turn a particular relation between the axion mass and its decay constant, which controls the size of its couplings to the SM. Many experiments have been and are currently searching for the QCD axion, from energies at the sub-eV up to the TeV range [184].

Evading this dependence, a generic axion-like particle (ALP) has been considered in plenty other models in the literature, namely as a *relaxion* which takes the role of μ_H^2 and slowly rolls down its potential until stabilizing at a small negative value, therefore providing a dynamical explanation for the HP [185]; as a *ma-xion* [186] responsible for generating neutrino Majorana masses; or an *axiflavon* which, taking a VEV, can generate the hierarchical fermion masses according to the Forggatt-Nielsen mechanism [187]. Furthermore, an ALP is a promising candidate to solve some of the apparent anomalies observed in different experiments, such as the galactic center (GC) excess [188] and the deviations from the SM prediction of the anomalous magnetic moments of charged leptons [189, 190]. In this last case, the pseudoscalar singlet can contribute at tree or loop level to the $A\ell^+\ell^-$ effective vertex, and hence be responsible for

an extra contribution that fits the $(g-2)$ anomalies[2], the CP-charge of the new scalar being important to explain the correct sign of the observed deviations. Such pseudoscalar can also provide the necessary conditions for EW baryogenesis, namely providing extra sources of CP violation during the EW PT [98].

In spite of stirring up such great theoretical interest, pseudoscalar singlets at the EW scale are very difficult to detect: first, because they do not have renormalizable interactions with the gauge bosons and the production cross section via an off-shell Higgs boson is too small (being out of reach even of future 100 TeV colliders [110, 192]); second, because any sizable scalar mixing is excluded by measurements of EDMs. As such, finding alternative production mechanisms for such particle is an ongoing subject of great activity. Since the LHC is a factory of top quarks (even before the next luminosity phase starts), a promising possibility is the production of EW pseudoscalars via top decays.

To study this possibility, let us consider the regime in which the LH quarks are embedded in the representation $\mathbf{6}$, while RH up quarks transform in both the $\mathbf{6}$ and the $\mathbf{15}$:

$$Q_L^\alpha = \frac{1}{\sqrt{2}}(\mathrm{i}d_L^\alpha, d_L^\alpha, \mathrm{i}u_L^\alpha, -u_L^\alpha, 0, 0)\ ; \tag{117}$$

$$U_{R_1}^\alpha = (0,0,0,0,\mathrm{i}\gamma^q u_R^\alpha, u_R^\alpha) \qquad \text{and} \qquad U_{R_2}^\alpha = \mathrm{i}(T^{12}-T^{34})u_R^\alpha\ . \tag{118}$$

The LO Yukawa Lagrangian is obtained from the contraction of two $SO(5)$ invariants, $\mathbf{1}_L \times \mathbf{1}_{R_1}$ and $\mathbf{5}_L \times \mathbf{5}_{R_2}$, obtained in the decomposition of the $\mathbf{6} = \mathbf{1}\oplus\mathbf{5}$ and the $\mathbf{15} = \mathbf{5}\oplus\mathbf{10}$ under the unbroken group. Keeping the same notation as section 4.5,

$$\begin{aligned}\mathcal{L}_{\text{yuk}} &= f y^{(1)}_{\alpha\beta}\overline{q_L}^\alpha_I \left(\Lambda^I_{L,D}\right)^\dagger_6 \left(\Lambda_{L,R_1}\right)_6 u_R^\beta + y^{(2)}_{\alpha\beta} f \overline{q_L}^\alpha_I \left(\Lambda^I_{L,D}\right)^\dagger_m \left(\Lambda_{L,R_2}\right)_{m6} u_R^\beta + \text{h.c.} \\ &= \frac{1}{\sqrt{2}}\overline{u_L^\alpha} h u_R^\beta \left[y^{(1)}_{\alpha\beta}\left(-1 + \mathrm{i}\gamma^q \frac{S}{f} + \frac{h^2}{2f^2} + \frac{S^2}{2f^2}\right) + y^{(2)}_{\alpha\beta} + \cdots \right] + \text{h.c.}\,,\end{aligned} \tag{119}$$

with $m = 1,\ldots,5$ being associated to the components along the broken generators and the ellipsis representing terms further suppressed by powers of $1/f$. The dressed spurions are defined as $\Lambda^I_{L,D} = U^{-1}\Lambda^I_L$; $\Lambda_{R_1,D} = U^{-1}\Lambda_{R_1}$; and $\Lambda_{R_2,D} = U^{-1}U_{R_2}U$. (We work in the approximation that the CKM matrix is diagonal.)

This construction shows explicitly that the singlet Yukawa matrix, $\sim \gamma^q y^{(1)}$, is not aligned with the Higgs Yukawa matrix, $\sim y^{(1)} - y^{(2)}$, in general. The singlet can therefore mediate FCNCs in the quark sector. We assume that no FCNCs arise in the leptonic one. This is realized, for instance, if the leptons are embedded in the fundamental representation, such that the singlet leptonic Yukawa matrix is automatically diagonal in the physical basis: $\boldsymbol{y}^l_{\alpha\alpha} \sim \gamma^l y^e_{\alpha\alpha}$.

[2]The magnetic moment of charged leptons is given by $g_\ell e/(2m_\ell)$, with $g_\ell = 2$ [21]. The deviation from this value is predicted in the SM at the loop level, the dominant contribution coming from the exchange of virtual photons. The anomaly refers to $\Delta a_\ell = a_\ell^{\text{exp}} - a_\ell^{\text{SM}}$, where $a_\ell \equiv (g_\ell - 2)/2$. The largest discrepancy between the SM predictions and experiment is found in the muon channel and is currently at the 4.2σ level, after combining the Brookhaven and Fermilab results [191].

Such FCNCs have been studied previously in Ref. [193] assuming that $S \to \bar{b}b, \gamma\gamma$. (For $m_S > m_t$, the scalar singlet can instead mediate four fermion interactions making the top quark decay non-resonantly. A sensitivity study for this process was subsequently presented in Ref. [194].) We complement the discussion therein by studying the collider signals of a *leptophilic* S. This regime is specially motivated if the embeddings of quarks preserve a $S \to -S$ symmetry, making the scalar decay into leptons the only possibility to probe the model. This scenario triggers rare top decays into two singlets instead of one, $t \to SSj$, which were not previously considered in the literature. Searches for these processes might additionally provide constraints in models with DM.

5.1.2 Collider signatures

Both the derivative and non-derivative pNGB interactions enter the Higgs width as follows:

$$\Gamma(h \to SS) = \frac{1}{32\pi m_h}\sqrt{1-\frac{4m_S^2}{m_h^2}}\left[\lambda_{HS} + \frac{\left(m_h^2 - 2m_S^2\right)}{2f^2} + O\left(\frac{v^2}{f^2}\right)\right]^2 , \tag{120}$$

where $\lambda_{HS} \sim g_*^2 y_\psi^2 N_C/(4\pi)^2$, according to equation 110, and the second coefficient is fixed by the kinetic Lagrangian in equation 109. Therefore, values of $m_S < m_h/2$ are *a priori* constrained by the Higgs decay width, $\Gamma_H \lesssim 10$ MeV [195]. This bound can be evaded provided that the combined contribution of the coefficients within the brackets is $\lesssim 0.5$. (Studying the effect of each contribution separately, this bound translates into $g_* \lesssim 5$ if λ_{HS} dominates over the derivative interactions; and $1/f^2 \lesssim 5$ TeV^{-2}, for $m_S \sim 50$ GeV, in the inverse case.)

Furthermore, the Yukawa matrices in equation 119 are subject to several constraints. In the following, we denote the S and S^2 Yukawa matrices by $\mathcal{Y}^q_{\alpha\beta} \sim \gamma^q y^{(1)}_{\alpha\beta}$ and $\widetilde{\mathcal{Y}}^q_{\alpha\beta} \sim y^{(1)}_{\alpha\beta}$. The relevant entries for this study are the 3α and $\alpha 3$ for which we have found no direct limits. Indirect constraints from flavour experiments, namely contributions to the $D^0 - \overline{D}^0$ ($D^0 \equiv c\overline{u}$) oscillation amplitude, involve always products of two Yukawas, $\mathcal{Y}_{ut}$ and $\mathcal{Y}_{ct}$ [196]; they are therefore negligible if one of these entries vanishes.

The singlet Yukawa matrices can be instead tested in the following rare top decays:

$$\Gamma(t \to q^\alpha S) = \frac{v^2}{64\pi f^2}\left[(\mathcal{Y}^q_{\alpha 3})^2 + (\mathcal{Y}^q_{3\alpha})^2\right] m_t \left(1-x^2\right)^2 ; \tag{121}$$

$$\Gamma(t \to q^\alpha SS) = \frac{v^2}{512\pi^3 f^4}\left[(\tilde{\mathcal{Y}}^q_{\alpha 3})^2 + (\tilde{\mathcal{Y}}^q_{3\alpha})^2\right] m_t^3 \left[\frac{1}{3}\sqrt{1-4x^2}\left(1+5x^2-6x^4\right)\right.$$
$$\left. + 2\left(x^2 - 2x^4 + 2x^6\right)\log\frac{2x^2}{1-2x^2+\sqrt{1-4x^2}}\right], \tag{122}$$

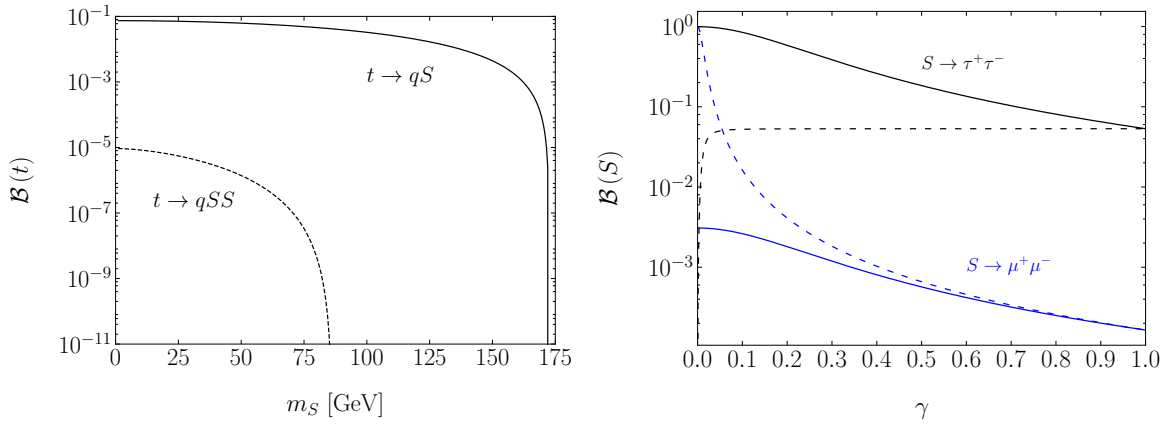

Figure 4: (Left) Exotic branching ratios of the top quark as a function of the singlet mass. We assumed $\mathcal{Y}^q_{i3} = \tilde{\mathcal{Y}}^q_{i3} = 1$, the same for the transposed entries, and $f = 1$ TeV. (Right) Singlet branching ratios into muons (in blue) and tau leptons (in black) as a function of γ, for $m_S = 100$ GeV. We assumed $\gamma^\ell = \gamma^\tau = 1$ and $\gamma^q = \gamma$ in the solid lines; while $\gamma^\ell = 1$ and $\gamma^\tau = \gamma^q = \gamma$ in the dashed lines.

where we have defined $x = m_S/m_t$. The branching ratio of the top quark into Sq and SSq is represented in the left panel of figure 4, setting the relevant Yukawa entries to 1 and $f = 1$ TeV. We take the top decay width to be $\Gamma_t \sim 1.4$ GeV [9].

The singlet can subsequently decay into fermions. Since quarks and leptons can transform differently under the global symmetry (which is primary motivated by their different masses and mixings), we show, in the right panel of figure 4, the branching ratio of S to taus and muons for different assumptions on the $\mathbb{Z}_2$ breaking parameter[3]. We verify that, even for $\gamma^q = \gamma^\tau$, the branching ratio into tau leptons is sizable ~ 0.1. In the *leptophilic* scenario ($\gamma^q = 0$), it is clearly the dominant mode. Moreover, in spite of the decay into muons being a factor of $m_\mu^2/m_\tau^2 \sim 10^{-3}$ smaller, it can be enlarged if the tau lepton transforms in a representation that breaks only softly (or not at all, in the case of the **15**) the singlet $\mathbb{Z}_2$ symmetry. If the latter applies also to quarks, the top can only decay via $t \longrightarrow SSj$.

Current multileptonic analyses could potentially be sensitive to this scenario. One example is the ATLAS search for $t \longrightarrow Zq$ [197] which defines the control region "CR1", where three light leptons are required. In addition, the $\ell^+\ell^-$ pair with invariant mass closest to m_Z must satisfy $|m_{\ell^+\ell^-} - 15\,\text{GeV}| > m_Z$; which makes the analysis sensitive to generic EW resonances in the leptophilic regime. However, the sensitivity to $\mathcal{Y}^q$ is only marginal [6].

We therefore propose three new dedicated analyses to test the parameter space of this model at the LHC: $pp \longrightarrow tS + j$, in both $S \longrightarrow \mu^+\mu^-$ and $S \longrightarrow \tau^+\tau^-$ channels; and $pp \longrightarrow tSS + j$, with $S \longrightarrow \mu^+\mu^-$. In our signal definition, we consider that the FCNC vertex can be present either in the production or the decay of the top quark; see figure 5. To subsequently study the reach of the different analyses, we define

[3]Hereafter, we denote any lepton by l and light leptons *i.e.* the muon and the electron by ℓ.

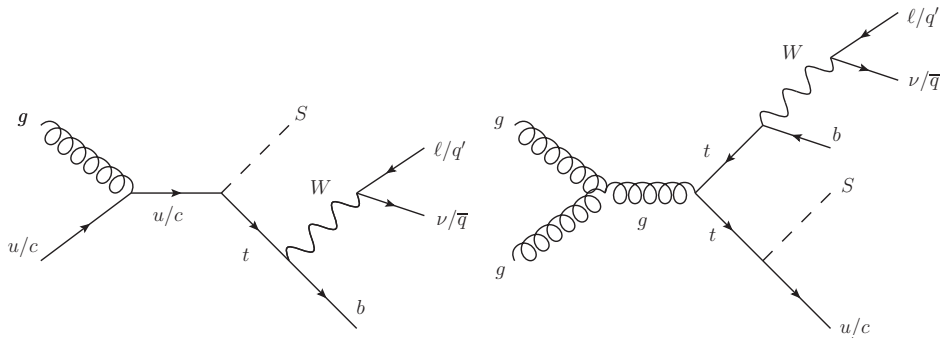

Figure 5: Production mechanisms of the top quark relevant for this work. On the left, the FCNC vertex is present in the production; on the right, the FCNC vertex is considered on the decay of the top quark.

the following benchmark points (BPs):

$$
\begin{aligned}
&\text{BP1}: \quad \mathcal{Y}_{\alpha 3} = \mathcal{Y}_{3\alpha} = 0.01\,, \quad f = 5\ \text{TeV} \implies \mathcal{B}(t \to Sq) \sim 10^{-8} - 10^{-7}\,,\\
&\text{BP2}: \quad \mathcal{Y}_{\alpha 3} = \mathcal{Y}_{3\alpha} = 0.10\,, \quad f = 5\ \text{TeV} \implies \mathcal{B}(t \to Sq) \sim 10^{-6} - 10^{-5}\,,\\
&\text{BP3}: \quad \mathcal{Y}_{\alpha 3} = \mathcal{Y}_{3\alpha} = 0.10\,, \quad f = 1\ \text{TeV} \implies \mathcal{B}(t \to Sq) \sim 10^{-4} - 10^{-3}\,,\\
&\text{BP4}: \quad \widetilde{\mathcal{Y}}_{\alpha 3} = \widetilde{\mathcal{Y}}_{3\alpha} = 1.00\,, \quad f = 5\ \text{TeV} \implies \mathcal{B}(t \to SSq) \sim 10^{-11} - 10^{-8}\,,\\
&\text{BP5}: \quad \widetilde{\mathcal{Y}}_{\alpha 3} = \widetilde{\mathcal{Y}}_{3\alpha} = 0.20\,, \quad f = 1\ \text{TeV} \implies \mathcal{B}(t \to SSq) \sim 10^{-10} - 10^{-7}\,,\\
&\text{BP6}: \quad \widetilde{\mathcal{Y}}_{\alpha 3} = \widetilde{\mathcal{Y}}_{3\alpha} = 1.00\,, \quad f = 1\ \text{TeV} \implies \mathcal{B}(t \to SSq) \sim 10^{-8} - 10^{-5}\,,
\end{aligned}
$$

with $i = 1, 2$. The range in the branching ratio follows from the values of $m_S \in [20, 150]$ GeV that are considered in this study.

5.1.3 New analyses at the LHC

In this section, we describe our proposed searches for the scalar particle triggering both two and four muon final states. We discuss the results from the top-up quark transition, which is the one leading to the most stringent upper limits on the scalar mass. This is mainly a parton distribution function effect: the probability to find a charm-quark in a proton that carries a sizable fraction of the initial energy is much smaller than for the up-quark [9]. In turn, while both processes in figure 5 are important for $t \longrightarrow Su$, only the one on the right contributes sizably if $\mathcal{Y}_{13} = \mathcal{Y}_{31} = 0$. (The signal efficiencies are comparable in the two channels.)

Signal and background samples are generated as described in section 3.3. At the reconstruction level, we assume the default CMS detector card in `Delphes`, which in particular requires electrons (muons) to have $p_T > 15$ GeV and $|\eta| < 2.5\ (2.4)$. We additionally demand that the transverse momentum of the hardest lepton is above 25 GeV. Jets are defined using the anti-k_T algorithm with $R = 0.5$ and required to have $p_T > 25$ GeV and $|\eta| < 2.5$. On top of these, the selection cuts particular to each search are described below.

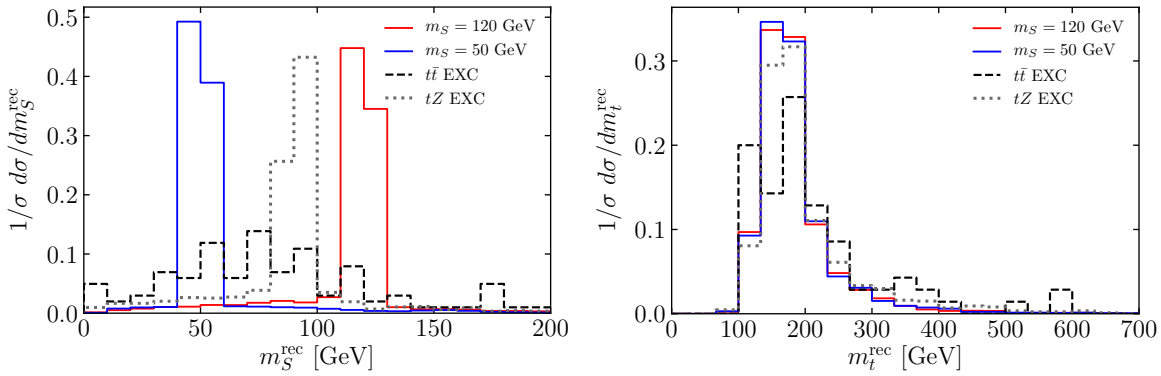

Figure 6: (Left) The reconstructed scalar mass distribution in the analysis proposed for $t \to Su$, $S \to \mu^+\mu^-$, immediately after the cut on particle multiplicity. Two signal BPs are confronted with the two major background components. The latter are generated EXClusively, *i.e.* only the gauge boson decays into muons are considered. (Right) The same for the reconstructed SM top quark mass.

5.1.3.1 Di-muon final states

In the $S \to \mu^+\mu^-$ search, we consider only leptonic decays of the W boson. Hence, at the detector level, we expect three charged leptons, multiple jets and MET. Among the set of events produced after running `Delphes`, we keep those with exactly three isolated leptons (two of them being necessarily opposite charged muons), at least one jet and exactly one b-tagged jet.

The scalar resonance is reconstructed from the hardest $\mu^+\mu^-$ pair; its invariant mass being denoted $m_S^{\rm rec}$. The corresponding normalized distribution is shown on the left panel of figure 6, for two signal BPs and the most dominant backgrounds originating from tZ and $t\bar{t}$ production. The transverse momentum of the neutrino is identified by knowing the transverse momenta of all visible particles in the final state. On the other hand, the longitudinal component is obtained by requiring that $(p_\ell + p_\nu) = m_W^2$, where p_ℓ (p_ν) is the four-momentum of the lepton not coming from the scalar decay (neutrino). The smallest value solution is chosen and $m_W = 81.2$ GeV is used as the reference mass. Both p_ℓ and p_ν are then added to the four-momentum of the b-jet to reconstruct the SM top quark; its invariant mass being denoted $m_t^{\rm rec}$. The corresponding distribution for two signal BPs and the dominant backgrounds is shown on the right panel of figure 6. We require that all events satisfy $|m_t^{\rm rec} - m_t| < 50$ GeV, taking the reference top mass to be $m_t = 172.5$ GeV.

An additional cut must be imposed to guarantee the validity of the EFT, making sure no energy bin sensitive to the UV resonance is used. We therefore require that $m_{\rm total} < 1$ TeV, with $m_{\rm total}$ being the invariant mass of the total system (that is, the reconstructed top, the reconstructed singlet and the MET). The effect of this last cut is minor: for $m_S = 50$ GeV, $\gtrsim 98\%$ of the signal events are kept. The complete cut-flow tables for other signal mass points and background samples are presented in Ref. [6].

It is clear from the reconstructed scalar mass distribution in figure 6 that the signal peaks sharply

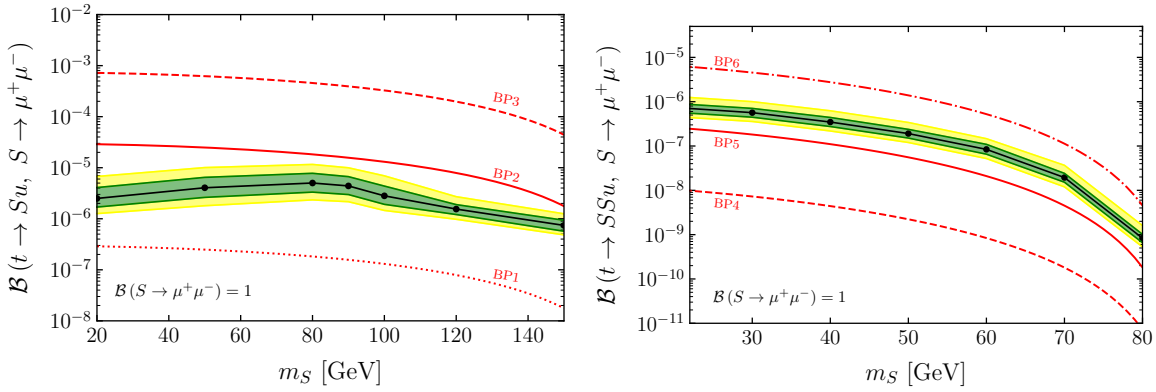

Figure 7: (Left) The 95% CL upper limits on the top branching ratio that can be tested in the $S \longrightarrow \mu^+\mu^-$ channel, in the analysis proposed for $t \longrightarrow Su$. Such limits are obtained for a collected luminosity $L = 150\,\text{fb}^{-1}$. The green and yellow bands assume, respectively, $\pm 1\sigma$ and $\pm 2\sigma$ level uncertainties on the limits. (Right) The same for the case in which $t \longrightarrow SSu$.

around the input scalar mass, while the background does not (with the exception of tZ, producing two muons with an invariant mass distribution that peaks around m_Z). For the final selection cut, we therefore impose that $|m_S^{\text{rec}} - m_S| < 30$ GeV (losing sensitivity to $m_S \sim m_Z$). The corresponding signal, $t\bar{t}$ and tZ efficiencies are $\approx 70,\ 40$ and 15%, respectively, for $m_S = 50$ GeV.

The distribution of the reconstructed scalar mass is used as discriminant variable to set the upper limits, which are derived using the `OpTHyLic` tool assuming the background-only hypothesis. For an integrated luminosity $L = 150\,\text{fb}^{-1}$, we find that production cross sections $\sigma \gtrsim 10^{-3}$ pb could be excluded at the 95% CL at the LHC; the highest sensitivity being attained for $m_S \sim 150$ GeV. The exclusion limits on the cross section can be translated into a maximum allowed coupling, by rescaling the theoretical cross section until the upper limit is reached; this coupling is subsequently used in equation 121 to obtain the limits on the exotic branching ratio of the top quark. (We assume that corrections to the top decay width from the new physics are negligible.)

The expected 95% CL limits, as well as the $\pm 1\sigma$ and $\pm 2\sigma$ level bands, resulting from this procedure are presented in the left panel of figure 7. Assuming $\mathcal{B}(S \longrightarrow \mu^+\mu^-) = 1$, this search could exclude models where the new physics coupling and scale are $(\mathcal{Y}^u_{13},\ f) = (0.1,\ 5\ \text{TeV})$, corresponding to the BP 2. For $\mathcal{O}(1)$ couplings in the UV, the highest sensitivity reach implies a lower bound on $f \gtrsim 90$ TeV.

5.1.3.2 Four muon final states

In comparison to single production, the double production of the pseudoscalar is phase space suppressed. We therefore expect to obtain weaker constraints in this case. Such constraints can be, however, the only way to probe the model in the limit where $S \longrightarrow -S$ is preserved by the quark sector.

Only hadronic decays of the W boson are considered this time. Hence, at the detector level, we require four isolated leptons and at least three jets, one of which must be b-tagged.

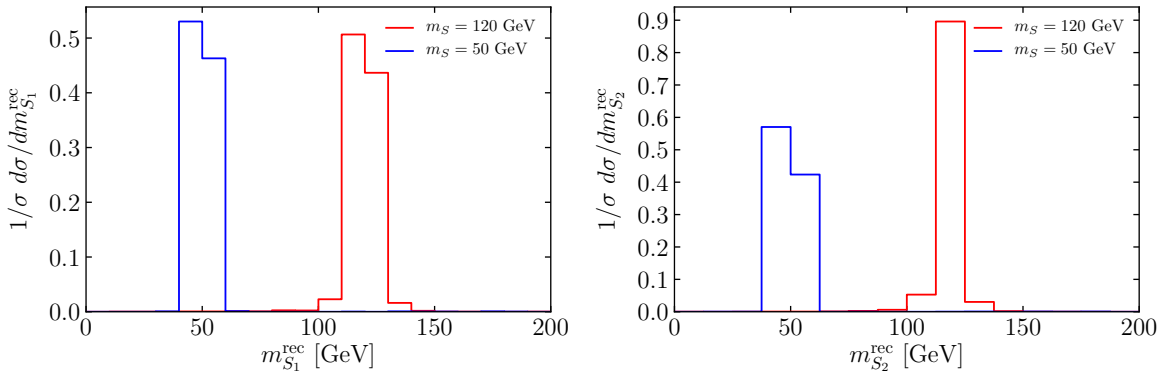

Figure 8: The two reconstructed scalar mass distributions in the analysis proposed for $t \to SSu$, $S \to \mu^+\mu^-$, immediately after the cut on particle multiplicities. The labels are as in figure 6.

The top quark decaying into the SM is reconstructed from a W candidate and the b-jet; the W being reconstructed from the two light jets whose invariant mass is closest to m_W. The corresponding mass distributions are label as before and the same mass window cuts are applied, including the one on the invariant mass of the total system, composed by the top quark and the two scalars S_1 and S_2.

In this case, however, we need to decide which $\mu^+\mu^-$ pair, among the two, is assigned to each scalar resonance. To do so, we compute all combinations and choose the one that minimizes $|m^{\rm rec}_{S_1} - m^{\rm rec}_{S_2}|$, with $m^{\rm rec}_{S_{1,2}}$ being the invariant mass of each pair of opposite sign muons. The corresponding distributions are represented in figure 8; it is apparent that the algorithm can differentiate correctly the leptons coming from each scalar. After the initial cut on the multiplicity of particles, the backgrounds are reduced to negligible levels, therefore no such distributions are shown in these plots.

The invariant mass distributions of the reconstructed scalars are finally used as discriminant variables to set the upper limits. For an integrated luminosity $L = 150$ fb^{-1}, we find that production cross sections $\sigma \gtrsim 10^{-3}$ pb could be excluded at the 95% CL at LHC; the highest sensitivity being attained for $m_S \sim 80$ GeV. The results, translated into the maximum allowed branching ratios of the top quark, are presented in the right panel of figure 7. Assuming $\mathcal{B}(S \to \mu^+\mu^-) = 1$, this search could potentially exclude models where the new physics coupling and scale are $(\widetilde{\mathcal{Y}}^u_{13},\ f) = (1.0,\ 1\ \text{TeV})$, corresponding to the BP 6. For $\mathcal{O}(1)$ couplings in the UV, the strongest limits translate into a lower bound on $f \gtrsim 2$ TeV.

5.1.4 Outlook

We have demonstrated that pseudoscalar singlet FCNCs in the top sector can arise in the next-to-minimal CHM and lead to sizable effects at the LHC. This contrasts with those mediated by the Higgs boson, which are typically very small because *(1)* they arise at higher-orders in the pNGBs EFT; *(2)* the signal peaks in regions of the phase space where the SM background is more prominent; *(3)* the Higgs branching ratios into the cleanest final states are overly small. On the other hand, if the heaviest fermions are embedded

in representations of $SO(6)$ that break only softly the singlet shift-symmetry, S can decay mainly into a pair of muons. Under this assumption, new physics scales as large as $f \sim \mathcal{O}(100)$ TeV could potentially be probed with a collected luminosity $L = 150$ fb^{-1}.

If opened, the τ-channel will however dominate the dynamics of a leptophilic singlet. In such case, the fact that tau leptons decay into hadrons before being detected renders the analysis more involved and dirtier than the previous one. This in conjunction with the smaller tau-tagging reconstruction efficiency, $\lesssim 60\%$, lead to weaker limits on the model parameter space. In particular, for $\mathcal{B}(S \to \tau^+\tau^-) = 1$, new physics scales $f \sim 75$ TeV could be probed ($\sim 20\%$ smaller than the ones we found in the muonphilic scenario). Note also that, as both the leptonic W and the tau-jets decay into MET, we cannot reconstruct the top invariant mass in this case. To guarantee the validity of the EFT, we have therefore imposed a maximum value (500 GeV) for the transverse, rather than the invariant, mass of the total system.

Finally, using the results in figure 7, we can make a naive rescaling of the statistical significance with the luminosity $\mathcal{S}'/\mathcal{S} = \sqrt{L'/L}$ (assuming the same systematic uncertainties on the event samples), to estimate the sensitivity prospects at the HL-LHC. With $L' = 3\,\text{ab}^{-1}$, we can therefore expect that compositeness scales as large as $f \gtrsim 200\ (3)$ TeV could be probed in $pp \to tS + j$ ($pp \to tSS + j$) searches, assuming that the pseudoscalar decays mainly into muons. Such flavour searches could provide a powerful constraint on the parameter space of the EW ALP.

5.2 EW phase transition at colliders and astrophysical observatories

5.2.1 The $SO(7)/G_2$ model

In the next sections, we turn the discussion into the $SO(7)$ global group. To start, we focus on the symmetry pattern $SO(7)/G_2$, which can be accomplished if a fundamental field transforming in the spinorial representation $\mathbf{8}$ of $SO(7)$ develops a VEV [101]. An eight-dimensional representation of the 21 $SO(7)$ generators, as well as the embedding of the G_2 subgroup, has been constructed in the work cited above. The generators that span the coset manifold (and so the corresponding NGBs) transform in the representation $\mathbf{7}$ of G_2, which decomposes as $(\mathbf{2},\ \mathbf{2}) \oplus (\mathbf{3},\ \mathbf{1})$ under the chiral group. Therefore, the physical spectrum of the model comprises a Higgs doublet and three extra states that, depending on which of the two $SU(2)$ groups is gauged, can transform as a triplet or three singlets under $\mathcal{G}_{\text{EW}}$. The former constitutes a version of the inert triplet model [198]; we will focus on this case hereafter, denoting the EW triplet by Φ.

Among the smallest representations where q_L and t_R can transform, we find the $\mathbf{8} \oplus \mathbf{8}$ and the $\mathbf{35} \oplus \mathbf{1}$. In the last case, the relevant shift-symmetry breaking interactions of equation 110 can be generated at LO. The potential is constructed out of two $\mathcal{H}$-invariants, the $\mathbf{1}_L \times \mathbf{1}_L$ and the $\mathbf{7}_L \times \mathbf{7}_L$ arising from the

decomposition of the $\mathbf{35} = \mathbf{1} \oplus \mathbf{7} \oplus \mathbf{27}$ under G_2. Under $SU(2)_L \times SU(2)_R$, the $\mathbf{7} = (\mathbf{2},\ \mathbf{2}) \oplus (\mathbf{3},\ \mathbf{1})$, while the $\mathbf{27} = (\mathbf{5},\ \mathbf{1}) \oplus (\mathbf{4},\ \mathbf{2}) \oplus (\mathbf{3},\ \mathbf{3}) \oplus (\mathbf{2},\ \mathbf{2}) \oplus (\mathbf{1},\ \mathbf{1})$. The LH quark can therefore mix with both doublets in these representations, the degree of mixing being denoted γ (following the notation of the last section). An explicit construction of such embedding Λ_L can be found in Ref. [171].

As before, we have freedom to choose γ such that Φ is CP-odd. In this case, the trilinear coupling to the Higgs boson in equation 110 automatically vanishes (assuming CP is preserved in the Higgs sector) and the renormalizable potential becomes accidentally $\mathbb{Z}_2$ symmetric:

$$\begin{aligned} V^{\mathbf{35}\oplus\mathbf{1}} &= c_1 f^4 \left|\left(\Lambda^I_{L,D}\right)_{88}\right|^2 + c_2 f^4 \left|\left(\Lambda^I_{L,D}\right)_{m8}\right|^2 \\ &= \mu_H^2|H|^2 + \lambda_H|H|^4 + \frac{1}{2}\mu_\Phi^2|\Phi|^2 + \frac{1}{4}\lambda_\Phi|\Phi|^4 + \lambda_{H\Phi}|H|^2|\Phi|^2\,, \end{aligned} \tag{123}$$

where the dressed spurion is $\Lambda^I_{L,D} = U^{-1}\Lambda^I_L U$, $m = 1, \ldots, 7$ and we have traded the two UV constants $c_{1,2}$ by the Higgs mass and its quartic coupling. Therefore, $V(\Phi)$ can be entirely determined up to $(\gamma,\ f)$. In particular, for $\gamma \to 0$, the triplet mass reads $\mu_\Phi^2 \approx \frac{2}{3} f^2 \lambda_H$ which can be naturally at the EW scale; moreover, $\mu_\Phi^2 > 0$ and $\lambda_{H\Phi} > 0$ guarantee that the triplet VEV is $\langle\Phi\rangle = 0$.

In this limit, the neutral component of the triplet is stable and hence a potential DM candidate. Since it is charged, the DM in this scenario annihilates sizably into the EW gauge bosons; to account for the relic abundance, a large new physics scale is therefore required, $f \sim 9$ TeV [171].

The accidental $\mathbb{Z}_2$ symmetry in the renormalizable Lagrangian is the reason why the triplet model is basically inert. On the other hand, the effective operators — arising from integrating the composite resonances out — change drastically the phenomenology. To clarify this point, we compute the Yukawa Lagrangian

$$\mathcal{L}_{\text{yuk}} = f y_{\alpha\beta} \overline{q_L}^\alpha_I \left(\Lambda^I_{L,D}\right)^\dagger_{88} u_R^\beta + \text{h.c.} = y^q_{\alpha\beta} \overline{q_L}^\alpha \tilde{H} \left[-1 + \mathrm{i}\gamma \frac{\Phi}{f} + \ldots \right] u_R^\beta + \text{h.c.}\,; \tag{124}$$

analogously for the down sector. This matches equation 111 with $c_\kappa = \mathrm{i}\gamma y$. The product of the doublet with the triplet $\mathbf{2}_{-1/2} \times \mathbf{3}_0 = \mathbf{2}_{-1/2} \oplus \mathbf{4}_{-1/2}$ under G_{EW}. Therefore, identifying the triplet components with $\Phi = (\phi^+, -\phi^0, \phi^-)^T$, we can write the resulting doublet as

$$\tilde{H}\Phi = \begin{pmatrix} \phi_0 h_0^* - \sqrt{2}\phi^+ h^- \\ \phi_0 h^- - \sqrt{2}\phi^- h_0^* \end{pmatrix}. \tag{125}$$

(In the down sector, $H\Phi$ reads as above upon the replacements $h_0^* \to h^+$ and $h^- \to -h_0$.) As such, in the unitary gauge after EWSB, we obtain:

$$\mathcal{L}_{\text{yuk}} \supset \frac{v}{\sqrt{2}} \frac{\gamma}{f} \left\{ \mathrm{i} y^t \phi_0 \bar{t}\gamma_5 t - \mathrm{i} y^b \phi_0 \bar{b}\gamma_5 b - \left[\sqrt{2}\mathrm{i}\phi^- \bar{b}(y^t P_R + y^b P_L) t + \text{h.c.} \right] \right\}. \tag{126}$$

The triplet components can therefore decay promptly at colliders, for natural values of the new physics scale.

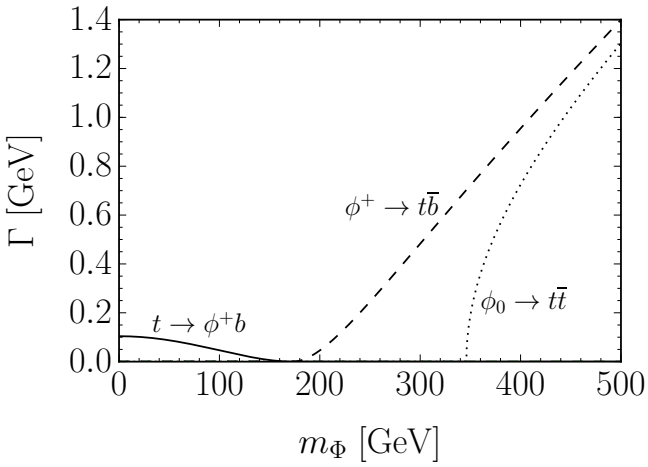

Figure 9: Partial decay widths of the different heavy particles in the triplet model. We set $f = 1$ TeV.

5.2.2 Collider signatures

The renormalizable Lagrangian of the triplet model is subject to several constraints. Bounds from LEP, using $\sqrt{s} = 209$ GeV data, have excluded triplet masses $\lesssim 100$ GeV [199]; we therefore restrict our analysis to the $]100,\ 500]$ GeV mass range.

The quartic interaction between the triplet and the Higgs boson triggers $h \longrightarrow \gamma\gamma$ at the loop level. The corresponding decay width reads:

$$\Gamma(h \to \gamma\gamma) = \frac{\alpha_{\text{em}}^2 m_H^3}{1024\pi^3}\left\{\frac{2}{v}\left[A_1(\tau_W) + \frac{4}{3}A_{1/2}(\tau_t)\right] + \lambda_{H\Phi}\frac{v}{m_\Phi^2}A_0(\tau_\Phi)\right\}^2, \tag{127}$$

with $\alpha_{\text{em}} = e^2/4\pi$ and $\tau_i = 4m_i^2/m_H^2$. The loop functions, as well as the explicit calculation of the scalar contribution, are detailed in appendix B. We denote by m_Φ the triplet mass which is $m_\Phi^2 = \mu_\Phi^2 + \lambda_{H\Phi}v^2/2$ at tree level. The last combined measurement of this decay performed by the ATLAS and the CMS collaborations gives $\Gamma(h \to \gamma\gamma)/\Gamma(h \to \gamma\gamma)_{\text{SM}} = 1.14^{+0.19}_{-0.18}$ [200]. Values of $\lambda_{H\Phi} \gtrsim 2\ (6)$ are consequently excluded for $m_\Phi \sim 200\ (300)$ GeV.

Furthermore, equation 126 triggers triplet decays into $\bar{q}q$ final states. Likewise, for $m_t > m_\Phi$, the top quark can decay into the triplet and a b quark. The corresponding decay widths read:

$$\Gamma\left(\phi_0 \to \bar{q}q\right) = \frac{3(y_q)^2 v^2}{16\pi}\frac{\gamma^2}{f^2}m_\phi\sqrt{1 - \frac{4m_q^2}{m_\phi^2}}\,; \tag{128}$$

$$\Gamma\left(\phi^+ \to \overline{q'}q\right) = 3\frac{(y_q)^2 + (y_{q'})^2}{16\pi}\frac{\gamma^2 v^2}{f^2}m_\phi\left[1 - \frac{m_q^2}{m_\phi^2}\right]^2\,; \tag{129}$$

$$\Gamma\left(t \to \phi^+ b\right) = \frac{(y_b)^2 + (y_t)^2}{32\pi}\frac{\gamma^2 v^2}{f^2}m_t\left[1 - \frac{m_\phi^2}{m_t^2}\right]^2. \tag{130}$$

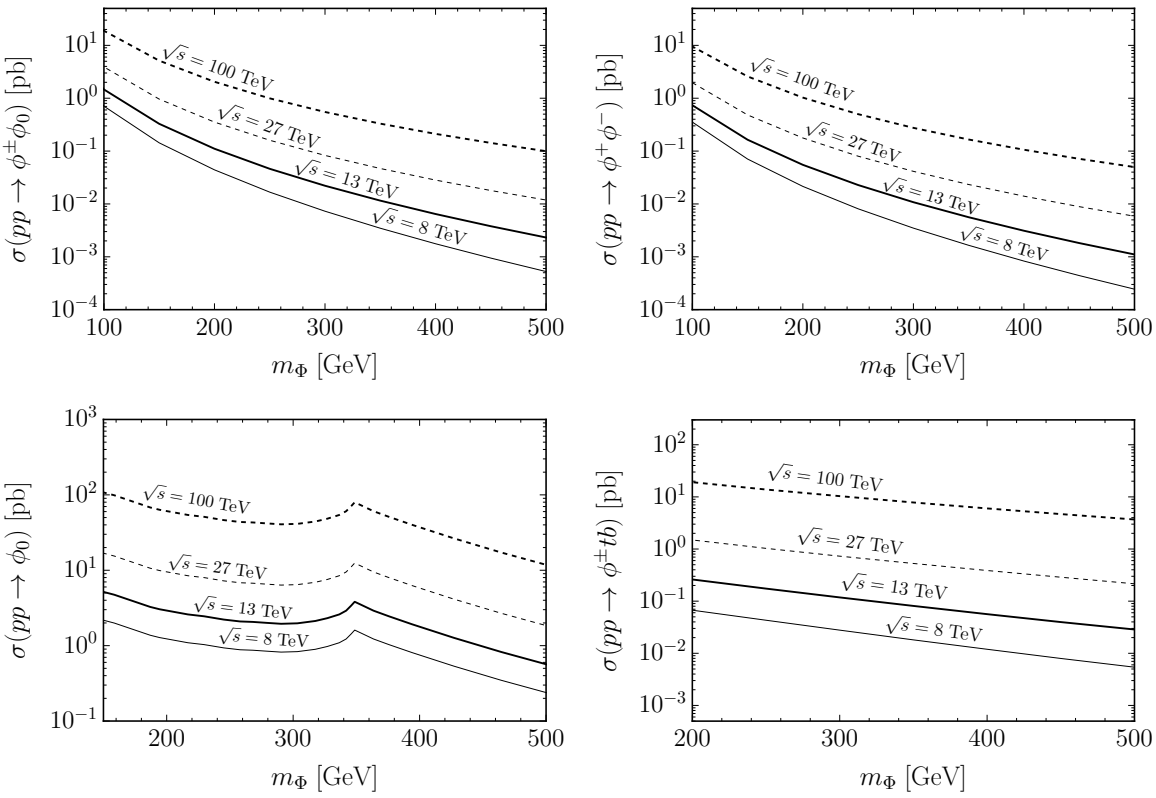

Figure 10: Single and pair-production cross section of the scalar triplet at pp colliders, in different production modes, as obtained with `MadGraph`. The different lines in the plots refer to different c.m.e., assuming $\gamma/f = 1\ \text{TeV}^{-1}$. The production cross section of ϕ_0 via gluon fusion was obtained by rescaling the results in Ref. [201], at $\sqrt{s} = 13$ TeV. To estimate the cross sections for other c.m.e., we computed the corresponding ratio by implementing the `ggHFullLoop` model in `MadGraph`.

In the second equation, we assumed $m_q \gg m_{q'}$, which holds if the former is a c or t quark and the latter a s or a b quark. Partial widths as a function of m_Φ are depicted in figure 9. Had we assumed also CP violation interactions, the trilinear coupling $\sim \kappa H^\dagger \Phi H$ would allow the triplet to gain a VEV $v' \sim \kappa v^2/m_\Phi^2$. The latter modifies the ρ-parameter and is therefore constrained to be $v' \lesssim$ GeV [202]. Therefore, $\Gamma(\phi^0 \to hh) \sim \kappa^2/m_\Phi$ would still be subdominant with respect to $\Gamma(\phi \to \bar{q}q)$ even for $f \sim 10$ TeV.

The effective couplings, entering in the expressions above, are constrained by several searches at pp colliders. To recast such constraints, we have obtained the signal cross section at $\sqrt{s} = 8$ and 13 TeV for different triplet masses; for purposes of illustration and future sensitivity studies, we also plot in figure 10 the results for $\sqrt{s} = 27$ and 100 TeV. The leading diagrams contributing to the triplet production are represented in figure 11.

The list below summarizes the main searches which constrain the parameter space of this model, defining each colored region in figure 12:

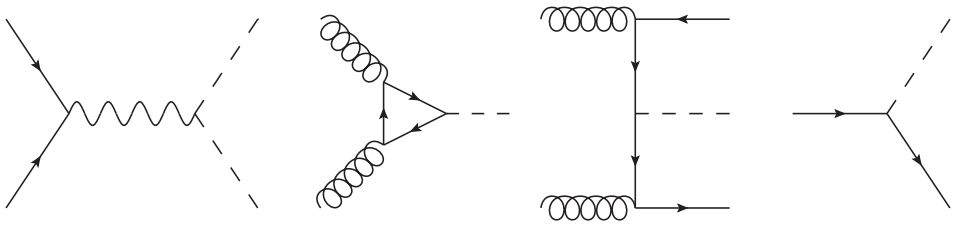

Figure 11: Representative diagrams of the main production mechanisms of the triplet at pp colliders. The diagrams from left to right correspond to: pair production via EW currents; single production via gluon fusion; production in association with $t\bar{b}$ ($\bar{t}b$); and prodcution from the decay of a top quark.

- **In blue:** Searches looking for $\bar{b}b$ or $\bar{t}t$ resonances constrain the ϕ_0 interaction. The production cross section of the neutral component is dominated by gluon fusion processes, since the Drell-Yann production is suppressed by the small $\left(y_q v/f\right)^2$ factor. For $m_\Phi < 2m_t$, the most constraining search up to date was performed by the CMS collaboration [203]. The limits obtained with $L = 35.9\,\text{fb}^{-1}$ of data at $\sqrt{s} = 13$ TeV exclude the region enclosed by the solid blue line. At the HL-LHC, it is expected that such limits become a factor of $\sqrt{L'/L} = \sqrt{3\,\text{fb}/35.9\,\text{ab}} \sim 9$ stronger. In this case, the region enclosed by the dashed blue line could be excluded. There are no resonant searches probing directly the $m_\Phi > 2m_t$ regime.

- **In green:** Searches for an EW resonance produced in association with a top and a bottom quarks are sensitive to $\phi^\pm$. For $m_\Phi > m_t$, the most constraining and recent study was published by the ATLAS collaboration [204], using $L = 36.1\,\text{fb}^{-1}$ of data collected at $\sqrt{s} = 13$ TeV. The corresponding limits on $\sigma(pp \to tb\phi^\pm) \times \mathcal{B}(\phi^\pm \to tb)$ constrain the region enclosed by the solid green line. With the enhancement of the luminosity, cross sections ~ 0.1 times smaller could be tested at the HL-LHC; the region delimited by the dashed green line could be correspondingly excluded if no deviations from the SM are observed.

- **In red:** Searches for exotic decays of the top quark also constrain the model for $m_\Phi < m_t$. In particular, CMS carried a search for $t\bar{t}$ production with $t \to \phi^\pm b, \phi^\pm \to \overline{q'}q$ at $\sqrt{s} = 8$ TeV and with $L = 19.7\,\text{fb}^{-1}$ [205], setting an upper bound on $\mathcal{B}(t \to \phi^\pm b, \phi^\pm \to jj) \lesssim 0.01$–$0.02$ for $m_\Phi \sim$ 100–160 GeV. Using equation 128, we converted this constraint into a bound on the $(m_\Phi, \gamma/f)$ plane. The region enclosed by the solid red line is consequently excluded. The dashed red line delimits the parameter space that could be tested at the HL-LHC.

The scalar triplet can be also pair-produced via EW charged currents (CCs), $pp \to W^{\pm(*)} \to \phi^\pm\phi_0$, as well as via neutral currents (NCs), $pp \to Z/\gamma \to \phi^+\phi^-$. Provided that Φ decays promptly, the cross section of these processes is independent of γ/f in good approximation.

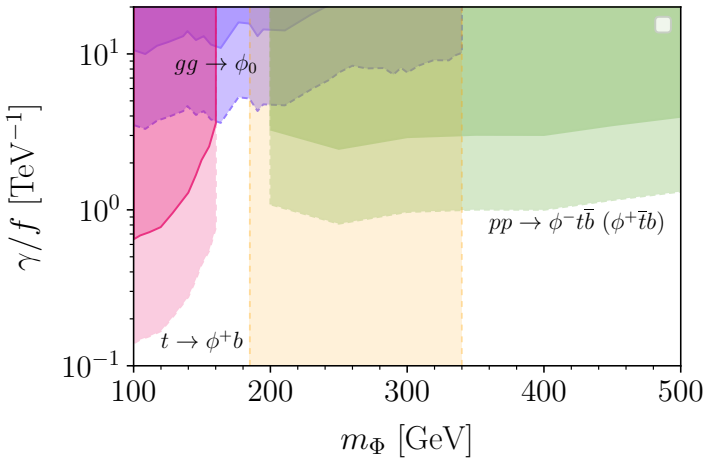

Figure 12: Current (solid) and future (dashed) collider bounds on the triplet Yukawa coupling, as a function of the triplet mass; see the text for details. The vertical orange band could be tested at the HL-LHC using our proposed analysis.

For $m_\Phi < m_t$, the charged and neutral triplet components decay mainly into $\overline{q'}q$ and $\bar{b}b$ final states, respectively. Searches for di-jet resonances could therefore be sensitive to this regime, the most constraining one being presented in Ref. [206]. The pair of quarks from each resonance is typically very collimated and can be reconstructed as a single jet. As such, both two- and four-jet signatures were considered in the analysis, the latter relying on advanced techniques to explore the sub-structure of jets. The upper limits on the cross section, obtained with 35.9 fb^{-1} of data collected at $\sqrt{s} = 13$ TeV, range from ~ 170 pb $(100\,\text{GeV})$ to ~ 20 pb $(170\,\text{GeV})$. No parameter space of the model is therefore constrained by this search; see figure 10. At the HL-LHC, cross sections ~ 0.1 times smaller could be probed; still, this analysis would be basically insensitive to our model.

For $m_t < m_\Phi < 2m_t$, the NC process produces more commonly a $\bar{t}bt\bar{b}$ final state. The CMS search at $\sqrt{s} = 8$ TeV presented in Ref. [207] could potentially probe this channel. Knowing the enhancement of the signal and background cross sections with the c.m.e., we projected these limits for the current run of the LHC. Again, we found that no region of the parameter space is or could be constrained at the HL-LHC. Likewise, the CC produces a $\bar{b}b\bar{t}b(t\bar{b})$ final state; to the best of our knowledge, there are however no dedicated searches for this process.

For $m_\Phi > 2m_t$, the CC leads to $\bar{t}t\bar{t}b(t\bar{b})$ instead, which no dedicated search currently available can probe. The lack of sensitivity to these final states has been also pointed out in Ref. [208]. The uncolored pair production of new physics that decays back into the SM is specially difficult for the LHC due to the small signal cross section and similarity with the backgrounds. Furthermore, as discussed by the authors, 13 TeV model-specific searches are set towards more massive resonances, making generic searches for multiple fermions with no beyond the SM source of large p_T or MET rarer at the present LHC run, in comparison to similar studies performed at 8 TeV.

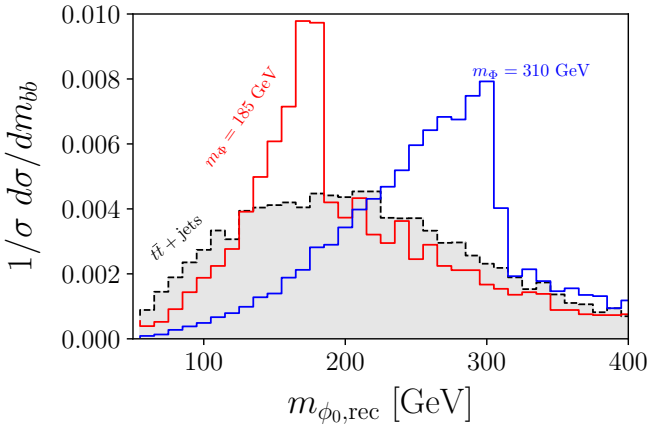

Figure 13: The mass distribution of the reconstructed neutral component of the triplet in the analysis proposed for $pp \to \phi^\pm\phi^0 \to t\bar{b}(\bar{t}b)b\bar{b}$. The solid red and blue lines correspond, respectively, to the signal for $m_\Phi = 185$ and 310 GeV; in comparsion, the main background distribution is represented by the dashed black line.

We therefore propose a new dedicated analysis to test the triplet model at the LHC, aiming to overcome the large gap on the parameter space left by the experimental searches. We focus on pair production sourced by the EW CCs, leading to $pp \to \phi^\pm\phi^0 \to t\bar{b}(\bar{t}b)b\bar{b}$, and consider only leptonic decays of the top quark.

5.2.3 New analysis at the LHC

Signal and background events are generated following the procedure described in section 3.3. The main backgrounds are $t\bar{t}$ + jets, $t\bar{t}b\bar{b}$, $t(\bar{t}) + 3b$ and $W + 4b$. Jets are defined using the anti-k_T algorithm with $R = 0.4$. At the reconstruction level, a lepton is considered isolated if the hadronic energy within a cone of radius $R = 0.3$ is smaller than 10 % of the lepton p_T.

We require exactly one isolated lepton with $|y| < 2.5$ and $p_T > 15$ GeV, as well as at least four jets with $p_T > 30$ GeV. The longitudinal component of the missing neutrino is reconstructed as described in section 5.1.3. The neutrino and lepton four-momenta are then added to the jet which gives a total invariant mass closest to m_t; the invariant mass of the reconstructed top being denoted m_t^{rec}. The latter is required to be within $|m_t^{\mathrm{rec}} - m_t| < 50$ GeV. Three b-tagged jets are also required to be found among those not coming from the leptonic top. To assign these jets to ϕ_0 and $\phi^\pm$, all combinations are computed and that minimizing $|m_{\phi_0}^{\mathrm{rec}} - m_{\phi^\pm}^{\mathrm{rec}}|$ is chosen; with m_ϕ^{rec} denoting the invariant mass of the scalar candidates. The normalized distribution of $m_{\phi_0}^{\mathrm{rec}}$ in the main background and two signal BPs is depicted in figure 13. The reconstructed masses of ϕ_0 and $\phi^\pm$ are subsequently required to be no more than 50 GeV away from each other. Finally, all events must satisfy $|m_{\phi_0}^{\mathrm{rec}} - m_{\phi_0}| < 30$ GeV and $|m_{\phi^\pm}^{\mathrm{rec}} - m_{\phi^\pm}| < 40$ GeV.

The cut-flows for the signal and background are given in Ref. [3]. Knowing the final number of events that survived the selection cuts, the experimental sensitivity can be estimated following equation 37. We

have obtained that $\mathcal{S}$ ranges from $2.7 - 4.3$, for $m_\Phi \in [185, 340]$ GeV, at the HL-LHC. These values are conservative, as the reconstruction relies on inclusive cuts with large mass windows and no matching procedure in the generation of the background sample is applied. Still, by performing this dedicated analysis, the entire mass interval $m_t < m_\Phi \lesssim 2m_t$ could be probed at the next luminosity phase of the LHC. This corresponds to the region enclosed by the dashed orange line in figure 12.

5.2.4 The electroweak phase transition

In this section, we focus on the implications of the presence of the exotic triplet in the past high-temperature history of our Universe. In particular, the renormalizable interactions between this scalar and the Higgs boson introduce significant corrections to the one-loop effective potential:

$$V(h, \phi_0) = V_{\text{tree}} + \Delta V_{\text{CW}} + \Delta V_T \ + C\,, \tag{131}$$

where C is a constant that cancels $V(0,0)$ and V_{tree} stands for the tree level potential. The one-loop correction to V_{tree} at zero temperature, ΔV_{CW}, is explicitly computed in appendix C.1 for a scalar field theory. Generalizing equation 379 to include loops of other types of fields leads to [209]:

$$\Delta V_{\text{CW}} = \frac{1}{64\pi^2} \sum_i (\pm) n_i m_i^4 \left[\log \frac{m_i^2}{v^2} - c_i \right], \tag{132}$$

where i runs over all bosons (+) and fermions (–). The n_i factor denotes the $d.o.f.$ of each field, while c_i is $5/6$ for gauge bosons and $3/2$ otherwise. On the other hand, the finite temperature corrections ΔV_T read:

$$\Delta V_T = \frac{T^4}{2\pi^2} \sum_i (\pm) n_i \int_0^\infty y^2 \log \left[1 \mp e^{-\sqrt{\frac{m_i^2}{T^2} + y^2}} \right]. \tag{133}$$

Similarly to the previous case, we derive the contribution from only scalar fields in appendix C.2. The field-dependent masses entering in the equations above are:

$$m_W^2 = \frac{1}{4} g^2 (h^2 + 4\phi_0^2)\,, \tag{134}$$

$$m_Z^2 = \frac{1}{4} (g^2 + g'^2) h^2\,, \tag{135}$$

$$m_{G^{0,\pm}}^2 = -\mu_H^2 + \lambda_H h^2 + \frac{1}{2} \lambda_{H\Phi} \phi_0^2\,, \tag{136}$$

$$m_{\phi^\pm}^2 = \mu_\Phi^2 + \frac{1}{2} \lambda_{H\Phi} h^2 + \lambda_\Phi \phi_0^2\,, \tag{137}$$

$$m_t^2 = \frac{1}{2} y_t^2 h^2\,, \tag{138}$$

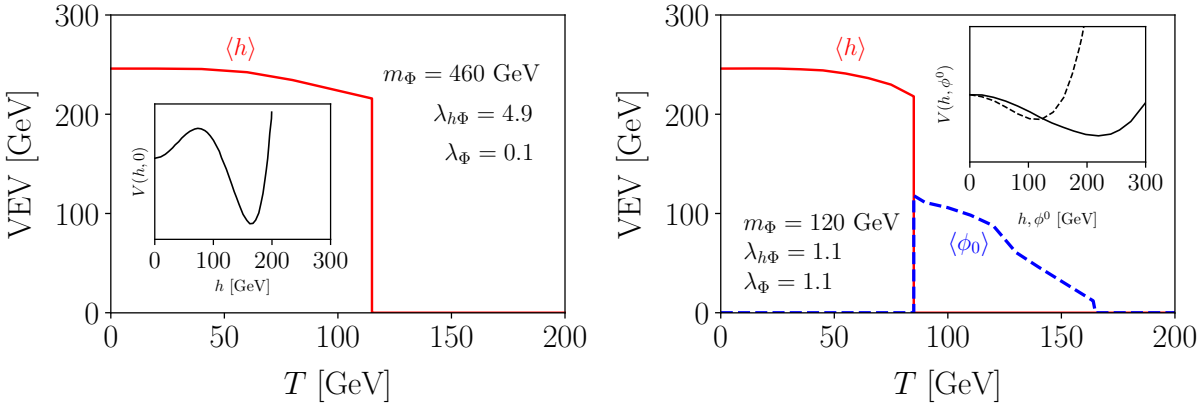

Figure 14: (Left) The scalar VEV as a function of the temperature, for a given point in the parameter space. At high temperatures, the potential is EW symmetric. At $T = 115$ GeV, the Higgs field develops a VEV, while $\langle\phi_0\rangle$ vanishes for all T. This illustrates a one–step EW PT. In the small window, the shape of the scalar potential at this specific temperature is also shown. (Right) The same as before, for a parameter space point leading to a two–step EW PT. The first symmetry breaking transition $(\langle h\rangle\langle\phi_0\rangle) = (0,0) \longrightarrow (0,10)$ GeV occurs at $T \sim 160$ GeV, evolving until $T \sim 85$ GeV. At this point, the second PT takes place, with $(0,120) \longrightarrow (220,0)$ GeV.

in addition to the physical scalar masses, obtained from diagonalizing the mixing matrix

$$\mathcal{M}^2 = \begin{bmatrix} -\mu_H^2 + 3\lambda_H h^2 + \frac{1}{2}\lambda_{H\Phi}\phi_0^2 & \lambda_{H\Phi} h\phi_0 \\ \lambda_{H\Phi} h\phi_0 & \mu_\Phi^2 + 3\lambda_\Phi\phi_0^2 + \frac{1}{2}\lambda_{H\Phi} h^2 \end{bmatrix} . \tag{139}$$

In the following computation of the potential, we take m_Φ, $\lambda_{H\Phi}$ and λ_Φ as input parameters. The remaining ones, namely μ_H^2, μ_Φ^2 and λ_H, are obtained numerically after requiring that the $T = 0$ potential has a minimum

$$\left.\frac{\partial V}{\partial h}\right|_{(v,0)} = 0\,, \quad \text{where} \quad \left.\frac{\partial^2 V}{\partial h^2}\right|_{(v,0)} = m_H^2 \quad \text{and} \quad \left.\frac{\partial^2 V}{\partial \phi_0^2}\right|_{(v,0)} = m_\Phi^2\,.$$

At tree level, $(v,0)$ is guaranteed to be an extreme provided that $\lambda_\Phi, \lambda_{H\Phi} > 0$ and $\mu_\Phi^2 > -1/2v^2\lambda_{H\Phi}$.

At high temperatures, the effective potential is EW symmetric. As the Universe cools down, a PT occurs as the potential develops a new minimum which becomes energetically more favorable. In the SM, the EW PT occurs smoothly, through a crossover. (The classification of PTs is discussed in appendix C.3.) However, the new $d.o.f.$ modify the transition of $\langle h\rangle = 0 \longrightarrow \langle h\rangle = v_c$ which can become first order, producing a barrier between the symmetric and non-symmetric vacuum states. We denote by T_c the critical temperature at which the Higgs first order PT occurs, that is when these two minima are degenerate; correspondingly, $v_c \equiv v(T = T_c)$. One example of such transition is given in the left panel of figure 14.

Furthermore, if the EW triplet also develops a VEV, the first order PT can proceed in two-steps:

$$\left(\langle h\rangle, \langle\phi_0\rangle\right) = (0,0) \xrightarrow{T_1} \left(\langle h\rangle, \langle\phi_0\rangle\right) = (0,\ v_c') \xrightarrow{T_2<T_1} \left(\langle h\rangle, \langle\phi_0\rangle\right) = (v_c,\ 0)\,, \tag{140}$$

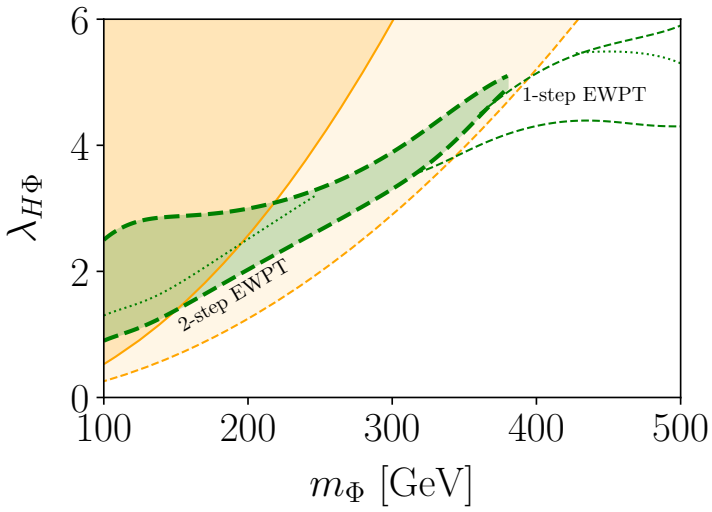

Figure 15: Complementarity between collider and GW searches in the $(m_\Phi, \lambda_{H\Phi})$ plane. In the region enclosed by the two dashed green lines, the EW PT is strongly first order; the nature of the strongest PT is also labeled. Within this region, the dotted line delimits the area which could be potentially tested at Laser Interferometer Space Antenna (LISA). On the other hand, the region enclosed by the solid (dashed) orange line is (could be) excluded by current (future) measurements of the partial decay width of the Higgs to di-photons; see equation 127.

as depicted in the right panel of figure 14.

Phenomenologically, it is of interest when such first order PT is strong, that is, when $v_c/T_c > 1$. This condition is fulfilled in the region enclosed by the dashed green line in figure 15. The nature of the strongest PT is also labeled. Superimposed in orange is the region which can be excluded at the 95% CL by the measurement of $h \longrightarrow \gamma\gamma$; see equation 127. The expectation at the HL-LHC is that ratios outside the range $\Gamma(h \longrightarrow \gamma\gamma)/\Gamma(h \longrightarrow \gamma\gamma)_{\text{SM}} = 1.0 \pm 0.1$ will be excluded [210]. Translating this bound into the $(m_\Phi,\ \lambda_{H\Phi})$ plane, we find that the region enclosed by the dashed orange line could be entirely probed.

In figure 15, we find a non-negligible region where a strong two-step EW PT can occur. Its curved shape is mostly due to two facts. First, the triplet squared-term is $\sim \mu_\Phi^2 + T^2$, which cannot be negative for $\mu_\Phi^2 > 0$; therefore, the two-step PT can only occur if the triplet minimum exists already at $T = 0$. For a fixed m_Φ, this is realized above $\lambda_{H\Phi}^{\text{min}} = 2m_\Phi^2/v^2$ at tree level. Second, the potential at the triplet minimum, $V(0, \langle\phi_0\rangle) \sim -|\mu_\Phi|^4/\lambda_\Phi$, cannot be deeper than the Higgs one. This requirement can be translated into a $\lambda_{H\Phi}^{\text{max}}$ above which the theory is unstable.

5.2.5 Astrophysical signatures

During a first order PT, the Universe evolves from the false to the true vacuum via thermal tunneling at finite T. This process can be understood in terms of the formation of spherical bubbles of the broken phase in the sea of the old vacuum which eventually spread throughout the whole Universe. The tunneling

probability per unit time per unit volume is given by [211]

$$\mathcal{P} \sim T^4 e^{-S_3/T}\,, \tag{141}$$

where S_3 is the three-dimensional euclidean action of the field that describes the bubble solution. In the *thin-wall* bubble limit, the spherically symmetric configuration has a well defined interior of radius R, separated from the exterior by a wall of thickness $L \ll R$, such that it can be divided in three regions: the inside, the outside and the bubble wall. Within this approximation [212],

$$S_3 \sim 4\pi\sigma R^2 - \frac{4\pi}{3}\epsilon R^3\,, \tag{142}$$

where σ and ϵ are, respectively, the surface tension and the potential energy difference between the outside and the inside of the bubble, *i.e.* between the metastable and true minima. There is therefore a critical radius $R_c = 2\sigma/\epsilon$, obtained by extremizing the action, below which the surface tension dominates and the bubble shrinks. Therefore, only bubbles with $R > R_c$ are large enough to grow after formation. The onset of the phase transition at $T = T_n$ is characterized by the nucleation of one bubble per horizon volume on average, which corresponds to [213]

$$\frac{S_3}{T_n} \sim \mathcal{O}(100)\,, \tag{143}$$

for EW-scale PTs.

There are two parameters constructed out of the quantities presented above which characterize the PT: the normalized vacuum energy density (α) that is released, and its duration time (β^{-1}) . They are defined as:

$$\alpha \equiv \frac{\rho_{\text{vac}}}{\rho_{\text{rad}}} \sim \frac{\epsilon(T_n)}{35T_n^4} \quad \text{and} \quad \frac{\beta}{H(T_n)} = T_n \frac{\partial}{\partial T}\frac{S_3}{T}\Big|_{T_n}\,, \tag{144}$$

where $\rho_{\text{rad}} = \pi^2 g_* T^4/30$ is the energy density during radiation era, with g_* denoting the number of effective $d.o.f.$, and $H \sim \sqrt{g_*}T^2/M_P$ is the Hubble parameter. The larger α and β^{-1} are, the stronger the PT.

It is a well known result that the collision of the bubbles (destroying their spherical symmetry) and the effects in the cosmic fluid resulting from its propagation (leading, for instance, to turbulence in the plasma) produce a stochastic GW spectrum [214]. This signal can be observed by long-baseline experiments using interferometry, such as LIGO [215] or the future LISA [216]. The spectrum of GWs from EW first order PTs typically peaks at the milliHertz range [217] and is therefore only accessible by the latter.

LISA is planned to start operating in about ten years, so technical details have not yet been finalized; as such, the predictions for detecting a given new physics model are not ultimately robust. LISA Pathfinder [218] was launched to space in 2015 as a proof-of-concept to test the signal to background ratio; the mission was successfully completed two years later, finding that the noise levels were even smaller than the required to achieve the experimental goals. The most promising configuration properties of the

apparatus is called "C1", consisting on a five million km arm length, an exposure of five years and noise levels corresponding to what was expected to be found by the LISA Pathfinder [217]. We will study the sensitivity of the triplet model considering this configuration definitions.

The PT parameters α and β can be computed using `CosmoTransitions` [219], which takes as input the tree level potential and the field-dependent particle spectrum. Knowing these parameters, we have used appendix A in Ref. [217] to check which (α, β) points, for $T_n \sim 100$ GeV, could be constrained by LISA under the assumptions that the wall velocity is close to 1 (in good approximation for strong PTs) and that the effects of long-lasting waves are negligible. Under these criteria, the region of the parameter space that could be potentially probed by this experiment lies above the green dotted line in figure 15.

5.2.6 Baryogenesis at the electroweak scale

In a significant region of the testable parameter space, the triplet model fulfills the necessary conditions for baryogenesis, which became known as the three Sakharov conditions [2]. We summarize them below, focusing on the ingredients which are insufficient in the SM but can be supplied by the new interactions with the exotic field.

1. Baryon number violation: Interactions violating baryon number exist in the SM, since B and L are anomalously violated in weak interactions; see equation 16.

2. C and CP violation: These symmetries are also violated in the EW theory, due to the presence of the complex phase in the CKM matrix. This effect is too small to explain the observed baryon asymmetry [31]. However, extra CP violation can be attained while the CP-odd triplet develops a VEV.

3. Departure from thermal equilibrium: This condition is absent in the SM, since the EW PT occurs through a crossover. In the SM extended with Φ, this PT can become first order, so that the baryon number violating interactions are out-of-equilibrium in the bubble walls.

In appendix D, we discuss the need for each of these conditions in detail. In particular, we discuss the nature of the SM solutions that violate baryon number. Altough they are completely negligible at present, they could have been sizable at high temperature as shown in equations 391 and 392, describing the rate of B-violating interactions by sphaleron fields. In the presence of these fields, baryogenesis during a first order PT might have proceeded as follows.

According to equation 391, $\Delta B \neq 0$ processes are unsuppressed at high T and occur instantly in the symmetric phase of the Universe, therefore being able to create a net of baryon charge. If there are interactions violating CP at the bubble wall, this excess can migrate to the interior of the bubble. There, the rate of sphaleron transitions can be strongly suppressed, which avoids the washing out of this asymmetry. Using equation 392, this requires $v_c/T_c \gg 1$, which is exactly the condition we used before to define a strong PT.

In our model, CP is indeed violated spontaneously during the second transition in the two–step case, where both ϕ_0 and h change VEV, generating a complex phase in the quarks mass:

$$m_t = \frac{v}{\sqrt{2}} y_t \left[1 + \mathrm{i}\gamma \frac{v'}{f} \right] \equiv |m_t| e^{i\theta(t)} \ . \tag{145}$$

At $T = 0$, this phase can be removed by a redefinition of the top quark and is therefore unphysical. However, during the PT, θ changes with time and therefore cannot be rotated away. The variation of this parameter is fixed by the the baryon-to-entropy ratio that we observe today [220],

$$\eta_s \equiv \frac{n_B}{s_E} \sim 10^{-10} \ , \tag{146}$$

where s_E is the entropy density. Since the total entropy $S_E = a^3 s_E$ is conserved in the expanding Universe, a denoting the scale factor, the number of baryons in a comoving volume can be written as $N_B = a^3 n_B \propto n_B / s_E$. Therefore, after particle freeze-out, this ratio remains constant.

In related models [98], it was found that the variation $\Delta\theta(t)$ needed to reproduce equation 146 requires that $\gamma \Delta v / f \gtrsim 0.1$, where Δv is the change in VEV during the EW PT. In our framework, Δv can be easily $\gtrsim 100$ GeV (see figure 14); therefore, baryogenesis can be explained with $\gamma / f \sim 1\,\mathrm{TeV}^{-1}$.

There is just one complication left to deal with: while the triplet has a non-vanishing VEV, the $\mathbb{Z}_2$ symmetry of the potential is broken spontaneously; consequently, causally disconnected regions in the Universe can end up in either the $+v'$ or $-v'$ vacuum. To go across these regions, the field must take the value of zero somewhere, which is not a minimum of the potential. Since this solution cannot be continuously deformed into the true vacuum, a topological defect is formed. The type of defect that is formed is determined by the vacuum manifold; In this case, it has a two-fold degeneracy, so a domain wall is produced.

Domain walls are problematic because, if existent, they dominate the energy density of the Universe. Since this is not observed, new physics models producing such defects face strong bounds. However, the temperature at which domain walls start dominating is well below the typical temperatures of the EW PT [98], after which the symmetry along the Φ direction is restored. Still, if different patches of the Universe end up lying in oppositely charged vacua $\pm v'$, some regions could produce an excess of baryons, while others an excess of anti-baryons, resulting in an overall zero baryon charge.

This can be avoided if there exists a small CP-breaking term in the potential $\sim \kappa H^\dagger \Phi H$ which can generate, via loop effects, a shifting between the two minima of the order $\Delta V \sim \kappa T^3 / (4\pi)^2$. As a result, there will be a pressure acting on the critical bubbles characterizing the triplet PT to collapse the regions where the field develops the higher-energy value. A sufficient condition for these regions to vanish at the time of the EW PT is $\Delta V / T_n^4 \gg H / T_n \sim 10^{-16}$ [98], where $1/H$ is the Hubble radius. This is satisfied for a very small $\kappa \gtrsim 10^{-12}$ GeV.

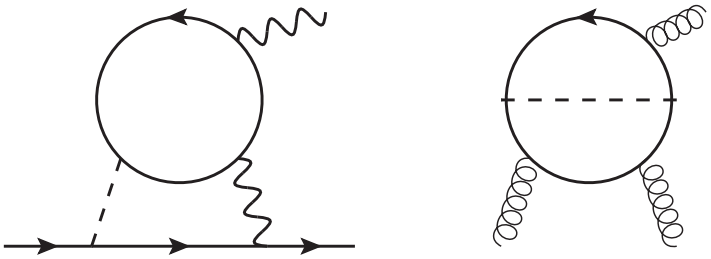

Figure 16: The main contributions to the EDMs of the electron (on the right) and of the neutron (on the left), arising in our model.

5.2.7 CP violation constraints

In spite of being very small, the CP violating coefficient is strongly constrained by measurements of the neutron and electron EDMs. They arise due to the mixing between H and Φ after EWSB.

Indeed, when the Higgs boson gains a VEV, the physical Yukawa couplings develop a small imaginary component:

$$y^{\psi}\left[h\bar{\psi}\psi + \mathrm{i}v\frac{\gamma}{f}\phi_0\bar{\psi}\gamma^5\psi\right] \longrightarrow y^{\psi}h^{\mathrm{phy}}\left[c_\theta\bar{\psi}\psi - \mathrm{i}s_\theta v\frac{\gamma}{f}\bar{\psi}\gamma^5\psi\right] + \dots\,, \tag{147}$$

where the dots include other interactions of the triplet in the mass basis and $s_\theta \sim \kappa v/m_\Phi^2$ is the sine of the scalar mixing angle. The latter is small, so $c_\theta \sim 1$ in good approximation.

The main contribution to the electron EDM is a two-loop process, as that depicted in the left panel of figure 16. Plugging the relevant parameters in equation 16 of Ref. [221], we obtain:

$$\left|\frac{d_e}{e}\right| \sim \frac{\alpha_{\mathrm{em}}v^2\gamma}{6\pi^3 m_t f}y_t\frac{\kappa y_e}{m_\Phi^2}\left[f(m_t^2/m_H^2) + g(m_t^2/m_H^2)\right], \tag{148}$$

with

$$f(z) = \frac{1}{2}z\int_0^1 \frac{1-2x(1-x)}{x(1-x)-z}\log\frac{x(1-x)}{z}dx\,; \tag{149}$$

$$g(z) = \frac{1}{2}z\int_0^1 \frac{1}{x(1-x)-z}\log\frac{x(1-x)}{z}dx\,. \tag{150}$$

For the values of $(\gamma/f, \kappa)$ compatible with baryogenesis, the model prediction is much smaller than the latest bound, $|d_e| \sim 10^{-42}$ e cm versus $|d_e| < 1.1\times10^{-29}$ e cm [181].

On the other hand, the neutron EDM arises mainly from the running of the diagram on the right panel of figure 16. Using equation 29 in Ref. [222], we find:

$$\left|\frac{d_n}{e}\right| \sim 20\ \mathrm{MeV}\frac{g_3^3}{(4\pi)^4}\frac{y_t^2v^2}{m_t^2m_\Phi^2}\frac{\gamma\kappa}{f}h(m_t^2/m_H^2)\,, \tag{151}$$

with

$$h(z) = z^2\int_0^1 dx\int_0^1 dy\frac{x^3y^3(1-x)}{[zx(1-xy)+(1-x)(1-y)]^2}\,. \tag{152}$$

Similarly to the previous case, for g_3 evaluated at ~ 1 GeV, we obtain that $|d_n| \sim 10^{-38}$ e cm, more than ten orders of magnitude smaller the current bound $\sim 10^{-26}$ e cm [180].

5.2.8 Outlook

We have studied the interplay between the Higgs boson and a triplet pseudoscalar in the $SO(7)/G_2$ NMCHM. Being a pNGB, the triplet phenomenology is mainly dictated by the effective Yukawa operators leading to a significantly different phenomenology at colliders, relatively to what is expected from the renormalizable Lagrangian. In particular, the only relevant interaction allowing the triplet to decay into hh is so suppressed by EWPD that decays mediated by the dimension five operators actually dominate the decay width.

Surprisingly, we have found that in the mass range $m_t < m_\Phi \lesssim 2m_t$ no single search constrains the parameter space of the model; see figure 12. It turns out that this is exactly where a (strong) two–step EW PT can occur (see figure 15), and therefore where EW baryogenesis can be explained. Given this holdback, we have proposed an analysis to test the $pp \to \phi^\pm \phi_0 \to t\bar{b}(\bar{t}b), b\bar{b}$ channel, showing that this whole interval of masses could be tested at the HL-LHC. We have furthermore studied the complementarity between the collider and astrophysical probes. In particular, if no departure from the SM prediction on the Higgs to di-photon rate is observed, only single peak GW signatures of the model are expected to be detected by LISA; see figure 15.

Finally, note that in this minimal setup one can actually link the phenomenology at low- and high-energies: if a signal of the pseudoscalar triplet was indeed observed at the LHC, it could be traced back to the mechanism of baryogenesis, since the same operator that triggers the triplet decays is *the* source of spontaneous CP violation at large temperature.

5.3 Testing lepton flavour universality at the precision frontier

5.3.1 The $SO(7)/SO(6)$ model

In this section, we explore the breaking pattern $SO(7)/SO(6)$, which can be achieved by the VEV of a field transforming in the fundamental vector representation of $SO(7)$. In this case, two extra NGBs are produced, on top of the Higgs doublet, which transform as singlets of the SM gauge group. We denote them by a_1 (–) and a_2 (+) and give them different CP charges (in parenthesis). This is the minimal setup where we can study the interplay among the exotic scalar particles and the consequent implications to the phenomenology at different experiments. In this regard, we will consider two regimes, characterized

by small and large scalar masses. We explore the former in the following; while the latter will be the focus of the next section.

The smallest representations of $SO(7)$ under which the composite resonances can transform are the $\mathbf{1}$, $\mathbf{7}$, $\mathbf{21}$ and $\mathbf{27}$. The most general embedding of the LH fields in the latter is:

$$L_L = \frac{1}{2}\begin{pmatrix} 0_{4\times4} & \theta\mathbf{v_1}^T & \gamma\mathbf{v_2}^T & \mathbf{v_2}^T \\ \theta\mathbf{v_1} & 0 & 0 & 0 \\ \gamma\mathbf{v_2} & 0 & 0 & 0 \\ \mathbf{v_2}^T & 0 & 0 & 0 \end{pmatrix}, \tag{153}$$

where the field vectors read $\mathbf{v_1} = (e_L, -\mathrm{i}e_L, \nu_L, \mathrm{i}\nu_L)$ and $\mathbf{v_2} = (\mathrm{i}e_L, e_L, \mathrm{i}\nu_L, -\nu_L)$, for leptons. A similar embedding is obtained for quarks, after replacing $e_L \to b_L$ and $\nu_L \to t_L$. Under $SO(6)$, the symmetric representation decomposes as $\mathbf{27} = \mathbf{1} \oplus \mathbf{6} \oplus \mathbf{20}$; with the $\mathbf{6} = \mathbf{1} \oplus \mathbf{5} = \mathbf{1} \oplus \mathbf{1} \oplus \mathbf{4}$ under $SO(5)$ and $SO(4)$, respectively, and the $\mathbf{20} = \mathbf{14} \oplus \mathbf{5} \oplus \mathbf{1} = \mathbf{9} \oplus \mathbf{4} \oplus \mathbf{1} \oplus \mathbf{4} \oplus \mathbf{1}$. Therefore, the LH fields can couple to three doublets in this decomposition, $\theta, \gamma \in \mathbb{R}$ being the corresponding degrees of mixing.

Writing explicitly the one-loop induced potential, we find (assuming CP conserving interactions):

$$\begin{aligned} V^{\mathbf{27}\oplus\mathbf{1}} &= c_1 f^4 \left|\left(\Lambda^I_{L,D}\right)_{77}\right|^2 + c_2 f^4 \left|\left(\Lambda^I_{L,D}\right)_{m7}\right|^2 \\ &= 4f^3 c_2 \gamma\Sigma a_2 + 2f\left(c_1 - 2c_2\right)\gamma\Sigma a_2 h^2 + \left(c_1 - 2c_2\right)\left[\left(\theta^2-1\right)a_1^2 + \left(\gamma^2-1\right)a_2^2 - h^2\right]h^2 \\ &+ \frac{1}{2}c_2 f^2\left[\left(\gamma^2+\theta^2-7+2\frac{c_1}{c_2}\right)h^2 + 4\left(\theta^2-1\right)a_1^2 + 4\left(\gamma^2-1\right)a_2^2\right], \end{aligned} \tag{154}$$

where we have used the same notation as in the previous sections and the sum over α and $m = 1, \ldots, 6$ is implicit. We further expand this expression in powers of $1/f$, keeping terms up to dimension four. The resulting potential reads:

$$\begin{aligned} V \sim\ & 4f^3 c_2 \gamma a_2 + f^2 c_1 h^2 + 2f^2 c_2\left[\left(\gamma^2-1\right)a_2^2 + \left(\theta^2-1\right)a_1^2 + \frac{1}{4}\left(\theta^2-7\right)h^2\right] \\ &+ 2f\gamma\left[\left(c_1 - 3c_2\right)a_2 h^2 - c_2\left(a_1^2 + a_2^2\right)a_2\right] + \left(c_1 - 2c_2\right)\left[\left(\theta^2-1\right)a_1^2 + \left(\gamma^2-1\right)a_2^2 - h^2\right]h^2 . \end{aligned} \tag{155}$$

We focus in scenarios where only the leptons break the shift-symmetry of the singlet pNGBs. They lead to small scalar masses which can be well below the EW scale, according to the PC rule. Such leptophilic regimes are obtained if, for example, $q_L \oplus u_R = \mathbf{7} \oplus \mathbf{21}$; with the corresponding embeddings given by

$$Q_L = \frac{1}{\sqrt{2}}(\mathrm{i}d_L, d_L, \mathrm{i}u_L, -u_L, 0, 0) \quad \text{and} \quad U_R = \mathrm{i}(T^{12} - T^{34})u_R\,. \tag{156}$$

The LO potential constructed from these spurions is $V = c_1 f^2 h^2$, while NLO terms produce the quartic coupling of the Higgs boson. No shift-breaking terms for $a_{1,2}$ are generated.

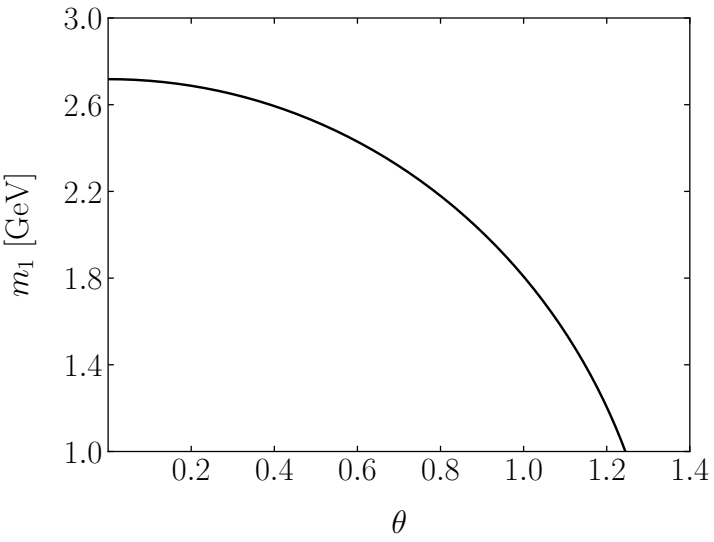

Figure 17: θ-dependence of the lightest scalar mass, obtained from the embedding of the LH leptons in the symmetric representation of $SO(7)$. We fixed $f = 1$ TeV.

Therefore, if $l_L \oplus e_R = \mathbf{27} \oplus \mathbf{1}$ while $q_L \oplus u_R = \mathbf{7} \oplus \mathbf{21}$, the scalar potential can be split as

$$V(h, a_1, a_2) = V_q(h) + V_l(h, a_1, a_2)\,, \tag{157}$$

where the first and second contributions come from loops of quarks and leptons, respectively. In such case, V_q is completely fixed by the measurements of the Higgs mass and its VEV, whereas V_l is identified with equation 155.

After EWSB, the interactions between h and a_2 in equation 155 lead to scalar mixing. In order to avoid bounds from Higgs searches, we choose $c_1 \sim 3c_2$ and $\gamma \sim 1$ to make these interactions very small. The tadpole can be subsequently removed by the field redefinition $a_2 \longrightarrow a_2 + \sqrt{2/3}f$. After these replacements, the scalar potential reads

$$V(a_1, a_2) = \frac{1}{2}m_1^2 a_1^2 + \frac{1}{2}m_2^2 a_2^2 + m_{12} a_2 a_1^2\,, \tag{158}$$

up to terms involving the Higgs boson. Without loss of generality, we assume $m_2 > m_1$. Furthermore, fixing $c_2 \sim g_*^2 y_l^2/(4\pi)^2 \sim 10^{-6}$, as expected by PC, as well as $f \sim 1$ TeV and $g_* \gtrsim 3$, we find

$$m_2 \approx 3.1 \text{ GeV} \quad \text{and} \quad m_{12} \approx 0.002 \text{ GeV}\,, \tag{159}$$

while m_1 depends solely on θ. We represent this dependence in figure 17. Scalar masses of $O(1)$ GeV are therefore very likely in this setup. (Note that, in spite of finding motivation in this explicit realization, we do not aim to probe this model in particular; therefore, departures from the previous assumptions will be considered too in the following, which can be accommodated in smaller representations than the $\mathbf{27}$.)

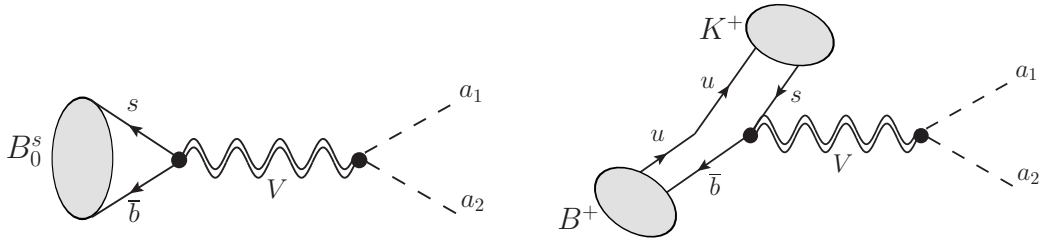

Figure 18: Tree level Feynman diagrams for the decays $B_s^0 \to a_1 a_2$ (on the left) and $B^+ \to K^+ a_1 a_2$ (on the right).

On another front, the Yukawa Lagrangian to dimension five reads:

$$\begin{aligned}\mathcal{L}_{\text{yuk}} &= y^e_{\alpha\beta} f \overline{l_{LI}}^{\alpha} \left(\Lambda^I_{L,D}\right)^{\dagger}_{77} e^{\beta}_R + \text{h.c.} \\ &= y^e_{\alpha\beta} \overline{l_L}^{\alpha} H \left[-1 + \frac{1}{f}\left(\mathrm{i}\theta a_1 - \gamma a_2\right) + \dots \right] e^{\beta}_R + \text{h.c.}\,,\end{aligned} \tag{160}$$

which matches equation 111 with $c_\kappa = \mathrm{i}\theta y$ and $c_\eta = -y$ for $\gamma = 1$.

Finally, heavy-light state couplings naturally arise in the composite model, since the pNGBs belong to the same sector as the heavy vector and fermionic resonances. We focus on interactions with the former, which are entirely fixed by the CCWZ construction. The vector resonance is assumed to transform in the adjoint representation of the global group. Expanding the second term in equation 104, we obtain:

$$\mathcal{L}_V = \sqrt{2} g_* \frac{V_\mu a_2 \overleftrightarrow{\partial^\mu} a_1}{1 + \Xi/f^2} \sim \frac{g_*}{\sqrt{2}} V_\mu a_2 \overleftrightarrow{\partial^\mu} a_1 + \mathcal{O}\left(\frac{a_1^2}{f^2}, \frac{a_2^2}{f^2}\right), \tag{161}$$

with $\Xi = f^2(1 - h^2/f^2 - a_1^2/f^2 - a_2^2/f^2)^{1/2}$. We identify V with the component of the vector resonance associated to the generator T^{56} (which is the one that transforms as a singlet of $SO(4)$). Such V can couple directly to the RH quarks[4], but not to the LH ones. The couplings to the latter are triggered by insertions of the Higgs field; hence, $g_{qq} \sim \xi g_* \lesssim 0.1$.

At energies well below its mass, V can be integrated out, giving rise to effective operators of the form qqa_1a_2. Provided that V has flavour-violating couplings to quarks, such operators trigger rare decays of bottom mesons into multiple leptons; see figure 18. Such couplings are strongly motivated by the LFU anomalies, as we discuss in the next section.

5.3.2 On flavour anomalies and model building

Let us revisit the two main flavour problems in the SMEFT. First, there is the SM flavour problem associated with the fact that $y_e \ll y_t$. Second, the so-called "new physics flavour problem" ensues from the

[4]Note that not even the coupling to the RH quarks arises if u_R is embedded in a single $SO(4)$ irreducible representation contained in the $\mathbf{21}$, such as the $(\mathbf{1},\mathbf{3})$. Indeed, in appendix C of Ref. [175], it is showed that, in this case, there is a discrete parity $P_6 \in O(7)$ under which V is odd while the SM quarks are even. Only if u_R is embedded in a linear combination of P-even and P-odd spurions, as the ones transforming in the $(\mathbf{1},\mathbf{3}) \oplus (\mathbf{1},\mathbf{1})$, can such coupling arise.

experimental bounds on higher dimensional four-fermion operators with a generic flavour structure, which imply[5] $\Lambda \gtrsim 10^{2-5}$ TeV. This rendered the belief that new sizable flavour-violating physics should be at very large scales, in contrast to what is expected from the EW HP. For this reason, an approach that was thoroughly considered in the recent past was to separate these tuning problems in the SMEFT and assume that the new physics which is responsible for stabilizing the Higgs mass would most likely be flavour-blind, or that the sources of flavour breaking would be minimal [160].

However, not only we have found no evidence of new physics so far (pushing the solutions to the EW HP itself to larger scales), but large deviations from the SM have been observed in tests of LFU. These deviations seem to point towards new flavour-violating dynamics around the TeV scale coupled mainly to the third generation, exactly as expected from the pattern of the Yukawa couplings in the SM. (Note that bounds on the cutoff of flavour-violating operators made out of third generation quarks can be nearly one order of magnitude less severe than those involving lighter generations[6].) This motivates the possibility of the two tuning problems being actually connected [162, 223] and is the first hint that the SM quantum numbers of the different generations might just be an accidental property of the low-energy physics, as signaled by their different masses.

Indeed, several B-factories around the world have been observing a different behavior of the lepton flavours in both charged and neutral currents that manifests in the ratios of

$$R_{D^{(*)}} = \frac{\Gamma\left(B \to D^{(*)}\tau\overline{\nu_\tau}\right)}{\Gamma\left(B \to D^{(*)}\ell\overline{\nu_\ell}\right)} \quad \text{and} \quad R_{K^{(*)}} = \frac{\Gamma\left(B \to K^{(*)}\mu^+\mu^-\right)}{\Gamma\left(B \to K^{(*)}e^+e^-\right)}, \tag{162}$$

which deviate significantly from unity. The first encodes a $b \to c$ transition, while the second a $b \to s$ one. (It is convenient to express these quantities as ratios to cancel uncertainties in the SM, coming from QCD and the CKM factors.) The latest result from the LHCb collaboration, after collecting $9\,\text{fb}^{-1}$ of data, shows a 3.1σ level tension with the SM from the measurement of R_K alone [224]. This increased statistical significance in the FCNC channel makes the chance of it being a pure statistical fluctuation less and less probable. In comparison, the *combined* results by BaBar, Belle and LHCb show $\gtrsim 3\sigma$ deviations from the SM prediction on the R_D and R_{D^*} observables[7].

Taken together, these anomalies are the largest coherent set of deviations observed so far of beyond the SM physics, since the observation of neutrino masses. Focusing on $b \to s\ell^+\ell^-$ transitions, fits to the LFU ratio (as well as to other anomalies in the muon sector, namely the smallness of the $B_s^0 \to \mu^+\mu^-$ branching ratio) [225] strongly favor LH current–current operators of the form

$$\mathcal{O}_{qq\ell\ell} = \frac{c_{ijkm}}{\Lambda^2}\overline{q_L^i}\gamma^\mu q_L^j\,\overline{\ell_L^k}\gamma_\mu \ell_L^m\,, \quad \text{with} \quad c_{ijkm} \sim \delta_{i3}\delta_{j3}\delta_{k2}\delta_{m2}\,, \tag{163}$$

[5] See https://indico.cern.ch/event/1019282/attachments/2230204/3780852/FlavourEFTLecture3.pdf.

[6] See footnote 5.

[7] See https://hflav-eos.web.cern.ch/hflav-eos/semi/spring19/html/RDsDsstar/RDRDs.html.

to explain the pattern of the observations. (To describe the FCCC channel, sizable interactions with the tau leptons are required too.)

Heavy colorless vectors such as our V are promising candidates to mediate these interactions; in particular, provided that

$$g_{qq} \sim 0.05 \left(\frac{m_V}{\text{TeV}}\right)^2 \tag{164}$$

and the vector coupling to the SM leptons is large, $g_{\ell\ell} \sim 1$, the $R_{K^{(*)}}$ anomalies can be explained at 1σ level [143]. Such vectors are constrained by other observables, including four-quark and four-lepton processes to which they contribute at tree level, as well as multi-lepton searches at the LHC (see section 4.6.1). Bounds on composite vectors are however weakened given that new decay channels open, for example $V \to a_1 a_2$ can easily dominate over other modes since the corresponding width involves the strong (rather than the elementary) coupling.

In leptophilic scenarios, the light scalars can subsequently decay into muons. This is accomplished if all leptons break the shift-symmetry of the singlet, but the decay into the third generation is kinematically closed; or if only muons break this symmetry. In the next sections, we study the collider probes of these scenarios, in particular to test the parameter space where equation 164 is satisfied.

We remark that combined explanations for the two LFU anomalies have been also considered in the literature. In this case, the leptoquark solution [226] is particularly motivated since the fit to $R_{D^{(*)}}$ requires large couplings of the effective operators which in turn imply smaller masses of the mediator. This is less problematic for a leptoquark than V, since the former can more easily evade collider and flavour bounds, contributing to meson mixing only at the loop level.

5.3.3 Collider signatures

Under the assumptions discussed in section 5.3.1, the relevant Lagrangian for our study is

$$\mathcal{L} = \frac{1}{2}m_V^2 + \frac{1}{2}m_1^2 a_1^2 + \frac{1}{2}a_2^2 m_2^2 + m_{12} a_2 a_1^2 + V^\mu \left[g_{12} a_1 \overleftrightarrow{\partial_\mu} a_2 + g_{qq} \left(\overline{q_L} \gamma_\mu q_L + \text{h.c.}\right) \right] , \tag{165}$$

where all parameters are free but their natural range is fixed by the composite model predictions. Assuming that g_{qq} complies with equation 163, then after EWSB, the last term in the Lagrangian becomes

$$\mathcal{L}_V \supset g_{qq} V_\mu \begin{pmatrix} \overline{s_L} & \overline{b_L} \end{pmatrix}^T \gamma^\mu V_{dL}^\dagger \begin{pmatrix} 0 & 0 \\ 0 & 1 \end{pmatrix} V_{dL} \begin{pmatrix} s_L & b_L \end{pmatrix} , \tag{166}$$

where we have considered just two fermion generations, for illustration purposes. Therefore, V can couple not only to $\overline{b_L} b_L$, but also to $\overline{b_L} s_L + \overline{s_L} b_L$. In the basis where the up-quark Yukawa matrix is already diagonal, we can identify $V_{dL} \equiv V_{\text{CKM}}$; hence, the flavour-violating coupling reads:

$$g_{sb} = g_{qq} \left(V_{dL}\right)^*_{21} \left(V_{dL}\right)_{22} = g_{qq} \left(V_{\text{CKM}}\right)_{ts} \left(V_{\text{CKM}}\right)_{tb} \sim 0.04\, g_{qq} . \tag{167}$$

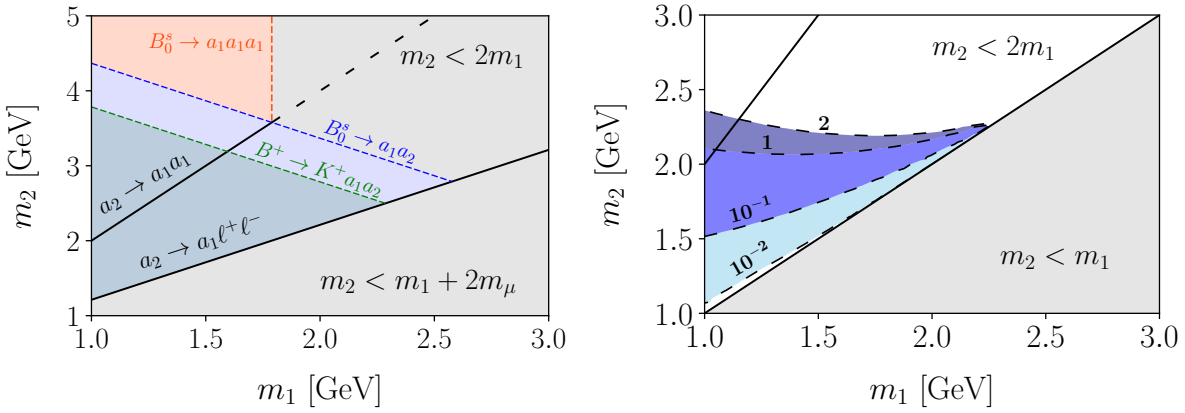

Figure 19: (Left) The dominant decays in each kinematic region considered in this analysis, represented in the plane (m_1, m_2). The gray areas are not studied. (Right) In the same plane, we represent $\Gamma(B_s^0 \to a_1 a_2)/\Gamma(B^+ \to K^+ a_1 a_2)$. This ratio vanishes along the line $m_1 = m_2$.

The B-meson decays depend on this physical coupling and on the kinematic regions defined by the light scalar masses, see the left panel in figure 19:

- If $m_{B_s^0} > m_1 + m_2$, the two-body decay $B_s^0 \to a_1 a_2$ is kinematically opened;
- If $m_{B_s^0} < m_1 + m_2$ and $m_{B_s^0} > 3m_1$, the decay mode $B \to a_1 a_1 a_1$ opens instead, the corresponding width being unsuppressed by the lepton Yukawa coupling, contrarily to $\Gamma(B_s^0 \to a_1 \ell^+ \ell^-)$;
- If $m_B^+ > m_1 + m_2 + m_K^+$, the decay mode $B^+ \to K^+ a_1 a_2$ can dominate the dynamics. This is true for any other meson satisfying this relation.

The decay widths of all processes enumerated above are computed in appendix F. All calculations take into account the meson form factors, that describe the quark–antiquark transition into a bound state; from Lorentz invariance, we know that such form factors are functions of momenta, whose constants are determined from experiment. Summarizing the results, we have:

$$\Gamma(B_s^0 \to a_1 a_2) \sim \frac{(g_{sb} g_{12})^2}{16\pi m_V^4} \frac{\left(m_1^2 - m_2^2\right)^2}{m_B} ; \tag{168}$$

$$\Gamma(B^0 \to a_1 a_1 a_1) \sim \frac{3\,(g_{sb} g_{12})^2}{256\pi^3} \frac{f_B^2 m_{12}^2}{m_V^4} m_B ; \tag{169}$$

$$\Gamma(B^+ \to K^+ a_1 a_2) \sim \frac{(g_{sb} g_{12})^2}{3072\pi^3 m_V^4} m_B^5 , \tag{170}$$

in the limit where all masses of the final state particles are taken to zero (except in equation 168, which vanishes in this limit) and the form factors f_B, $f_+(q^2)$, $f_-(q^2) \to 1$. In the right panel of figure 19,

we represent the ratio between the first and the third of these widths. It is clear that the three-body dominates over the two-body decay when $m_1 \sim m_2$. This can be understood from the fact that, in this limit, the two degenerate scalars transform as a complex scalar field $\Phi = a_1 + \mathrm{i}a_2$. At the same time, the model Lagrangian becomes invariant under $\Phi \to e^{\mathrm{i}\alpha}\Phi$ rotations, up to spurion effects of $\mathcal{O}(m_{12})$ which explicitly break the symmetry. Upon integrating V out, the effective interaction between Φ and the SM quarks can be written as $\sim (\bar{q}\gamma_\mu q)(\Phi\partial^\mu\Phi^\dagger - \Phi^\dagger\partial^\mu\Phi) \equiv (\bar{q}\gamma_\mu q)J^\mu$, with J^μ being the Noether current associated with the $U(1)$ global symmetry. Employing the B-meson form factor, this interaction becomes $\sim (\partial_\mu B)J^\mu \overset{\text{IBP}}{=} B(\partial_\mu J^\mu) \to 0$ in this limit.

We assume that each scalar decays subsequently to muons. Therefore, the exotic decay $B_0^s \to a_1 a_2$ can produce four muons in the final state. The LHCb collaboration has performed dedicated analyses to probe this process, the most stringent limit being [227]

$$\mathcal{B}(B_0^s \to 2\mu^+ 2\mu^-) < 2.5 \times 10^{-9} \,. \tag{171}$$

There are however compelling **reasons to look for alternative decays**.

First, provided that $m_2 > 2m_1$, the scalar decay width of the heaviest singlet,

$$\Gamma(a_2 \to a_1 a_1) = \frac{m_{12}^2}{8\pi m_2}\left(1 - \frac{4m_1^2}{m_2^2}\right)^{1/2} , \tag{172}$$

can dominate over the leptonic one,

$$\Gamma(a_2 \to \ell^+\ell^-) = \frac{y_\ell^2\gamma^2}{8\pi}\left(\frac{v}{\sqrt{2}f}\right)^2\left(1 - \frac{4m_\ell^2}{m_2^2}\right)^{3/2} m_2 \,. \tag{173}$$

This is true whenever $m_{12}/m_2 \gg y_\ell\gamma v/f$; we make this assumption hereafter. Note that, from PC, we expect $m_{12} \sim m_2$, so that this inequality holds trivially. (The $\mathbf{27}\oplus\mathbf{1}$ model we have worked out in previous sections renders smaller values for m_{12}; see equation 159. The Yukawa together with the ξ suppression can make the leptonic width sub-leading even in this case.)

If instead $m_2 < 2m_1$, a_2 can either decay into a lepton pair, or $a_1\ell^+\ell^-$ with width

$$\Gamma(a_2 \to a_1\ell^+\ell^-) \approx \frac{y_\ell^2\theta^2}{64\pi^3 m_2^3}\left(\frac{v}{\sqrt{2}f}\right)^2 m_{12}^2 m_1^2\left(1 + \frac{m_2}{m_1}\right)\left(\frac{m_2}{m_1} - 1\right)^5 , \tag{174}$$

where we have worked in the $m_2/m_1 \sim 1$ limit. This decay mode dominates provided that $\theta \gtrsim 100\gamma$. We assume $\theta\sqrt{\xi} \sim 1$ and $\gamma\sqrt{\xi} \sim 0.01$ in the following. In this case, a_2 decays into four leptons, mediated by a_1 which can be either on- or off-shell. For the previous choice of parameters, the two scalars have decay widths smaller than 10 MeV and lifetimes shorter than 10 fs. Consequently, both $a_{1,2}$ would appear not to have any experimentally measurable flight distance[8] and would appear to have zero width.

[8] Departures from this assumption are also plausible: while the values of $m_{12} \sim m_{1,2}$ make a_2 very likely short-lived; if *e.g.* $\theta \sim 0.1$ and $f \sim 5$ TeV, still compatible with $\Gamma(a_2 \to a_1\ell^+\ell^-) > \Gamma(a_2 \to \ell^+\ell^-)$, the a_1 flight distance could be measured experimentally at the LHCb.

	$m_X \geq m_1 + m_2$		$m_X < m_1 + m_2$
	$m_2 \geq 2m_1$	$m_2 < 2m_1$	$m_X \geq 3m_1$
$B_s^0 \to 3\mu^+3\mu^-$	[0.02,0.03]	[0.01,0.02]	[0.02,0.03]
limit ($\times 10^{-9}$)	$[6.7, 11.6]$	$[7.9, 18.2]$	$[6.0, 11.9]$
$B^+ \to K^+3\mu^+3\mu^-$	[0.007,0.009]	[0.003,0.009]	four-body
limit ($\times 10^{-9}$)	$[5.9, 8.0]$	$[6.0, 16.6]$	four-body

Table 5: In the first and third rows, we present the maximum and minimum efficiencies for selecting signal events in the channels $B_s^0 \to 3\mu^+3\mu^-$ ($m_X = m_{B_s^0}$) and $B^+ \to K^+3\mu^+3\mu^-$ ($m_X = m_{B^+} - m_{K^+}$), for the different kinematic regions defined in figure 19. These results are used to obtained the upper limits on the branching ratios, for $3\,\text{fb}^{-1}$ of data, as shown in the second and fourth rows. We have used values of $m_2 < 10$ GeV and $m_1 \geq 1.1$ GeV, the efficiency being negligible for smaller values of m_1.

Several precision experiments, such as Belle and BaBar, have set bounds on the parameter space of light leptophilic scalars. The Yukawa suppression in the equations above makes our model basically insensitive to such bounds, even taken into account the projected limits at future facilities [189]. We conclude that, if indeed a_2 decays mostly according to equations 172 and 174, six (rather than four) muon final states are expected. There are no dedicated searches which can probe these processes.

Second, in the limit of degenerate scalars, searches for B decays into only muons cannot constrain the model; the tagging of extra mesons is required instead. No analysis exists either to probe this kind of channels, *e.g.* $B^+ \to K^+3\mu^-3\mu^-$. Remarkably, not even channels with a smaller multiplicity of leptons, in particular $B^+ \to K^+2\mu^+2\mu^-$, have been tested so far. A sensitivity study of this process is presented in Ref. [228].

In the next section, we therefore present the first proposed analyses to study the aforementioned processes at the LHCb.

5.3.4 New analyses at the LHCb

The largest backgrounds to six muon processes come from the resonant productions of J/Ψ and φ mesons that subsequently decay into muons. These backgrounds can be removed by vetoing all reconstructed a_1 particles with an invariant mass close to where these SM resonances peak. After this cut, the analyses become essentially background-free (as in the case of the four muons search [227]). Therefore, we can estimate the upper limit on $\mathcal{B}(B_0^s \to 3\mu^+3\mu^-)$ using the result obtained for $\mathcal{B}(B_0^s \to 2\mu^+2\mu^-)$, after normalizing the efficiency ϵ with respect to the four muons case[9]. With that aim, we follow the analysis

[9] In both cases, the maximum number of signal events which can be excluded is the same (see equation 35); hence, $\epsilon_{2\mu^+2\mu^-}\sigma_{\text{max}}^{2\mu^+2\mu^-} L \sim \epsilon_{3\mu^+3\mu^-}\sigma_{\text{max}}^{3\mu^+3\mu^-} L'$, where σ_{max} is given by the B-production cross section times the maximum allowed branching ratio.

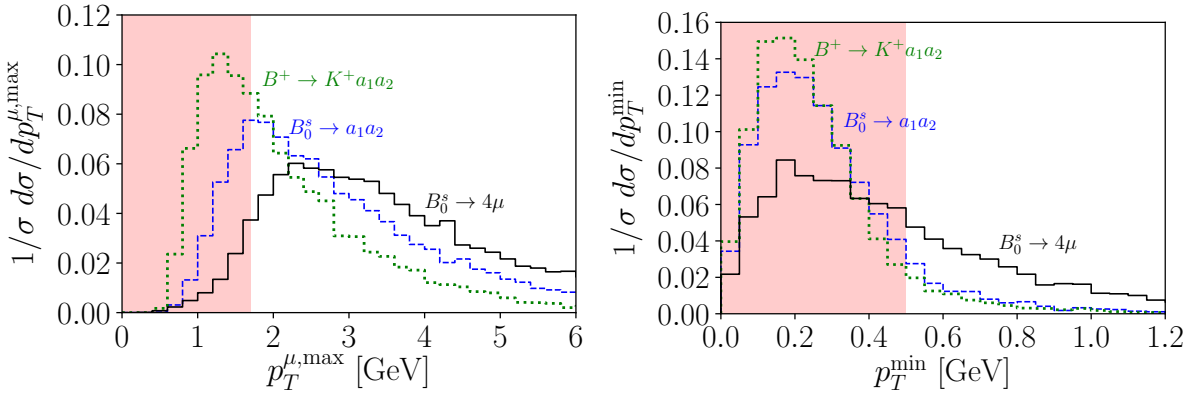

Figure 20: (Left) Normalized distribution of the transverse momentum of the hardest muon for $B_s^0 \to a_1 a_2$ and $B^+ \to K^+ a_1 a_2$. These distributions are compared with that of $B_0^s \to 2\mu^+ 2\mu^-$. We fixed $m_1 = 1$ GeV and $m_2 = 2.5$ GeV. (Right) The same for the softest track.

strategy presented in Ref. [227], requiring that all events have:

1. Six muons with vanishing total charge;

2. At least one muon with $p_T > 1.7$ GeV, to simulate the same hardware trigger as the one used at $\sqrt{s} = 8$ TeV;

3. All tracks with $p_T > 0.5$ GeV and within a pseudorapidity volume defined by $2.5 < \eta < 5.0$;

4. All muons with a total momentum larger than 2.5 GeV, to simulate the threshold for positive muon identification at the LHCb detector;

5. No pairs of zero charge muons with an invariant mass in the range $[0.95,\ 1.09] \bigcup [3.0,\ 3.2]$ GeV.

The efficiencies after these selection cuts are presented in table 5. For comparison, in the four muons channel, we obtain $\epsilon_{2\mu^+ 2\mu^-} \approx 0.14$. Below, we detail the effects of these cuts in the analyses with and without the tagging of an extra meson.

5.3.4.1 Six muon final states

The efficiencies obtained in the $B_s^0 \to 3\mu^+ 3\mu^-$ channel are nearly one order of magnitude smaller than in the four muons case. The reason for this is two-fold. Due to the larger muons multiplicity, there are more events in which no single muon has $p_T > 1.7$ GeV; see the left panel of figure 20. In the same way, the probability to find a muon with $p_T < 0.5$ GeV is larger; see the right panel in figure 20.

Given the previous discussion, we can estimate the upper limit on the branching ratio of the new

process at $\sqrt{s} = 14$ TeV and luminosity L' as

$$\mathcal{B}^{3\mu^+3\mu^-}_{\text{max}} \sim \frac{\mathcal{B}^{2\mu^+2\mu^-}_{\text{max}} \times \varepsilon_{2\mu^+2\mu^-}}{1.8 \times \varepsilon_{3\mu^+3\mu^-}} \times \frac{L}{L'}, \tag{175}$$

where $\mathcal{B}^{2\mu^+2\mu^-}_{\text{max}}$, given by equation 171, was obtained with $L = 3\,\text{fb}^{-1}$ and $\sqrt{s} = 8$ TeV. The factor 1.8 stands for the enhancement of the B^0_s production cross section from $\sqrt{s} = 8$ TeV to $\sqrt{s} = 14$ TeV. The results on the maximum branching ratio are presented in table 5, for the different kinematic regions analysed in this work.

5.3.4.2 Six muons+meson final states

In the analysis for $B^+ \to K^+3\mu^+3\mu^-$, on top of the selection criteria above, we require the presence of an additional charged track. Practically, no additional requirement to identify the charged kaon is necessary, since the particle identification system of the LHCb detector is optimized for the momentum range of the heavy meson decay products (the efficiency for positive kaon identification being $\gtrsim 95\%$ in the momentum range 10–40 GeV and for pion mis-tagging probability below 1% [229]).

Due to the occurrence of the extra track, the selection efficiencies for this process are smaller in comparison to the previous case; they are presented in table 5. The limit on the branching ratio can be again obtained as

$$\mathcal{B}^{3\mu^+3\mu^-K^+}_{\text{max}} \sim \frac{\mathcal{B}^{2\mu^+2\mu^-}_{\text{max}} \times \varepsilon_{2\mu^+2\mu^-}}{1.8 \times 3.7 \times \varepsilon_{3\mu^+3\mu^-K^+}} \times \frac{L}{L'}, \tag{176}$$

where the additional factor 3.7 is due to the larger production cross section of B^+ in comparison to B^0_s. The corresponding upper limits on branching ratio are presented in table 5. As can be seen, the growth in the production cross section compensates the smaller efficiencies in this channel, actually leading to the most stringent bounds. This fact, together with the theoretical observation that this decay mode dominates for $m_1 \sim m_2$, strongly motivates searches for $B^+ \to K^+3\mu^+3\mu^-$.

Finally, we note that if a signal is observed in these six muon channels, the mass of the light scalars could be reconstructed at the LHCb. To show that this is the case, let us first assume $m_2 > 2m_1$, so that a_2 decays mainly into a_1a_1. We start by computing the difference $\delta = |m^{\text{rec}}_i - m^{\text{rec}}_j| + |m^{\text{rec}}_j - m^{\text{rec}}_k|$; with m^{rec}_i being the invariant mass of any combination of two opposite-sign muons. Those that minimize δ are then assigned to the three a_1 particles involved. The two a_1 candidates that subsequently reconstruct a_2 are the ones with a minimum ΔR between themselves; see the left panel in figure 21.

If instead $m_2 < 2m_1$, a_2 decays mostly into $a_1\mu^+\mu^-$. In this case, we reconstruct the two a_1 particles by minimizing the difference $|m^{\text{rec}}_i - m^{\text{rec}}_j|$. The heavier scalar is subsequently reconstructed by combining the two muons which were left unassigned, plus the a_1 candidate which is closest in ΔR to the former. The corresponding mass distributions are plotted in the right panel of figure 21, for a given BP.

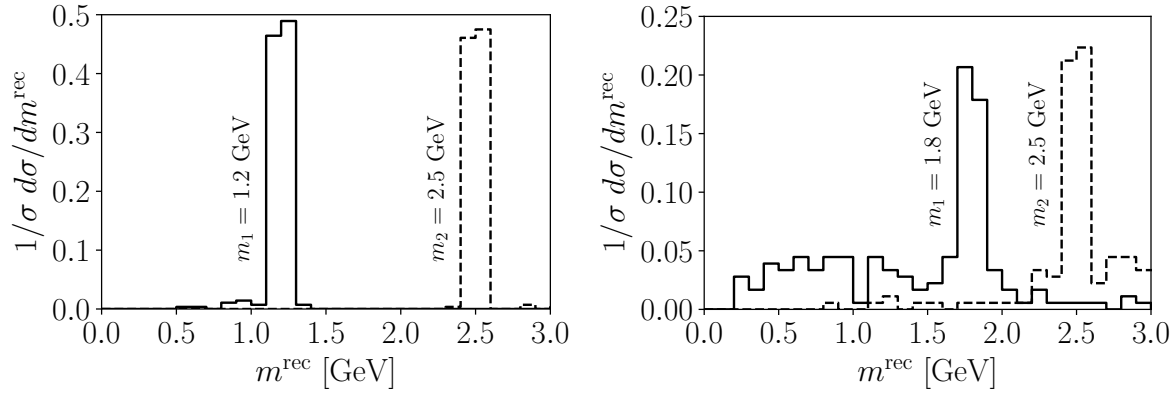

Figure 21: (Left) Normalized distribution of the reconstructed m_1 (solid) and m_2 (dashed) for $m_2 > 2m_1$. (Right) The same for $m_2 < 2m_1$.

5.3.5 Outlook

We have studied the signatures of light leptophilic scalars coupled to a flavour-violating heavy vector boson, all assumed to be part of the same non-minimal composite sector. Such vector boson mediates rare decays of B-mesons which can in turn explain the anomalies observed in tests of LFU by several experiments.

In the low-mass regime, the scalars can decay into muons, triggering the processes $B_s^0 \to 3\mu^+3\mu^-$ and $B^+ \to K^+3\mu^+3\mu^-$, none of which has been *yet* explored experimentally. By performing new dedicated analyses to test these channels at the LHCb, we have found that branching ratios as small as 6.0×10^{-9} and 5.9×10^{-9} could be probed, respectively, at the current run of this facility. In particular, the three-body decay can not only lead to the strongest bounds on the model but is also *the* key signature when the two pNGBs are approximately degenerate.

For illustration, we translated the (weakest) upper bounds on these processes to the $(g_{sb},\ m_V)$ plane; see the top panel in figure 22. It is clear that, for certain points of the parameter space where $(m_2 - m_1) \lesssim 1$ GeV, the stringent bounds on the vector mass are obtained in the $B^+ \to K^+a_1a_2$ channel. Notably, after Upgrade II of the LHCb detector, where 300 fb^{-1} of data are expected to be collected, branching ratios a hundred times smaller could be probed; consequently, vector masses as large as $m_V \sim 15$ TeV could be excluded if no signal is observed in these channels. Therefore, our proposed analyses could potentially outperform the bounds from meson mixing on $\Delta M_s \equiv M_H^s - M_L^s$, corresponding to the mass difference between the heavy (H) and light (L) eigenstates of the $B_s^0 - \overline{B}_s^0$ system. (We did not include in the plot the latest SM prediction for ΔM_s, as reported in Ref. [143], because the inputs from lattice calculations are still to be confirmed). Finally, the dotted-dashed line in this plot represents the combination of mass and coupling for which the heavy vector can explain the anomalies in $R_K^{(*)}$ at 1σ level, according to equation 164. Our analyses can entirely probe this region as well.

In the bottom panel of figure 22, we plotted instead the obtained bounds on the $(m_1,\ m_2)$ plane,

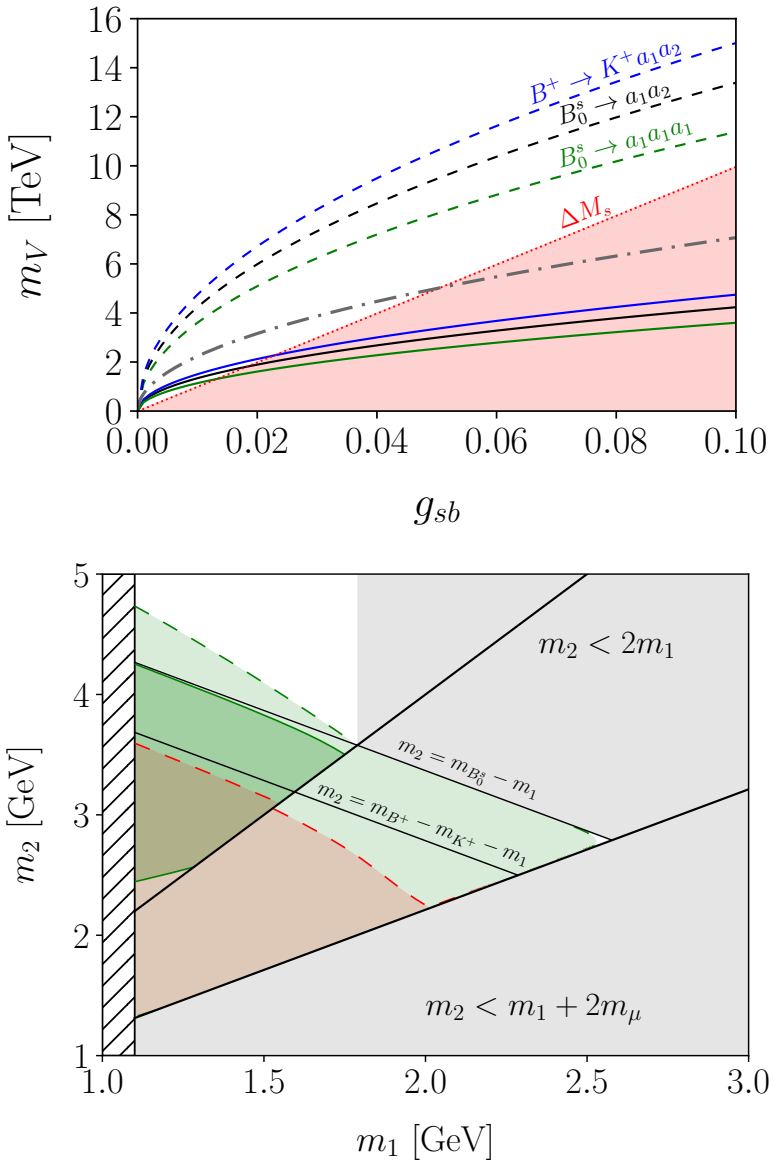

Figure 22: (Top) Maximum vector mass that can be tested with our proposed analyses. The blue, black and green lines stand for the different channels analysed in this work, the solid (dashed) ones corresponding to a collect luminosity of 3 (300) fb^{-1}. The red dotted line delimits the region excluded by measurements of ΔM_s. Along the dash-dotted line, the $R_{K^{(*)}}$ anomalies can be explained; see the text for details. We fixed $g_{12} = 0.5$ as well as $m_1 = 1.2$ GeV. The heavy scalar mass was set to $m_2 = 2.0$ GeV for both $B_0^s \to a_1 a_2$ and $B^+ \to K^+ a_1 a_2$ channels; for $B_0^s \to a_1 a_1 a_1$, we used $m_2 = m_{12} = 5$ GeV instead. (Bottom) The upper limits on branching ratio translated to the plane (m_1, m_2). The regions that can be tested in searches for $B_s^0 \to 3\mu^+ 3\mu^-$ and $B^+ \to K^+ 3\mu^+ 3\mu^-$ are enclosed by the green and red lines, respectively. We fixed $g_{sb} = 0.04$, $m_V = 4$ TeV and $g_{12} = 0.5$, as well as $m_{12} = 1$ GeV (only relevant in the upper left region). The sensitivity is negligible in the slashed region.

fixing $g_{sb} = 0.04$ and $m_V = 4$ TeV; such values are not yet excluded by measurements of ΔM_s. We conclude that almost the entire low-mass parameter space could be probed at Upgrade II of the LHCb detector. Currently, the region where $m_2 < 2m_1$ cannot be excluded for the particular BP we chose, since the decay $B_s^0 \to a_1 a_2$ is very suppressed close to the line $m_1 = m_2$. Moreover, the upper limit obtained in this region is weaker than for $m_2 > 2m_1$. (Note that our analyses lead to negligible sensitivity for $m_{1,2} \sim 1$ GeV, due to the veto on the invariant mass of muon pairs close to m_φ.)

The heavy vector can trigger also b–d transitions, in which case we expect new rare decays, such as $B^0 \to 3\mu^+3\mu^-$. Given the growth in production cross section of B^0 in comparison to B_s^0, we estimate that $\mathcal{B}(B^0 \to 3\mu^+3\mu^-) \gtrsim 1.6 \times 10^{-9}$ could be probed with $3\,\text{fb}^{-1}$ of data at the current run of the LHCb. This channel vanishes for $m_1 \sim m_2$. In this limit, we propose searching for $B_s^0 \to K^{*0}3\mu^-3\mu^+$ instead. Assuming the $K^{*0} \to K^+\pi^-$ mode for the reconstruction of the unstable kaon, with a branching ratio $\sim 2/3$ [9], we obtain efficiencies around two times smaller than for $B_s^0 \to 3\mu^+3\mu^-$, upon performing the analysis described in section 5.3.4. Consequently, we estimate that the LHCb could reach $\mathcal{B}(B_s^0 \to K^{*0}3\mu^-3\mu^+) \gtrsim 1.8 \times 10^{-8}$, with $L = 3\,\text{fb}^{-1}$. Testing different flavour transitions is specially relevant to probe different flavour structures of SMEFT operators extended with light scalars, *e.g.* $\bar{q}q\bar{q}qa^2$. Such EFT formulation has become one of the favorite tools to interpret the bounds on ALPs [184, 230].

Finally, we remark that, at the next update of the LHCb detector, it is expected that the hardware trigger is completely removed and that the threshold for muon identification can be lowered, so that muon tracks with $p_T \lesssim 0.25$ GeV could be detected. In this way, efficiencies $\gtrsim 3$ times larger could be attained. The results presented in table 5 are therefore conservative.

5.4 Composite dark sectors

5.4.1 Still the $SO(7)/SO(6)$ model

In this section, we consider the same realization of the CHM presented in section 5.3.1, but assume instead the large mass regime for the pNGBs. This is accomplished when the main breaking of the shift-symmetry comes from integrating out the quarks mixing with the composite sector. In this case, the two singlet particles, η (+) and κ (–), can naturally be at the EW scale. (We assign them the CP-charges in parenthesis.) We aim to study the conditions under which η is a DM candidate. If the CHM is to explain other problems in particles physics beyond DM, for example EW baryogenesis, extra pNGBs such as κ must also be present. Since the latter is part of the same composite sector as the DM candidate, this setup provides not only a Higgs portal to the SM, but also an exotic mediator between the dark and visible sectors which can affect the phenomenology non-trivially.

Contrary to the minimal composite DM model, the $SO(7)$ global group does not admit a WZW term. Therefore, assuming that the stabilizing DM symmetry is respected at the classical level, it is automatically

preserved at the quantum level as well[10]. It follows that the minimal non-anomalous composite DM model necessarily contains additional pNGB states.

Several NMCHMs with DM have been considered in the literature but, in most constructions, it is assumed that the unstable exotic pNGBs are heavier than the DM and therefore decoupled from its phenomenology. This is the case if the fermions which break the shift-symmetry of the unstable pNGBs are heavier than those that break the DM's. There is however no theoretical motivation to prefer this over the inverse hierarchy; and, in fact, the latter can be favored experimentally. Indeed, if the DM can annihilate sizably into the additional pNGBs, it can freeze out even in the absence of couplings to the SM, in which case the current very strong constraints from DM experiments can be avoided.

To probe both the Higgs and the exotic portal couplings in this scenario, we make two different choices for the embeddings of the elementary fermions: in Regime I (RegI), we assume that $q_L \oplus t_R = \mathbf{27} \oplus \mathbf{1}$; while in Regime II (RegII), $q_L \oplus t_R = \mathbf{7} \oplus \mathbf{7}$. Below, we study the predictions emerging from these regimes.

5.4.1.1 Regime I

In this regime, the radiatively induced potential is obtained as in equation 155, with $\gamma \longrightarrow 0$ to assure the DM stability. Trading c_1 and c_2 by the Higgs mass and its quartic coupling, we obtain:

$$V_{\text{RegI}} = \frac{\mu_H^2}{2}h^2 + \frac{\lambda_H}{4}h^4 + \left[\frac{\lambda_H f^2 + 2\mu_H^2}{3-\theta^2}\right]\eta^2 + \frac{1}{4}\lambda_H \eta^2 h^2 + \left[\frac{(\lambda_H f^2 + 2\mu_H^2)(\theta^2-1)}{\theta^2-3}\right]\kappa^2 + \frac{1}{4}\lambda_H(1-\theta^2)h^2\kappa^2 \,. \tag{177}$$

Therefore, $m_\kappa \leq m_\eta$ for all values of $\theta \in]0,1]$. For example, for $\theta \sim 0.5$, the physical scalar masses read $m_\eta^{\text{phys}} \approx 210$ GeV and $m_\kappa^{\text{phys}} \approx 170$ GeV.

On another front, the Yukawa Lagrangian to dimension six reads:

$$\begin{aligned}\mathcal{L}_{\text{yuk}} &= y f \overline{q_{LI}} \left(\Lambda_D^I\right)^\dagger_{77} u_R + \text{h.c.} \\ &= -y_q \frac{h}{\sqrt{2}} \overline{u_L} u_R \left[\sqrt{1 - \frac{h^2}{f^2} - \frac{\eta^2}{f^2} - \frac{\kappa^2}{f^2}} + \mathrm{i}\theta\frac{\kappa}{f}\right] + \text{h.c.} \\ &= -y_q \frac{h}{\sqrt{2}} \overline{u_L} u_R \left[1 + \mathrm{i}\theta\frac{\kappa}{f} - \frac{\eta^2 + \kappa^2 + h^2}{2f^2}\right] + \mathcal{O}\left(\frac{1}{f^4}\right) + \text{h.c.}\,,\end{aligned} \tag{178}$$

which matches equation 111 with $c_\kappa = -\theta y$, $c_\eta = 0$ and $c_{\eta^2} = -y$.

[10] We are assuming that the UV does not break the DM parity symmetry at higher order in derivatives than that corresponding to the WZW term. This is not guaranteed in the CHM under study since the parity symmetry is not part of the global group $SO(7)$. Instead, we could uplift $SO(7) \longrightarrow O(7)$, in which case the kinetic Lagrangian would preserve the parity symmetry exactly. Still, the absence of the WZW term (that arises already at dimension five in the $SO(6)/SO(5)$ CHM), together with the fact that such breaking terms could appear at much higher orders in $1/f$, is an important motivation to go beyond minimality.

For $\theta = 0$, the singlet κ becomes also stable. In this case, (η, κ) transforms as a complex scalar under $SO(2) \cong U(1)$ that belongs to the unbroken $SO(6)$ symmetry group. The corresponding phenomenology is studied in Ref. [175]. For $\theta = 1$, κ becomes massless; its shift-symmetry remains unbroken. These values are therefore stable under radiative corrections and hence *technically* natural. In this range of values, $\langle\eta\rangle = \langle\kappa\rangle = 0$. However, for $1 < \theta < \sqrt{3}$, we can also have $\langle\kappa\rangle \neq 0$, leading to spontaneous CP violation. Since this is very constrained experimentally (see section 5.2.7), in the following we consider only θ-values that satisfy $\langle\kappa\rangle = 0$. On the other hand, for $\theta > \sqrt{3}$, η can gain a VEV and becomes unstable. Requiring that both CP and the $\mathbb{Z}_2$ DM symmetries are not broken spontaneously therefore assures that the hierarchy $m_\kappa \leq m_\eta$ is always respected. We restrict to this case hereafter.

In equation 177, we can further trade $(f,\ \theta)$ for $(m_\eta,\ m_\kappa)$, to make the physical parameters more apparent in the potential:

$$V_{\text{Regl}} = \frac{\mu_H^2}{2}h^2 + \frac{\lambda_H}{4}h^4 + \frac{1}{2}m_\eta^2\eta^2 + \frac{1}{4}\lambda_H\eta^2h^2 + \frac{1}{2}m_\kappa^2\kappa^2 + \frac{1}{4}\lambda_H\left(\frac{m_\kappa}{m_\eta}\right)^2 h^2\kappa^2\,, \tag{179}$$

with

$$f \sim \frac{m_\eta}{\sqrt{\lambda_H}}\left[1 + \frac{m_\kappa^2}{2m_\eta^2}\right]^{1/2}\,. \tag{180}$$

In this framework, the compositeness scale can therefore be constrained by DM observables.

5.4.1.2 Regime II

In the second regime, we use the following embeddings for fields in the fundamental representation of $SO(7)$:

$$\mathsf{T}_R = \left(0,0,0,0,0,\mathrm{i}\theta t_R, t_R\right) \quad \text{and} \quad \mathsf{Q}_L = \frac{1}{\sqrt{2}}\left(-\mathrm{i}b_L, b_L, \mathrm{i}t_L, t_L, 0, 0, 0\right)\,. \tag{181}$$

Under $SO(6)$, the $\mathbf{7} = \mathbf{6} \oplus \mathbf{1}$; therefore, only one independent invariant can be built at LO in the spurions expansion for each field, leading to:

$$V = c_1 f^2\left[h^2 + (1-\theta^2)\kappa^2 + \eta^2\right] + \frac{c_2}{2}f^2h^2\,. \tag{182}$$

The $m_\kappa \leq m_\eta$ hierarchy, for $\theta \in]0,1]$, is also attained. Nevertheless, NLO terms are mandatory to obtain the complete renormalizable potential. There are eight non-redundant invariants that we can build, including the two used in the equation above:

$$\begin{aligned}
I_1 &\equiv \left[\left(\Lambda^{\mathbf{1}*}_{D,R}\right)\left(\Lambda^{\mathbf{1}}_{D,R}\right)\right] = f^2\left[f^2 - h^2 - \eta^2 - \kappa^2\left(1-\theta^2\right)\right]\,,\\
I_2 &\equiv \left[\left(\Lambda^{\mathbf{1}*}_{D,L}\right)^I\left(\Lambda^{\mathbf{1}}_{D,L}\right)^I\right] = \frac{1}{2}h^2f^2\,,\\
I_3 &\equiv \left[\left(\Lambda^{\mathbf{1}*}_{D,R}\right)\left(\Lambda^{\mathbf{1}}_{D,R}\right)\right]^2 = \left[h^2 + \kappa^2\left(1-\theta^2\right) + \eta^2 - f^2\right]^2\,,
\end{aligned}$$

$$
\begin{aligned}
I_4 &\equiv \left[\left(\Lambda^{\mathbf{6}*}_{D,R}\right)^m \left(\Lambda^{\mathbf{6}}_{D,R}\right)_m\right]^2 = \left[h^2+\kappa^2\left(1-\theta^2\right)+\eta^2+\theta^2 f^2\right]^2,\\
I_5 &\equiv \left[\left(\Lambda^{\mathbf{1}*}_{D,L}\right)^I \left(\Lambda^{\mathbf{1}}_{D,L}\right)_I\right]^2 = \frac{1}{4}h^4,\\
I_6 &\equiv \left[\left(\Lambda^{\mathbf{6}*}_{D,L}\right)^I_m \left(\Lambda^{\mathbf{6}}_{D,L}\right)^m_I\right]^2 = \frac{1}{4}\left(h^2-4f^2\right)^2,\\
I_7 &\equiv \left(\Lambda^{\mathbf{1}*}_{D,R}\right)\left(\Lambda^{\mathbf{1}}_{D,R}\right)\left(\Lambda^{\mathbf{1}*}_{D,L}\right)^I \left(\Lambda^{\mathbf{1}}_{D,L}\right)_I = \frac{1}{2}h^2\left[f^2-h^2-\eta^2-\kappa^2\left(1-\theta^2\right)\right],\\
I_8 &\equiv \left(\Lambda^{\mathbf{6}*}_{D,R}\right)^m \left(\Lambda^{\mathbf{6}}_{D,R}\right)_m \left(\Lambda^{\mathbf{1}*}_{D,L}\right)^I \left(\Lambda^{\mathbf{1}}_{D,L}\right)_I = \frac{1}{2}h^2\left[h^2+\eta^2+\kappa^2\left(1-\theta^2\right)+\theta^2 f^2\right].
\end{aligned}
$$

It is clear from the form of I_1–I_8 that the naive counting of nine operators constructed out of $\{h^2,\eta^2,\kappa^2\}$ is reduced to only five, by combining the two operators in $\{h^2,\eta^2+(1-\theta^2)\kappa^2\}$. The corresponding coefficients together with θ can be traded by the Higgs mass and its quartic coupling, plus the two singlet masses and two of their couplings. The new physics scale f remains a free parameter. After this replacement, we finally obtain:

$$
\begin{aligned}
V_{\text{RegII}} =& \frac{\mu_H^2}{2}h^2+\frac{\lambda_H}{4}h^4+\frac{1}{2}m_\eta^2\eta^2+\frac{1}{8}\lambda_{\eta\kappa}\left(\frac{m_\eta}{m_\kappa}\right)^2\eta^4+\frac{1}{2}m_\kappa^2\kappa^2+\frac{1}{8}\lambda_{\eta\kappa}\left(\frac{m_\kappa}{m_\eta}\right)^2\kappa^4\\
&+\frac{1}{4}\lambda_{\eta H}\eta^2h^2+\frac{1}{4}\lambda_{\eta\kappa}\eta^2\kappa^2+\frac{1}{4}\lambda_{\eta H}\left(\frac{m_\kappa}{m_\eta}\right)^2\kappa^2h^2.
\end{aligned}
\tag{183}
$$

Although less predictive than the previous case, this regime shows important consequences: for instance, the choice for the masses and $\lambda_{\eta H}$ determines the interaction between the Higgs and the pseudoscalar singlet. More importantly, the DM couplings to the singlet and to the Higgs boson can be chosen independently. Contrary to the previous case, they are both generated at $O(\lambda^4_{L,R})$. In order to study a complementary phenomenology to that of RegI, we assume $\lambda_{\eta H}\ll\lambda_{\eta\kappa}\sim\lambda_H$. This suppression can be achieved as a result of $\sim 1\%$ level of tuning in the model parameters[11]. Note that such levels of tuning are not uncommon in the composite framework [172]; they are actually required in all models where EWSB is not attained at LO, such as the $\mathbf{7}\oplus\mathbf{7}$ MCHM. Such model requires a *double tuning* in the scalar potential, which can be of the same order as the one required in this setup: the first tuning is used to make the couplings of h^2 and h^4, α_{h^2} and β_{h^4}, comparable and so overcome the different orders in the spurions expansion at which they are generated; whereas the second one is necessary to make $\alpha_{h^2}/\beta_{h^4}\sim\xi\ll 1$, in agreement with the SM values.

Finally, the Yukawa Lagrangian reads exactly as in equation 178.

[11] To obtain this value, we use the known coefficient of the h^4 operator to find the order of magnitude of the NLO UV constants. To this aim, we assume that all $c_i\sim c$ ($i=3,\dots,8$) and solve for λ_H, obtaining $c\sim\lambda_H/10$. We then scan over the range $[0.1c,\ 10c[$, *assuming an uniform distribution*, to find the region where $\lambda_{\eta H}<0.1\lambda_{\eta\kappa}$. We finally study the stability of this region, by producing small changes in single parameters (up to 10%) and verify that they do not reintroduce the naive scaling. We can consequently quantify the level of tuning we are requiring as $\sim c^{\min}/\lambda\sim 10^{-2}$.

5.4.2 On dark matter models and constraints

Since DM has escaped detection so far (beyond gravitational), model builders have been prompted to think about new mechanisms to explain it, as well as more ways to search for it. Some proposals include very rich dark sectors, such as co-annihilation scenarios [231] or hypothetical dark gauge groups [232], enlarging the exotic spectrum associated to the DM problem and consequently predicting new phenomenological results.

WIMPs are, on the other hand, one of the oldest and simplest candidates for this problem. The defining feature of a WIMP is that the observed relic abundance[12] [233],

$$\Omega_{\text{obs}} h^2 = 0.1200 \pm 0.0012\,, \tag{184}$$

is naturally explained within the standard cosmology with a weak-scale cross section; see appendix E. It is not of little importance that this simple solution for DM points to new physics exactly at the same scale as the HP. These coincidence of scales is actually a prediction of CHMs, where additional pNGBs at the EW scale naturally arise, which can play the role of a WIMP if endowed with a stabilizing symmetry. We focus on this DM candidate from here on.

At large cosmological scales, the WIMP candidate behaves as cold, collisionless, weakly interacting DM which is in very good agreement with all observations [234]. Some discrepancies are however observed at scales smaller than $\mathcal{O}$(Mpc) [235], which are more sensitive to baryon interactions. At these small scales, structure formation is a complicated problem that has been taken care of using DM-*only* N-body simulations. The magnitude of these small scale effects is therefore still unclear and could be significantly reduced by including baryonic processes in the simulations [236]; we ignore these effects in the following analysis.

Not only must WIMPs (as any other DM candidate) respect the relic density bound in equation 184, but they are also severely constrained by collider searches, as well as direct and indirect detection searches for DM. At colliders, the DM particles are stable, so they are typically searched for in final states with large MET and at least an additional hard jet to trigger the event. On the other hand, direct detection experiments search for signs of DM in the recoils of atomic nucleus when scattered off by DM particles. These are Earth-based ultra-sensitive laboratories with low-backgrounds which provide the strongest bounds on the WIMP parameter space up to date. They are limited to the target size and the amount of DM particles available $\sim \rho_{\text{DM}}/m_{\text{DM}}$, hence they are typically sensitive to the mass range $1\,\text{GeV} \lesssim m_{\text{DM}} \lesssim$ few TeV [237]. Sub-GeV DM can be instead tested when scattering off electrons. This detection strategy has been recently proposed in the literature and studied intensively by both theory and experimental groups [238, 239].

Finally, in indirect detection, the stable products resulting from the DM annihilation into the SM particles are collected in large telescopes. In comparison to direct detection, these searches face larger backgrounds

[12] The density parameter Ω is defined as the ratio between the observed energy density of a given component and the critical density of the Universe today, $\rho_c^0 = 3H_0^2/8\pi G$. In addition, $h \sim 0.7$ in equation 184 is the reduced Hubble parameter [9].

from different astrophysical environments. For instance, the cosmic rays resulting from the DM annihilation diffuse through the magnetic fields in the Galaxy, which leads to significant changes in their spectrum from the source up until the collection point. To trace back their origin, we therefore need to rely on numerical simulation of their propagation and the modeling of the galactic magnetic field, which is quite non-trivial [240]. In comparison, the gamma-ray spectrum is much more reliable given that photons reach the detector in close to straight lines.

Although strong limits have been obtained on WIMP scattering and production at these facilities, the corresponding bounds do not show model-independent sensitivity to generic WIMP models. Instead, they assume specific annihilation fractions into the SM and other signal features which can only probe particular scenarios. Therefore, the lack of observations definitely does not rule out all WIMP candidates. There can be, for example, momentum suppression, or loop suppression, in the direct detection cross section that makes the experimental bounds much weaker while leaving the total annihilation cross section unchanged. Another possibility is the presence of a new mediator which can affect the direct and indirect detection processes non-trivially, specially if it lies below the DM scale, which is the hypothesis we take in this work.

In such case, it is *not* straightforward to quantify when the WIMP hypothesis is excluded using existent data. The experimental collaborations present bounds on $2\,\mathrm{DM} \longrightarrow 2\,\mathrm{SM}$ processes, whereas the presence of the intermediate step in the annihilation chain, $2\,\mathrm{DM} \longrightarrow 2\kappa \longrightarrow 4\,\mathrm{SM}$, doubles the number of SM particles in the final state. Consequently, the showering process is altered in this last case, leading to changes in the spectrum of stable particles and their fluxes at telescopes. Therefore, we cannot simply rescale the bounds presented by the collaborations to constrain our model, but have to simulate all steps in the annihilation process up until detection. Likewise, collider searches for WIMPs alone are not sufficient to probe the model, but searches for the visible scalar are necessary as well. In the next sections, the signatures of our model at these facilities are explored in detail.

5.4.3 Relic density

The DM annihilation cross section into Higgs bosons in the limit of small DM velocity v[13] reads

$$\sigma v(\eta\eta \to hh) \simeq \frac{1}{64\pi m_\eta^2}\left[\lambda_{\eta H} - \frac{4m_\eta^2}{f^2}\right]^2\left[1 - \frac{m_H^2}{m_\eta^2}\right]^{1/2}, \tag{185}$$

where the second term in the effective vertex comes from the derivative interactions in equation 109. This expression holds similarly for the EW gauge bosons by virtue of the Equivalence Theorem, provided that $m_\eta \gg m_W$; and for $\eta\eta \to \kappa\kappa$ upon the replacements $m_H, \lambda_{\eta H} \to m_\kappa, \lambda_{\eta\kappa}$. In RegI, there is a partial cancellation between the portal coupling to the Higgs boson and the effective coupling, in the first bracket of equation 185. The extra scalar can therefore dominate the DM annihilation. In RegII, this cancellation

[13] We use the same letter to denote the velocity and the Higgs VEV in this section; the right meaning is obvious from the context.

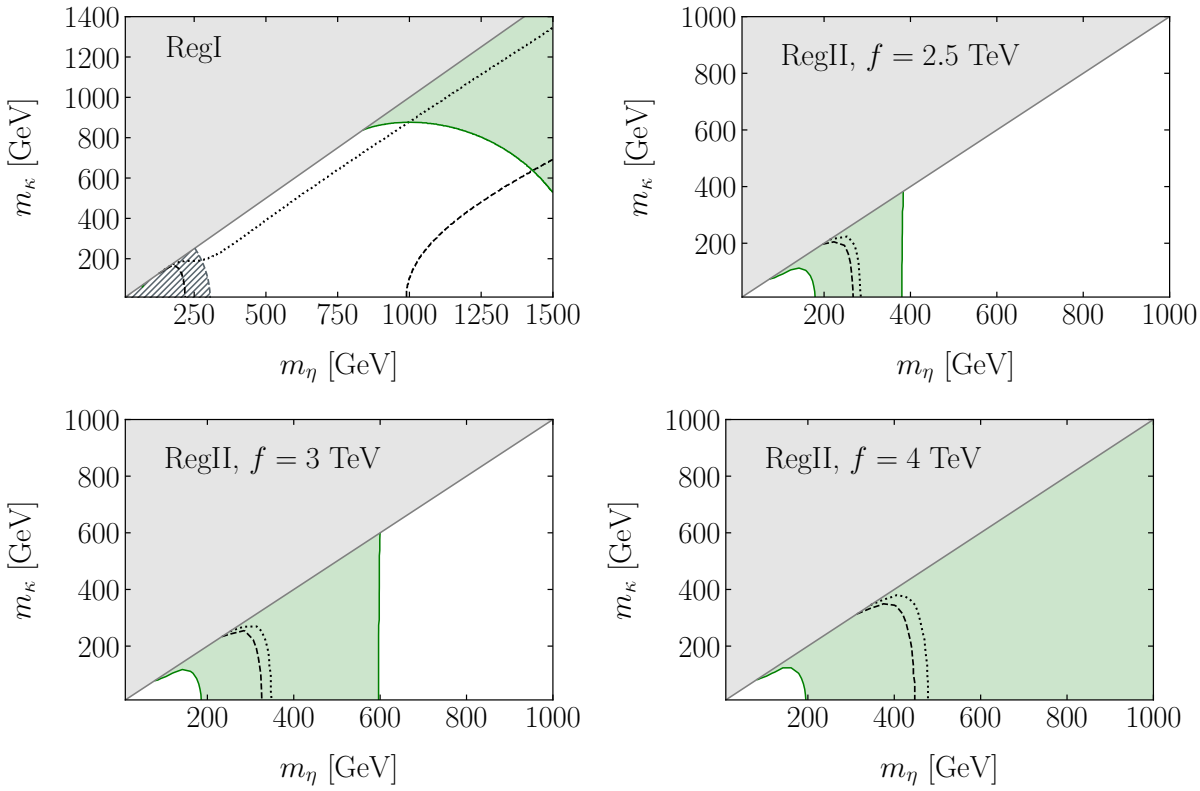

Figure 23: The parameter space excluded by the relic density constraint (in green) assuming that the DM is a thermal relic. The dotted (dashed) black lines correspond to an annihilation fraction into $\kappa\kappa$ equal to 0.2 (0.3). The area enclosed by the solid gray line is theoretically forbidden. The upper left panel and the upper right, bottom left and bottom right panels stand for RegI and RegII with $f = 2.5, 3$ and 4 TeV, respectively. In RegI, the slashed area is ruled out by EWPD.

occurs instead in $\sigma v\,(\eta\eta \to \kappa\kappa)$. After EWSB, there are additional contributions from a Higgs particle exchange in the s-channel, which are further suppressed by a factor of μ_H^2/m_η^2.

To clarify this behavior, we determine the region of the plane (m_η, m_κ) for which the relic density is above the measured value; see equation 184. With this aim, we use `micrOmegas` [241] with a model implemented in `Feynrules` [78] (we cross-checked the limits using `MadDM` [242] and found perfect agreement). The corresponding area is enclosed by the solid green line in figure 23 for RegI and for RegII with $f = 2.5, 3, 4$ TeV (the parameter space for $f = 1$ TeV is unconstrained). Contour lines of constant annihilation fraction into $\kappa\kappa$ are also plotted. In RegI, the slashed gray area corresponds to values of f excluded by EWPD; see section 4.6.2. We assume that the leading contribution to these observables is the modification of the scalar-vectors coupling due to the pNGB nature of the Higgs boson; in turn, scales $f \lesssim 900$ GeV [159] are excluded.

Let us first focus on RegII and analyse the results for $f = 2.5$ TeV. It is clear that the behavior of the relic density can be described in three regions of increasing m_η:

1. $m_\eta^2/f^2 \ll 1$: the annihilation cross section $\sigma v(\eta\eta \to \kappa\kappa)$ grows quadratically with $\lambda_{\eta\kappa} \sim \lambda_H$,

being large enough to make $\Omega_\eta h^2 < \Omega_{\text{obs}} h^2$;

2. $m_\eta^2/f^2 \sim \lambda_{\eta\kappa}$: in this regime, there is destructive interference between the two terms in equation 185, leading to overabundance of the DM;

3. $m_\eta^2/f^2 \gg 1$: the derivative term dominates the dynamics and the DM abundance decreases again.

Note that, during the last transition, the observed relic abundance is attained quite independently from m_κ. For a given f, the value of m_η at which this transition takes place matches the one from equation 12 in Ref. [175]. Furthermore, note that, for $m_\eta \sim 200$ GeV, a thermal η can be all the DM in our Universe while annihilating sizably into the exotic pNGB; it can therefore freeze out even in the absence of couplings to the SM.

This three-phase picture is modified in RegI where $f \propto m_\eta$ (see equation 180), making the derivative interactions already significant at small m_η. Explicitly,

$$\sigma(\eta\eta \to hh) \propto \frac{\lambda_H^2}{m_\eta^2}\left(1 - \frac{4}{1+\frac{m_\kappa^2}{2m_\eta^2}}\right)^2 \quad \text{while} \quad \sigma(\eta\eta \to \kappa\kappa) \propto \frac{\lambda_H^2}{m_\eta^2}\left(\frac{4}{1+\frac{m_\kappa^2}{2m_\eta^2}}\right)^2 . \tag{186}$$

Therefore, by increasing m_κ while keeping m_η fixed (*i.e.* increasing f), the effective couplings become smaller and η becomes overabundant. Increasing m_η instead while keeping m_κ fixed leads to the opposite effect; however, as the cross sections scale with m_η^{-2}, this will eventually lead to overabundance as well. Altogether, the previous arguments explain the shape of the upper left panel in figure 23.

Let us further note that the requirement $\Omega_\eta h^2 = \Omega_{\text{obs}} h^2$ establishes a relation between m_η and m_κ, effectively removing one free parameter. (This conclusion fails if the DM is non-thermal.) In RegI, the corresponding relation reads approximately

$$\begin{aligned} m_\kappa\left(m_\eta\right) \approx \big[&-5461.99 + 21.002\left(m_\eta/\text{GeV}\right) - 2.6313\times10^{-2}\left(m_\eta/\text{GeV}\right)^2 \\ &+ 1.4988\times10^{-5}\left(m_\eta/\text{GeV}\right)^3 - 3.3382\times10^{-9}\left(m_\eta/\text{GeV}\right)^4 \big]\ \text{GeV}, \end{aligned} \tag{187}$$

for $m_\eta \in [800, 1500]$ GeV. This relation implies a bound on $2.8 \lesssim f \lesssim 3.3$ TeV. This contrasts with CHMs without DM, in which this upper bound relies on naturalness arguments, rather than on actual observables. Interestingly, for WIMPs, the relic density constraint favors natural new physics scales, not yet excluded by other data.

5.4.4 Direct Detection

The spin-independent (SI) elastic scattering cross section of η on a nucleus reads [53]:

$$\sigma_{\text{SI}} = \frac{1}{\pi}\left(\frac{m_\eta m_n}{m_\eta + m_n}\right)^2 \frac{\left[Z f_p + (A-Z) f_n\right]^2}{A^2}\,, \tag{188}$$

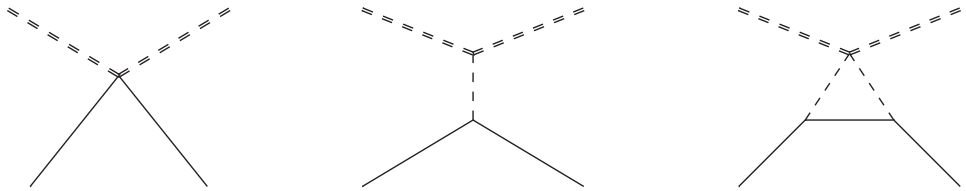

Figure 24: Contributions to the $\eta^2\bar{q}q$ effective operator at low energies from the contact interaction (left), the exchange of a Higgs particle (center) and a loop induced by interactions with κ (right).

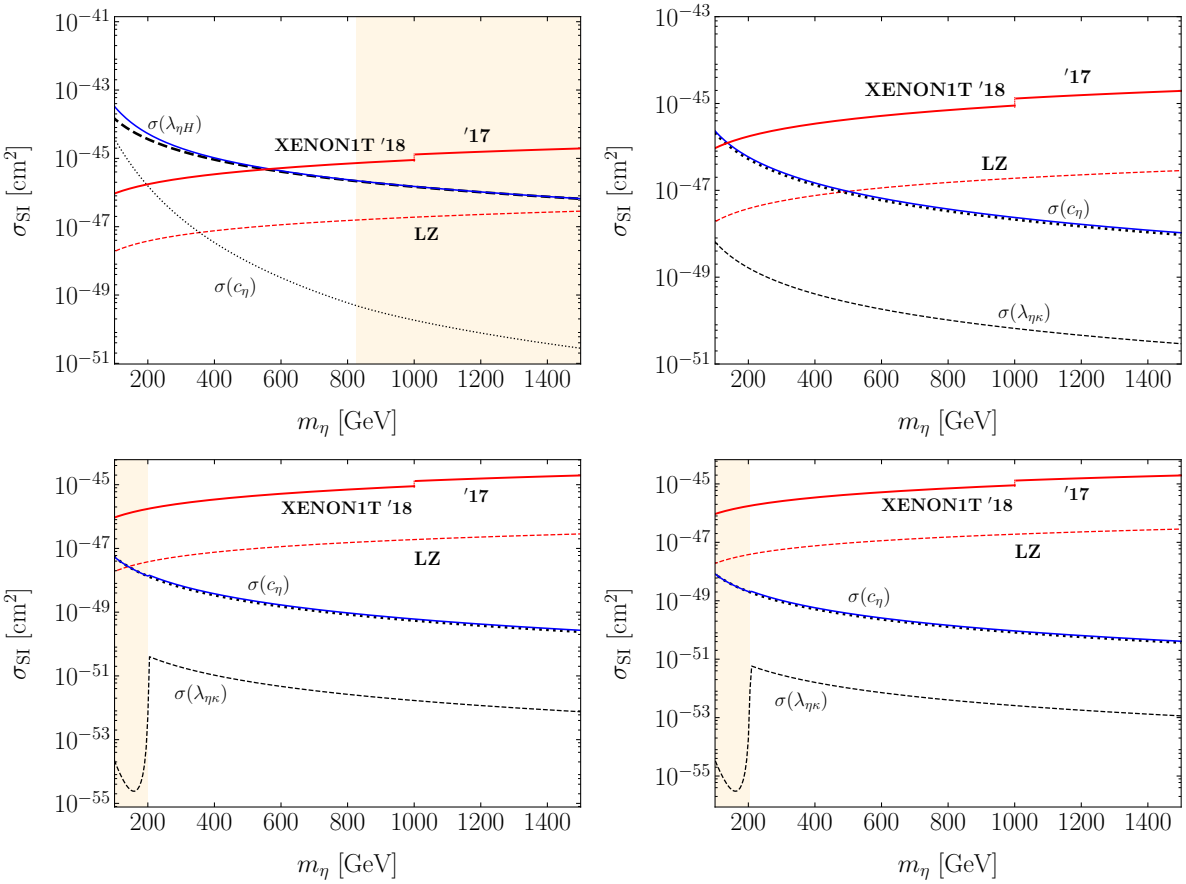

Figure 25: Spin independent cross section for direct detection as a function of the DM mass, in RegI (upper left panel) and RegII with $f = 1,\ 2.5$ and 4 TeV (upper right, bottom left and bottom right panels, respectively). The black dashed and dotted lines stand for the scalar mediated and contact interaction contributions in each regime, whereas the blue line represents the sum of all contributions. The solid red and dashed curves are for the XENON1T and LZ exclusion limits, respectively. Across all masses, we assume that η makes up all the DM in the Universe. In particular, η is a thermal relic in the orange region, where m_κ is fixed by equation 187.

where $m_n \sim 1$ GeV is the neutron mass; Z and $A - Z$ are the numbers of protons and neutrons in the nucleus, respectively; and the form factors are defined as

$$f_{n,p} = \sum_{q=u,d,s} f_{T_q}^{(n,p)} a_q \frac{m_{n,p}}{m_q} + \frac{2}{27} f_{T_G}^{(n,p)} \sum_{q=c,b,t} a_q \frac{m_{n,p}}{m_q} \,. \tag{189}$$

The matrix elements f_{T_q} parameterize the quark content of the nucleon; we take them from Ref. [53]. The DM coupling to gluons, via loops of heavy quarks, is encoded in $f_{T_G} = 1 - \sum_{q=u,d,s} f_{T_q}$. Finally, a_q stands for the coefficient of the effective operator $m_q \eta^2 \bar{q} q$ at low energies. In our model, it is generated at tree level by the left and central diagrams in figure 24, and at the loop level by the diagram on the right:

$$a_q = \frac{m_q}{m_\eta} \left[\frac{c_\eta}{2f^2} + \frac{\lambda_{\eta H}}{2m_h^2} + \frac{\lambda_{\eta\kappa} c_\kappa^2}{32\pi^2} \left(\frac{m_q}{m_\kappa f} \right)^2 \right]. \tag{190}$$

We assumed that m_κ is the largest scale involved in the nuclear interaction to obtain the third term in the equation above. In figure 25, we represent each of these contributions to the SI scattering cross section as a function of the DM mass. The scalar couplings are defined according to section 5.4.1; we fixed $\theta = 1$, to explore the flavour universal scenario. The total SI scattering cross section is plotted in blue. Superimposed are the current (in solid red) and future (in dashed red) bounds from the XENON1T [243, 244] and the LZ [245] experiments. They both use liquid xenon as the target for direct detection, which is very efficient in converting the nuclear recoils into scintillation and ionization signals and very sensitive to the DM interactions due to its large A. In the orange region, we used the relation in equation 187 to study the scenario where a thermal η is all the observed DM in the Universe. To probe the non-minimal setup, we fixed $m_\kappa = 10$ GeV outside this region.

While RegI is partially ruled out by XENON1T, RegII leads to theoretical cross sections which are typically two (four) orders of magnitude below the LZ projected limit for a non-zero (zero) c_η. Moreover, in the region where $\Omega_\eta h^2 = \Omega_{\text{obs}} h^2$, the cross section is much more suppressed. This regime therefore evades all direct detection constraints, even at future facilities. Complementary probes are therefore of extreme importance.

5.4.5 Indirect Detection

To predict the indirect detection signals of our model, we resort to `MadDM` [242], where we can compute the spectra resulting from the DM annihilating into an arbitrary number of exotic final states. The simulation (in the *precise* mode; see the manual for details) proceeds in three steps: *(1)* the annihilation cross section is computed at parton level with `MadGraph`; *(2)* the subsequent decay, showering and hadronization of the final state particles is performed by `Pythia`; *(3)* the energy spectrum dN/dE of a given stable particle species is generated at the source. Examples of the prompt gamma ray spectra produced in different DM annihilation channels are provided in figure 26. The presence of the exotic κ leads to a shift effect in the resulting spectra to the left, due to the larger multiplicity of SM particles which are produced in the final state.

The results in figure 26 can be subsequently used to obtain the gamma ray flux from DM annihilation

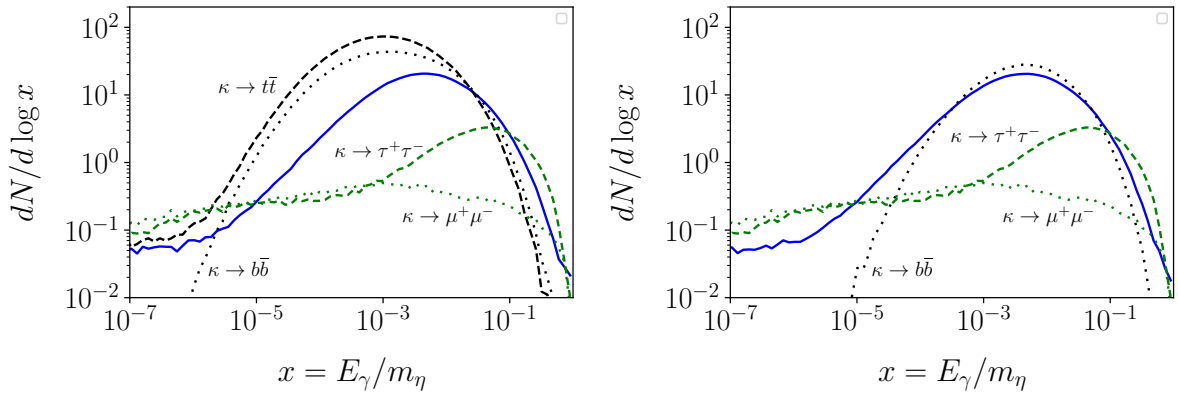

Figure 26: Energy spectra of prompt gamma rays at the production point. The blue line corresponds to $\eta\eta \to hh + W^+W^- + ZZ$ (no intermediate step). The other curves stand for the annihilation into $\kappa\kappa$, in different decay modes. (The gamma-ray spectrum from $\kappa \to e^+e^-$ is very similar to that of $\kappa \to \mu^+\mu^-$; we therefore do not show it.) These plots correspond to a BP with $m_\eta = 2m_\kappa$ along the line where the DM thermal abundance equals the observed value; see figure 23. The left (right) panel refers to RegI, with $m_\eta \sim 1.3$ TeV (RegII, with $f = 2.5$ TeV and $m_\eta \sim 180$ GeV).

at different facilities:

$$\Phi\left(\Delta\Omega, E_{\text{min}}, E_{\text{max}}\right) \propto \frac{\langle\sigma v\rangle}{m_\eta^2} \int_{E_{\text{min}}}^{E_{\text{max}}} \frac{dN_\gamma}{dE_\gamma} dE_\gamma \times \int_{\Delta\Omega}\int_{\Delta l} \rho^2_{\text{DM}}(\vec{r}(l)) dl d\Omega \,, \tag{191}$$

where $\langle\sigma v\rangle$ is the velocity averaged DM annihilation cross section and N_γ (E_γ) is the number (kinetic energy) of prompt photons in the final state. The second term in this equation is the so-called "*J*-factor", a geometric function that depends on the integration of the DM density over the solid angle ($\Delta\Omega$) and the line of sight (Δl).

To be finally able to constrain the model, `MadDM` includes the Fermi-LAT likelihoods for gamma rays from dwarf spheroidal galaxies [246]. These satellite galaxies are the most reliable sources for indirect detection due to their proximity, large DM density and the fact that they are nearly free from other gamma-ray emission. In contrast, the GC, in spite of being the brightest DM source in the sky, has also bright astrophysical backgrounds with large uncertainties which vary significantly with the DM density profile [247, 248]. For these reasons, we do not consider the bounds from the H.E.S.S. [249] experiment, for example, which can be the strongest for $m_\eta \gtrsim 1$ TeV.

Instead, we focus on the combined analysis performed by Fermi-LAT involving 45 stellar systems, among which 28 confirmed DM–dominated dwarfs (Pass 8 data), with a sensitivity window between 500 MeV $< E_\gamma <$ 500 GeV [246]. No significant global excess was observed and therefore strong bounds can be set on the gamma ray flux predicted from this model, which can be reinterpreted in terms of cross section constraints, for a given DM mass. The expected upper limits at the 95 % CL are plotted in figure 27, for the different regimes. We set $m_\kappa = m_\eta$ and $m_\kappa = 20$ GeV outside the orange region for RegI and RegII, respectively. For comparison, we also plot the bounds on the DM annihilation cross section into the

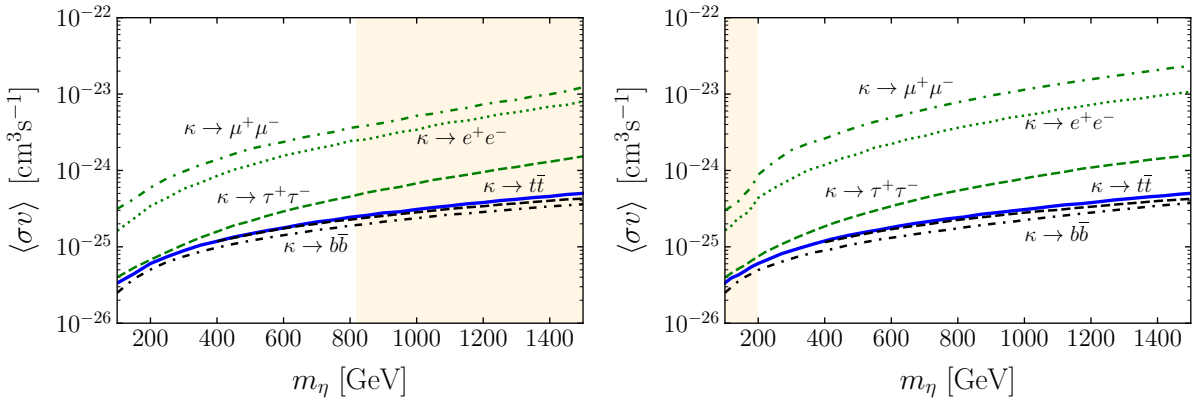

Figure 27: The new Fermi-LAT upper bounds in the plane $(m_\eta, \langle\sigma v\rangle)$, for different decay channels of the exotic particle. The solid blue line stands for $\eta\eta \longrightarrow hh + W^+W^- + ZZ$, giving the dominant contribution to the DM $\longrightarrow$ SM annihilation in the limit of large masses. In the orange area, m_κ is a function of m_η to fit $\Omega_{\text{obs}}h^2$. The results for RegI and RegII ($f = 2.5$ TeV) are shown in the left and right panels, respectively.

SM bosons ,with no intermediate exotic step. To the best of our knowledge, the results of this dedicated simulation are new in the literature; they can be furthermore used to constrain other DM models with new $d.o.f.$ below the DM scale.

From figure 27, it is clear that the exotic decays into the light leptons are the most weakly constrained. On the other hand, final states with quarks produce hadrons, namely neutral pions that decay $\sim 100\%$ [9] into low-energy photons, making the gamma spectrum much larger. Moreover, after running identical simulations for $\eta\eta \longrightarrow \bar{\psi}\psi$, we found that the light lepton channels are also the most affected by the inclusion of the intermediate step in the annihilation chain $\eta\eta \longrightarrow \kappa\kappa \longrightarrow \bar{\psi}\psi\bar{\psi}\psi$, particularly muons, whose photon spectrum originates mainly from final state radiation and becomes very flat; see figure 26. Generically, the impact of the exotic step in the indirect detection bounds can lead to two opposite effects: on one side, the shift of the spectrum peak to the left leads to a larger number of photons in the lowest energy bins, where the noise levels are typically larger, therefore weakening the bounds; on the other side, for large DM masses, the intermediate step might rather strengthen the constraints by moving the spectrum that is above the 500 GeV threshold back to the Fermi window.

Let us also remark that if a thermal η explains the totality of the DM abundance, its annihilation cross section should be of the order $\langle\sigma v\rangle \sim 3 \times 10^{-26}\,\text{cm}^3\ \text{s}^{-1}$ (just using the parameters in equation 399). This cross section is unconstrained by the Fermi data in both regimes. Next-generation Cherenkov telescopes, with an improved capability to discriminate the GC radiation components, such as CTA [250], might strengthen the Fermi bound by one-to-two orders of magnitude [248]. In this case, the all DM scenario could be excluded if η annihilates entirely into the SM or into $\kappa\kappa$, with $\kappa \longrightarrow \bar{q}q$. The leptophilic scenario would still be, on the other hand, entirely unconstrained. Note that there is freedom in the CHM to make κ leptophilic, as $c_\kappa \propto \theta$ (this is not the case for the DM coupling to the SM fermions; see

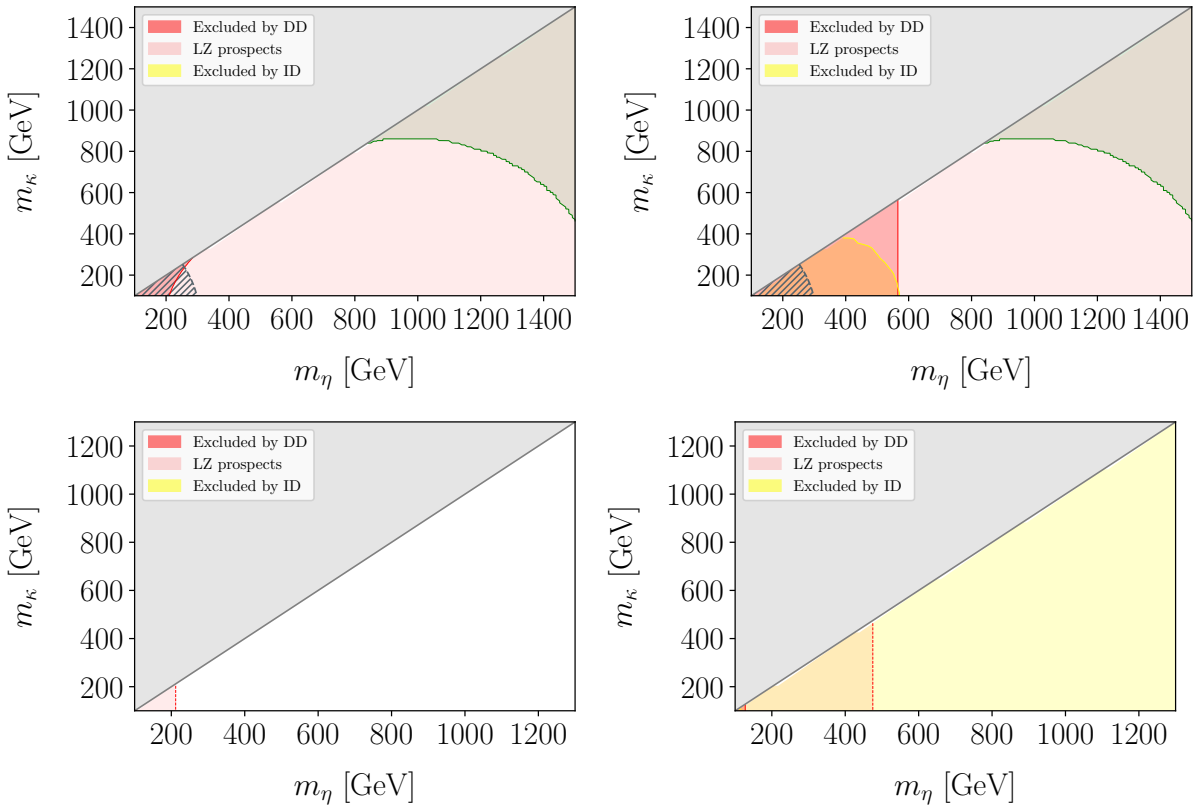

Figure 28: Combined constraints from the different DM searches. The green region is excluded by the observed relic density. The red and yellow regions are excluded by direct and indirect detection searches, respectively; while the red light region could be potentially tested at the future LZ experiment. In the slashed region, f is ruled out by EWPD. The upper left (right) panel corresponds to the thermal (non-thermal) scenario in RegI. The same holds for the bottom left and right panels in RegII, for $f = 1$ TeV.

equation 178). In particular, if all quarks are embedded in $SO(7)$ representations that do not break the shift-symmetry of κ, we are led to $\theta^q = 0 \neq \theta^\ell$.

Assuming instead $\theta = 1$ for all the fermions[14] (universal scenario), we gathered in figure 28 all the DM constraints obtained for each regime. The green region is excluded by the relic density; while the red and yellow regions are excluded by the current direct and indirect searches, respectively. The future LZ experiment could additionally probe the light red region. The left and right panels correspond, respectively, to the case of thermal and non-thermal DM. In the thermal scenario, if η is under-abundant, we take into account the possibility that the missing fraction of the relic density might arise from other species (such as primordial black holes) and therefore rescale all fluxes for direct and indirect detection by $r = (\Omega_\eta h^2)/(\Omega_{\rm obs} h^2)$ and r^2, respectively. In the non-thermal scenario, no rescaling is applied; see Ref. [251] for an explicit realization. As can be seen, some regimes could be entirely probed at future direct detection facilities, or even by the new bounds we derived for indirect detection. In contrast, RegII

[14]Note that, for the heaviest fermions which give the leading contribution to the scalar potential, we have traded this parameter for the scalar masses, that is $\theta \approx 1 - m_\kappa^2/2m_\eta^2$. In the present discussion, we keep only the LO term for purposes of illustration.

with thermal DM escapes all constraints. Together with the leptophilic scenario, this strongly motivates other searches, such as those at colliders.

5.4.6 Collider signals

We focus on LHC probes of the pNGB particles produced in the decay of heavy VLQs, which are the *smoking gun* prediction of compositeness. (Moreover, other production mechanisms for these scalars in the SM are suppressed, as they are singlets of the gauge group.)

We focus on scenarios with light singlet top partners [119, 252]. In the $\mathbf{27} \oplus \mathbf{1}$ model, such partners can transform in the $\mathbf{1}$, $\mathbf{6}$ or $\mathbf{20}$ representations of the $SO(6)$ group. We denote the full singlet by $\tilde{T}$, and the other $SO(5)$ and $SO(4)$ singlets in the $\mathbf{6} = \mathbf{5} \oplus \mathbf{1} = \mathbf{4} \oplus \mathbf{1} \oplus \mathbf{1}$ by T' and T'', respectively. (We ignore the largest representation of the $\mathcal{H}$-group in the following discussion.) The relevant phenomenology of these top partners is determined from the linear couplings to the SM:

$$\mathcal{L}_{\mathbf{1}} = \cdots + f U_7^i U_7^j \left(\overline{Q_L^{\mathbf{27}}}\right)_{ij} T_R^{\mathbf{1}} + \text{h.c.} = \left[\ldots - h\overline{t_L} - \mathrm{i}\theta \frac{v}{f} \kappa \overline{t_L}\right] \tilde{T}_R + \text{h.c.}\,; \tag{192}$$

$$\begin{aligned} \mathcal{L}_{\mathbf{6}} &= \cdots + f U_7^i U_k^j \left(\overline{Q_L^{\mathbf{27}}}\right)_{ij} \left(T_R^{\mathbf{6}}\right)^k + \text{h.c.} \\ &= \frac{3}{4}\frac{v}{f}\eta \overline{t_L} T_R' + \left[\frac{3}{4}\frac{v}{f}\kappa \overline{t_L} - \mathrm{i}\theta \frac{1}{2} h \overline{t_L}\right] T_R'' + \text{h.c.} \end{aligned} \tag{193}$$

The same equations hold for bottom partners.

We explore the pair-production of these VLQs in pp collisions, which is dominated by model-independent QCD processes. The corresponding cross section drops sharply with the mass M and therefore VLQ searches in this context are more adequate for future colliders [176]. In particular, the QCD production of T' typically yields a $t\bar{t} + E_T^{\text{miss}}$ final state. This signal is equivalent to that of pair-produced stops decaying into stable neutralinos in SUSY; the prospects to test this process at a future 100 TeV collider have been studied in Ref. [253]. By rescaling the results with the VLQ production cross section, to account for the different spin of particles in the initial state, the authors of Ref. [176] have set bounds on the plane (M, m_η). For a collected luminosity of $1\,\text{ab}^{-1}$ and assuming $\mathcal{B}\left(T' \to \eta t\right) = 1$, the authors found that masses $M \lesssim 9\,\text{TeV}$ and $m_\eta \lesssim 3$ TeV could be excluded, if no deviation from the SM predictions is observed.

Nonetheless, the non-minimal structure of the model can be only established if, together with the process above, decays of the VLQs into κ are observed. No specific searches for this channel have been proposed for 100 TeV colliders and only limits in a narrow mass range have been obtained using LHC results [165, 254–263]. Thus, we provide dedicated searches for this case. We focus on $pp \to B\overline{B} \to \kappa\kappa b\bar{b}$, assuming a hierarchical parameter space where $M \in [1000, 9000]$ GeV and $m_\kappa \in [50, 400]$ GeV.

There are, in fact, additional reasons to concentrate mostly on this channel: *(1)* if $\tilde{B}$ is the lightest resonance, the DM channel is absent, while decays into κ will be in general present, providing the only

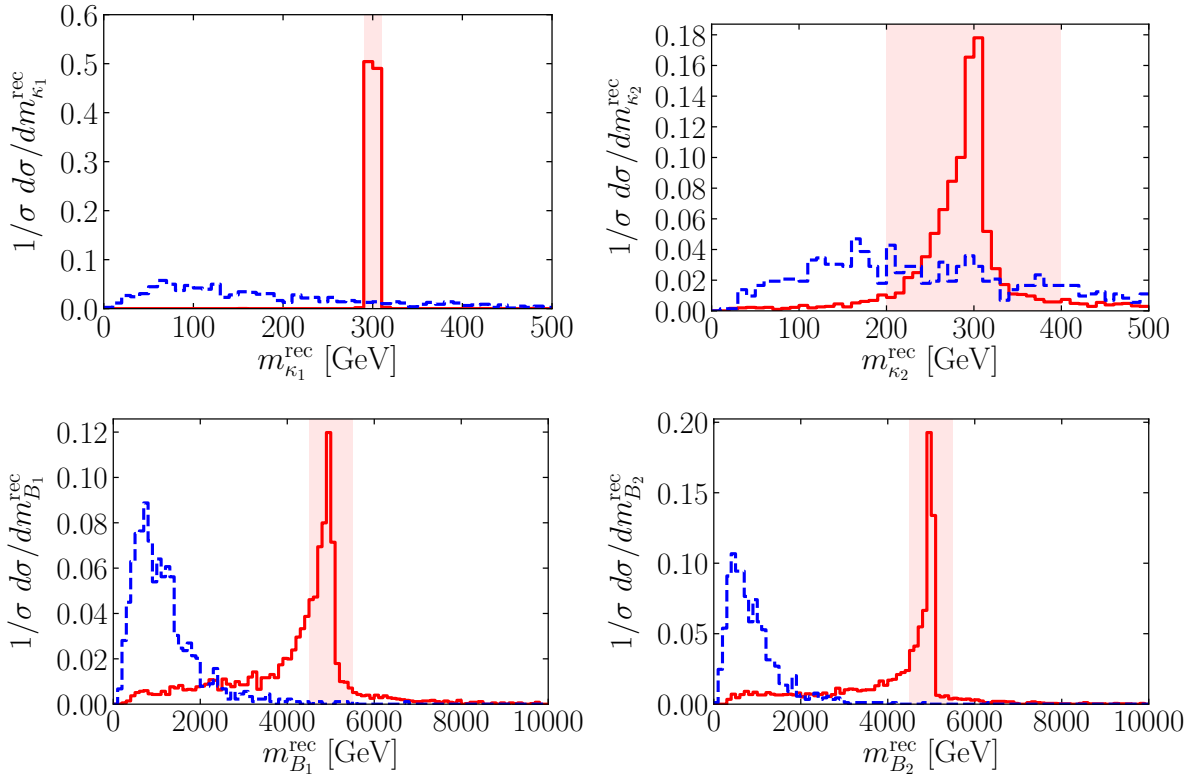

Figure 29: Normalized distributions of $m^{\rm rec}_{\kappa_1}$ (upper left), $m^{\rm rec}_{\kappa_2}$ (upper right), $m^{\rm rec}_{B_1}$ (bottom left) and $m^{\rm rec}_{B_2}$ (bottom right) in the signal for $M = 5$ TeV and $m_\kappa = 300$ GeV (solid red) and in the SM background (dashed blue), in the analysis proposed for $pp \to B\overline{B} \to \kappa\kappa b\overline{b}$, $\kappa\kappa \to \gamma\gamma b\overline{b}$. Subsequent cuts are imposed to make the different variables lie within the light red regions.

insight into the composite structure of the model; *(2)* if the sextuplet is the lightest one, B'' will decay mainly into κb[15] under our previous assumption that $\theta \leq 1$; *(3)* after the decay of κ, this channel gives rise to a very clean signature, allowing to reconstruct the masses of κ and B relatively easily. Another advantage of this channel is that it can be used to constrain other CHMs not necessarily having DM, such as the $SO(6)/SO(5)$ model.

Regarding the decays of the unstable singlet, we study three possibilities:

1. $\kappa\kappa \to b\overline{b}\gamma\gamma$: this combines the large branching ratio of the singlet decay into third generation quarks (in the universal scenario) with the good mass resolution and low backgrounds of the photon channel. Such final state has been considered in many other studies; see, for example, Refs. [264, 265].

2. $\kappa\kappa \to b\overline{b}b\overline{b}$: in this case, both singlets decay via the dominant mode, for the mass range considered in this study.

3. $\kappa\kappa \to \mu^+\mu^-\mu^+\mu^-$: finally, this channel is intended to complement the very weak bounds from

[15] This contrasts with the results from Ref. [119], which were obtained under the assumption that the derivative interactions $c_R\overline{T_R}d_\mu\gamma^\mu t_R$ dominate over those in equation 193. Our statement in *(2)* is therefore applicable only if $c_R \ll 1$.

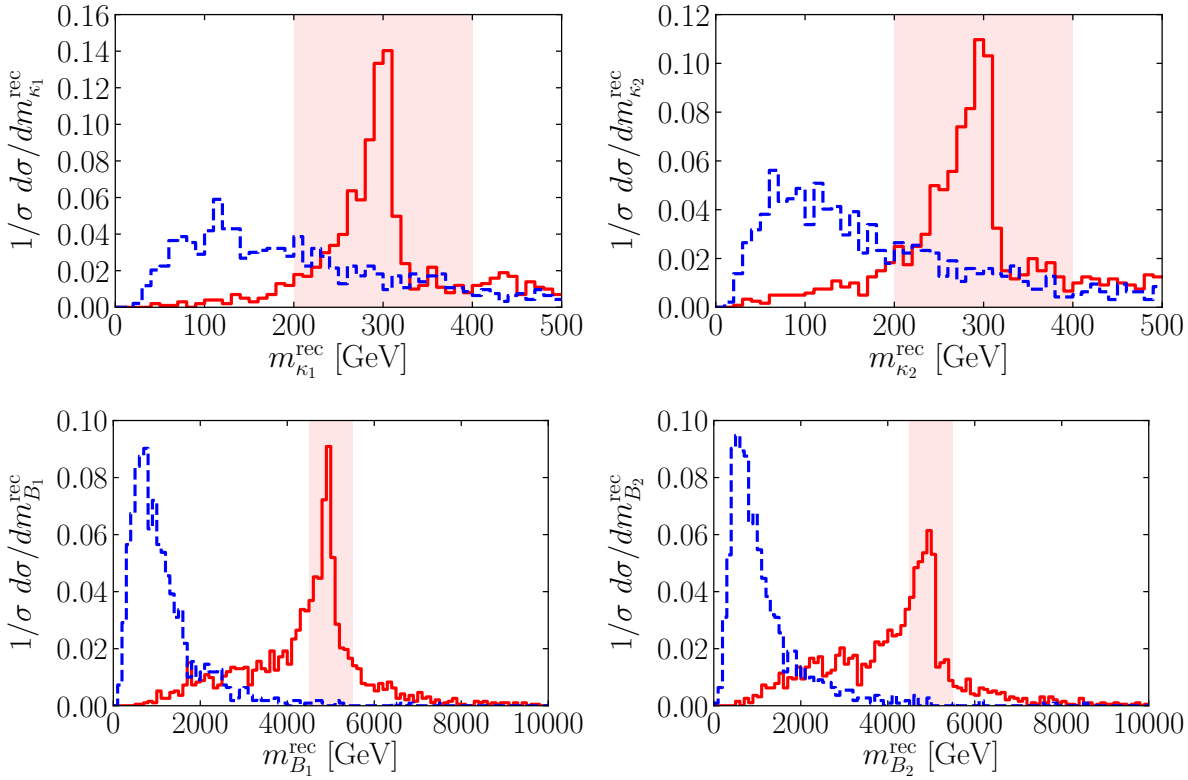

Figure 30: Normalized distributions of $m^{\rm rec}_{\kappa_1}$ (upper left), $m^{\rm rec}_{\kappa_2}$ (upper right), $m^{\rm rec}_{B_1}$ (bottom left) and $m^{\rm rec}_{B_2}$ (bottom right) in the signal for $M = 5$ TeV and $m_\kappa = 300$ GeV (solid red) and in the SM background (dashed blue), in the analysis proposed for $pp \to B\bar{B} \to \kappa\kappa b\bar{b}$, $\kappa\kappa \to b\bar{b}b\bar{b}$.

DM detection experiments we have obtained in the leptophilic scenario.

Below, we describe our proposed searches for each of these processes. Signal and background events are generated at $\sqrt{s} = 100$ TeV using `MadGraph`. The signal sample is produced with no parton level cuts. Both samples are subsequently showered and hadronized according to the procedure described in section 3.3. For the data analyses, we use dedicated routines based on `ROOT` and `Fasjet` [266] with no detector simulation.

In all cases, a lepton is considered isolated at the reconstruction level if the hadronic activity deposited in a cone of radius $\Delta R = 0.2$ is smaller than 10% of its p_T. Likewise for the photons. Furthermore, leptons (photons) are required to have $p_T > 20$ GeV and $|\eta| < 2.47$ ($|\eta| < 2.5$). We define jets using the anti-k$_t$ algorithm with $R = 0.4$. A jet is considered to be b-tagged if the angular separation between itself and a B-meson is $\Delta R < 0.2$, the tagging efficiency being fixed to 0.7.

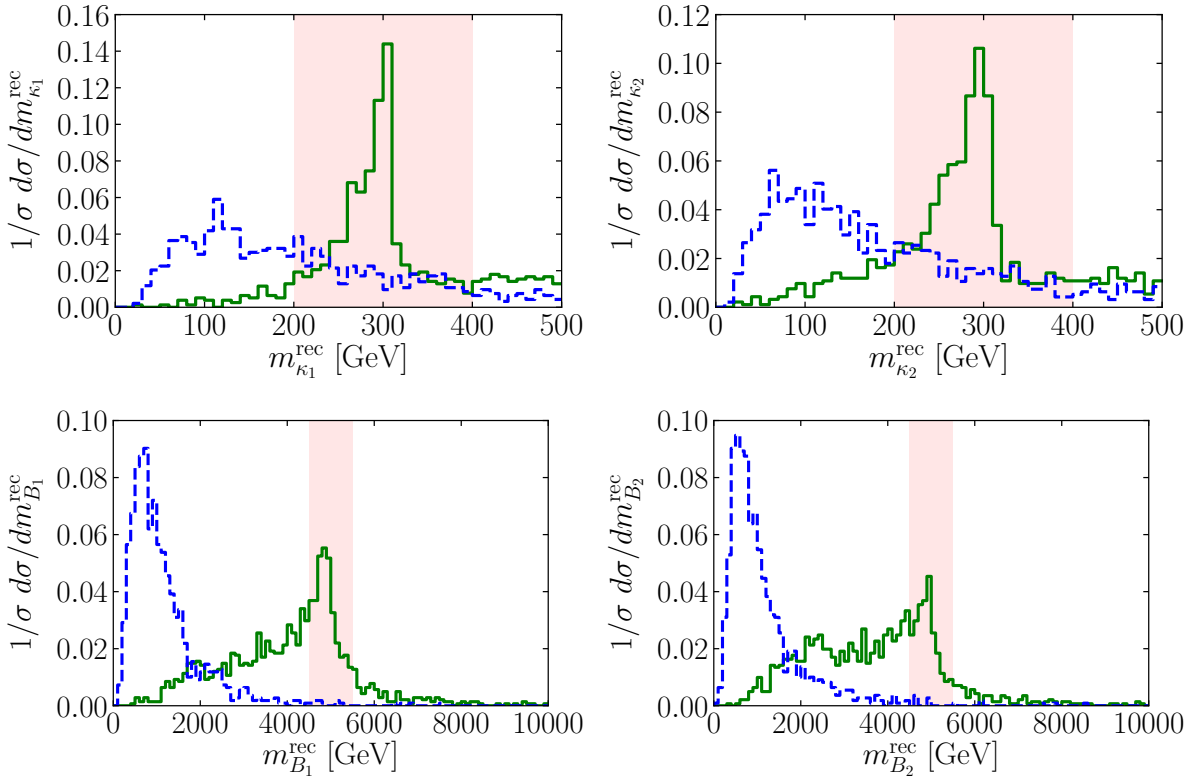

Figure 31: Normalized distributions of $m_{\kappa_1}^{\rm rec}$ (upper left), $m_{\kappa_2}^{\rm rec}$ (upper right), $m_{B_1}^{\rm rec}$ (bottom left) and $m_{B_2}^{\rm rec}$ (bottom right) in the signal for a top partner with $M = 5$ TeV and $m_\kappa = 300$ GeV (solid green) and in the SM background (dashed blue), in the analysis proposed for $pp \to B\bar{B} \to \kappa\kappa b\bar{b}$, $\kappa\kappa \to b\bar{b}b\bar{b}$.

5.4.6.1 $b\bar{b}\gamma\gamma$ final states

For the background, we consider the irreducible $pp \to b\bar{b}b\bar{b}\gamma\gamma$, with $p_T^{b_1} > 500$ GeV and $p_T^\gamma > 20$ GeV, where b_1 stands for the hardest b-quark. The cross section in this region of the phase space is ~ 0.006 pb. We require exactly two isolated photons and at least four b-tagged jets with $p_T > 20$ GeV. We also veto all events with a non-vanishing number of isolated leptons.

The invariant mass of the two photon system is denoted by $m_{\kappa_1}^{\rm rec}$. The momentum of the hadronically decaying scalar is considered to be the sum of the momenta of the two b-tagged jets with invariant mass closest to $m_{\kappa_1}^{\rm rec}$; its invariant mass being denoted $m_{\kappa_2}^{\rm rec}$. There is a two-fold ambiguity in assigning the remaining two hardest b-jets to either κ_1 or κ_2 to reconstruct the two vector-like B-quarks. In order to solve it, we choose the combination that minimizes $|m_{B_1}^{\rm rec} - m_{B_2}^{\rm rec}|$, with $m_{B_i}^{\rm rec}$ the invariant mass of the corresponding three-particle system.

In figure 29, we plot the normalized distributions of all these reconstructed masses, in both the signal and the background, for a BP defined by $M = 5$ TeV and $m_\kappa = 300$ GeV. The discriminating power of the observables is apparent. Thus, we select events fulfilling $|m_{\kappa_1}^{\rm rec} - m_\kappa| < 10$ GeV, $|m_{\kappa_2}^{\rm rec} - m_\kappa| < 100$ GeV, $|m_{B_1}^{\rm rec} - m_B| < 500$ GeV and $|m_{B_2}^{\rm rec} - m_B| < 500$ GeV. After such requirements, the analysis becomes

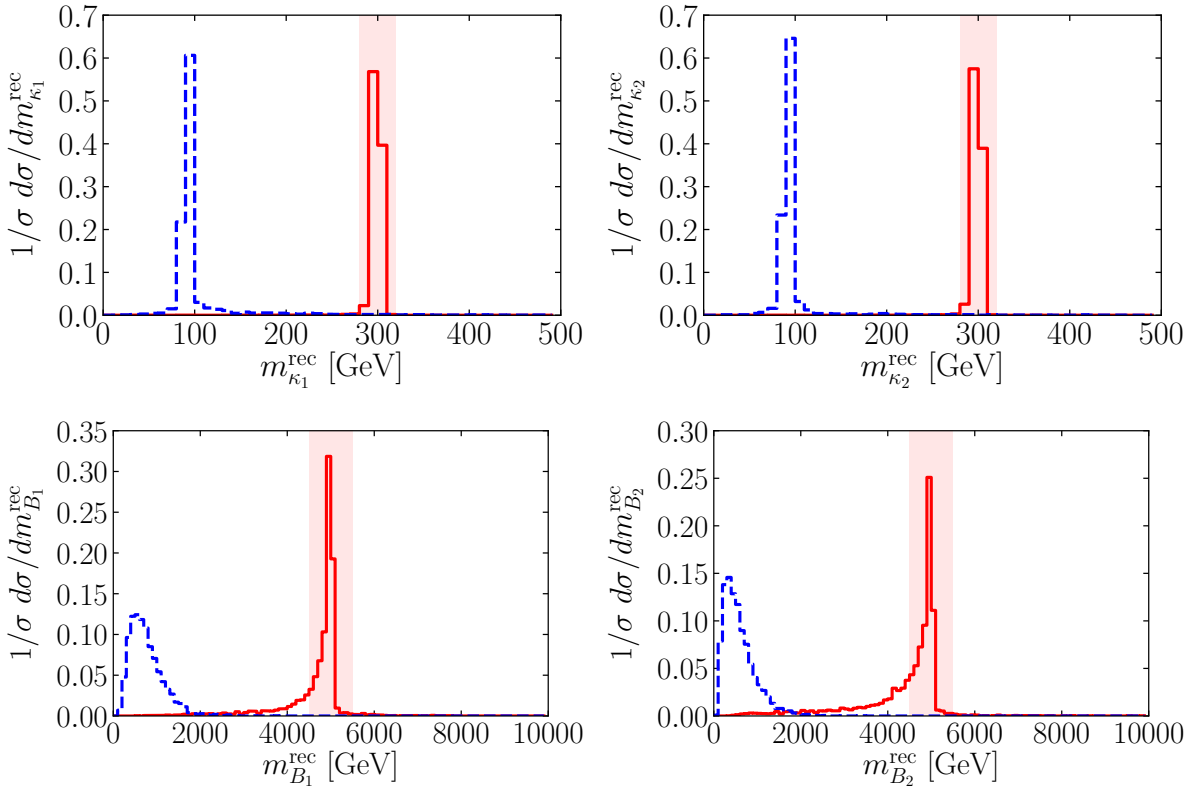

Figure 32: Normalized distributions of $m^{\rm rec}_{\kappa_1}$ (upper left), $m^{\rm rec}_{\kappa_2}$ (upper right), $m^{\rm rec}_{B_1}$ (bottom left) and $m^{\rm rec}_{B_2}$ (bottom right) in the signal for $M = 5$ TeV and $m_\kappa = 300$ GeV (solid red) and in the SM background (dashed blue), in the analysis proposed for $pp \to B\bar{B} \to \kappa\kappa b\bar{b}$, $\kappa\kappa \to \mu^+\mu^-\mu^+\mu^-$.

essentially background-free.

We make use of the CL_s method in ROOT to calculate exclusion limits; see section 3.4. (We use a linear interpolation of the CL_s results to cover the mass points that were not simulated.) The signal region which could be probed at the 95% CL is shown in the left panel of figure 33 for an integrated luminosity $L = 100$ fb^{-1}. The colored lines assume different values of $\mathcal{B}(\kappa \to \bar{b}b)$: 1, in orange; 0.8, in green; 0.4, in blue; and 0.1, in red. We have fixed[16] $\mathcal{B}(\kappa \to \gamma\gamma) = 10^{-3}$.

5.4.6.2 $b\bar{b}b\bar{b}$ final states

For the background, we consider $pp \to b\bar{b}b\bar{b}$, with $p_T^{b_1} > 500$ GeV; the extra two b-jets required to match the signal are to be found among the products of the Pythia shower. We checked explicitly that both $pp \to b\bar{b}b\bar{b}$ and $pp \to b\bar{b}b\bar{b}b\bar{b}$ have very similar distributions, validating the use of the former as the background sample[17]. This sample is normalized to the cross section of the actual background as

[16] We can naively estimate the decay widths of κ into the relevant final states, to obtain the branching ratio into di-photons: $\Gamma(\kappa \to \gamma\gamma) \sim \alpha_{\rm em}^2/(4\pi)^2(v/f)^2 m_\kappa^2/v$ while $\Gamma(\kappa \to \bar{\psi}\psi) \sim y_\psi^2(v/f)^2 m_\kappa$. Hence, $\mathcal{B}(\kappa \to \gamma\gamma) \sim \alpha_{\rm em}^2/(y_\psi 4\pi)^2 m_\kappa/v$.

[17] We will further assume systematic uncertainties in the background in the computation of the exclusion limits, to infer the impact of this assumption.

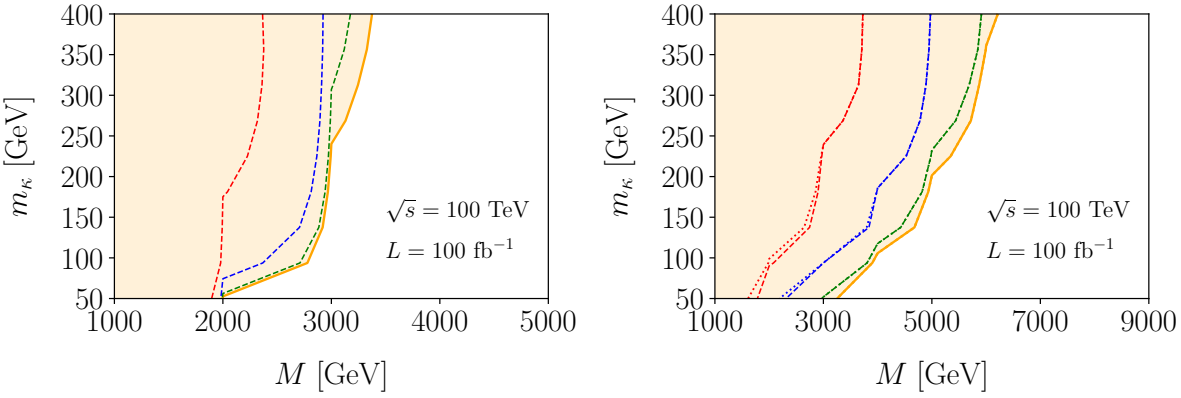

Figure 33: Exclusion lines at 95% CL in the plane (M, m_κ) for the first two analyses: $pp \to B\overline{B} \to \kappa\kappa b\bar{b}$, with $\kappa\kappa \to b\bar{b}\gamma\gamma$ (left) and $\kappa\kappa \to b\bar{b}b\bar{b}$ (right). We assume that the bottom partner decays 100% into this final state. The results are presented for a future 100 TeV collider with a collected luminosity of $100\,\text{fb}^{-1}$. The colored area enclosed by the orange solid, green dashed, blue dashed and red dashed lines could be excluded assuming that $\mathcal{B}(\kappa \to \bar{b}b) = 1,\ 0.8,\ 0.4$ and 0.1, respectively. In the left panel, we have set $\mathcal{B}(\kappa \to \gamma\gamma) = 10^{-3}$. In the right one, the dashed and solid (dotted) lines are obtained assuming a systematic uncertainty of 20% (50%) in the computation of the limits.

computed with `MadGraph`, roughly ~ 13 pb in this region of the phase space.

We require no isolated leptons and at least six b-tagged jets. The b-tagged jets reconstructing the two κ's are those minimizing $|m^{\text{rec}}_{\kappa_1} - m^{\text{rec}}_{\kappa_2}|$ among the four with smallest p_T, where m^{rec}_κ stands now for the invariant mass of two b-jets. The ambiguity in assigning the two hardest jets to any of the two heavy quarks is solved in the same way as before.

The normalized distributions of $m^{\text{rec}}_{\kappa_1}$, $m^{\text{rec}}_{\kappa_2}$, $m^{\text{rec}}_{B_1}$ and $m^{\text{rec}}_{B_2}$ are shown in figure 30, for the same BP used in the previous analysis. All events are finally required to satisfy $|m^{\text{rec}}_{\kappa_1} - m_\kappa| < 100$ GeV, $|m^{\text{rec}}_{\kappa_2} - m_\kappa| < 100\,\text{GeV}$, $|m^{\text{rec}}_{B_1} - m_B| < 500$ GeV and $|m^{\text{rec}}_{B_2} - m_B| < 500$ GeV. Note that this search is also sensitive to the channel $pp \to T\overline{T} \to \kappa\kappa t\bar{t}$; see figure 31.

Performing a statistical analysis equivalent to the one used in the last subsection, we obtain the plot in the right panel of figure 33. The dashed (dotted) lines are obtained assuming a systematic uncertainty of 20% (50%) in the number of background events. Given that the analysis becomes nearly background-free for $M \gtrsim 3$ TeV, such levels of uncertainty have a minor impact on the results.

5.4.6.3 $\mu^+\mu^-\mu^+\mu^-$ final states

For the background, we consider $pp \to b\bar{b}\mu^+\mu^-\mu^+\mu^-$, with $p_T^{b_1} > 500$ GeV. The corresponding cross section is $\sim 10^{-5}$ pb. We require no isolated electrons, two pairs of muons with vanishing electric charge and exactly two b-tagged jets.

The muon pairs reconstructing the two κ's are those minimizing $|m^{\text{rec}}_{\kappa_1} - m^{\text{rec}}_{\kappa_2}|$, where m^{rec}_κ stands for the invariant mass of two oppositely charged muons. To decide which b-jet is assigned to each κ, we

choose again the combination that gives the minimum difference between the reconstructed heavy quark masses.

The normalized mass distributions in both the signal and the background are plotted in figure 32 for the BP considered in the previous cases. We require all events to have $|m^{\text{rec}}_{\kappa_1} - m_\kappa| < 20$ GeV, $|m^{\text{rec}}_{\kappa_2} - m_\kappa| < 20$ GeV, $|m^{\text{rec}}_{B_1} - m_B| < 500$ GeV and $|m^{\text{rec}}_{B_2} - m_B| < 500$ GeV. After this last cut, the analysis becomes essentially background-free.

For the VLQ masses considered in this study, the signal efficiency is nearly constant (≈ 0.1–0.2); therefore, the exclusion lines in the (M, m_κ) plane are close to vertical. We find that all masses up to $M \sim 5\ (8)$ TeV could be excluded at the 95% CL at a future 100 TeV collider with $L = 1$ ab^{-1}, assuming that $\mathcal{B}(\kappa \to \mu^+\mu^-) = 0.1\ (0.4)$.

5.4.7 Outlook

We have studied the DM phenomenology in a NMCHM where extra $d.o.f.$ are present below the DM scale. Not only this hierarchy is theoretically plausible, as we have shown in explicit realizations of the $SO(7)/SO(6)$ model, but also experimentally driven as strong bounds from DM searches can be eluded in this case.

We showed that in large regions of the phase space, namely for $\mathcal{O}(100)$ GeV masses, the DM can annihilate sizably into the lighter pNGB and therefore freeze out in the absence of couplings to the SM. This is due to the destructive interference between the portal coupling and derivative interactions characteristic of the Goldstone nature, which suppresses (enhances) effectively the annihilation cross section (relic abundance).

In the scenario where the LH fermions couple to VLQs in the symmetric representation of $SO(7)$, we found that the relic density constraint excludes compositeness scales $f \gtrsim 3.3$ TeV. This contrasts with other models where the bound on f originates solely from fine-tuning arguments. Furthermore, in this scenario, the portal coupling to the Higgs boson is predicted to be $\mathcal{O}(\lambda_H)$. Consequently, all DM masses up to 1.5 TeV could be potentially probed at the future LZ experiment.

On the other hand, if the SM fermions couple to composite operators in smaller representations of the global group, the portal coupling to the Higgs boson can be instead marginal and the dominant scalar contribution to the DM-nucleon cross section becomes (one-loop) suppressed, with no chance of being probed even at future direct detection facilities.

To further test the model, we have recast indirect detection constraints from the Fermi-LAT experiment taking into account the presence of the exotic step, $\eta\eta \to \kappa\kappa$, in the annihilation. To obtain such constraints, we performed dedicated simulations to include the new showering effects due to the decay of κ into the SM, assuming different decay modes. The new Fermi-LAT limits obtained in this procedure are presented in figure 27, for particular choices of the scalar masses. The leptophilic regime is very weakly

constrained by this experiment, while searches at other indirect detection facilities are still dominated by large uncertainties. Even if the Fermi bounds could be strengthen by an order of magnitude in the future, a thermal relic that decays mainly into a muonphilic κ would still be able to explain all the DM in the Universe.

Finally, we developed dedicated collider analyses for a future 100 TeV pp collider to probe these regimes. We focused on pair-production of VLQs that decay into their SM partner and the extra singlet, therefore providing an insight both into the compositeness and the non-minimal nature of the model. We found that in the $b\bar{b}\gamma\gamma$ and $b\bar{b}b\bar{b}$ channels, VLQ masses as large as ~ 3 and 6 TeV could be probed, respectively, with a collected luminosity of $100\,\text{fb}^{-1}$. In the four muons channel, all masses up to ~ 9 TeV could be probed with ten times larger luminosities. These searches could therefore have an important complementary role and probe regions of the parameter space that escape entirely the constraints from DM experiments.

Altogether, in spite of the growing efforts to build alternative models of DM, this study shows that by dropping the requirement of minimality (which, in the context of CHMs, is equivalent to demand that the model is anomaly-free), the familiar WIMP can still be a compelling and natural DM candidate in the composite framework. (Similar conclusions have been drawn in model-independent studies playing with different annihilation fractions of the DM into the SM [267].)

Chapter 6

Non-minimal EFT analysis

In the last chapter, we have considered different quantum numbers for the composite resonances in the UV, namely VLQs transforming in the fundamental, adjoint and symmetric representations of the global group of the strong sector, and integrated them out to obtain the low-energy interactions. Formally, we were therefore matching the UV onto the SMEFT Lagrangian extended with the lightest exotic $d.o.f.$ and studying only the reduced set of operators which arose in this procedure.

In this chapter, we consider a complementary approach in which we are ignorant about the UV and consider instead all the interactions which can arise at low-energy, up to a given order in the new physics scale and in the number of exotic $d.o.f.$ We focus on the minimal setup, extending the SMEFT with only one exotic particle at a time.

To find out the most promising candidates to include, we must figure out which resonances of the composite sector are expected to be the lightest; and find a sufficiently large separation of scales such that heavier resonances are decoupled from the low-energy phenomenology.

As argued in previous chapters, a very plausible mass hierarchy between composite particles is

$$m_{\Pi} \ll m_{\Psi} \ll m_V \sim m_* \,, \tag{194}$$

given both theoretical and experimental considerations. Indeed, the pNGBs are expected to be much lighter than m_*, due to their approximate shift-symmetry. Such scalars must lie at a scale not far from the heavy fermion masses, since the latter are directly responsible for the generation of m_{Π}. On the other side, some composite vectors (in contrast with what is found in QCD) have been pushed to scales $\sim 3-4$ TeV, significantly larger than those allowed for VLQs, which might have masses ~ 1 TeV; revisit the discussion in section 4.6.1. Furthermore, the heavy vectors do not influence the Higgs mass directly, so this hierarchy is expected even theoretically. Regarding the fermionic sector itself, we remark that VLLs are experimentally

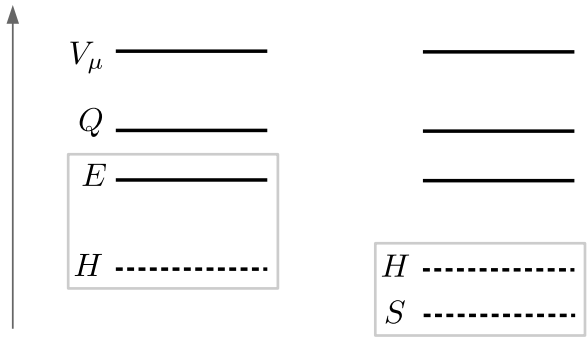

Figure 34: Plausible mass hierarchy between the composite resonances; see the text for details. The arrow points in the direction of increasing mass. Each square demarks the composite $d.o.f.$ that will make up the EFTs of interest.

allowed to be significantly lighter than the VLQs, as masses ~ 200 GeV are compatible with the data. At the theoretical level, the type of vector-like fermion that is considered to be the most low-lying depends on the particle physics problem we aim to solve.

Given these considerations, we will assume the mass scheme plotted in figure 34 and study the following two EFTs:

1. The EFT of the SM+VLL, the latter being denoted by E (see section 6.1): this is a suitable description of the MCHM at energies $\mu \sim v$, as well as NMCHMs where the extra pNGBs are decoupled from the EW scale. Even in the first case, we go beyond minimality by considering non-renormalizable interactions which can trigger the single production $pp \to E\ell$. To the best of our knowledge, this is the first time such EFT is studied. Furthermore, the contribution of renormalizable interactions to this process is very suppressed and constrained by other data, which strongly motivates the inclusion of operators beyond the LO. The corresponding cross section grows with the energy and can therefore dominate the large $\sqrt{s}$ region of the phase space.

2. The EFT of the SM+ALP, the latter being denoted by S (see section 6.2): singlets are one of the most common types of NGBs arising in NMCHMs, CP-odd ones being specially promising from a phenomenological point of view (as supported by basically all studies presented in the last chapter). In turn, the ALP EFT has been thoroughly studied in the literature [184, 230]. However, the corresponding bases of operators usually assume the case of a shift-symmetric particle, so *e.g.* its renormalizable coupling to the Higgs boson is often dismissed. Moreover, we will argue that the most common shift-symmetric basis involves redundancies and might not even be the most accurate to describe the pure axion field. On the other hand, we construct a minimal basis for a generic pseudoscalar singlet and compute the RGEs of all Wilson coefficients in the EFT, both before and after EWSB. The latter is discussed for the first time in the context of this work.

6.1 The SM extended with a vector-like lepton

We extend the SM with a singlet VLL E with $Y = -1$. The relevant Lagrangian for our study, up to dimension six, reads[1]:

$$\begin{aligned}\mathcal{L}_E = &\overline{E}\left(i\not{D} - M_E\right)E - \left(y\overline{l_L}HE + \text{h.c.}\right) \\ &+ \Big[f_{ue}\left(\overline{u_R}\gamma^\mu u_R\right)\left(\overline{e_R}\gamma_\mu E\right) + f_{de}\left(\overline{d_R}\gamma^\mu d_R\right)\left(\overline{e_R}\gamma_\mu E\right) + f_{qe}\left(\overline{q_L}\gamma^\mu q_L\right)\left(\overline{e_R}\gamma_\mu E\right) \\ &+ f_{qdl}\left(\overline{q_L}d_R\right)\left(\overline{E}l_L\right) + f_{qul}\left(\overline{q_L}u_R\right)\epsilon\left(\overline{l_L}^T E\right) + f_{luq}\left(\overline{l_L}u_R\right)\epsilon\left(\overline{q_L}^T E\right) + \text{h.c.}\Big],\end{aligned} \tag{195}$$

where $f_i = c_i/\Lambda^2$ is dimensionfull. After EWSB, E and ℓ can therefore mix. (We assume that the SM lepton Yukawa matrix is already diagonalized.) The mass terms become diagonal after the following rotations:

$$\begin{pmatrix} e_{R,L} \\ E_{R,L}\end{pmatrix} = \begin{pmatrix} c_{R,L} & s_{R,L} \\ -s_{R,L} & c_{R,L}\end{pmatrix}\begin{pmatrix} e_{R,L} \\ E_{R,L}\end{pmatrix} \equiv V_{R,L}e', \tag{196}$$

where $s_{R,L}$ and $c_{R,L}$ are, respectively, the sine and cosine of the rotation angles which are

$$s_L \to \frac{yv}{\sqrt{2}m_E} \quad \text{and} \quad s_R \to 0\,, \tag{197}$$

in the limit of $y \to 0$. In this limit, the electron is massless whereas the mass of the VLL is

$$m_E = \sqrt{M_E^2 + \frac{y^2v^2}{2}}\,. \tag{198}$$

The renormalizable interactions in $\mathcal{L}_E$ modify the lepton couplings to gauge bosons. To see how, let us denote the extended vector of leptons, in equation 196, by e'^a, with $a = e, E$ (for purposes of the discussion, we ignore the two other lepton flavours in the SM). Since the components in e'_L have different isospin charges, lepton FCNCs can arise in the LH sector of the model. (In contrast, the couplings to the photon remain diagonal.) Explicitly,

$$\mathcal{L}_{\text{kin}} \supset \frac{g_1}{c_\omega}Z_\mu\overline{e'_L}\gamma^\mu\left[V_L^\dagger\mathcal{G}_L V_L\right]e'_L\,, \quad \text{where} \quad \mathcal{G}_L = \begin{pmatrix} -\frac{1}{2} + s_\omega^2 & 0 \\ 0 & s_\omega^2\end{pmatrix}. \tag{199}$$

This leads to:

$$\mathcal{L}_{\text{kin}} \supset \frac{g_1}{2c_\omega}(\underbrace{-1 + 2s_\omega^2}_{\text{SM}} + s_L^2)Z_\mu\overline{e_L}\gamma^\mu e_L - \frac{g_1}{2c_\omega}s_L c_L Z_\mu\left[\overline{e_L}\gamma^\mu E_L + \text{h.c.}\right] + \ldots\,, \tag{200}$$

where the dots include Z-boson interactions triggering pair production of the VLL. We will ignore the latter production mechanism in this work, for two main reasons: *(1)* it is phase space suppressed; *(2)* it is not

[1] Note that derivative terms such as $\overline{E}i\not{D}e_R$ can be removed upon suitable field redefinitions.

significantly enhanced by the effective interactions. On the other hand, single production of the VLL is negligible before EWSB and severely constrained in the broken phase, allowing the EFT interactions to play the leading role.

Indeed, the beyond the SM coupling in the first term of the equation above is strongly constrained by EWPD, requiring that [268]

$$|s_L| < 0.021 \Rightarrow |y| < 0.06\,, \tag{201}$$

at the 95% CL, for $m_E = 0.5$ TeV; slightly larger values are found if E couples instead to the muon. We therefore assume $y \ll 1$ in the following.

To leading order in θ_ω and neglecting $m_Z \ll \sqrt{s}$, the (differential) single production cross sections read:

$$\frac{d\sigma}{d\theta}(u\bar{u} \to E\ell) = \frac{\sin\theta}{32\pi s}\left(1 - \frac{m_E^2}{s}\right)\left\{ -\frac{\pi^2\alpha_{\rm em}^2}{3s_\omega^4 s^2} s_L^2\,(s+t)\left(m_E^2 - s - t\right)\right. \tag{202}$$
$$\left. + \frac{1}{3\Lambda^4}\left[s\left(s - m_E^2\right)\left(\frac{c_{qul}^2}{4} + c_{ue}^2\right) + t\left(t - m_E^2\right)\left(\frac{c_{luq}^2}{4} + c_{ue}^2 + c_{qe}^2\right) + st\left(2c_{ue}^2 - \frac{1}{2}c_{qul}c_{luq}\right)\right]\right\},$$

for $\bar{u}u$ initiated processes; and

$$\frac{d\sigma}{d\theta}(d\bar{d} \to E\ell) = \frac{\sin\theta}{32\pi s}\left(1 - \frac{m_E^2}{s}\right)\left\{ -\frac{\pi^2\alpha_{\rm em}^2}{3s_\omega^4 s^2} s_L^2\,(s+t)\left(m_E^2 - s - t\right)\right. \tag{203}$$
$$\left. + \frac{1}{3\Lambda^4}\left[s\left(s - m_E^2\right)\left(\frac{c_{qdl}^2}{4} + c_{de}^2\right) + t\left(t - m_E^2\right)\left(c_{qe}^2 + c_{de}^2\right) + 2stc_{de}^2\right]\right\},$$

for those triggered by $\bar{d}d$. In these expressions, θ is the angle between initial $p_i = \sqrt{s}/2$ and final $p_f = \left(s - m_E^2\right)/\left(2\sqrt{s}\right)$ momenta, in the center-of-mass frame; accordingly, the Mandelstam variable $t = m_E^2 - 2p_i\left(\sqrt{m_E^2 + p_f^2} - p_f\cos\theta\right)$.

To compare the purely SM and EFT contributions, we plot in figure 35 the total single E production cross section, for fixed values of f_{qe} and the maximum allowed value for y. The SM contribution is obtained by making $\Lambda \to \infty$ in the equations above. It is apparent that the effective interactions dominate even for Wilson coefficients $f \sim 10^{-2}$ TeV^{-2}. The corresponding contribution grows with $\sigma \sim s/\Lambda^4$ while the SM one is dumped by the Z boson propagator, $\sigma \sim 1/s$. This, together with the y suppression, makes the EFT interactions dominate the dynamics of production at large $\sqrt{s}$.

Having showed their leading role in the production, let us see if the effective interactions can also dominate the subsequent decay of the VLL. The Yukawa coupling y triggers not only $E \to Z/h\ell$, but also $E \to W\nu$ decays, since the interaction

$$\frac{g_2}{\sqrt{2}} W_\mu^+ \overline{\nu'_L}\gamma^\mu \begin{pmatrix} 1 & 0 \\ 0 & 0 \end{pmatrix} V_L e'_L + \text{h.c.} \tag{204}$$

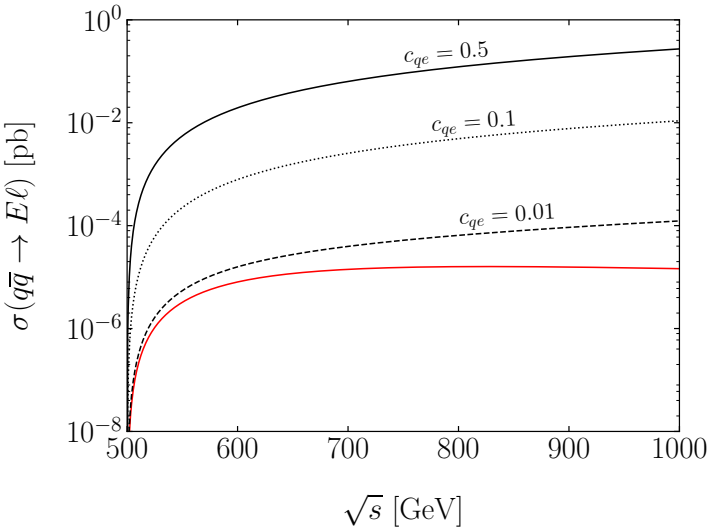

Figure 35: Single E production cross section as a function of $\sqrt{s}$, for $m_E = 500$ GeV and $y = 0.1$. In the black lines, c_{qe} takes different values while $\Lambda = 1$ TeV. All other Wilson coefficients are set to zero. The red line shows the contribution from the SM mediated process.

is not flavour-diagonal in the mass basis. The corresponding decay widths read:

$$\Gamma(E \to Z\ell) = y^2 \frac{\alpha}{16 s_\omega^2 c_\omega^2} \left(\frac{v}{m_Z}\right)^2 m_E \,, \tag{205}$$

in the same limit where $y \to 0$ and $m_Z \ll m_E$. This equation holds for all EW bosons, by virtue of the Equivalence Theorem.

Regarding the three-body decay of the VLL, we focus on $E \to \ell\bar{q}q$. The latter is triggered by the effective operators which are already in our basis. This channel is expected to dominate over the leptonic one, in either the flavour universal (where E couples equally to all fermions) or the hierarchical scenario (where E couples to all fermions according to their masses). In the first case, because there are $N_C = 3$ copies of each quark; in the second case, due to the smallness of the lepton Yukawa couplings which we assume to be the only source of flavour-breaking.

The differential decay widths for $E \to \ell u\bar{u}$ and $E \to \ell d\bar{d}$ read, respectively,

$$\begin{aligned}\frac{d\Gamma'}{dE_1 dE_2} = \frac{3}{128\pi^3 m_E}\Big[&2E_1 m_E \left(m_E^2 - 2E_1 m_E\right)\left(f_{luq}^2 + 4f_{qe}^2\right) + 8E_2 f_{ue}^2 m_E \left(m_E^2 - 2E_2 m_E\right) \\ &+ 2f_{luq}f_{qul}\left(m_E^2 - 2E_1 m_E\right)\left(m_E^2 - 2E_3 m_E\right) + 2E_3 f_{qul}^2 m_E \left(m_E^2 - 2E_3 m_E\right)\Big]\,;\end{aligned} \tag{206}$$

and

$$\begin{aligned}\frac{d\Gamma'}{dE_1 dE_2} = \frac{3}{128\pi^3 m_E}\Big[&8E_1 f_{qe}^2 m_E \left(m_E^2 - 2E_1 m_E\right) + 8E_2 f_{de}^2 m_E \left(m_E^2 - 2E_2 m_E\right) \\ &+ 2E_3 f_{qdl}^2 m_E \left(m_E^2 - 2E_3 m_E\right)\Big]\,,\end{aligned} \tag{207}$$

where E_1, E_2 and E_3 are the energies of $u(d)$, $\overline{u}(\overline{d})$ and ℓ, respectively. Upon integration over the phase space, we obtain:

$$\Gamma' = \frac{m_E^5}{2048\pi^3}\left[f_{luq}^2 + f_{luq}f_{qul} + f_{qul}^2 + f_{qdl}^2 + 4\left(2f_{qe}^2 + f_{ue}^2 + f_{de}^2\right)\right]. \tag{208}$$

By comparing equations 205 and 208, we finally find that

$$\Gamma' > \Gamma \quad \text{for} \quad y \lesssim 0.2\left(\frac{m_E}{\Lambda}\right)^2, \tag{209}$$

considering $\mathcal{O}(1)$ couplings and including all types of quarks. For example, for $m_E = (0.5,\ 0.3\,, 0.25)\ \Lambda$, the hierarchy above requires that $y \lesssim (0.05,\ 0.02,\ 0.008)$. These values are very close to the bound from EWPD in equation 201, so it is very likely that E decays mainly via the EFT operators indeed.

6.1.1 Recast of LHC searches

From the previous analysis, we expect that the single production of E gives rise to a final state comprised of two light leptons and several jets at colliders (focusing on hadronic decays of the top quark). The experimental analysis presented in Ref. [269] can therefore constrain this scenario, although it is specially suitable to probe the VLL decays into light quarks.

Among the most relevant cuts, an electron (muon) is assumed to be isolated if the sum of the p_T of all tracks within a cone of radius $\Delta R = 0.3$ around its direction is less than $3\ (10)\%$ of the electron (muon) p_T. Electrons (muons) are furthermore required to have $p_T > 35\ (25)$ GeV and to lie in a pseudorapidity volume defined by $|\eta| < 1.44$ and $1.56 < |\eta| < 2.50$ ($|\eta| < 2.4$). Furthermore, the leading lepton must have $p_T > 230$ GeV (electron) or 53 GeV (muon) to trigger the event. Jets are clustered using the anti-k_T algorithm with $R = 0.4$ and required to have $p_T > 50$ GeV. The two hardest same-flavour leptons are selected, along with the two hardest jets. Finally, the invariant mass of the two leptons is required to be $m_{\ell\ell} > 500$ GeV, to suppress the majority of the Drell-Yann background.

Subsequently, the invariant mass of the total system $m_{\ell\ell jj}$ is used as the discriminating variable between signal and background and split in several energy bins: $[0.5,\ 1.5]$, $[1.5,\ 2.5]$, $[2.5,\ 3.5]$, $[3.5,\ 4.5]$ and $[4.5,\ 10]$ TeV. In order to set limits on the Wilson coefficients, we will restrict the analysis to the second one and consider $\ell = \mu$. In this case, even Wilson coefficients as large as $f \sim \mathcal{O}(1)$ TeV^{-2} are allowed by perturbative unitarity constraints (see the appendix in the original paper [7]).

From equations 202 and 203, it is clear that the EFT operators contribute to only six different signal regions. Therefore, the full cross section, or equivalently the number of events in each bin, can be

	process	I_1^u	I_2^u	I_3^u	I_1^d	I_2^d	I_3^d
prod.	$q\bar{q} \to \mu E$	c_{qul}	c_{luq}	c_{ue}	c_{qdl}	c_{qe}	c_{de}
decay	$E \to \mu u\bar{u}$	–	–	–	c_{ue}	–	c_{ue}
	$E \to \mu d\bar{d}$	c_{de}	c_{de}	c_{de}	–	–	–

Table 6: Cumulative set of EFT parameters which were turned on to fix the kinematic coefficients used in the master equation 210. The null entry means that only the Wilson coefficient in the first line was used. In the decay process, u and d refer to any type of up- or down-quarks.

parameterized by

$$N = \frac{1}{\Lambda^4}\left[\mathcal{I}_1^u\left(\frac{c_{qul}^2}{4} + c_{ue}^2\right) + \mathcal{I}_2^u\left(\frac{c_{luq}^2}{4} + c_{ue}^2 + c_{qe}^2\right) + \mathcal{I}_3^u\left(2c_{ue}^2 - \frac{1}{2}c_{qul}c_{luq}\right)\right.$$
$$\left. + \mathcal{I}_1^d\left(\frac{c_{qdl}^2}{4} + c_{de}^2\right) + \mathcal{I}_2^d\left(c_{de}^2 + c_{qe}^2\right) + 2\mathcal{I}_3^d c_{de}^2\right], \tag{210}$$

where the I_i coefficients can be obtained from simulation. With this aim, we have generated the signal events with `MadGraph` and `Pythia`, for different masses of the VLL and three possible decay channels: $E \to \ell q\bar{q}$, $E \to \ell b\bar{b}$ and $E \to \ell t\bar{t}$. To obtain each I_i, we have set different Wilson coefficients to non-zero values; see table 6. For example, I_1^u was fixed by $c_{qul} \neq 0$ in the case where E decays to up-type quarks. To realize the decay into the down-type, a second coefficient was given a non-zero value, namely $c_{de} \neq 0$.

The events obtained in this way were subsequently filtered to match the analysis we have described following Ref. [269]. The latter was recast using dedicated routines based on `Fastjet` and `ROOT`. No detector simulation was included. (A validity test was performed by generating and applying the analysis to the dominant background, that is Drell-Yann production, finding good agreement with the number of events reported in Ref. [269].) The results from the simulation are presented in table 7, assuming $m_E = 500\,\text{GeV}$.

6.1.2 Global constraints

Comparing the prediction for the number of signal events using this table with what was actually obtained in the simulation, we have found deviations of at most $\pm 15\%$. We have taken this as a systematic error to obtain the maximum number of signal events allowed by the data analysed in Ref. [269]. The results,

		Bins in $2\ell 2j$ mass [TeV]				
		$0.5-1.5$	$1.5-2.5$	$2.5-3.5$	$3.5-4.5$	$4.5-10$
$E\to\mu d\bar{d}$	$\mathcal{I}_1^q/10^2$	390 (150)	530 (240)	220 (96)	62 (19)	22 (5.5)
	$\mathcal{I}_2^q/10^2$	140 (88)	180 (100)	74 (35)	19 (9.2)	8.4 (2.9)
	$\mathcal{I}_3^q/10^2$	-190 (-73)	-260 (-120)	-110 (-49)	-29 (-9.1)	-11 (-2.8)
$E\to\mu b\bar{b}$	$\mathcal{I}_1^q/10^2$	380 (150)	480 (210)	210 (88)	55 (22)	18 (3.5)
	$\mathcal{I}_2^q/10^2$	140 (85)	170 (97)	68 (33)	22 (7.4)	5.5 (2.1)
	$\mathcal{I}_3^q/10^2$	-190 (-79)	-240 (-110)	-100 (-44)	-29 (-11)	-9.2 (-1.7)
$E\to\mu t\bar{t}$	$\mathcal{I}_1^q/10^2$	170 (160)	200 (120)	73 (27)	20 (5.7)	4.3 (1.4)
	$\mathcal{I}_2^q/10^2$	93 (57)	85 (48)	24 (9.6)	5.3 (1.4)	1.0 (0.36)
	$\mathcal{I}_3^q/10^2$	-82 (-79)	-110 (-64)	-37 (-13)	-11 (-2.5)	-2.1 (-0.53)
SM		949 ± 115	161 ± 25	13.7 ± 3.7	1.2 ± 0.6	0.48 ± 0.32
Data		949	151	11	0	1
$\mathbf{s_{max}}$		291	60	14	4	5

Table 7: Kinematic coefficients I_i^q [TeV^4], with $q=u$ (d), for the process $pp\to\mu^+\mu^- qq$ obtained upon recasting the analysis in Ref. [269]. The results are presented for $\sqrt{s}=13$ TeV and $L=77.4$ fb^{-1}. We have assumed $\mathcal{B}(E\to\mu d\bar{d})=1$, $\mathcal{B}(E\to\mu b\bar{b})=1$ and $\mathcal{B}(E\to\mu t\bar{t})=1$ in the upper, middle and bottom panels, respectively. The number of SM expected events, the data and the maximum allowed signal $s_{\mathtt{max}}$ at 95% CL are also displayed; see the text for details.

obtained with the CL$_s$ method, are reported in table 7. In this table, the uncertainties on the background which were included in the computations are also displayed.

Note that, since no b-tagging was applied in the analysis, the results reported in table 7 for light and bottom quarks are very similar. As such, we derived bounds on the Wilson coefficients as a function of

$$\mathcal{B}(E\to\ell jj)\equiv\mathcal{B}(E\to\ell d\bar{d})+\mathcal{B}(E\to\ell b\bar{b})=1-\mathcal{B}(E\to\ell t\bar{t})\,. \tag{211}$$

The results are plotted in the left panel of figure 36, for $m_E=500$ GeV. (Studies for other masses are presented in the original Ref. [7].) For setting bounds on f_{luq}, we marginalized over f_{qul}; and vice-versa. (These are the only two coefficients in the EFT that interfere.) The final results can be interpreted as global limits on the EFT since turning on other operators would increase the signal. On that account, the upper bounds in figure 36 show *the largest* value each Wilson coefficient is allowed to take.

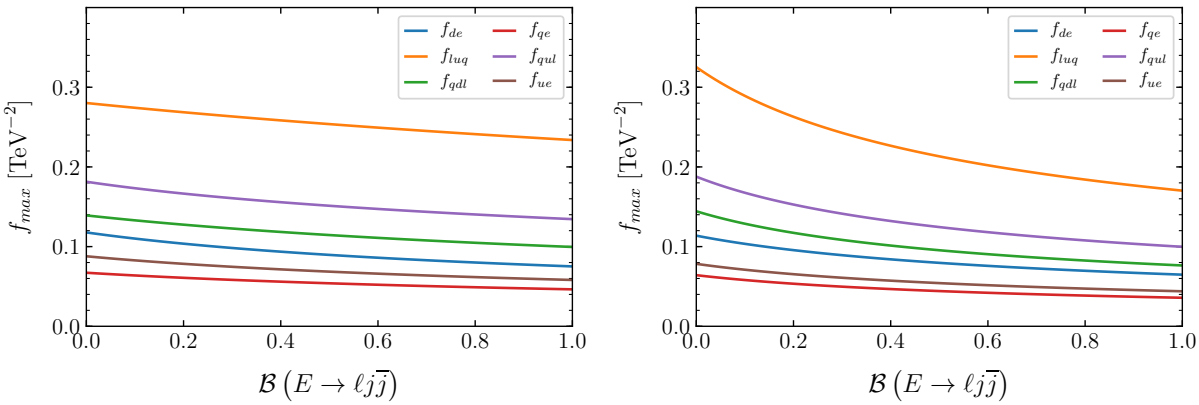

Figure 36: The global limits at 95% CL on the Wilson coefficients, f, obtained for $m_E = 0.5$ TeV and using the second (left) and the third (right) energy bins defined in table 7.

For comparison, we also plotted in the right panel of figure 36 the results obtained using the third energy bin defined in table 7, which are very similar to the previous ones. In fact, we do not expect drastic changes in the cross section unless we get close to the unitarity bound[2]. For the Wilson coefficients $f \sim \mathcal{O}(0.1)$ TeV^{-2} that we can probe, such bound is at $\sqrt{\hat{s}} \sim 20$ TeV ($\sqrt{\hat{s}}$ denoting the partonic c.m.e.), very far from the energies considered even in the fourth bin. This would not be the case if we could probe $f \sim \mathcal{O}(1)$ TeV^{-2} instead, for which the cross section *explodes* at $\sqrt{\hat{s}} \sim 5$ TeV [7].

Note also that the worst limits are in the region where $\mathcal{B}(E \to \ell j \bar{j}) \ll 1$. This is expected, since the analysis is not sensitive to the top quark. This point, in particular, has motivated us to extend the previous analysis with relevant cuts on new observables, which can make it more sensitive to the SM+E EFT. One of these observables is the invariant mass of the reconstructed VLL, its four-momentum being reconstructed as the sum of the momenta of the softest lepton and the two hardest jets in an event.

Additional modifications should be employed to gain sensitivity in the case $\mathcal{B}(E \to \ell b \bar{b}) \approx 1$ or $\mathcal{B}(E \to \ell t \bar{t}) \approx 1$. In the bottom channel, we have therefore applied a b-tagging algorithm, following the same lines described in section 5.4.6, and required the presence of exactly two of such b-jets. In the top channel, in addition to the latter, at least three light jets were required. Making optimized mass cut windows for each channel, we have found that Wilson coefficients $\sim 50\%$ smaller could be probed with this improved analysis. (The selection efficiencies for signal and background were found to be, in good approximation, bin and operator independent. The corresponding values, as well as the maximum number of signal events obtained for each case, are reported in Ref. [7], assuming the same uncertainties as before and that no deviation from the SM is observed.)

[2] Using the unitarity of the S-matrix in QFT and expanding a given amplitude in terms of partial waves, it is possible to derive bounds on the corresponding coefficients; these are the so-called unitarity bounds [21]. In particular, if an EFT amplitude has no angular dependence, the unitarity bound is violated for $\sqrt{\hat{s}} > \sqrt{16\pi}\Lambda$, assuming $c = 1$.

6.1.3 Phenomenological applications

In this section, we give concrete examples to illustrate the usefulness of the *master formula* in equation 210. Let us consider the SM+E extended with a heavy colored scalar $\Pi_7 \sim (3,2)_{7/6}$ under the SM gauge group. The relevant Lagrangian to match onto our EFT is

$$\mathcal{L}_{\Pi_7+E} = -\Pi_7^\dagger \left[y^E \overline{E} q_L + y^{lu} \epsilon \overline{l_L}^T u_R + y^{eq} \overline{e_R} q_L \right] + \text{h.c.} \tag{212}$$

Integrating out the UV particle at tree level, we obtain[3]:

$$f_{luq} = \frac{-y^{lu} y^E}{m_\Pi^2} \quad \text{and} \quad f_{qe} = -\frac{y^{eq} y^E}{2m^2} \,. \tag{213}$$

Assuming $m_E = 500$ GeV, we can use equation 210 and table 7 to derive bounds on the UV couplings *taking both operators into account*. The results are plotted in figure 37, for the current and improved analyses. Superimposed are also the expected limits at the HL-LHC. In black, we plot the expected limit if only O_{luq} (giving the strongest bounds) is included; the corresponding results are $\sim 24\%$ less accurate. For other single-field extensions of the SM+E [7], the discrepancy might be even larger. This fact, together with its functional form, makes equation 210 not only adequate but really the correct approach to interpret the experimental results. For comparison, we also show in figure 37 the bounds on the new scalar from $pp \to jj$ LHC searches [270]. For $y^E \gtrsim 3$, the bound on $y^{lu} = y^{eq}$ from our study is more than four times stronger than that from other data.

Furthermore, our results can be extended to four-fermion operators involving the second and the third generations of quarks. This contrasts with those presented in Ref. [269] which used all bins up to 10 TeV to derive limits. Since the single E production cross section initiated by bottom quarks is around two orders of magnitude smaller than that initiated by light quarks, the bounds on the EFT operators involving bottom quarks are expected to be ~ 10 times weaker. In turn, the unitarity bound is at $\sqrt{\hat{s}} \sim 5$ TeV [7]. The use of energy bins above this threshold is therefore completely wrong. On the other hand, the bounds from our study (restricted to $\sqrt{\hat{s}} \lesssim 2.5$ TeV) are compatible with the validity of the EFT.

In particular, such bounds can be used to constrain the model presented in section 5.3. The heavy vector V in this model, whose Lagrangian is defined in equation 165, can also couple to $E\mu$ (with strength $g_{E\ell}$), as both V and E are part of the composite sector. Upon integrating V out at tree level, a single effective operator in our basis is generated:

$$f_{qe} = -\frac{g_{qq} g_{E\ell}}{m_V^2} \sim -0.05 g_{E\ell}\ \text{TeV}^{-2} \,, \tag{214}$$

where we employed equation 164 to account for the possibility that V explains the LFU anomalies in $R_{K^{(*)}}$. Within the current analysis, values of $f_{qe} \sim 0.05 \times \sqrt{3000/77.4} \approx 0.3\ \text{TeV}^{-2}$ (see figure 36) could be

[3] To match onto the EFT, we have to reorder some operators using Fierz identities, for example $(\overline{q_L}\gamma^\mu q_L)(\overline{e_R}\gamma_\mu E_R) = -2(\overline{q_L} E_R)(\overline{e_R} q_L)$.

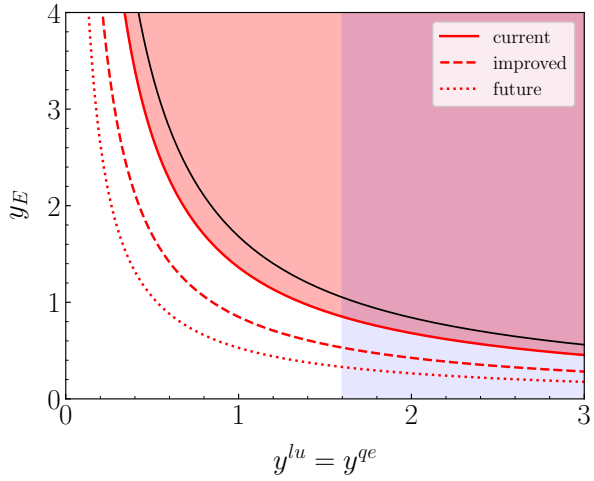

Figure 37: Constraints on the UV completion of the SM+E EFT presented in equation 212; see the text for details. We assumed that all couplings to the SM fields are equal. The current, improved and future results refer to the LHC analyses proposed in this study, assuming the $E \to \mu\bar{q}q$ channel and the second energy bin. The masses of the VLL and the heavy mediator were set to $m_E = 500$ GeV and $m_{\Pi_7} = 5$ TeV, respectively. The light blue region is excluded from di-jet searches at the LHC.

probed at the HL-LHC. Consequently, all vectors with $m_V > 2.5$ TeV and $g_{E\ell} > 6$ [4] could be excluded. This analysis, together with the direct search for $V \to E\ell$, $E \to Z/h\ell$ described in Ref. [106], could potentially probe a significant region of the parameter space where the LFU anomalies can be explained.

Finally, we remark that, in spite of having matched these UV models onto the EFT relevant for single E production, other SMEFT operators could arise which can be better constrained by other data. Since such operators are functions of the same UV couplings as the operators in our basis, it is worth checking that a composite completion exists such that bounds on the SMEFT operators do not spoil the dominance of the $E\ell\bar{q}q$ contact interactions at large $\sqrt{s}$. The example provided in appendix G fulfills this goal.

6.1.4 Outlook

We have constructed the most generic EFT involving the SM and a single E to dimension six, assuming only $\Delta L = 0$ interactions. The corresponding operators trigger $pp \to E\ell$ followed by $E \to \ell\bar{q}q$ (with no intermediate SM state) which can dominate the dynamics of the VLL at large $\sqrt{s}$. This hints towards a different signal region than those assumed by standard experimental analyses, where the VLL (as other resonances) is commonly searched for in $E \to Z\ell$ and $E \to Wv$ final states [137–141].

We have shown that there are other searches sensitive to our scenario, although very limited in scope. For example, Ref. [269] presents limits for a single EFT operator and cannot be straightforwardly recast to set bounds on the whole EFT basis. Furthermore, there is no rigorous treatment of the EFT validity in that

[4] Such large values are likely in the composite framework, as $g_{E\ell}$ is enhanced by g_*/g_e with respect to $g_{\ell\ell}$; see equation 105.

analysis, since energy bins up to 10 TeV are used to derive upper limits. Therefore, such limits cannot be translated to any model predicting new particles below this large cutoff, or even couplings to sea quarks.

In this way, not only we aim to motivate different searches for the VLLs, but to provide a meaningful way to organize the results from experimental searches, in order to make them more useful for the theoretical community. (Similar efforts were also pursued in the analysis of Ref. [271], in the context of neutrino physics). Indeed, equation 210, together with the kinematic coefficients obtained upon simulation, can be used to constrain any UV model *taking into account all operators which are generated* in the IR. We have obtained such coefficients for light, bottom and top quarks separately, thereby extending the applicability of the previous analysis.

Globally, we have found that Wilson coefficients as small as ~ 0.05 TeV^{-2} are already ruled out in the muon channel. Although not explicitly shown, the results in the electron channel are very similar, being typically $\sim 4\%$ weaker. Considering single-field UV completions of the SM+E EFT and translating such bounds into limits on the couplings to purely SM currents, we have found that our analysis can outperform bounds from di-jet searches by almost an order of magnitude.

6.2 The SM extended with an axion-like particle

We extend the SM with a singlet pseudoscalar S with $Y = 0$. The most general renormalizable Lagrangian for such ALP is[5]

$$\mathcal{L}_S = \frac{1}{2}\left(\partial_\mu S\right)\left(\partial^\mu S\right) - \frac{1}{2}m_S^2 S^2 - \frac{\kappa_S}{3!}S^3 - \frac{\lambda_S}{4!}S^4 - \kappa_{SH}S|H|^2 - \frac{\lambda_{SH}}{2}S^2|H|^2\,, \tag{215}$$

with all coefficients real.

The first tower of effective operators arises at dimension five. In table 8, we provide a Green basis of such set of operators, independent under algebraic or IBP identities. The operators labeled by $\mathcal{O}$ constitute the minimal basis which is non-redundant on-shell.

(The choice of the on-shell basis is not unique. In particular, we could work with an effective Lagrangian where the Yukawa-like operators, rather than the derivative ones, have been removed. Therefore, it might seem surprising that, in our basis, $S(p_1)H(p_2) \to H(p_3)Z(p_4)$ cannot be induced at tree level; while, in the derivative basis, the $\mathcal{R}_{SH\Box}$ operator could trigger this process. However, an explicit calculation shows that the corresponding amplitude squared is $|i\mathcal{M}|^2 \sim r_{SH\Box}^2 p_4^2 = 0$ when evaluated on-shell.)

In the following, we compute the energy evolution of the ALP EFT parameters in the unbroken EW phase, assuming only that the new physics does not violate CP. This amounts to take κ_S and κ_{SH} in the renormalizable Lagrangian, as well as the Wilson coefficients of all the scalar operators in table 8 together with $\mathcal{O}_{SG}$, $\mathcal{O}_{SW}$ and $\mathcal{O}_{SB}$, to zero. Under this assumption, contributions to CP-odd operators only arise if

[5] Our broad definition of this particle is not the most commonly used in the literature, where it is often assumed that the only term breaking the ALP shift-symmetry is the mass.

Scalar	Yukawa	Derivative	Gauge
$\mathcal{O}_{S^5} = S^5$	$\mathcal{O}^{\alpha\beta}_{SHu} = S\overline{q^\alpha_L}\widetilde{H}u^\beta_R$	$\mathcal{R}_{S\Box} = S^2\partial^2 S$	$\mathcal{O}_{SG} = SG^A_{\mu\nu}G^{\mu\nu}_A$
$\mathcal{O}_{S^3} = S^3\lvert H\rvert^2$	$\mathcal{O}^{\alpha\beta}_{SHd} = S\overline{q^\alpha_L}Hd^\beta_R$	$\mathcal{R}_{SH\Box} = SH^\dagger D^2 H$	$\mathcal{O}_{S\widetilde{G}} = SG^A_{\mu\nu}\widetilde{G}^{\mu\nu}_A$
$\mathcal{O}_S = S\lvert H\rvert^4$	$\mathcal{O}^{\alpha\beta}_{SHe} = S\overline{l^\alpha_L}He^\beta_R$	$\mathcal{R}_{HS\Box} = \lvert H\rvert^2\partial^2 S$	$\mathcal{O}_{SW} = SW^a_{\mu\nu}W^{\mu\nu}_a$
		$\mathcal{R}^{\alpha\beta}_{Sq} = S\overline{q^\alpha_L}\mathrm{i}\not{D}q^\beta_L$	$\mathcal{O}_{S\widetilde{W}} = SW^a_{\mu\nu}\widetilde{W}^{\mu\nu}_a$
		$\mathcal{R}^{\alpha\beta}_{Sl} = S\overline{l^\alpha_L}\mathrm{i}\not{D}l^\beta_L$	$\mathcal{O}_{SB} = SB_{\mu\nu}B^{\mu\nu}$
		$\mathcal{R}^{\alpha\beta}_{Su} = S\overline{u^\alpha_R}\mathrm{i}\not{D}u^\beta_R$	$\mathcal{O}_{S\widetilde{B}} = SB_{\mu\nu}\widetilde{B}^{\mu\nu}$
		$\mathcal{R}^{\alpha\beta}_{Sd} = S\overline{d^\alpha_R}\mathrm{i}\not{D}d^\beta_R$	
		$\mathcal{R}^{\alpha\beta}_{Se} = S\overline{e^\alpha_R}\mathrm{i}\not{D}e^\beta_R$	

Table 8: The Green basis of dimension five operators of the SM+ALP EFT. The h.c. counterpart is implicit for all the operators in the Yukawa class, $\mathcal{R}_{SH\Box}$ and $\mathcal{R}_{5-9}$.

the remaining CP-even ones are dressed with the SM complex phases in the quark sector. The goal of this work is to study the CP-even sector in isolation, ignoring this effect. Nevertheless, we present the results for arbitrary Yukawa couplings, so that the mixing with the CP-odd sector via the imaginary part of y^q can be easily obtained.

Under these considerations, the CP-even effective Lagrangian relevant to our study is

$$\begin{aligned}\mathcal{L}_{\text{CP-even}} \supset & \sum_{\psi=u,d,e}\left[\mathrm{i}a^{\alpha\beta}_{SH\psi}\mathcal{O}^{\alpha\beta}_{SH\psi} + \text{h.c.}\right] + \sum_{X=B,W,G} a_{S\widetilde{X}}\mathcal{O}_{S\widetilde{X}} \\ & + \left[\mathrm{i}r_{SH\Box}\mathcal{R}_{SH\Box} + \text{h.c.}\right] + \sum_{\psi=q,l,u,d,e}\left[\mathrm{i}r_{S\psi}\mathcal{R}_{S\psi} + \text{h.c.}\right],\end{aligned} \tag{216}$$

with all the Wilson coefficients being real or real matrices in flavour space.

6.2.1 One-loop divergences in the ALP SMEFT

In appendix H.1, we compute the divergences generated by 1PI diagrams at one-loop with off-shell momenta and to order $\mathcal{O}(1/\Lambda)$, Λ being the cutoff scale of the SM+ALP EFT. We use the background field method (BFM) [272] and work in the Feynman gauge in dimensional regularization with spacetime dimensions $\mathrm{d} = 4 - 2\epsilon$. All counterterms obtained in this way are gauge invariant. We implemented the model in `Feynrules` and evaluated by hand the Yukawa and scalar pieces of each of the Feynman diagrams obtained with `QGRAF` [273]. We used `FeynArts` [274] and `FormCalc` [275] to compute the gauge corrections, as well as to cross-check the previous calculations.

The divergences, produced in the processes enumerated below, are absorbed by the following EFT couplings:

- $SH^\dagger \to q_L\overline{u_R}$:

$$a'_{SHu} = \frac{1}{(4\pi)^2\epsilon}\left[\lambda_{SH}a_{SHu} - y^d y^{d\dagger}a_{SHu} - a_{SHd}y^{d\dagger}y^u + y^d a^\dagger_{SHd}y^u - a_{SHu}\left(\frac{25g_1^2}{36} + \frac{3g_2^2}{4} + \frac{16g_3^2}{3}\right)\right]. \tag{217}$$

- $SH \to q_L\overline{d_R}$:

$$a'_{SHd} = \frac{1}{(4\pi)^2\epsilon}\left[\lambda_{SH}a_{SHd} - y^u y^{u\dagger}a_{SHd} - a_{SHu}y^{u\dagger}y^d + y^u a^\dagger_{SHu}y^d - a_{SHd}\left(\frac{g_1^2}{36} + \frac{3g_2^2}{4} + \frac{16g_3^2}{3}\right)\right]. \tag{218}$$

- $SH \to l_L\overline{e_R}$:

$$a'_{SHe} = \frac{1}{(4\pi)^2\epsilon}a_{SHe}\left[a_7 - \left(\frac{9g_1^2}{4} + \frac{3g_2^2}{4}\right)\right]. \tag{219}$$

- $S \to HH^\dagger$:

$$r_{SH\Box} = \frac{1}{16\pi^2\epsilon}\left\{\mathrm{Tr}\left[y^e a^\dagger_{SHe}\right] + 3\mathrm{Tr}\left[y^d a^\dagger_{SHd} - a_{SHu}y^{u\dagger}\right]\right\}. \tag{220}$$

- $S \to \psi\overline{\psi}$:

$$r_{Sq} = \frac{1}{32\pi^2\epsilon}\left[acd_{SHu}y^{u\dagger} + a_{SHd}y^{d\dagger} - \frac{1}{3}\left(a_{S\widetilde{B}}g_1^2 + 27a_{S\widetilde{W}}g_2^2 + 48a_{S\widetilde{G}}g_3^2\right)\right], \tag{221}$$

$$r_{Sl} = \frac{1}{32\pi^2\epsilon}\left[a_{SHe}y^{l\dagger} - 3\left(a_{S\widetilde{B}}g_1^2 + 3a_{S\widetilde{W}}g_2^2\right)\right], \tag{222}$$

$$r_{Su} = \frac{-1}{16\pi^2\epsilon}\left[a^\dagger_{SHu}y^u - \frac{8}{3}\left(a_{S\widetilde{B}}g_1^2 + 3a_{S\widetilde{G}}g_3^2\right)\right], \tag{223}$$

$$r_{Sd} = \frac{-1}{16\pi^2\epsilon}\left[a^\dagger_{SHd}y^d - \frac{2}{3}\left(a_{S\widetilde{B}}g_1^2 + 12a_{S\widetilde{G}}g_3^2\right)\right], \tag{224}$$

$$r_{Se} = \frac{-1}{16\pi^2\epsilon}\left[a^\dagger_{SHe}y^l - 6a_{S\widetilde{B}}g_1^2\right]. \tag{225}$$

All other coefficients vanish. Regarding the gauge operators in table 8, no diagram exists for the process $S \to BB$. On the other hand, some of the amplitudes corresponding to $S \to WW$ and $S \to GG$ are

divergent; see equations 474–478. However, all the divergent contributions cancel out upon summation. Furthermore, note that the CP-even renormalizable couplings do not get contributions from the dimension five operators at one-loop. Indeed, the former are even under $S \to -S$ while the latter are odd, and therefore no corrections to the renormalizable Lagrangian are generated.

We partially checked the consistency of the previous results by computing some amplitudes which could possibly generate CP-odd operators or which are related to the ones above by gauge invariance. In the first case, we have for example checked that all divergences coming from the (box) diagrams contributing to $S \to HH^\dagger HH^\dagger$ cancel out. In the second case, we computed $SV \to \overline{\psi}\psi$ and therefore cross-checked the anti-symmetric part of $r_{S\psi}$.

6.2.2 Anomalous dimensions in the ALP SMEFT

Having matched all possible divergences into the Green basis, we can redefine the redundant operators into the minimal set. Such procedure is described in appendix H.3. Using equations 526–528, we can therefore determine the on-shell divergent Lagrangian,

$$-\mathcal{L}_{\text{div}} = \mathcal{O}_i a_i' \equiv \frac{1}{32\pi^2\epsilon}\mathcal{O}_i \alpha_{ij} a_j\,, \tag{226}$$

where i, j run over all operators (including those of different flavour) and α includes all renormalizable couplings. The divergences in $\mathcal{L}_{\text{div}}$ are absorbed through renormalization, which amounts to redefine the bare coefficients and fields of the dimension five Lagrangian as

$$\mathcal{O}_i^{(0)} a_i^{(0)} \to \mathcal{O}_i Z_i^F Z_{ij} a_j = \mathcal{O}_i a_i + \mathcal{O}_i \left(Z_i^F Z_{ij} - \delta_{ij}\right) a_j\,, \tag{227}$$

where the Z_F-factor collects the wave function renormalization (WFR) constants of all fields in $\mathcal{O}_i$. Let us also define, following the nomenclature and the approach of Ref. [276],

$$Z = 1 + \frac{\kappa}{32\pi^2\epsilon} \qquad \text{and} \qquad Z^F = 1 + \frac{\kappa^F}{32\pi^2\epsilon}\,, \tag{228}$$

with

$$\kappa = \alpha - \kappa^F\,, \tag{229}$$

in order to cancel the divergences in $\mathcal{L}_{\text{div}}$.

Next, we add the tree level anomalous dimension n_i of c_i^0 (in $a \equiv c/\Lambda$), by making $Z_{ij} \to \mu^{n_i\epsilon} Z_{ij}$. In dimensional regularization, such parameter is required to maintain the coupling dimensionless. Differentiating the bare coupling with respect to $t \equiv \log\mu$ and requiring that it does not depend on the energy, we obtain:

$$\frac{dc}{dt} = -\epsilon Z^{-1}\cdot n\cdot Z\cdot c - Z^{-1}\cdot\frac{dZ}{dt}\cdot c = \frac{1}{32\pi^2}\left[(\kappa\cdot n - n\cdot\kappa)\,c - \frac{d\kappa}{\epsilon dt}\cdot c\right], \tag{230}$$

in matrix notation and up to one-loop. This matches equation 35 in Ref. [276]. Furthermore, note that κ — being adimensional — can only depend on couplings, so:

$$\kappa = C g^{n_g} y^{n_y} (\sqrt{\lambda})^{n_{\sqrt{\lambda}}}, \tag{231}$$

where C is some constant and the superscripts refer to the number of gauge (g), Yukawa (y) and square-root scalar ($\sqrt{\lambda}$) couplings involved. In this way, working out for example the contribution from the gauge coupling, we can derive the general form of the second term in equation 230, as

$$\kappa = C(g^0 \mu^{-\epsilon} Z_g^{-1})^{n_g} = C(g^0 \mu^{-\epsilon} + \dots)^{n_g} \Rightarrow \frac{d\kappa}{dt} = -\epsilon n_g C g^{n_g} = -\epsilon n_g \kappa, \tag{232}$$

with the dots including one-loop terms which multiplied by the other factors in equation 230 would become of higher order.

Finally, taking into account that the tree level anomalous dimension associated with a given operator $\mathcal{O} = X_{\mu\nu}^{N_X} H^{N_S} D^{N_D} \psi^{N_F}$ is

$$n_{\mathcal{O}} = N_X + N_S + N_F - 2, \tag{233}$$

we obtain the master formula for one-loop renormalization:

$$\beta_{a_i} = 16\pi^2 \mu \frac{da_i}{d\mu} = \frac{1}{2}\left[(n_j - n_i) + n_{\text{coupl}_{ij}}\right] k_{ij} a_j \equiv \gamma_{ij} a_j, \tag{234}$$

where γ is the anomalous dimension matrix and $n_{\text{coupl}_{ij}}$ counts the number of couplings[6] $(g, y, \sqrt{\lambda})$ in k_{ij}.

The WFR factors of each field present in the EFT are obtained from the divergences associated to the kinetic Lagrangian, which can be parameterized as

$$\begin{aligned}\mathcal{L}_{\text{kin}} = {} & \overline{\psi_L}(1 + \delta Z_{\psi L}) \mathrm{i} \not{D} \psi_L + \overline{\psi_R}(1 + \delta Z_{\psi R}) \mathrm{i} \not{D} \psi_R + \frac{1}{2}(1 + \delta Z_S)(\partial_\mu S)^2 + (1 + \delta Z_H)(\partial_\mu H)^2 \\ & - \frac{1}{4}(1 + \delta Z_B) B_{\mu\nu} B^{\mu\nu} - \frac{1}{4}(1 + \delta Z_W) W_{I\mu\nu} W^{I\mu\nu} - \frac{1}{4}(1 + \delta Z_G) G^A_{\mu\nu} G^{A\,\mu\nu},\end{aligned} \tag{235}$$

after rescaling the bare fields $\psi^0 \to \sqrt{Z}\psi = (1 + \delta Z/2 + \dots)\,\psi$. In this way, the extra contributions $\delta Z \equiv Z - 1$ can be used to cancel the divergences contributing to this Lagrangian, that are computed in appendix H.2. The final results read:

$$Z_{l_L} = 1 - \frac{1}{64\pi^2 \epsilon}\left[g_1^2 + 3g_2^2 + 2 y^e y^{e\dagger}\right]; \tag{236}$$

$$Z_{e_R} = 1 - \frac{1}{16\pi^2 \epsilon}\left[g_1^2 + y^{e\dagger} y^e\right]; \tag{237}$$

$$Z_{d_R} = 1 - \frac{1}{48\pi^2 \epsilon}\left[\frac{1}{3} g_1^2 + 4 g_3^2 + 3 y^{d\dagger} y^d\right]; \tag{238}$$

[6] We will drop the subscript in n_{coupl} from here on.

$$Z_{u_R} = 1 - \frac{1}{48\pi^2\epsilon}\left[\frac{4}{3}g_1^2 + 4g_3^2 + 3y^{u\dagger}y^u\right]; \tag{239}$$

$$Z_{q_L} = 1 - \frac{1}{96\pi^2\epsilon}\left[\frac{1}{6}g_1^2 + \frac{9}{2}g_2^2 + 8g_3^2 + 3y^u y^{u\dagger} + 3y^d y^{d\dagger}\right]; \tag{240}$$

$$Z_H = 1 + \frac{1}{32\pi^2\epsilon}\left[g_1^2 + 3g_2^2 - 2\gamma_H^{(Y)}\right]; \tag{241}$$

$$Z_B = 1 - \frac{g_1^2}{32\pi^2\epsilon}\left[\frac{1}{3} + n_G\left(2 + \frac{22N_C}{27}\right)\right] = 1 - \frac{41g_1^2}{96\pi^2\epsilon}; \tag{242}$$

$$Z_W = 1 + \frac{g_2^2}{32\pi^2\epsilon}\left[\frac{43}{3} - \frac{2}{3}n_G\left(1 + N_C\right)\right] = 1 + \frac{19g_2^2}{96\pi^2\epsilon}; \tag{243}$$

$$Z_G = 1 + \frac{g_3^2}{32\pi^2\epsilon}\left[\frac{22}{3}N_C - \frac{8}{3}n_G\right] = 1 + \frac{14g_3^2}{32\pi^2\epsilon}, \tag{244}$$

having defined

$$\gamma_H^{(Y)} \equiv \mathrm{Tr}\left[y^e y^{e\dagger} + 3\left(y^d y^{d\dagger} + y^u y^{u\dagger}\right)\right], \tag{245}$$

and leaving the number of colors N_C and generations n_G unreplaced, in the first equality, to make these expressions generic.

These expressions can be subsequently employed to obtain the renormalization factors of each operator in our minimal basis:

$$Z^F_{O_{SHu}} = \sqrt{Z_{q_L} Z_H Z_{u_R}}, \qquad Z^F_{O_{s\widetilde{G}}} = Z_G, \tag{246}$$

$$Z^F_{O_{SHd}} = \sqrt{Z_{q_L} Z_H Z_{d_R}}, \qquad Z^F_{O_{s\widetilde{W}}} = Z_W, \tag{247}$$

$$Z^F_{O_{SHe}} = \sqrt{Z_{l_L} Z_H Z_{e_R}}, \qquad Z^F_{O_{s\widetilde{B}}} = Z_B. \tag{248}$$

Together with the previous results, this fixes κ in equation 229. We now have all ingredients to compute the RGEs.

6.2.2.1 Yukawa-like operators

Let us take, for example, the operator $i = O_{SHu}$. Then, $\Delta n \equiv n_j - n_i = 0$ in equation 234, whenever j is associated with another operator of the same class. (This term vanishes trivially for the WFR contribution.) The corresponding counterterms in the physical basis are functions of one λ_{SH} or two Yukawa couplings, hence $n_{ij} = 2$. For the mixing with the gauge operators, from equation 526, we have instead $\Delta n = -1$ and $n_{ij} = 3$ since the corresponding counterterm expressions involve a Yukawa and two gauge couplings. Therefore, every term in the RGE has the same weight after summing the two contributions in equation 234. Similar considerations are taken for the RGEs of the other Yukawa-like operators.

Altogether, we have:

$$\beta_{a_{SHu}} = 2\Bigg[\left(\lambda_{SH} - \frac{17g_1^2}{24} - \frac{9g_2^2}{8} - 4g_3^2 + \frac{1}{2}\gamma_H^{(Y)}\right)a_{SHu} - \frac{3}{4}y^d y^{d\dagger} a_{SHu} + \frac{5}{4}y^u y^{u\dagger} a_{SHu} + a_{SHu} y^{u\dagger} y^u + y^d a_{SHd}^\dagger y^u - \frac{1}{2}a_{SHd} y^{d\dagger} y^u - \left(\frac{17g_1^2}{6}a_{s\widetilde{B}} + \frac{9g_2^2}{2}a_{s\widetilde{W}} + 16g_3^2 a_{s\widetilde{G}} + \mathrm{Tr}\left[y^e a_{SHe}^\dagger + 3y^d a_{SHd}^\dagger - 3a_{SHu} y^{u\dagger})\right]\right)y^u\Bigg]; \tag{249}$$

$$\beta_{a_{SHd}} = 2\Bigg[\left(\lambda_{SH} - \frac{5g_1^2}{24} - \frac{9g_2^2}{8} - 4g_3^2 + \frac{1}{2}\gamma_H^{(Y)}\right)a_{SHd} - \frac{3}{4}y^u y^{u\dagger} a_{SHd} + \frac{5}{4}y^d y^{d\dagger} a_{SHd} + a_{SHd} y^{d\dagger} y^d + y^u a_{SHu}^\dagger y^d - \frac{1}{2}a_{SHu} y^{u\dagger} y^d - \left(\frac{5g_1^2}{6}a_{s\widetilde{B}} + \frac{9g_2^2}{2}a_{s\widetilde{W}} + 16g_3^2 a_{s\widetilde{G}} - \mathrm{Tr}\left[y^e a_{SHe}^\dagger + 3y^d a_{SHd}^\dagger - 3a_{SHu} y^{u\dagger})\right]\right)y^d\Bigg]; \tag{250}$$

$$\beta_{a_{SHe}} = 2\Bigg[a_{SHe}\left(\lambda_{SH} - \frac{15g_1^2}{8} - \frac{9g_2^2}{8} + \frac{1}{2}\gamma_H^{(Y)}\right) + \frac{5}{4}y^e y^{e\dagger} a_{SHe} + a_{SHe} y^{e\dagger} y^e - \left(\frac{15g_1^2}{2}a_{s\widetilde{B}} + \frac{9g_2^2}{2}a_{s\widetilde{W}} - \mathrm{Tr}\left[y^e a_{SHe}^\dagger + 3y^d a_{SHd}^\dagger - 3a_{SHu} y^{u\dagger})\right]\right)y^e\Bigg]; \tag{251}$$

6.2.2.2 Gauge operators

No divergences are mapped into these operators; therefore, they run only due to the non-trivial WFR of the gauge bosons:

$$\beta_{s\widetilde{G}} = -14g_3^2 a_{s\widetilde{G}}; \tag{252}$$

$$\beta_{s\widetilde{W}} = -\frac{19}{3}g_2^2 a_{s\widetilde{W}}; \tag{253}$$

$$\beta_{s\widetilde{B}} = \frac{41}{3}g_1^2 a_{s\widetilde{B}}. \tag{254}$$

A more graphic picture of the operator mixing can be obtained in the limit in which the different fermion families factorize, so that all dimension five Wilson coefficients are flavour-diagonal $a_{\alpha\beta} = \delta_{\alpha\beta}a_\alpha$ (and neglecting also off-diagonal entries in the Yukawa matrices). Using the notation of equation 234, where i runs over O_{SHu}^α, O_{SHd}^α, O_{SHe}^α, $O_{s\widetilde{G}}$, $O_{s\widetilde{W}}$ and $O_{s\widetilde{B}}$, and j over the same operators but with flavour

index ρ, we can write the anomalous dimension matrix in the following form:

$$\gamma = \begin{pmatrix} \gamma_{11} + 6y^u_\alpha y^u_\rho & y^d_\alpha y^u_\alpha - 6y^u_\alpha y^d_\rho & -2y^u_\alpha y^e_\rho & -32g_3^2 y^u_\alpha & -9g_2^2 y^u_\alpha & -\frac{17}{3}g_1^2 y^u_\alpha \\ y^u_\alpha y^d_\alpha - 6y^d_\alpha y^u_\rho & \gamma_{22} + 6y^d_\alpha y^d_\rho & 2y^d_\alpha y^e_\rho & -32g_3^2 y^d_\alpha & -9g_2^2 y^d_\alpha & -\frac{5}{3}g_1^2 y^d_\alpha \\ -6y^e_\alpha y^u_\rho & 6y^e_\alpha y^d_\rho & \gamma_{33} + 2y^e_\alpha y^e_\rho & 0 & -9g_2^2 y^e_\alpha & -15g_1^2 y^e_\alpha \\ 0 & 0 & 0 & -14g_3^2 & 0 & 0 \\ 0 & 0 & 0 & 0 & -\frac{19}{3}g_2^2 & 0 \\ 0 & 0 & 0 & 0 & 0 & \frac{41}{3}g_1^2 \end{pmatrix}, \tag{255}$$

where $\delta_{\alpha\rho}$ is implicit in every entry where the ρ-index does not appear, and we have defined:

$$\gamma_{11} = 2\lambda_{SH} - \frac{3}{2}\left(y^d_\alpha\right)^2 + \frac{9}{2}\left(y^u_\alpha\right)^2 - \frac{17}{12}g_1^2 - \frac{9}{4}g_2^2 - 8g_3^2 + \gamma_H^{(Y)};$$

$$\gamma_{22} = 2\lambda_{SH} - \frac{3}{2}\left(y^u_\alpha\right)^2 + \frac{9}{2}\left(y^d_\alpha\right)^2 - \frac{5}{12}g_1^2 - \frac{9}{4}g_2^2 - 8g_3^2 + \gamma_H^{(Y)};$$

$$\gamma_{33} = 2\lambda_{SH} + \frac{9}{2}\left(y^e_\alpha\right)^2 - \frac{15}{4}g_1^2 - \frac{9}{4}g_2^2 + \gamma_H^{(Y)}.$$

Based on the structure of the RGE matrix, we can draw the following conclusions:

1. The Yukawa-like operators are renormalized by all the others in our basis (the only zero in the third line is trivial given that leptons are not $SU(3)$ charged);

2. Even in the limit where the different families factorize, there is inter-generation mixing due to the trace contributions in the redundant operator $\mathcal{R}_{SH\Box}$, that is redefined into $O_{SHu,SHd,SHe}$ upon the use of the EOMs.

3. The bottom part matrix is block-diagonal. This is in agreement with the non-renormalization theorems provided in Refs. [277, 278].

In appendix H.4, we translate these results into a basis more commonly found in the literature, whose operators take the form $(\partial_\mu S)\overline{\psi}\gamma^\mu\psi$. We show that such basis is over-complete and derive the RGEs in a new minimal shift-symmetric basis. A comparison between our results and partial computations of the anomalous dimension matrix found in the literature is also presented in this appendix.

One of the main reasons such derivative basis is adopted is to describe the case of a *pure* axion (not necessarily the QCD one) which is a periodic field. We remark that, even in this case and in full generality, the Lagrangian should also include the term [190]

$$\mathcal{L} \supset \sum_{n\in\mathbb{Z}} \overline{\psi_L} c_n e^{inS/\Lambda} H\psi_R + \text{h.c.}, \tag{256}$$

which is invariant under $S \longrightarrow S + 2\pi\Lambda$. Upon expansion of the exponential, we obtain the Yukawa-like operators in our basis. These must be therefore included to describe correctly the phenomenology of the

axion up to a certain order in the EFT expansion (although the truncation itself makes us unable to visualize the full periodicity of the interaction). Moreover, such operators emerge naturally from the CCWZ Lagrangian of spontaneously broken theories, therefore making the non-derivative basis a convenient choice to match the EFT onto *e.g.* CHMs.

6.2.3 Matching and running below the electroweak scale

At energies below the EW scale, the ALP phenomenology can be described by a low-energy effective field theory (LEFT), where the massive SM bosons and the top quark are no longer present, that is valid up to $\mu \approx v$. Assuming still CP invariance, the most generic ALP LEFT Lagrangian up to dimension five is

$$\begin{aligned}\mathcal{L}_{\text{LEFT}} = &\frac{1}{2}\partial_\mu S \partial^\mu S - \frac{1}{2}\tilde{m}_S^2 S^2 - \frac{1}{4!}\tilde{\lambda}_S S^4 - \frac{1}{4}A_{\mu\nu}A^{\mu\nu} - \frac{1}{4}G^A_{\mu\nu}G^{A\mu\nu} \\ &+ \sum_{\psi=u,d,e}\left\{\overline{\psi^\alpha}\,\mathrm{i}\not{D}\psi^\alpha - \left[(\tilde{m}_\psi)_{\alpha\beta}\overline{\psi^\alpha_L}\psi^\beta_R - \mathrm{i}S(\tilde{c}_\psi)_{\alpha\beta}\overline{\psi^\alpha_L}\psi^\beta_R + \text{h.c.}\right]\right\} \\ &+ \tilde{a}_{S\widetilde{G}} S G^A_{\mu\nu}\tilde{G}^{A\mu\nu} + \tilde{a}_{S\widetilde{A}} S A_{\mu\nu}\tilde{A}^{\mu\nu} \\ &+ \sum_{\psi=u,d,e}\left\{S^2(\tilde{a}_\psi)_{\alpha\beta}\overline{\psi^\alpha_L}\psi^\beta_R + (\tilde{a}_{\psi A})_{\alpha\beta}\overline{\psi^\alpha_L}\sigma^{\mu\nu}\psi^\beta_R A_{\mu\nu} + (\tilde{a}_{\psi G})_{\alpha\beta}\overline{\psi^\alpha_L}\sigma^{\mu\nu}T_A u^\beta_R G^A_{\mu\nu} + \text{h.c.}\right\},\end{aligned} \tag{257}$$

where the Wilson coefficients can be fixed at the Higgs scale by demanding that both theories before and after EWSB describe the same physics. Performing this procedure at tree level, we obtain:

$$\tilde{e} = g_2 s_\omega = g_1 c_\omega\,, \qquad \tilde{g}_3 = g_3\,, \tag{258}$$

$$\tilde{m}_S^2 = m_S^2 + \frac{\lambda_{SH}}{2}v^2\,, \qquad \tilde{\lambda}_S = \lambda_S - 3\frac{v^2}{m_H^2}\lambda_{SH}^2\,, \tag{259}$$

$$\tilde{m}_u = \frac{v}{\sqrt{2}}y^u\,, \qquad \tilde{m}_d = \frac{v}{\sqrt{2}}y^d\,, \tag{260}$$

$$\tilde{m}_e = \frac{v}{\sqrt{2}}y^e\,, \qquad \tilde{c}_u = \frac{v}{\sqrt{2}}a_{SHu}\,, \tag{261}$$

$$\tilde{c}_d = \frac{v}{\sqrt{2}}a_{SHd}\,, \qquad \tilde{c}_e = \frac{v}{\sqrt{2}}a_{SHe}\,, \tag{262}$$

$$\tilde{a}_{S\widetilde{G}} = a_{S\widetilde{G}}\,, \qquad \tilde{a}_{S\widetilde{A}} = a_{S\widetilde{W}}s_\omega^2 + a_{S\widetilde{B}}c_\omega^2\,. \tag{263}$$

Given that the heavy particle generating $\tilde{a}_\psi = y^\psi \lambda_{SH} v/(2\sqrt{2}m_H^2)$ is the SM Higgs boson which sets the scale of light masses, *i.e.* because $y^\psi \sim m_\psi/v$, the coefficient $\tilde{a}_\psi$ is of order $1/v^2$ and therefore negligible in the LEFT. All coefficients not explicitly shown vanish identically.

It is also clear from the matching conditions that the integration of the massive particles, with the exception of the Higgs boson, produces no effect. This can be cross-checked with the power counting derived in Ref. [279]. Generically, a tree level graph with heavy internal particles generates operators with

mass dimension

$$D-4=\sum_i (d_i-4)+\frac{F_i}{2}+B_i \equiv \sum_i \omega_i\,, \tag{264}$$

with d, F and B being, respectively, the operator dimension in the high-energy EFT, the number of heavy fermions and the number of heavy bosons. The i sums over the vertices in any tree level graph. To construct the ALP LEFT up to dimension five, we therefore need $\sum_i \omega_i \leq 1$. The operators containing at least one heavy field[7] which satisfy this requirement are:

$$\omega=0: \quad hS^2\,; \qquad\qquad \omega=\frac{1}{2}: \quad \psi tA,\ \psi tG,\ \psi tS\,; \tag{265}$$

$$\omega=1: \quad t^2A,\ t^2G,\ t^2S,\ h\psi^2,\ Z\psi^2,\ W\psi^2\,. \tag{266}$$

For tree level matching, there are at least two vertices per graph. Therefore, to comply with the maximum weight, we can either *(1)* combine two vertices with $\omega = 1/2$; *(2)* combine one vertex with $\omega = 1$ and another with $\omega = 0$; and *(3)* combine a vertex with $\omega = 0$ with others of the same weight or in conjunction with the previous cases. In case *(1)*, there is actually just one possibility, given that the photon and the gluon couple diagonally to the fermions. By integrating the top at tree level, we generate $c\psi^2S^2$, with $c \sim v/\Lambda^2$ which is parametrically of the same order as the dimension six terms we have neglected. In case *(2)*, there is no possibility to use the vertices involving two top quarks internally in a tree graph, but we can combine $h\psi^2$ with hS^2. The remaining case *(3)* allows us to combine the hS^2 vertex with itself, producing a contribution to S^4. All these cases have been accounted for along equations 258–263.

Nonetheless, in the following, we adopt a more general approach in which we are ignorant about the LEFT completion in the UV and therefore consider all the operators in equation 257, namely $S^2\overline{\psi}\psi$. In such approach, we need to include also the purely SMEFT dimension five operators in the last line of equation 257, the so-called dipole operators; in particular, these can be induced by the SVV couplings, so it would be inconsistent to ignore them in this analysis. The RGEs obtained this way can be used to describe phenomena at any energy $\mu < v$, excluding confinement effects below the QCD scale. Once we reach a light fermion threshold, we simply have to remove the index referring to the particle being integrated out and keep calculating in the EFT with generic Wilson coefficients. To be able to capture these effects, we leave the flavour number unreplaced.

On top of the minimal basis in equation 257, the following redundant operators must be included to absorb all possible off-shell divergences that arise at dimension five:

$$\mathcal{L}_R = \sum_{\psi=u,d,e} \left[\left(\tilde{r}_{\psi\Box}\right)_{\alpha\beta} \overline{\psi_L^\alpha} D^2 \psi_R^\beta + \mathrm{i}\left(\tilde{r}_{S\psi_L}\right)_{\alpha\beta} S\overline{\psi_L^\alpha} \mathrm{i}\not{D}\psi_L^\beta + \mathrm{i}\left(\tilde{r}_{S\psi_R}\right)_{\alpha\beta} S\overline{\psi_R^\alpha} \mathrm{i}\not{D}\psi_R^\beta + \mathrm{h.c.} \right], \tag{267}$$

where again the flavour matrices are taken to be real for CP-even operators.

[7] Operators with no heavy fields match directly into the LEFT.

Furthermore, to absorb contributions from non-diagonal $\psi \longrightarrow \psi$ processes, we will work with generic fermion masses. In order to do so, we consider a spurion background field (BF) φ coupled to massless fermions:

$$\mathcal{L}_{\text{BF}} = -\left(\tilde{m}_u\right)_{\alpha\beta} \varphi \bar{u}_L^\alpha u_R^\beta - \left(\tilde{m}_d\right)_{\alpha\beta} \varphi \bar{d}_L^\alpha d_R^\beta - \left(\tilde{m}_e\right)_{\alpha\beta} \varphi \bar{e}_L^\alpha e_R^\beta + \text{h.c.}\,, \tag{268}$$

and assume that it develops a VEV $\langle\varphi\rangle = 1$ by the end of the computations. In this way, we can calculate any process involving n external φ-fields to account for n insertions of the fermions mass.

6.2.4 One-loop divergences in the ALP LEFT

Similarly to section 6.2.1, we fix the counterterm Lagrangian of the ALP LEFT by computing the $1/v$ term of all 1PI one-loop divergent amplitudes in the off-shell basis. (The running of the dimension four couplings with other dimension four ones can be obtained with automatized tools, namely `Pyr@te` [280]; we will retain some of these contributions in the final results, written in gray, as a manual cross-check.)

We use directly the `FormCalc` output, after having verified most of the results in the unbroken theory and fixed small typos in the conversion of the `FeynRules` model to `FeynArts` in terms involving the Levi-Civita tensor; see footnote 1. Still, some amplitudes of the considered processes need to be reduced further in order to match onto our LEFT. The identities used in this procedure, as well as the diagrams generated in each process, are presented in appendix I.1.

Matching the divergences onto the Green basis consisting of the operators in equations 257 and 267, we obtain:

- $S \longrightarrow S$:

$$\begin{aligned}\tilde{m}_S'^2 = {}& \frac{3}{4\pi^2\epsilon}\left(\text{Tr}\left[\tilde{m}_d^\dagger \tilde{a}_d \tilde{m}_d^\dagger \tilde{m}_d + \tilde{m}_d^\dagger \tilde{m}_d \tilde{a}_d^\dagger \tilde{m}_d\right] + \text{Tr}\left[\tilde{m}_u^\dagger \tilde{a}_u \tilde{m}_u^\dagger \tilde{m}_u + \tilde{m}_u^\dagger \tilde{m}_u \tilde{a}_u^\dagger \tilde{m}_u\right]\right) \\ & + \frac{1}{4\pi^2\epsilon}\text{Tr}\left[\tilde{m}_e^\dagger \tilde{a}_e \tilde{m}_e^\dagger \tilde{m}_e + \tilde{m}_e^\dagger \tilde{m}_e \tilde{a}_e^\dagger \tilde{m}_e\right]\,.\end{aligned} \tag{269}$$

- $\psi \longrightarrow \psi$:

$$\tilde{m}_e' = \frac{3}{8\pi^2\epsilon}\tilde{e}\left(\tilde{m}_e \tilde{m}_e^\dagger \tilde{a}_{eA} + \tilde{a}_{eA} \tilde{m}_e^\dagger \tilde{m}_e\right) - \frac{1}{16\pi^2\epsilon}\tilde{m}_S^2 \tilde{a}_e\,, \tag{270}$$

$$\begin{aligned}\tilde{m}_u' = {}& -\frac{2}{8\pi^2\epsilon}\tilde{e}\left(\tilde{m}_u \tilde{m}_u^\dagger \tilde{a}_{uA} + \tilde{a}_{uA} \tilde{m}_u^\dagger \tilde{m}_u\right) - \frac{1}{2\pi^2\epsilon}\tilde{g}_3\left(\tilde{m}_u \tilde{m}_u^\dagger \tilde{a}_{uG} + \tilde{a}_{uG} \tilde{m}_u^\dagger \tilde{m}_u\right) \\ & - \frac{1}{16\pi^2\epsilon}\tilde{m}_S^2 \tilde{a}_u\,,\end{aligned} \tag{271}$$

$$\begin{aligned}\tilde{m}_d' = {}& \frac{1}{8\pi^2\epsilon}\tilde{e}\left(\tilde{m}_d \tilde{m}_d^\dagger \tilde{a}_{dA} + \tilde{a}_{dA} \tilde{m}_d^\dagger \tilde{m}_d\right) - \frac{1}{2\pi^2\epsilon}\tilde{g}_3\left(\tilde{m}_d \tilde{m}_d^\dagger \tilde{a}_{dG} + \tilde{a}_{dG} \tilde{m}_d^\dagger \tilde{m}_d\right) \\ & - \frac{1}{16\pi^2\epsilon}\tilde{m}_S^2 \tilde{a}_d\,.\end{aligned} \tag{272}$$

- $SS \to SS$:

$$\tilde{\lambda}'_S = \frac{3}{\pi^2\epsilon}\left[\mathrm{Tr}_e^{\tilde{\lambda}} + 3\left(\mathrm{Tr}_u^{\tilde{\lambda}} + \mathrm{Tr}_d^{\tilde{\lambda}}\right)\right], \tag{273}$$

with

$$\mathrm{Tr}_\psi^{\tilde{\lambda}} \equiv \mathrm{Tr}\Big[\tilde{a}_\psi \tilde{c}_\psi^\dagger \tilde{c}_\psi \tilde{m}_\psi^\dagger + \tilde{a}_\psi \tilde{m}_\psi^\dagger \tilde{c}_\psi \tilde{c}_\psi^\dagger - \tilde{a}_\psi^\dagger \tilde{c}_\psi \tilde{m}_\psi^\dagger \tilde{c}_\psi - \tilde{a}_\psi \tilde{c}_\psi^\dagger \tilde{m}_\psi \tilde{c}_\psi^\dagger + \tilde{a}_\psi^\dagger \tilde{c}_\psi \tilde{c}_\psi^\dagger \tilde{m}_\psi + \tilde{a}_\psi^\dagger \tilde{m}_\psi \tilde{c}_\psi^\dagger \tilde{c}_\psi\Big].$$

- $S \to \psi\overline{\psi}$:

$$\begin{aligned}
\tilde{c}'_e &= \frac{-1}{8\pi^2\epsilon}\left(\tilde{a}_e \tilde{m}_e^\dagger \tilde{c}_e + \tilde{c}_e \tilde{m}_e^\dagger \tilde{a}_e\right) - \frac{3\tilde{e}}{8\pi^2\epsilon}\left(\tilde{m}_e \tilde{c}_e^\dagger \tilde{a}_{eA} + \tilde{a}_{eA} \tilde{c}_e^\dagger \tilde{m}_e\right. && (274)\\
&\left. -\tilde{c}_e \tilde{m}_e^\dagger \tilde{a}_{eA} - \tilde{a}_{eA} \tilde{m}_e^\dagger \tilde{c}_e\right), \\
\tilde{c}'_u &= \frac{2\tilde{e}}{8\pi^2\epsilon}\left(\tilde{m}_u \tilde{c}_u^\dagger \tilde{a}_{uA} + \tilde{a}_{uA} \tilde{c}_u^\dagger \tilde{m}_u - \tilde{c}_u \tilde{m}_u^\dagger \tilde{a}_{uA} - \tilde{a}_{uA} \tilde{m}_u^\dagger \tilde{c}_u\right) && (275)\\
&- \frac{1}{8\pi^2\epsilon}\left(\tilde{a}_u \tilde{m}_u^\dagger \tilde{c}_u + \tilde{c}_u \tilde{m}_u^\dagger \tilde{a}_u\right) + \frac{\tilde{g}_3}{2\pi^2\epsilon}\left(\tilde{m}_u \tilde{c}_u^\dagger \tilde{a}_{uG} + \tilde{a}_{uG} \tilde{c}_u^\dagger \tilde{m}_u - \tilde{c}_u \tilde{m}_u^\dagger \tilde{a}_{uG} - \tilde{a}_{uG} \tilde{m}_u^\dagger \tilde{c}_u\right), \\
\tilde{c}'_d &= -\frac{\tilde{e}}{8\pi^2\epsilon}\left(\tilde{m}_d \tilde{c}_d^\dagger \tilde{a}_{dA} + \tilde{a}_{dA} \tilde{c}_d^\dagger \tilde{m}_d - \tilde{c}_d \tilde{m}_d^\dagger \tilde{a}_{dA} - \tilde{a}_{dA} \tilde{m}_d^\dagger \tilde{c}_d\right) && (276)\\
&- \frac{1}{8\pi^2\epsilon}\left(\tilde{a}_d \tilde{m}_d^\dagger \tilde{c}_d + \tilde{c}_d \tilde{m}_d^\dagger \tilde{a}_d\right) + \frac{\tilde{g}_3}{2\pi^2\epsilon}\left(\tilde{m}_d \tilde{c}_d^\dagger \tilde{a}_{dG} + \tilde{a}_{dG} \tilde{c}_d^\dagger \tilde{m}_d - \tilde{c}_d \tilde{m}_d^\dagger \tilde{a}_{dG} - \tilde{a}_{dG} \tilde{m}_d^\dagger \tilde{c}_d\right).
\end{aligned}$$

These processes fix also the following non-renormalizable couplings:

$$\begin{aligned}
\tilde{r}'_{Se_L} &= \frac{1}{16\pi^2\epsilon}\tilde{a}_e \tilde{c}_e^\dagger - \frac{3}{2\pi\epsilon}\tilde{\alpha}_{\mathrm{em}}\tilde{a}_{S\widetilde{A}} + \frac{3\tilde{e}}{16\pi^2\epsilon}\tilde{c}_e \tilde{a}_{eA}^\dagger, && (277)\\
\tilde{r}'_{Se_R} &= \frac{-1}{16\pi^2\epsilon}\tilde{a}_e^\dagger \tilde{c}_e + \frac{3}{2\pi\epsilon}\tilde{\alpha}_{\mathrm{em}}\tilde{a}_{S\widetilde{A}} - \frac{3\tilde{e}}{16\pi^2\epsilon}\tilde{c}_e^\dagger \tilde{a}_{eA}, && (278)\\
\tilde{r}'_{Su_L} &= \frac{1}{16\pi^2\epsilon}\tilde{a}_u \tilde{c}_u^\dagger - \frac{2}{\pi\epsilon}\left(\frac{\tilde{\alpha}_{\mathrm{em}}}{3}\tilde{a}_{S\widetilde{A}} + \tilde{\alpha}_3 \tilde{a}_{S\widetilde{G}}\right) - \frac{2\tilde{e}}{16\pi^2\epsilon}\tilde{c}_u \tilde{a}_{uA}^\dagger - \frac{1}{4\pi^2\epsilon}\tilde{g}_3 \tilde{c}_u \tilde{a}_{uG}^\dagger, && (279)\\
\tilde{r}'_{Su_R} &= \frac{-1}{16\pi^2\epsilon}\tilde{a}_u^\dagger \tilde{c}_u + \frac{2}{\pi\epsilon}\left(\frac{\tilde{\alpha}_{\mathrm{em}}}{3}\tilde{a}_{S\widetilde{A}} + \tilde{\alpha}_3 \tilde{a}_{S\widetilde{G}}\right) + \frac{2\tilde{e}}{16\pi^2\epsilon}\tilde{c}_u^\dagger \tilde{a}_{uA} - \frac{1}{4\pi^2\epsilon}\tilde{g}_3 \tilde{c}_u^\dagger \tilde{a}_{uG}, && (280)\\
\tilde{r}'_{Sd_L} &= \frac{1}{16\pi^2\epsilon}\tilde{a}_d \tilde{c}_d^\dagger - \frac{2}{\pi\epsilon}\left(\frac{\tilde{\alpha}_{\mathrm{em}}}{12}\tilde{a}_{S\widetilde{A}} + \tilde{\alpha}_3 \tilde{a}_{S\widetilde{G}}\right) + \frac{\tilde{e}}{16\pi^2\epsilon}\tilde{c}_d \tilde{a}_{dA}^\dagger - \frac{1}{4\pi^2\epsilon}\tilde{g}_3 \tilde{c}_d \tilde{a}_{dG}^\dagger, && (281)\\
\tilde{r}'_{Sd_R} &= \frac{-1}{16\pi^2\epsilon}\tilde{a}_d^\dagger \tilde{c}_d + \frac{2}{\pi\epsilon}\left(\frac{\tilde{\alpha}_{\mathrm{em}}}{12}\tilde{a}_{S\widetilde{A}} + \tilde{\alpha}_3 \tilde{a}_{S\widetilde{G}}\right) - \frac{\tilde{e}}{16\pi^2\epsilon}\tilde{c}_d^\dagger \tilde{a}_{dA} - \frac{1}{4\pi^2\epsilon}\tilde{g}_3 \tilde{c}_d^\dagger \tilde{a}_{dG}. && (282)
\end{aligned}$$

- $V \to \psi\overline{\psi}$:

$$\begin{aligned}
\tilde{a}'_{eA} &= \frac{\tilde{e}}{16\pi^2\epsilon}\left(\tilde{e}\tilde{a}_{eA} + 2\tilde{c}_e \tilde{a}_{S\widetilde{A}}\right), && (283)\\
\tilde{a}'_{uA} &= \frac{\tilde{e}}{12\pi^2\epsilon}\left(\frac{1}{3}\tilde{e}\tilde{a}_{uA} + \tilde{c}_u \tilde{a}_{S\widetilde{A}}\right) - \frac{\tilde{e}}{18\pi^2\epsilon}\tilde{g}_3 \tilde{a}_{uG}, && (284)
\end{aligned}$$

$$\tilde{a}'_{dA} = \frac{\tilde{e}}{24\pi^2\epsilon}\left(\frac{1}{6}\tilde{e}\tilde{a}_{dA} - \tilde{c}_d\tilde{a}_{S\widetilde{A}}\right) + \frac{\tilde{e}}{36\pi^2\epsilon}\tilde{g}_3\tilde{a}_{dG}\,, \tag{285}$$

$$\tilde{r}'_{e\Box} = -\frac{3}{8\pi^2\epsilon}\tilde{e}\tilde{a}_{eA}\,, \tag{286}$$

$$\tilde{r}'_{u\Box} = \frac{1}{4\pi^2\epsilon}\tilde{e}\tilde{a}_{uA} + \frac{1}{2\pi^2\epsilon}\tilde{g}_3\tilde{a}_{uG}\,, \tag{287}$$

$$\tilde{r}'_{d\Box} = -\frac{1}{8\pi^2\epsilon}\tilde{e}\tilde{a}_{dA} + \frac{1}{2\pi^2\epsilon}\tilde{g}_3\tilde{a}_{dG}\,, \tag{288}$$

$$\tilde{a}'_{uG} = -\frac{1}{8\pi^2\epsilon}\tilde{g}_3\tilde{c}_u\tilde{a}_{S\widetilde{G}} - \frac{7}{6\pi\epsilon}\tilde{\alpha}_3\tilde{a}_{uG} + \frac{1}{24\pi^2\epsilon}\tilde{e}\tilde{g}_3\tilde{a}_{uA}\,, \tag{289}$$

$$\tilde{a}'_{dG} = -\frac{1}{8\pi^2\epsilon}\tilde{g}_3\tilde{c}_d\tilde{a}_{S\widetilde{G}} - \frac{7}{6\pi\epsilon}\tilde{\alpha}_3\tilde{a}_{dG} - \frac{1}{48\pi^2\epsilon}\tilde{e}\tilde{g}_3\tilde{a}_{dA}\,. \tag{290}$$

These processes also contribute to the redundant operators in the previous item and can therefore be used as a cross-check.

- $SS \to \psi\overline{\psi}$:

$$\begin{aligned}\tilde{a}'_e = &-\left[\frac{1}{\pi\epsilon}\tilde{\alpha}_{\mathsf{em}} - \frac{\tilde{\lambda}_S}{32\pi^2\epsilon}\right]\tilde{a}_e - \frac{1}{16\pi^2\epsilon}\left(\tilde{c}_e\tilde{a}^\dagger_e\tilde{c}_e - 2\tilde{a}_e\tilde{c}^\dagger_e\tilde{c}_e - 2\tilde{c}_e\tilde{c}^\dagger_e\tilde{a}_e\right)\\ &- \frac{3\tilde{e}}{8\pi^2\epsilon}\left(\tilde{c}_e\tilde{c}^\dagger_e\tilde{a}_{eA} + \tilde{a}_{eA}\tilde{c}^\dagger_e\tilde{c}_e\right)\,,\end{aligned} \tag{291}$$

$$\begin{aligned}\tilde{a}'_u = &-\left[\frac{4}{3\pi\epsilon}\left(\frac{1}{3}\tilde{\alpha}_{\mathsf{em}} + \tilde{\alpha}_3\right) - \frac{\tilde{\lambda}_S}{32\pi^2\epsilon}\right]\tilde{a}_u - \frac{1}{16\pi^2\epsilon}\left(\tilde{c}_u\tilde{a}^\dagger_u\tilde{c}_u - 2\tilde{a}_u\tilde{c}^\dagger_u\tilde{c}_u - 2\tilde{c}_u\tilde{c}^\dagger_u\tilde{a}_u\right)\\ &+ \frac{\tilde{e}}{4\pi^2\epsilon}\left(\tilde{c}_u\tilde{c}^\dagger_u\tilde{a}_{uA} + \tilde{a}_{uA}\tilde{c}^\dagger_u\tilde{c}_u\right) + \frac{\tilde{g}_3}{2\pi^2\epsilon}\left(\tilde{c}_u\tilde{c}^\dagger_u\tilde{a}_{uG} + \tilde{a}_{uG}\tilde{c}^\dagger_u\tilde{c}_u\right)\,,\end{aligned} \tag{292}$$

$$\begin{aligned}\tilde{a}'_d = &-\left[\frac{1}{3\pi\epsilon}\left(\frac{1}{3}\tilde{\alpha}_{\mathsf{em}} + 4\tilde{\alpha}_3\right) - \frac{\tilde{\lambda}_S}{32\pi^2\epsilon}\right]\tilde{a}_d - \frac{1}{16\pi^2\epsilon}\left(\tilde{c}_d\tilde{a}^\dagger_d\tilde{c}_d - 2\tilde{a}_d\tilde{c}^\dagger_d\tilde{c}_d - 2\tilde{c}_d\tilde{c}^\dagger_d\tilde{a}_d\right)\\ &- \frac{\tilde{e}}{8\pi^2\epsilon}\left(\tilde{c}_d\tilde{c}^\dagger_d\tilde{a}_{dA} + \tilde{a}_{dA}\tilde{c}^\dagger_d\tilde{c}_d\right) + \frac{\tilde{g}_3}{2\pi^2\epsilon}\left(\tilde{c}_d\tilde{c}^\dagger_d\tilde{a}_{dG} + \tilde{a}_{dG}\tilde{c}^\dagger_d\tilde{c}_d\right)\,.\end{aligned} \tag{293}$$

- $S \to VV$:

$$\tilde{a}_{S\widetilde{A}} = \frac{\tilde{e}}{8\pi^2\epsilon}\mathsf{Tr}\left[\left(\tilde{c}_e\tilde{a}^\dagger_{eA} + \tilde{c}^\dagger_e\tilde{a}_{eA}\right) + \left(\tilde{c}_d\tilde{a}^\dagger_{dA} + \tilde{c}^\dagger_d\tilde{a}_{dA}\right) - 2\left(\tilde{c}_u\tilde{a}^\dagger_{uA} + \tilde{c}^\dagger_u\tilde{a}_{uA}\right)\right], \tag{294}$$

$$\tilde{a}_{S\widetilde{G}} = \frac{-\tilde{g}_3}{16\pi^2\epsilon}\mathsf{Tr}\left[\tilde{c}_d\tilde{a}^\dagger_{dG} + \tilde{c}^\dagger_d\tilde{a}_{dG} + \tilde{c}_u\tilde{a}^\dagger_{uG} + \tilde{c}^\dagger_u\tilde{a}_{uG}\right]\,. \tag{295}$$

All other coefficients vanish. The processes $V \to \overline{\psi}\psi$, as well as $\psi \to \psi$, give also contributions to the fermion kinetic terms; see equation 546. We use them to cross-check the WFR factors which are presented in the next section.

6.2.5 Anomalous dimensions in the ALP LEFT

The WFR factors of light fields, required to compute the β-functions in the ALP LEFT, are obtained analogously to what was done in appendix H.2. They read[8]:

$$Z_{e_L} = 1 - \frac{\tilde{\alpha}_{\text{em}}}{4\pi\epsilon} - \frac{\tilde{c}_e\tilde{c}_e^\dagger}{32\pi^2\epsilon} - \frac{3\tilde{e}}{16\pi^2\epsilon}\left(m_e\tilde{a}_{eA}^\dagger + \tilde{a}_{eA}m_e^\dagger\right), \tag{296}$$

$$Z_{e_R} = 1 - \frac{\tilde{\alpha}_{\text{em}}}{4\pi\epsilon} - \frac{\tilde{c}_e^\dagger\tilde{c}_e}{32\pi^2\epsilon} - \frac{3\tilde{e}}{16\pi^2\epsilon}\left(\tilde{a}_{eA}^\dagger m_e + m_e^\dagger\tilde{a}_{eA}\right), \tag{297}$$

$$\begin{aligned} Z_{d_L} = 1 &- \frac{1}{3\pi\epsilon}\left[\frac{1}{12}\tilde{\alpha}_{\text{em}} + \tilde{\alpha}_3\right] - \frac{\tilde{c}_d\tilde{c}_d^\dagger}{32\pi^2\epsilon} \\ &- \frac{\tilde{e}}{16\pi^2\epsilon}\left(m_d\tilde{a}_{dA}^\dagger + \tilde{a}_{dA}m_d^\dagger\right) + \frac{\tilde{g}_3}{4\pi^2\epsilon}\left(m_d\tilde{a}_{dG}^\dagger + \tilde{a}_{dG}m_d^\dagger\right), \end{aligned} \tag{298}$$

$$\begin{aligned} Z_{d_R} = 1 &- \frac{1}{3\pi\epsilon}\left[\frac{1}{12}\tilde{\alpha}_{\text{em}} + \tilde{\alpha}_3\right] - \frac{\tilde{c}_d^\dagger\tilde{c}_d}{32\pi^2\epsilon} \\ &- \frac{\tilde{e}}{16\pi^2\epsilon}\left(\tilde{a}_{dA}^\dagger m_d + m_d^\dagger\tilde{a}_{dA}\right) + \frac{\tilde{g}_3}{4\pi^2\epsilon}\left(\tilde{a}_{dG}^\dagger m_d + m_d^\dagger\tilde{a}_{dG}\right), \end{aligned} \tag{299}$$

$$\begin{aligned} Z_{u_L} = 1 &- \frac{1}{3\pi\epsilon}\left[\frac{1}{3}\tilde{\alpha}_{\text{em}} + \tilde{\alpha}_3\right] - \frac{\tilde{c}_u\tilde{c}_u^\dagger}{32\pi^2\epsilon} \\ &+ \frac{2\tilde{e}}{16\pi^2\epsilon}\left(m_u\tilde{a}_{uA}^\dagger + \tilde{a}_{uA}m_u^\dagger\right) + \frac{\tilde{g}_3}{4\pi^2\epsilon}\left(m_u\tilde{a}_{uG}^\dagger + \tilde{a}_{uG}m_u^\dagger\right), \end{aligned} \tag{300}$$

$$\begin{aligned} Z_{u_R} = 1 &- \frac{1}{3\pi\epsilon}\left[\frac{1}{3}\tilde{\alpha}_{\text{em}} + \tilde{\alpha}_3\right] - \frac{\tilde{c}_u^\dagger\tilde{c}_u}{32\pi^2\epsilon} \\ &+ \frac{2\tilde{e}}{16\pi^2\epsilon}\left(\tilde{a}_{uA}^\dagger m_u + m_u^\dagger\tilde{a}_{uA}\right) + \frac{\tilde{g}_3}{4\pi^2\epsilon}\left(\tilde{a}_{uG}^\dagger m_u + m_u^\dagger\tilde{a}_{uG}\right), \end{aligned} \tag{301}$$

$$\begin{aligned} Z_A = 1 &- \frac{\tilde{\alpha}_{\text{em}}}{3\pi\epsilon}\left[n_\ell + \frac{1}{3}n_d + \frac{4}{3}n_u\right] \\ &+ \frac{\tilde{e}}{2\pi^2\epsilon}\text{Tr}\left[(\tilde{a}_{eA}^\dagger m_e + m_e^\dagger\tilde{a}_{eA}) - 2(\tilde{a}_{uA}^\dagger m_u + m_u^\dagger\tilde{a}_{uA}) + (\tilde{a}_{dA}^\dagger m_d + m_d^\dagger\tilde{a}_{dA})\right], \end{aligned} \tag{302}$$

$$Z_G = 1 + \frac{\tilde{\alpha}_3}{4\pi\epsilon}\left[11 - \frac{2}{3}(n_u + n_d)\right] - \frac{\tilde{g}_3}{4\pi^2\epsilon}\text{Tr}\left[\tilde{a}_{dG}^\dagger m_d + m_d^\dagger\tilde{a}_{dG} + \tilde{a}_{uG}^\dagger m_u + m_u^\dagger\tilde{a}_{uG}\right], \tag{303}$$

$$Z_S = 1 - \frac{1}{8\pi^2\epsilon}\text{Tr}\left[\tilde{c}_e\tilde{c}_e^\dagger + 3\left(\tilde{c}_d\tilde{c}_d^\dagger + \tilde{c}_u\tilde{c}_u^\dagger\right)\right]. \tag{304}$$

We can now move to the physical basis by using the redundancy relations in equations 580–585. All contributions from effective operators to the fermion kinetic terms are precisely canceled on-shell. The other WFR factors remain the same in the minimal basis.

Following the procedure[9] described in section 6.2.2, we can finally obtain the β-functions of the different parameters in the ALP LEFT (up to renormalizable contributions computed with `Pyr@te`).

[8] Although we are interested in computing only the $1/v$ term of the RGEs, we must keep the dimension four terms in the WFR factors, which will be multiplied by $1/v$ coefficients in the final equations.

[9] In the deduction of the master formula in section 6.2.2, we have factorized out the dimension five couplings, so that α

6.2.5.1 Fermionic masses

Let us first consider the pure SM LEFT limit. The contribution from effective operators to the running of the fermion masses comes, not only from the mixing with dipole operators, but also from the WFR of the fermion fields. Since the last contribution vanishes on-shell,

$$\beta_{\tilde{m}_e} = \frac{1}{2} k_{\tilde{m}_e,\tilde{c}_{eA}} \tilde{c}_{eA} \left(n_{\tilde{m}_e,\tilde{a}_{eA}} + \Delta n_{\tilde{a}_{eA},\tilde{m}_e} \right) . \tag{305}$$

The mass counterterm $k_{\tilde{m}_e,\tilde{a}_{eA}} \tilde{a}_{eA}$ can be directly read from equation 270, as well as the input parameters for the master formula $n_{\tilde{m}_e,\tilde{a}_{eA}} = \Delta n_{\tilde{a}_{eA},\tilde{m}_e} = 1$, where we used that the tree level anomalous dimension of $\tilde{a}_{eA}$ is 1. Hence,

$$\beta_{\tilde{m}_e} = 12\tilde{e} \left(\tilde{m}_e \tilde{m}_e^\dagger \tilde{a}_{eA} + \tilde{a}_{eA} \tilde{m}_e^\dagger \tilde{m}_e \right) . \tag{306}$$

This result agrees exactly with equation C.2 in Ref. [281].

Including also the contribution from dimension five operators involving the ALP, which adds

$$\frac{1}{2} k_{\tilde{m}_e,\tilde{a}_e} \tilde{a}_e \left(n_{\tilde{m}_e,\tilde{a}_e} + \Delta n_{\tilde{a}_e,\tilde{m}_e} \right) = -2\tilde{m}_S^2 \tilde{a}_e \tag{307}$$

to the previous β-function, where $n_{\tilde{m}_e,\tilde{a}_e} = 0$ and $\Delta n_{\tilde{a}_e,\tilde{m}_e} = 2$, we obtain the final result:

$$\beta_{\tilde{m}_e} = 12\tilde{e} \left(\tilde{m}_e \tilde{m}_e^\dagger \tilde{a}_{eA} + \tilde{a}_{eA} \tilde{m}_e^\dagger \tilde{m}_e \right) - 2\tilde{m}_S^2 \tilde{a}_e . \tag{308}$$

Similarly to the case of the electron, the contribution from chromomagnetic operators to the WFR of quarks is canceled on-shell. Therefore, we have:

$$\beta_{\tilde{m}_q} = -12\tilde{e} Q_q \left(\tilde{m}_q \tilde{m}_q^\dagger \tilde{a}_{qA} + \tilde{a}_{qA} \tilde{m}_q^\dagger \tilde{m}_q \right) - 16\tilde{g}_3 \left(\tilde{m}_q \tilde{m}_q^\dagger \tilde{a}_{qG} + \tilde{a}_{qG} \tilde{m}_q^\dagger \tilde{m}_q \right) - 2\tilde{m}_S^2 \tilde{a}_q , \tag{309}$$

where $Q_u = 2/3$ and $Q_d = -1/3$. Again, the pure SM LEFT terms agree with equations C.3 and C.4 in Ref. [281].

6.2.5.2 Gauge couplings

Because explicit gauge invariance is retained in the BFM, the renormalization factors of the gauge couplings and the corresponding gauge bosons are related [272]: $Z_g = Z_V^{-1/2}$. Hence, the β-functions of the gauge couplings can be determined from the WFR factors of the respective gauge bosons.

Let us quickly sketch the proof. First, as always, we require the bare coupling, $g_0 = Z_g \mu^\epsilon g$, to be independent of the energy:

$$16\pi^2 \mu \frac{\partial g_0}{\partial \mu} = 0 = 16\pi^2 Z_g \mu^\epsilon \left[g\epsilon + g\mu \frac{\partial \log Z_g}{\partial \mu} + \mu \frac{\partial g}{\mu} \right] , \tag{310}$$

in equation 226 was made of renormalizable couplings only. Any other factorization, namely the inverse, is valid too. In case α is instead made of dimension five couplings, the knowledge of their tree level anomalous dimensions is required, which can be trivially obtained from equation 233.

which leads to

$$\beta_g = -16\pi^2 g\left[\epsilon + \mu\frac{\partial \log Z_g}{\partial \mu}\right] = -16\pi^2 g\left[\epsilon - \frac{1}{2}\mu\frac{\partial \log Z_V}{\partial \mu}\right]. \tag{311}$$

Given that $Z_V = Z_V\left(\tilde{g}, \tilde{m}_\psi, \tilde{m}^\dagger_\psi, \tilde{a}_{\psi V}, \tilde{a}^\dagger_{\psi V}\right)$ in the LEFT, we can use the chain rule

$$16\pi^2\mu\frac{\partial}{\partial\mu} = \beta_{\tilde{g}}\frac{\partial}{\partial\tilde{g}} + \beta_{\tilde{a}^{\alpha\beta}_{\psi V}}\frac{\partial}{\partial\tilde{a}^{\alpha\beta}_{\psi V}} + \beta_{\tilde{a}^{\dagger\alpha\beta}_{\psi V}}\frac{\partial}{\partial\tilde{a}^{\dagger\alpha\beta}_{\psi V}}, \tag{312}$$

to simplify the result above. We obtain:

$$\beta_{\tilde{g}} = -\tilde{g}\left[16\pi^2\epsilon - \frac{1}{2}\beta_{\tilde{i}}\frac{\partial \log Z_V}{\partial \tilde{i}}\right]. \tag{313}$$

Now, $Z_V = 1 + \sum Z_V^{(1)}/\epsilon^n$. Since the β-function needs to be finite, the various powers of $1/\epsilon$ must cancel. In particular, the first power is canceled by the $O(\epsilon)$ term in $\beta_{\tilde{i}}$, with $\tilde{i}$ representing all the parameters in Z_V. (Such term is absent in the RGEs of $\tilde{m}_\psi$ and $\tilde{m}^\dagger_\psi$.) Therefore, taking $\epsilon \to 0$, the generalized BFM formula for the LEFT is

$$\beta_{\tilde{g}} = -8\pi^2\tilde{g}\left[\tilde{g}\frac{\partial}{\partial\tilde{g}} + \tilde{a}^{\alpha\beta}_{qV}\frac{\partial}{\partial\tilde{a}^{\alpha\beta}_{\psi V}} + \tilde{a}^{\dagger\alpha\beta}_{\psi V}\frac{\partial}{\partial\tilde{a}^{\dagger\alpha\beta}_{\psi V}}\right]Z_V^{(1)}. \tag{314}$$

Using equations 302 and 303, we find:

$$\beta_{\tilde{e}} = \frac{80\tilde{e}^3}{9} + 8\tilde{e}^2\mathrm{Tr}\Big[-(\tilde{a}^\dagger_{eA}\tilde{m}_e + \tilde{m}^\dagger_e\tilde{a}_{eA}) + 2(\tilde{a}^\dagger_{uA}\tilde{m}_u + \tilde{m}^\dagger_u\tilde{a}_{uA}) - (\tilde{a}^\dagger_{dA}\tilde{m}_d + \tilde{m}^\dagger_d\tilde{a}_{dA})\Big] \tag{315}$$

and

$$\beta_{\tilde{g}_3} = -\tilde{g}_3{}^3\frac{23}{3} + 4\tilde{g}_3{}^2\mathrm{Tr}\left[\tilde{a}^\dagger_{dG}\tilde{m}_d + \tilde{m}^\dagger_d\tilde{a}_{dG} + \tilde{a}^\dagger_{uG}\tilde{m}_u + \tilde{m}^\dagger_u\tilde{a}_{uG}\right], \tag{316}$$

in agreement with equations C.5 and C.6[10] in Ref. [281].

6.2.5.3 Dipole operators

The WFR factor contributing to the RGEs of the dipole operators is:

$$Z_F\tilde{a}_{\psi V} = 1 + \frac{\delta Z^\dagger_{\psi L}}{2}\tilde{a}_{\psi V} + \tilde{a}_{\psi V}\frac{\delta Z_{\psi R}}{2} + \tilde{a}_{\psi V}\frac{\delta Z_V}{2}, \tag{317}$$

where $\delta Z_{\psi L}$ and $\delta Z_{\psi R}$ are matrices in flavour space. Their renormalizable pieces can be read from equations 296–301. Including the contributions from the counterterms in the on-shell basis, in the photon case, we obtain:

$$\begin{aligned}\beta_{\tilde{a}_{eA}} &= 8\tilde{e}^2\tilde{a}_{eA} + 4\tilde{e}\tilde{c}_e\tilde{a}_{S\widetilde{A}} + 2\tilde{e}^2\tilde{c}_{eA} + \frac{1}{2}\left(\tilde{c}_e\tilde{c}^\dagger_e\tilde{a}_{eA} + \tilde{a}_{eA}\tilde{c}^\dagger_e\tilde{c}_e\right) + \frac{80}{9}\tilde{e}^2\tilde{a}_{eA} \\ &= \frac{170}{9}\tilde{e}^2\tilde{a}_{eA} + 4\tilde{e}\tilde{c}_e\tilde{a}_{S\widetilde{A}} + \frac{1}{2}\left(\tilde{c}_e\tilde{c}^\dagger_e\tilde{a}_{eA} + \tilde{c}_{eA}\tilde{c}^\dagger_e\tilde{c}_e\right),\end{aligned} \tag{318}$$

[10] To match the notation of Ref. [281] to ours, we have to replace $\tilde{g} \to -\tilde{g}$ and $\tilde{m}_\psi \to \tilde{m}^\dagger_\psi$.

where the first term agrees with equation C.10 in Ref. [281]. Likewise,

$$\begin{aligned}\beta_{\tilde{a}_{qA}} = {} & 10Q_q^2\tilde{e}^2\tilde{a}_{qA} - 4Q_q\tilde{e}\tilde{c}_q\tilde{a}_{s\widetilde{A}} + \frac{32Q_q\tilde{e}}{3}\tilde{g}_3\tilde{a}_{qG} \\ & + \frac{8}{3}\tilde{g}_3^2\tilde{a}_{qA} + \frac{1}{2}\left(\tilde{c}_q\tilde{c}_q^\dagger\tilde{a}_{qA} + \tilde{a}_{qA}\tilde{c}_q^\dagger\tilde{c}_q\right) + \frac{80}{9}\tilde{e}^2\tilde{a}_{qA}\,,\end{aligned} \tag{319}$$

in agreement with equations C.11 and C.12 in Ref. [281].

Finally, the dipole operators involving the gluon have the following RGE:

$$\begin{aligned}\beta_{\tilde{a}_{qG}} = {} & 8\tilde{g}_3Q_q\tilde{e}\tilde{c}_{qA} - 4\tilde{g}_3\tilde{c}_q\tilde{a}_{s\widetilde{G}} \\ & + 2Q_q^2\tilde{e}^2\tilde{a}_{qG} + \frac{1}{2}\left(\tilde{c}_q\tilde{c}_q^\dagger\tilde{a}_{qG} + \tilde{a}_{qG}\tilde{c}_q^\dagger\tilde{c}_q\right) - \frac{19}{3}\tilde{g}_3^2\tilde{a}_{qG}\,,\end{aligned} \tag{320}$$

which also matches equations C.13 and C.14 in the aforementioned work.

6.2.5.4 Singlet mass

Factorizing $j = \tilde{a}_\psi$ in equation 269, we obtain $n_{ij} = 0$ and $\Delta n_{ji} = 2$ ($i = \tilde{m}_S^2$) which can be employed in the master formula. Moreover, since there are no effective contributions in Z_S, $\beta_i = k_{ij}a_j$. Explicitly:

$$\begin{aligned}\beta_{\tilde{m}_S^2} = 8\Big\{ & 3\mathrm{Tr}\left[\tilde{m}_d^\dagger\tilde{a}_d\tilde{m}_d^\dagger\tilde{m}_d + \tilde{m}_d^\dagger\tilde{m}_d\tilde{a}_d^\dagger\tilde{m}_d\right] + 3\mathrm{Tr}\left[\tilde{m}_u^\dagger\tilde{a}_u\tilde{m}_u^\dagger\tilde{m}_u + \tilde{m}_u^\dagger\tilde{m}_u\tilde{a}_u^\dagger\tilde{m}_u\right] \\ & + \mathrm{Tr}\left[\tilde{m}_e^\dagger\tilde{a}_e\tilde{m}_e^\dagger\tilde{m}_e + \tilde{m}_e^\dagger\tilde{m}_e\tilde{a}_e^\dagger\tilde{m}_e\right]\Big\}\,.\end{aligned} \tag{321}$$

6.2.5.5 Single self-interaction

In this case, factorizing $j = \tilde{a}_\psi$ in equation 273 leads to $n_{ij} = 2$ and $\Delta n_{ji} = 0$ ($i = \tilde{\lambda}_S$), so that $\beta_i = k_{ij}a_j$. Hence:

$$\beta_{\tilde{\lambda}_S} = 96\left[\mathrm{Tr}_e^{\tilde{\lambda}} + 3\left(\mathrm{Tr}_u^{\tilde{\lambda}} + \mathrm{Tr}_d^{\tilde{\lambda}}\right)\right] + 8\mathrm{Tr}\left[\tilde{c}_e\tilde{c}_e^\dagger + 3\left(\tilde{c}_d\tilde{c}_d^\dagger + \tilde{c}_u\tilde{c}_u^\dagger\right)\right]\tilde{\lambda}_S\,. \tag{322}$$

(Note that we can *partially* cross-check the contributions from the renormalizable couplings to this running, written explicitly in the original Ref. [8], by keeping the four-dimensional terms that contribute to the WFR of the S^4 operator. We have added these terms in the equation above, for an example.)

6.2.5.6 Renormalizable Yukawa operators

The mixing parameters required for the master formula can be obtained from equations 274–276, together with the additional terms that arise upon reduction of the redundant operators. Altogether, the renormalizable Yukawa operators involving the ALP mix with three dimension five operators leading to the following

parameters: *(1)* $n_{\tilde{c}_\psi,\tilde{a}_\psi} = \Delta n_{\tilde{a}_\psi,\tilde{c}^1_\psi} = 1$; *(2)* $n_{\tilde{c}_\psi,\tilde{a}_{\psi V}} = 2$ and $\Delta n_{\tilde{a}_{\psi V},\tilde{c}_\psi} = 0$; *(3)* $n_{\tilde{a}_{SV},\tilde{c}_\psi} = 2$ and $\Delta n_{\tilde{a}_{SV},\tilde{c}_\psi} = 0$. Employing them in the master formula, we obtain:

$$\begin{aligned}\beta_{\tilde{c}_e} =& -24\tilde{e}^2\tilde{a}_{S\widetilde{A}}\tilde{m}_e + 2\left(\tilde{m}_e\tilde{c}_e^\dagger\tilde{a}_e + \tilde{a}_e\tilde{c}_e^\dagger\tilde{m}_e - 2\tilde{a}_e\tilde{m}_e^\dagger\tilde{c}_e - 2\tilde{c}_e\tilde{m}_e^\dagger\tilde{a}_e\right) \\ &- 12\tilde{e}\left[\tilde{m}_e\tilde{c}_e^\dagger\tilde{a}_{eA} + \tilde{a}_{eA}\tilde{c}_e^\dagger\tilde{m}_e - \tilde{c}_e\tilde{m}_e^\dagger\tilde{a}_{eA} - \tilde{a}_{eA}\tilde{m}_e^\dagger\tilde{c}_e\right] \\ &-6\tilde{e}^2\tilde{c}_e + 3\tilde{c}_e\tilde{c}_e^\dagger\tilde{c}_e + 2\mathrm{Tr}\left[\tilde{c}_e\tilde{c}_e^\dagger + 3\left(\tilde{c}_d\tilde{c}_d^\dagger + \tilde{c}_u\tilde{c}_u^\dagger\right)\right]\tilde{c}_e\,,\end{aligned} \tag{323}$$

$$\begin{aligned}\beta_{\tilde{c}_q} =& -8\left[3\tilde{e}^2Q_q^2\tilde{a}_{S\widetilde{A}} + 4\tilde{g}_3^2\tilde{a}_{S\widetilde{G}}\right]\tilde{m}_q + 2\left(\tilde{m}_q\tilde{c}_q^\dagger\tilde{a}_q + \tilde{a}_q\tilde{c}^\dagger\tilde{m}_q - 2\tilde{a}_q\tilde{m}_q^\dagger\tilde{c}_q - 2\tilde{c}_q\tilde{m}_q^\dagger\tilde{a}_q\right) \\ &+ 12Q_q\tilde{e}\left[\tilde{m}_q\tilde{c}_q^\dagger\tilde{a}_{qA} + \tilde{a}_{qA}\tilde{c}_q^\dagger\tilde{m}_q - \tilde{c}_q\tilde{m}_q^\dagger\tilde{a}_{qA} - \tilde{a}_{qA}\tilde{m}_q^\dagger\tilde{c}_q\right] \\ &+ 16\tilde{g}_3\left[\tilde{m}_q\tilde{c}_q^\dagger\tilde{a}_{qG} + \tilde{a}_{qG}\tilde{c}_q^\dagger\tilde{m}_q - \tilde{c}_q\tilde{m}_q^\dagger\tilde{a}_{qG} - \tilde{a}_{qG}\tilde{m}_q^\dagger\tilde{c}_q\right].\end{aligned} \tag{324}$$

Identifying $\tilde{c}_\psi = -\tilde{m}_\psi c_{ff}$ and $\tilde{a}_{S\tilde{V}} = \tilde{g}^2 C_{VV}$, where the couplings in the r.h.s. are defined in the basis of Ref. [184], we can exactly reproduce the $\log v/m_\psi$ piece of the ALP–fermion couplings induced by the ALP-gauge boson operators, in equations 26 and 31 of the aforementioned work.

(We have added to the first RGE the contributions from renormalizable couplings, as a further cross-check of the `Pyr@te` results [8]. Such contributions can be easily included by adding the WFR factors and the dimension four contributions in equations 551 and 552.)

6.2.5.7 Non-renormalizable Yukawa operators

The WFR factors of these operators can be read from the relevant Lagrangian written in terms of the renormalized fields,

$$\begin{aligned}(\tilde{a}_\psi)_{\alpha\beta}\overline{\psi}_L^\alpha\psi_R^\beta S^2 \to (\tilde{a}_\psi)_{\alpha\beta}\overline{\psi}_L^i\left[\delta_{i\alpha} + \frac{\left(\delta Z_{\psi L}^\dagger\right)_{i\alpha}}{2}\right]\left[\delta_{\beta j} + \frac{\left(\delta Z_{\psi R}\right)_{\beta j}}{2}\right]\psi_R^j\left[1+\delta Z_S\right]S^2 \\ \supset (\tilde{a}_\psi)_{\alpha\beta}\overline{\psi}_L^i\psi_R^j S^2\left(\frac{-1}{32\pi\epsilon}\right)\left\{2\left(Q_\psi^2\tilde{e}^2 + \frac{4}{3}\tilde{g}_3^2\right)\delta_{i\alpha}\delta_{\beta j} + \frac{\left(\tilde{c}_\psi\tilde{c}_\psi^\dagger\right)_{i\alpha}}{2}\delta_{\beta j} + \delta_{i\alpha}\frac{\left(\tilde{c}_\psi^\dagger\tilde{c}_\psi\right)_{\beta j}}{2}\right. \\ \left. + 4\mathrm{Tr}\left[\tilde{c}_e\tilde{c}_e^\dagger + 3\tilde{c}_d\tilde{c}_d^\dagger + 3\tilde{c}_u\tilde{c}_u^\dagger\right]\delta_{i\alpha}\delta_{\beta j}\right\} \\ = \left(\frac{-1}{32\pi\epsilon}\right)\overline{\psi}_L\left[2\left(Q_\psi^2\tilde{e}^2 + \frac{4}{3}\tilde{g}_3^2 + 2\mathrm{Tr}\left[\tilde{c}_e\tilde{c}_e^\dagger + 3\tilde{c}_d\tilde{c}_d^\dagger + 3\tilde{c}_u\tilde{c}_u^\dagger\right]\right)\tilde{c}_\psi + \tilde{c}_\psi\tilde{c}_\psi^\dagger\tilde{c}_\psi\right]\psi_R S^2\,.\end{aligned} \tag{325}$$

Moreover, the non-renormalizable Yukawa operators involving the ALP mix with two different operators in the LEFT, leading to the following mixing parameters: *(1)* $n_{\tilde{a}_\psi,\tilde{a}_{\psi V}} = 3$ and $\Delta n_{\tilde{a}_{\psi V},\tilde{a}_\psi} = -1$; *(2)* $n_{\tilde{a}_\psi,\tilde{a}_{S\tilde{V}}} = 3$ and $\Delta n_{S\tilde{V},\tilde{a}_\psi} = -1$.

The final RGEs are in turn given by:

$$\beta_{\tilde{a}_e} = \left(-6\tilde{e}^2 + \tilde{\lambda}_S \right) \tilde{a}_q - \left(24\tilde{e}^2 \tilde{a}_{S\widetilde{A}} \right) \tilde{c}_q + 2 \left(-\tilde{c}_e \tilde{a}_e^\dagger \tilde{c}_e + \frac{13}{4} \tilde{a}_e \tilde{c}_e^\dagger \tilde{c}_e + \frac{13}{4} \tilde{c}_e \tilde{c}_e^\dagger \tilde{a}_e \right) \tag{326}$$
$$+ 4\mathrm{Tr} \left[\tilde{c}_e \tilde{c}_e^\dagger + 3 \left(\tilde{c}_d \tilde{c}_d^\dagger + \tilde{c}_u \tilde{c}_u^\dagger \right) \right] \tilde{a}_e - 12\tilde{e} \left(\tilde{c}_e \tilde{c}_e^\dagger \tilde{a}_{eA} + \tilde{a}_{eA} \tilde{c}_e^\dagger \tilde{c}_e \right),$$

$$\beta_{\tilde{a}_q} = \left(-6Q_q^2 \tilde{e}^2 - 8\tilde{g}_3^2 + \tilde{\lambda}_S \right) \tilde{a}_q - \left(24\tilde{e}^2 Q_q^2 \tilde{a}_{S\widetilde{A}} + 32\tilde{g}_3^2 \tilde{a}_{S\widetilde{G}} \right) \tilde{c}_q \tag{327}$$
$$+ 2 \left(-\tilde{c}_q \tilde{a}_q^\dagger \tilde{c}_q + \frac{13}{4} \tilde{a}_q \tilde{c}_q^\dagger \tilde{c}_q + \frac{13}{4} \tilde{c}_q \tilde{c}_q^\dagger \tilde{a}_q \right) + 4\mathrm{Tr} \left[\tilde{c}_e \tilde{c}_e^\dagger + 3 \left(\tilde{c}_d \tilde{c}_d^\dagger + \tilde{c}_u \tilde{c}_u^\dagger \right) \right] \tilde{a}_q$$
$$+ 12Q_q \tilde{e} \left(\tilde{c}_q \tilde{c}_q^\dagger \tilde{a}_{qA} + \tilde{a}_{qA} \tilde{c}_q^\dagger \tilde{c}_q \right) + 16\tilde{g}_3 \left(\tilde{c}_q \tilde{c}_q^\dagger \tilde{a}_{qG} + \tilde{a}_{qG} \tilde{c}_q^\dagger \tilde{c}_q \right).$$

6.2.5.8 Gauge operators

Finally, the WFR of the photon field can be obtained from

$$SA_{\mu\nu}\widetilde{A}^{\mu\nu} \to \left[1 + \frac{\delta Z_S}{2} \right] \left[1 + \delta Z_A \right] SA_{\mu\nu}\widetilde{A}^{\mu\nu} \tag{328}$$
$$\supset -\frac{1}{32\pi^2\epsilon} \left(2\mathrm{Tr} \left[\tilde{c}_e \tilde{c}_e^\dagger + 3\tilde{c}_d \tilde{c}_d^\dagger + 3\tilde{c}_u \tilde{c}_u^\dagger \right] + \frac{160}{9} \tilde{e}^2 \right) SA_{\mu\nu}\widetilde{A}^{\mu\nu} .$$

Furthermore, equation 294 leads to the following identification of the mixing parameters: $n_{\tilde{a}_{S\widetilde{A}}, \tilde{a}_{\psi A}} = 2$ and $\Delta n_{\tilde{a}_{\psi A}, \tilde{a}_{S\widetilde{A}}} = 0$. Therefore,

$$\beta_{\tilde{a}_{S\widetilde{A}}} = -4\tilde{e}\mathrm{Tr} \left[-\left(\tilde{c}_e \tilde{a}_{eA}^\dagger + \tilde{c}_e^\dagger \tilde{a}_{eA} \right) - \left(\tilde{c}_d \tilde{a}_{dA}^\dagger + \tilde{c}_d^\dagger \tilde{a}_{dA} \right) + 2 \left(\tilde{c}_u \tilde{a}_{uA}^\dagger + \tilde{c}_u^\dagger \tilde{a}_{uA} \right) \right] \tag{329}$$
$$+ 2\mathrm{Tr} \left[\tilde{c}_e \tilde{c}_e^\dagger + 3\tilde{c}_d \tilde{c}_d^\dagger + 3\tilde{c}_u \tilde{c}_u^\dagger \right] \tilde{a}_{S\widetilde{A}} + \frac{160}{9} \tilde{e}^2 \tilde{a}_{S\widetilde{A}} .$$

In a complete analogous way,

$$\beta_{\tilde{a}_{S\widetilde{G}}} = -2\mathrm{Tr} \left[\tilde{c}_d \tilde{a}_{dG}^\dagger + \tilde{c}_d^\dagger \tilde{a}_{dG} + \tilde{c}_u \tilde{a}_{uG}^\dagger + \tilde{c}_u^\dagger \tilde{a}_{uG} \right] \tag{330}$$
$$+ 2\mathrm{Tr} \left[\tilde{c}_e \tilde{c}_e^\dagger + 3\tilde{c}_d \tilde{c}_d^\dagger + 3\tilde{c}_u \tilde{c}_u^\dagger \right] \tilde{a}_{S\widetilde{G}} - \frac{46}{3} \tilde{g}_3^2 \tilde{a}_{sG} .$$

These results are fully generic, not assuming that the EFT in the UV is the SM+ALP. Altogether, they show that the running in the LEFT can introduce two new important effects. First, dimension five operators can now contribute to the renormalizable couplings, in particular the fermion and ALP masses:

$$\delta\tilde{m}_\psi \sim \tilde{m}_S^2 \tilde{a}_\psi , \quad \delta\tilde{m}_S^2 \sim \tilde{m}_\psi^3 \tilde{a}_\psi . \tag{331}$$

(Such contributions are however absent if the UV completion is the SM+ALP EFT producing vanishing $\tilde{a}_\psi$ at all scales.) Second, the gauge operators are no longer scale invariant; instead, they can mix with the dipole operators. (Again, this effect cannot be obtained from the SM+ALP EFT since no dipole operator is generated up to dimension five.)

6.2.6 A comment on the non-renormalization results

A comment is in order regarding the non-renormalization of the ALP–gauge boson interactions in the EFT before EWSB and their breaking in the LEFT. With this aim, it is useful to consider the case of the θ-angles in the SMEFT and try to apply the same reasoning to the axion, which can be regarded as a dynamical θ.

It is a well known result that the CP-odd anomalous couplings in the SM cannot be multiplicatively renormalized at any order in perturbation theory [282, 283]. Since the corresponding operators $\alpha_X/(8\pi)X\widetilde{X} \equiv \alpha_X/(8\pi)\partial_\mu K^\mu$ are total derivatives, the corresponding Feynman rules are $\propto \sum p^\mu = 0$ in each vertex. Therefore, such terms alone will always give vanishing contributions to any perturbative calculation. Furthermore, because the θ-angle terms are topological (see equation 389), they have a 2π periodicity which leaves the path integral, and therefore the respective topological charge, well defined.

In the case of the axion which is, by definition, identified with a discrete symmetry $S \longrightarrow S + 2\pi\Lambda$, compatibility with the θ-angle period requires that in any operator of the form

$$a\frac{\alpha_X}{8\pi\Lambda}SX_{\mu\nu}\widetilde{X}^{\mu\nu}, \tag{332}$$

the coupling a is an integer. Therefore, the latter should not run under the continuous evolution of the renormalization group. We have confirmed this in the case of the ALP EFT, but not in the case of the ALP LEFT. While such quantization (and its implications for the running) holds when we consider the anomalous operators in isolation, it can be altered by the presence of fermions [284]. For example, if the fermions couple to the axion, we can make chiral rotations, $\psi_L \longrightarrow e^{ixS}\psi_L$ and $\psi_R \longrightarrow e^{-ixS}\psi_R$, that change $a \longrightarrow a + 2x$ (due to the chiral anomaly). In this case, it is rather a combination of several couplings in the theory that is quantized and it is no longer correct to require $a \in \mathbb{Z}$ [284].

Therefore, even in the theory above EWSB, the anomalous couplings need not to be quantized and could potentially mix with other operators under renormalization. However, since no other operator in the EFT basis gives corrections to these couplings, at one-loop, the corresponding RGEs remain scale invariant after factorizing out the gauge couplings; see appendix H.4.

On the other hand, below the EW scale, we see that the anomalous operators can indeed mix with the dipole ones. (Furthermore, assuming that the axion takes some VEV such that $\tilde{a}_{S\tilde{V}}S$ is as an effective angle and $\tilde{c}_\psi S$ is an effective fermion mass, the corresponding RGEs in equations 329 and 330 are functions of the same SM LEFT parameters as the θ-term RGEs in Ref. [281].)

6.2.7 Phenomenological applications

The energy dependence of the different parameters in the ALP EFTs has a profound impact on the phenomenology of these particles. Consider a UV theory where only a reduced set of couplings is present. We might be tempted to think that there is enough freedom to play with these couplings if they are loosely constrained by high-energy experiments. However, the running in the renormalization group can lead to

significant contributions which are not necessarily small, as there are $\mathcal{O}(1)$ numbers in the anomalous dimension matrix, in equation 255, which will become log enhanced. Moreover, the mixing with different operators in the RGEs can produce at smaller energies couplings which are much more constrained by low-energy experiments than those present in the UV.

To exemplify this point, let us consider the following Lagrangian, defined at the scale $\Lambda = 10$ TeV:

$$\mathcal{L}_{\text{UV}} = \mathcal{L}_{\text{SM}} + \frac{1}{2}\partial_\mu S \partial^\mu S + \frac{1}{2}\tilde{m}_S^2 S^2 + \frac{a_{S\widetilde{Z}}}{c_\omega^2 - s_\omega^2} S \left(c_\omega^2 W_{\mu\nu}\widetilde{W}^{\mu\nu} - s_\omega^2 B_{\mu\nu}\widetilde{B}^{\mu\nu} \right) , \tag{333}$$

where the relation between the gauge couplings is chosen to make S photophobic. Such construction arises, for instance, in the $SO(6)/SO(5)$ NMCHM; see equation 115. Since the ALP–gauge boson couplings are scale independent, $a_{S\widetilde{A}}$ remains vanishing at all scales (neglecting finite contributions). This holds in this particular model below the EW scale, because dipole operators are not generated by the Lagrangian in equation 333 up to $\mathcal{O}(1/\Lambda)$. The photophobic condition is therefore stable.

The coupling $a_{S\widetilde{Z}}$ can be directly constrained at colliders, namely in $pp \to ZS$ searches. The corresponding bounds are weak, allowing couplings $\sim 0.2\,(0.04)$ TeV^{-1} at the current run (HL phase) of the LHC [230]. However, $a_{S\widetilde{Z}}$ generates, through mixing via the RGEs, other couplings such as a_{SHe} which is much more constrained experimentally. Considering the physical ALP mass to be $\mathcal{O}$(KeV), the most stringent bound on the parameter space comes from the absence of extra cooling of Red Giants due to the emission of ALP radiation, implying [285]

$$\tilde{c}_e \lesssim 3 \times 10^{-13}, \quad \text{for a typical core temperature of } T \approx 10^8 \text{ K}. \tag{334}$$

To translate this constraint into a bound on $a_{S\widetilde{Z}}$, we run this coupling up to the EW scale using equation 323. (Assuming that there are no beyond the SM particles on top of the ALP, $\beta_{\tilde{c}_e} \propto \tilde{c}_e$.) Resumming equations (315) and (323), up to $\mathcal{O}(1/\Lambda)$ effects, we obtain:

$$\tilde{c}_e(v) \lesssim 2.8 \times 10^{-13}, \tag{335}$$

which corresponds to

$$a_{SHe}(v) \lesssim 1.6 \times 10^{-12}\ \text{TeV}^{-1}. \tag{336}$$

Solving numerically equations (249)-(254), for $\lambda_{SH} = 0$, as well as the RGEs of the gauge and Yukawa couplings above the EW scale (in appendix C of Ref. [8]), we find that the maximum allowed value for $a_{S\widetilde{Z}}$ is

$$a_{S\widetilde{Z}}(10\,\text{TeV}) \lesssim 4.8 \times 10^{-6}\ \text{TeV}^{-1}. \tag{337}$$

This bound is four orders of magnitude stronger than that expected from future direct searches, which shows the potential of our results to study the ALP phenomenology across several energy scales. The running solely in the LEFT corrects the result in equation 334 by $\sim 6\%$, which can be taken as a systematic error when working in the SM+ALP EFT.

Another interesting case is that of a top-philic ALP at $\Lambda = 10$ TeV, with Lagrangian

$$\mathcal{L}_{\text{UV}} = \mathcal{L}_{\text{SM}} + \frac{1}{2}\partial_\mu S \partial^\mu S + \frac{1}{2}\tilde{m}_S^2 S^2 + a_t S\left(\mathrm{i}\bar{q}_L \widetilde{H} t_R + \text{h.c.}\right) ; \tag{338}$$

in our notation, $a_t = (a_{SHu})_{33}$. The experimental bounds on such coupling are also very weak. To the best of our knowledge, no dedicated searches for $pp \to S\bar{t}t$ have been carried out and only indirect limits have been set on $a_t \lesssim \text{TeV}^{-1}$ [286].

Such coupling generates, via renormalization mixing, a non-vanishing a_{SHe}. Therefore, we can proceed in the same way as before, to translate the low-energy bound in equation 334 into constraints on the UV coupling, a_t. Solving numerically the relevant RGEs, we obtain

$$a_t(10\,\text{TeV}) \lesssim 4.3 \times 10^{-6}\ \text{TeV}^{-1}\,, \tag{339}$$

for an ALP at the KeV scale. This bound is six orders of magnitude stronger than that from other studies. Again, it becomes clear the importance of considering the RGE effects when setting constraints on a particular model (such constraints hardly replace direct searches, but they can have an important complementary role in probing the model parameter space).

6.2.8 Outlook

We have constructed the most generic CP-even EFT involving the SM and an ALP, up to dimension five, and have subsequently obtained the one-loop RGEs of the different couplings in the theory above and below the EW scale.

In the unbroken phase, partial computations of the RGEs have been previously obtained in several works assuming shift-symmetric operators only (apart from the ALP mass). Therefore, such works have dismissed, for example, the marginal coupling of the ALP to the Higgs boson as well as its self-interaction, which we have included in our computations. Furthermore, we have pointed out some redundancies that appear in the commonly used shift-symmetric basis and obtained conditions on the corresponding coefficients under which the operators form an irreducible set; see appendix H.4. Such conditions make the coefficients in this shift-symmetric and our bases unequivocally related which allowed us to obtain the RGEs in the former and therefore cross-check several results in the literature [184, 287, 288]. Subsequent independent works also found exact agreement with our results [289, 290].

It is worth noting that we have matched all the UV divergences onto an independent off-shell basis and wrote explicitly these results, to enlarge their applicability. In this way, the RGEs of extensions of our EFTs, with either new particles or higher-dimensional operators, can be built on our results.

In the ALP LEFT, relevant at low energies, in which the SM massive bosons, as well as the top quark, have been integrated out, we have computed the evolution of all parameters in the theory irrespective of the UV completion above the EW scale. To the best of our knowledge, the RGEs in this EFT were computed

for the first time in the context of our work[11]. We have found that, in general, effective interactions can renormalize dimension four ones and operators involving the ALP can mix with purely SMEFT operators. In this regard, it is interesting to note that even a theory photophobic in the UV might generate the ALP coupling to photons in the LEFT by mixing with dipole operators under renormalization. Although the running in this EFT is expected to produce small effects, the ALP–photon coupling is so constrained [184] that important bounds could be derived on UV models that generate the dipole operators.

Finally, let us emphasize the importance of these studies for the correct interpretation of the experimental results on the ALP parameter space. We have shown that, even for UV models poorly constrained by collider experiments, the RGE evolution can generate other couplings which can be severely constrained in astrophysical events, as the case of the ALP–electron coupling. In turn, the knowledge of the RGEs allows us to translate such bounds into upper limits on the relevant UV parameters. This provides a useful method to study the interplay between collider and astrophysical probes of NMCHMs, collected in various experiments at very different energy scales. As an example, we studied an explicit realization of the $SO(6)/SO(5)$ CHM, where the exotic pNGB — identified with the ALP — was assumed to couple only to gauge bosons, via the WZW term. The corresponding RGE constraint we have obtained, running up the bound on the ALP–electron coupling from Red Giants cooling, is more than four orders of magnitude stronger than that from direct searches at the LHC.

[11] Days after the publication of our work, Ref. [289] appeared which also computed the RGEs in the ALP LEFT, up to two-loop order in the gauge couplings, but assuming that the UV completion of the LEFT is the SM+ALP EFT.

Chapter 7

Conclusions

Ending as we started, we hold the idea that the paradigm in particle physics today is one of "rough water". The SM does not give us a complete understanding of Nature and mysteries that date back several decades, such as DM, are left unsolved.

The Higgs boson remains one of the most interesting directions we have to delve into these unknowns and one of the main motivations to cross the high-energy frontier. Indeed, in popular theories to embed the Higgs boson in a more fundamental framework, new particles arise which are promising candidates for many of our opened questions. This is the case of NMCHMs.

In such setups, we have shown that compositeness is an experimentally viable solution to the HP while addressing smoothly other issues that remain unsolved in the SM and which could re-enforce the demand for new physics next to the TeV scale. For example:

1. In the $SO(6)/SO(5)$ NMCHM, an EW pseudoscalar singlet S arises in FCNC decays of the top quark. Such ALP can provide a dynamical solution to the strong CP problem; serve as DM; help generating the matter-antimatter asymmetry; *etc.* The ALP FCNCs arise at dimension five in the pNGBs EFT and could potentially be observable in the decays $t \longrightarrow Sq$ and $t \longrightarrow SSq$ leading, respectively, to branching ratios of the order 10^{-4} and 10^{-10}, for a new physics scale $f \sim 1\,\text{TeV}$ and couplings $c \sim \mathcal{O}(0.1)$. Analyses currently performed at the LHC are not significantly sensitive to any of these interactions, which could provide a remarkable insight into the nature of the ALP and on the problems that it can solve.

2. In the $SO(7)/G_2$ NMCHM, an EW pseudoscalar triplet Φ arises along with the Higgs boson, changing drastically the nature of the EW PT, which can become first order. In such case, we found that baryogenesis can be explained for $c/f \sim 1\,\text{TeV}^{-1}$ and triplet masses $\sim m_t - 2m_t$. In this region, the triplet components can be pair-produced by EW currents and decay promptly into third generation quarks.

However, we have found no collider searches which can currently constrain this region.

3. In the low-mass regime of the $SO(7)/SO(6)$ NMCHM, leptophilic scalars with masses of $\mathcal{O}(1)$ GeV can couple to heavy flavour-violating vector bosons, triggering rare decays of B-mesons into multiple muons at the LHCb. Such vectors are promising candidates to explain the LFU anomalies, their composite nature being crucial to evade bounds from high-energy searches. (If such composite channels are opened, vector masses $\gtrsim 1.3$ TeV are not yet excluded.) Although the decay $B \to 2\mu^+2\mu^-$ has been probed experimentally, we found compelling reasons to test the channels $B \to 3\mu^+3\mu^-$ and $B \to 3\mu^+3\mu^- K$, mediated by the light pNGBs, which have not been searched for directly. One reason is that the tagging of extra mesons is required in the limit where the light scalars are degenerate, in which case the B decay into only muons vanishes. Moreover, other precision experiments cannot constrain this model.

4. In the high-mass regime of the $SO(7)/SO(6)$ NMCHM, we showed that composite DM naturally arises at the EW scale, with the right properties to explain the relic abundance in the Universe; while the presence of a lighter pNGB κ can weaken significantly the low-energy bounds. If the DM annihilates sizably into this exotic DM-SM mediator and the latter is CP-odd, the direct detection cross section is loop suppressed, being out of reach even of future facilities. In leptophilic regimes, future indirect detection facilities could also leave the possibility that our candidate is all the DM completely unprobed. At colliders, we focused on decays of pair-produced VLQs into the EW pNGBs, which constitutes a *double smoking gun* evidence of compositeness. The branching ratios in these channels can be larger than those into the SM bosons, rendering the current direct searches mostly insensitive to these scenarios. Furthermore, for our DM candidate to explain the totality of relic abundance, new physics scales ~ 3 TeV are typically required, which makes searches for the heavy quarks more suitable for future colliders. Although the reach of a 100 TeV collider has been explored for the DM channel, no specific searches for the visible one have been developed.

All the models above, built on low cutoff scales, justify our positive answer to the first question posed in the Introduction, extending the purpose of composite theories to well beyond the HP. Not only NMCHMs provide motivated solutions to problems from flavour anomalies to DM, but by addressing these solutions we were led to radically new and unexplored signatures, unlike the ones which have been persistently explored by the experimental collaborations. This last point answers directly the second question posed also in chapter 1.

We have therefore proposed new dedicated analyses to probe the non-standard signatures:

1. To test the ALP FCNCs, we have proposed an inclusive search for $pp \to tS(S) + j$. In the muon channel, we have shown that, for $\mathcal{O}(1)$ couplings in the UV and an integrated luminosity $L = 150\,\text{fb}^{-1}$, the LHC could probe $f \sim 90\,(3)$ TeV in single (pair) production.

2. To study the triplet model in the region where EW baryogenesis can be explained, we have proposed to search for $pp \to \phi^{\pm}\phi^{0} \to t\bar{b}(b\bar{t})b\bar{b}$, showing that this entire region could be tested at the HL-LHC. Moreover, we have demonstrated that a certain region of the parameter space that could be left untested by Higgs to di-photon measurements could be probed at the future GW observatory LISA. In this region, the strongest PT proceeds mainly in one–step and, therefore, only one peak signal structures might be expected.

3. To probe the signatures of light leptophilic scalars coupled to a heavy vector, we proposed dedicated LHCb searches for $B_s^0 \to 3\mu^+3\mu^-$ and $B^+ \to K^+3\mu^+3\mu^-$, as well as $B^0 \to 3\mu^+3\mu^-$ and $B_s^0 \to K^{0*}3\mu^+3\mu^-$, to test other flavour transitions. We found that, at Upgrade II of the LHCb detector, our proposed analyses could outperform bounds from meson mixing, as well as probe the region in which the anomalies in LFU can be explained. It is also worth mentioning that such searches have been considered one of the benchmark interests of the LHCb collaboration [229].

4. To explore the non-minimal nature of the DM model, we have developed new analyses to be performed at a future 100 TeV collider based on the search for $pp \to \overline{B}B \to \kappa\kappa\bar{b}b$. In the muonphilic scenario, that could elude the constraints from future DM searches, we found that all bottom partner masses up to ~ 9 TeV could be probed, with $L = 1\,\text{ab}^{-1}$.

In spite of the powerful constraints these numerous searches could set on the parameter space of NMCHMs, they are only sensitive to particular scenarios in the UV. With the aim of describing a wider parameter space of some CHMs, we rely on EFTs which include all effective operators that can be present at low energies. We constructed two of such EFTs, one in which we extended the SM with a VLL and another where we extended the SM with an ALP. Both these exotic particles are allowed to be close to the EW scale by current data and are common to the majority of CHMs.

In the SM+VLL EFT, we have considered all operators up to dimension six which could trigger the single production $pp \to E\ell$. We argued that such interactions can dominate the production and decay of the VLL E in the large $\sqrt{s}$ region of the parameter space. Again, this contrasts with the topology in which these particles are usually searched for at the LHC. By recasting a search for excited leptons, we derived global bounds on the Wilson coefficients, the most constrained one being $\sim 0.05\,\text{TeV}^{-2}$. We also provided a master formula to constrain any UV model taking into account all operators which are generated in the IR, extending the scope of previous analyses.

In the SM+ALP EFT, we have computed the full one-loop RGEs of all parameters in the theory up to dimension five, above and below the EW scale, assuming only that the new physics preserves CP. The knowledge of such equations is required for a consistent analysis of the constraints, collected by different experiments across a huge range of energies, that have been set on the parameter space of the ALP. As an example of the potential of our results, we explored the possibility of probing indirectly the ALP-Z interaction, that is predicted for example in the $SO(6)/SO(5)$ NMCHM, via its contribution to the

ALP-electron coupling, which is bounded by astrophysical signals. The corresponding RGE constraint on the UV coupling is four orders of magnitude stronger than that expected from future direct searches *e.g.* $pp \to SZ$, providing an important complementarity between collider and astrophysical probes.

In a time where model building and the search for alternative mechanisms to probe new physics are so intense, the conclusion of this thesis is particularly relevant: there are traditional solutions to the HP and other mysteries in particle physics which, in their realistic versions, are not ruled out by current data and which require significant experimental advances in upcoming facilities to be possibly refuted.

Bibliography

[1] F. Zwicky. "On the Masses of Nebulae and of Clusters of Nebulae." In: *Astrophysics. J.* 86 (Oct. 1937), p. 217. doi: 10.1086/143864.

[2] A. D. Sakharov. "Violation of CP Invariance, C asymmetry, and baryon asymmetry of the universe." In: *Pisma Zh. Eksp. Teor. Fiz.* 5 (1967), pp. 32–35. doi: 10.1070/PU1991v034n05ABEH002497.

[3] M. Chala, M. Ramos, and M. Spannowsky. "Gravitational wave and collider probes of a triplet Higgs sector with a low cutoff." In: *Eur. Phys. J. C* 79.2 (2019), p. 156. doi: 10.1140/epjc/s10052-019-6655-1. arXiv: 1812.01901 [hep-ph].

[4] A. Blance, M. Chala, M. Ramos, and M. Spannowsky. "Novel B-decay signatures of light scalars at high energy facilities." In: (2019). arXiv: 1907.13151 [hep-ph].

[5] M. Ramos. "Composite dark matter phenomenology in the presence of lighter degrees of freedom." In: *JHEP* 07 (2020), p. 128. doi: 10.1007/JHEP07(2020)128. arXiv: 1912.11061 [hep-ph].

[6] N. Castro, M. Chala, A. Peixoto, and M. Ramos. "Novel flavour-changing neutral currents in the top quark sector." In: *JHEP* 10 (2020), p. 038. doi: 10.1007/JHEP10(2020)038. arXiv: 2005.09594 [hep-ph].

[7] M. Chala, P. Kozów, M. Ramos, and A. Titov. "Effective field theory for vector-like leptons and its collider signals." In: *Phys. Lett. B* 809 (2020), p. 135752. doi: 10.1016/j.physletb.2020.135752. arXiv: 2005.09655 [hep-ph].

[8] M. Chala, G. Guedes, M. Ramos, and J. Santiago. "Running in the ALPs." In: *Eur. Phys. J. C* 81.2 (2021), p. 181. doi: 10.1140/epjc/s10052-021-08968-2. arXiv: 2012.09017 [hep-ph].

[9] M. Tanabashi et al. "Review of Particle Physics." In: *Phys. Rev. D* 98 (3 2018), p. 030001. doi: 10.1103/PhysRevD.98.030001. url: https://link.aps.org/doi/10.1103/PhysRevD.98.030001.

[10] P. W. Anderson. "Plasmons, Gauge Invariance, and Mass." In: *Phys. Rev.* 130 (1 1963), pp. 439–442. doi: 10.1103/PhysRev.130.439. url: https://link.aps.org/doi/10.1103/PhysRev.130.439.

[11] F. Englert and R. Brout. "Broken Symmetry and the Mass of Gauge Vector Mesons." In: *Phys. Rev. Lett.* 13 (9 1964), pp. 321–323. doi: 10.1103/PhysRevLett.13.321. url: https://link.aps.org/doi/10.1103/PhysRevLett.13.321.

[12] P. W. Higgs. "Broken Symmetries and the Masses of Gauge Bosons." In: *Phys. Rev. Lett.* 13 (16 1964), pp. 508–509. doi: 10.1103/PhysRevLett.13.508. url: https://link.aps.org/doi/10.1103/PhysRevLett.13.508.

[13] P. Zyla et al. "Review of Particle Physics." In: *PTEP* 2020.8 (2020), p. 083C01. doi: 10.1093/ptep/ptaa104.

[14] L. Wolfenstein. "Parametrization of the Kobayashi-Maskawa Matrix." In: *Phys. Rev. Lett.* 51 (21 1983), pp. 1945–1947. doi: 10.1103/PhysRevLett.51.1945. url: https://link.aps.org/doi/10.1103/PhysRevLett.51.1945.

[15] Y. Grossman and P. Tanedo. "Just a Taste: Lectures on Flavor Physics." In: *Theoretical Advanced Study Institute in Elementary Particle Physics: Anticipating the Next Discoveries in Particle Physics*. Nov. 2017. doi: 10.1142/9789813233348_0004. arXiv: 1711.03624 [hep-ph].

[16] S. L. Glashow, J. Iliopoulos, and L. Maiani. "Weak Interactions with Lepton-Hadron Symmetry." In: *Phys. Rev. D* 2 (7 1970), pp. 1285–1292. doi: 10.1103/PhysRevD.2.1285. url: https://link.aps.org/doi/10.1103/PhysRevD.2.1285.

[17] L. Maiani. "The GIM Mechanism: origin, predictions and recent uses." In: *48th Rencontres de Moriond on Electroweak Interactions and Unified Theories*. Mar. 2013. arXiv: 1303.6154 [hep-ph].

[18] M. K. Gaillard and B. W. Lee. "Rare decay modes of the K mesons in gauge theories." In: *Phys. Rev. D* 10 (3 1974), pp. 897–916. doi: 10.1103/PhysRevD.10.897. url: https://link.aps.org/doi/10.1103/PhysRevD.10.897.

[19] G. Lüders. "Proof of the TCP theorem." In: *Annals of Physics* 2.1 (1957), pp. 1–15. issn: 0003-4916. doi: https://doi.org/10.1016/0003-4916(57)90032-5. url: https://www.sciencedirect.com/science/article/pii/0003491657900325.

[20] J. S. Bell and R. Jackiw. "A PCAC puzzle: $\pi^0 \to \gamma\gamma$ in the σ model." In: *Nuovo Cim. A* 60 (1969), pp. 47–61. doi: 10.1007/BF02823296.

[21] M. D. Schwartz. *Quantum Field Theory and the Standard Model*. Cambridge University Press, Mar. 2014. isbn: 978-1-107-03473-0, 978-1-107-03473-0.

[22] J. E. Kim and G. Carosi. "Axions and the Strong CP Problem." In: *Rev. Mod. Phys.* 82 (2010). [Erratum: Rev.Mod.Phys. 91, 049902 (2019)], pp. 557–602. doi: 10.1103/RevModPhys.82.557. arXiv: 0807.3125 [hep-ph].

[23] M. Shifman and A. Vainshtein. "(In)dependence of Θ in the Higgs regime without axions." In: *Mod. Phys. Lett. A* 32.14 (2017), p. 1750084. doi: 10.1142/S0217732317500845. arXiv: 1701.00467 [hep-th].

[24] P. Fileviez Perez and H. H. Patel. "The Electroweak Vacuum Angle." In: *Phys. Lett. B* 732 (2014), pp. 241–243. doi: 10.1016/j.physletb.2014.03.064. arXiv: 1402.6340 [hep-ph].

[25] M. Shifman. *Advanced topics in quantum field theory.: A lecture course*. Cambridge, UK: Cambridge Univ. Press, Feb. 2012. isbn: 978-1-139-21036-2, 978-0-521-19084-8.

[26] G. Aad et al. "A search for the dimuon decay of the Standard Model Higgs boson with the ATLAS detector." In: *Phys. Lett. B* 812 (2021), p. 135980. doi: 10.1016/j.physletb.2020.135980. arXiv: 2007.07830 [hep-ex].

[27] S. Di Vita, C. Grojean, G. Panico, M. Riembau, and T. Vantalon. "A global view on the Higgs self-coupling." In: *JHEP* 09 (2017), p. 069. doi: 10.1007/JHEP09(2017)069. arXiv: 1704.01953 [hep-ph].

[28] "Study of the double Higgs production channel $H(\rightarrow b\bar{b})H(\rightarrow \gamma\gamma)$ with the ATLAS experiment at the HL-LHC." In: (Jan. 2017).

[29] T. Aoyama, M. Hayakawa, T. Kinoshita, and M. Nio. "Tenth-Order QED Contribution to the Electron $g-2$ and an Improved Value of the Fine Structure Constant." In: *Phys. Rev. Lett.* 109 (11 2012), p. 111807. doi: 10.1103/PhysRevLett.109.111807. url: https://link.aps.org/doi/10.1103/PhysRevLett.109.111807.

[30] L. Canetti, M. Drewes, and M. Shaposhnikov. "Matter and Antimatter in the Universe." In: *New J. Phys.* 14 (2012), p. 095012. doi: 10.1088/1367-2630/14/9/095012. arXiv: 1204.4186 [hep-ph].

[31] M. B. Gavela, P. Hernandez, J. Orloff, and O. Pene. "Standard model CP violation and baryon asymmetry." In: *Mod. Phys. Lett. A* 9 (1994), pp. 795–810. doi: 10.1142/S0217732394000629. arXiv: hep-ph/9312215.

[32] J. F. Donoghue. "General relativity as an effective field theory: The leading quantum corrections." In: *Phys. Rev. D* 50 (1994), pp. 3874–3888. doi: 10.1103/PhysRevD.50.3874. arXiv: gr-qc/9405057.

[33] M. Bardon, P. Norton, J. Peoples, A. M. Sachs, and J. Lee-Franzini. "Measurement of the Momentum Spectrum of Positrons from Muon Decay." In: *Phys. Rev. Lett.* 14 (12 1965), pp. 449–453. doi: 10.1103/PhysRevLett.14.449. url: https://link.aps.org/doi/10.1103/PhysRevLett.14.449.

[34] A. V. Manohar. "Introduction to Effective Field Theories." In: (Apr. 2018). Ed. by S. Davidson, P. Gambino, M. Laine, M. Neubert, and C. Salomon. doi: 10.1093/oso/9780198855743.003.0002. arXiv: 1804.05863 [hep-ph].

[35] I. Brivio and M. Trott. "The Standard Model as an Effective Field Theory." In: *Phys. Rept.* 793 (2019), pp. 1–98. doi: 10.1016/j.physrep.2018.11.002. arXiv: 1706.08945 [hep-ph].

[36] S. Weinberg. "Baryon- and Lepton-Nonconserving Processes." In: *Phys. Rev. Lett.* 43 (21 1979), pp. 1566–1570. doi: 10.1103/PhysRevLett.43.1566. url: https://link.aps.org/doi/10.1103/PhysRevLett.43.1566.

[37] W. Buchmuller and D. Wyler. "Effective Lagrangian Analysis of New Interactions and Flavor Conservation." In: *Nucl. Phys. B* 268 (1986), pp. 621–653. doi: 10.1016/0550-3213(86)90262-2.

[38] B. Grzadkowski, M. Iskrzynski, M. Misiak, and J. Rosiek. "Dimension-Six Terms in the Standard Model Lagrangian." In: *JHEP* 10 (2010), p. 085. doi: 10.1007/JHEP10(2010)085. arXiv: 1008.4884 [hep-ph].

[39] L. Lehman. "Extending the Standard Model Effective Field Theory with the Complete Set of Dimension-7 Operators." In: *Phys. Rev. D* 90.12 (2014), p. 125023. doi: 10.1103/PhysRevD.90.125023. arXiv: 1410.4193 [hep-ph].

[40] C. W. Murphy. "Dimension-8 operators in the Standard Model Eective Field Theory." In: *JHEP* 10 (), p. 174. doi: 10.1007/JHEP10(2020)174. arXiv: 2005.00059 [hep-ph].

[41] H.-L. Li, Z. Ren, J. Shu, M.-L. Xiao, J.-H. Yu, and Y.-H. Zheng. "Complete Set of Dimension-8 Operators in the Standard Model Effective Field Theory." In: (Apr. 2020). arXiv: 2005.00008 [hep-ph].

[42] Y. Liao and X.-D. Ma. "An explicit construction of the dimension-9 operator basis in the standard model effective field theory." In: *JHEP* 11 (2020), p. 152. doi: 10.1007/JHEP11(2020)152. arXiv: 2007.08125 [hep-ph].

[43] J. Ellis, M. Madigan, K. Mimasu, V. Sanz, and T. You. "Top, Higgs, Diboson and Electroweak Fit to the Standard Model Effective Field Theory." In: *JHEP* 04 (2021), p. 279. doi: 10.1007/JHEP04(2021)279. arXiv: 2012.02779 [hep-ph].

[44] M. Agostini et al. "Final Results of GERDA on the Search for Neutrinoless Double-β Decay." In: *Phys. Rev. Lett.* 125.25 (2020), p. 252502. doi: 10.1103/PhysRevLett.125.252502. arXiv: 2009.06079 [nucl-ex].

[45] A. Takenaka et al. "Search for proton decay via $p \to e^+\pi^0$ and $p \to \mu^+\pi^0$ with an enlarged fiducial volume in Super-Kamiokande I-IV." In: *Phys. Rev. D* 102.11 (2020), p. 112011. doi: 10.1103/PhysRevD.102.112011. arXiv: 2010.16098 [hep-ex].

[46] C. Grojean, G. Servant, and J. D. Wells. "First-order electroweak phase transition in the standard model with a low cutoff." In: *Phys. Rev. D* 71 (2005), p. 036001. doi: 10.1103/PhysRevD.71.036001. arXiv: hep-ph/0407019.

[47] M. Chala, C. Krause, and G. Nardini. "Signals of the electroweak phase transition at colliders and gravitational wave observatories." In: *JHEP* 07 (2018), p. 062. doi: 10.1007/JHEP07(2018)062. arXiv: 1802.02168 [hep-ph].

[48] A. Hook. "Naturalness without new particles." In: *JHEP* 04 (2021), p. 048. doi: 10.1007/JHEP04(2021)048. arXiv: 1902.06758 [hep-ph].

[49] R. Barbieri and G. Giudice. "Upper bounds on supersymmetric particle masses." In: *Nuclear Physics B* 306.1 (1988), pp. 63–76. issn: 0550-3213. doi: https://doi.org/10.1016/0550-3213(88)90171-X. url: https://www.sciencedirect.com/science/article/pii/055032138890171X.

[50] R. Tito D'Agnolo. "One Lecture on the Hierarchy Problem." In: *Cargese International Summer School*. 2018.

[51] N. Craig. "Naturalness and New Approaches to the Hierarchy Problem." In: *Prospects in Theoretical Physics*. 2017.

[52] J. Ellis and K. A. Olive. "Supersymmetric Dark Matter Candidates." In: (Jan. 2010). arXiv: 1001.3651 [astro-ph.CO].

[53] M. Frigerio, A. Pomarol, F. Riva, and A. Urbano. "Composite Scalar Dark Matter." In: *JHEP* 07 (2012), p. 015. doi: 10.1007/JHEP07(2012)015. arXiv: 1204.2808 [hep-ph].

[54] J. D. Wells. "Naturalness, Extra-Empirical Theory Assessments, and the Implications of Skepticism." In: *Found. Phys.* 49.9 (2019), pp. 991–1010. doi: 10.1007/s10701-018-0220-x. arXiv: 1806.07289 [physics.hist-ph].

[55] S. Koren. "The Hierarchy Problem: From the Fundamentals to the Frontiers." Doctoral dissertation. UC, Santa Barbara, 2020. arXiv: 2009.11870 [hep-ph].

[56] G. 't Hooft. "Naturalness, chiral symmetry, and spontaneous chiral symmetry breaking." In: *NATO Sci. Ser. B* 59 (1980). Ed. by G. 't Hooft, C. Itzykson, A. Jaffe, H. Lehmann, P. K. Mitter, I. M. Singer, and R. Stora, pp. 135–157. doi: 10.1007/978-1-4684-7571-5_9.

[57] "LHC Design Report Vol.1: The LHC Main Ring." In: (June 2004). Ed. by O. S. Bruning, P. Collier, P. Lebrun, S. Myers, R. Ostojic, J. Poole, and P. Proudlock. doi: 10.5170/CERN-2004-003-V-1.

[58] "LHC Design Report. 2. The LHC infrastructure and general services." In: (Nov. 2004). Ed. by O. Buning, P. Collier, P. Lebrun, S. Myers, R. Ostojic, J. Poole, and P. Proudlock. doi: 10.5170/CERN-2004-003-V-2.

[59] "LHC Design Report. 3. The LHC injector chain." In: (Dec. 2004). Ed. by M. Benedikt, P. Collier, V. Mertens, J. Poole, and K. Schindl. doi: 10.5170/CERN-2004-003-V-3.

[60] A. Airapetian et al. "ATLAS: Detector and physics performance technical design report. Volume 1." In: (May 1999).

[61] A. Airapetian et al. "ATLAS: Detector and physics performance technical design report. Volume 2." In: (May 1999).

[62] G. L. Bayatian et al. "CMS Physics: Technical Design Report Volume 1: Detector Performance and Software." In: (2006).

[63] G. L. Bayatian et al. "CMS technical design report, volume II: Physics performance." In: *J. Phys. G* 34.6 (2007), pp. 995–1579. doi: 10.1088/0954-3899/34/6/S01.

[64] S. Amato et al. "LHCb technical proposal: A Large Hadron Collider Beauty Experiment for Precision Measurements of CP Violation and Rare Decays." In: (Feb. 1998).

[65] A. A. Alves Jr. et al. "The LHCb Detector at the LHC." In: *JINST* 3 (2008), S08005. doi: 10.1088/1748-0221/3/08/S08005.

[66] "ALICE: Technical proposal for a large ion collider experiment at the CERN LHC." In: (Dec. 1995).

[67] T. Abe et al. "Belle II Technical Design Report." In: (Nov. 2010). arXiv: 1011.0352 [physics.ins-det].

[68] D. Boutigny et al. "BaBar technical design report." In: (Mar. 1995).

[69] "Design Report Tevatron 1 project." In: (Sept. 1984).

[70] "LEP Design Report: Vol.2. The LEP Main Ring." In: (June 1984).

[71] F. Abe et al. "Observation of top quark production in $\bar{p}p$ collisions." In: *Phys. Rev. Lett.* 74 (1995), pp. 2626–2631. doi: 10.1103/PhysRevLett.74.2626. arXiv: hep-ex/9503002.

[72] S. Abachi et al. "Observation of the top quark." In: *Phys. Rev. Lett.* 74 (1995), pp. 2632–2637. doi: 10.1103/PhysRevLett.74.2632. arXiv: hep-ex/9503003.

[73] M. D. Schwartz. "TASI Lectures on Collider Physics." In: *Proceedings, Theoretical Advanced Study Institute in Elementary Particle Physics : Anticipating the Next Discoveries in Particle Physics (TASI 2016): Boulder, CO, USA, June 6-July 1, 2016*. Ed. by R. Essig and I. Low. 2018. doi: 10.1142/9789813233348_0002. arXiv: 1709.04533 [hep-ph].

[74] G. P. Salam. "Towards Jetography." In: *Eur. Phys. J. C* 67 (2010), pp. 637–686. doi: 10.1140/epjc/s10052-010-1314-6. arXiv: 0906.1833 [hep-ph].

[75] M. Cacciari, G. P. Salam, and G. Soyez. "The anti-k_t jet clustering algorithm." In: *JHEP* 04 (2008), p. 063. doi: 10.1088/1126-6708/2008/04/063. arXiv: 0802.1189 [hep-ph].

[76] G. Aad et al. "ATLAS b-jet identification performance and efficiency measurement with $t\bar{t}$ events in pp collisions at $\sqrt{s} = 13$ TeV." In: *Eur. Phys. J. C* 79.11 (2019), p. 970. doi: 10.1140/epjc/s10052-019-7450-8. arXiv: 1907.05120 [hep-ex].

[77] J. Alwall, R. Frederix, S. Frixione, V. Hirschi, F. Maltoni, O. Mattelaer, H. S. Shao, T. Stelzer, P. Torrielli, and M. Zaro. "The automated computation of tree-level and next-to-leading order differential cross sections, and their matching to parton shower simulations." In: *JHEP* 07 (2014), p. 079. doi: 10.1007/JHEP07(2014)079. arXiv: 1405.0301 [hep-ph].

[78] N. D. Christensen and C. Duhr. "FeynRules - Feynman rules made easy." In: *Comput. Phys. Commun.* 180 (2009), pp. 1614–1641. doi: 10.1016/j.cpc.2009.02.018. arXiv: 0806.4194 [hep-ph].

[79] T. Sjöstrand, S. Ask, J. R. Christiansen, R. Corke, N. Desai, P. Ilten, S. Mrenna, S. Prestel, C. O. Rasmussen, and P. Z. Skands. "An Introduction to PYTHIA 8.2." In: *Comput. Phys. Commun.* 191 (2015), pp. 159–177. doi: 10.1016/j.cpc.2015.01.024. arXiv: 1410.3012 [hep-ph].

[80] S. Ovyn, X. Rouby, and V. Lemaitre. "DELPHES, a framework for fast simulation of a generic collider experiment." In: (Mar. 2009). arXiv: 0903.2225 [hep-ph].

[81] R. Brun and F. Rademakers. "ROOT: An object oriented data analysis framework." In: *Nucl. Instrum. Meth.* A389 (1997), pp. 81–86. doi: 10.1016/S0168-9002(97)00048-X.

[82] A. L. Read. "Presentation of search results: The CL(s) technique." In: *J. Phys.* G28 (2002). [,11(2002)], pp. 2693–2704. doi: 10.1088/0954-3899/28/10/313.

[83] A. L. Read. "Modified frequentist analysis of search results (The CL(s) method)." In: *Workshop on Confidence Limits*. Aug. 2000.

[84] E. Busato, D. Calvet, and T. Theveneaux-Pelzer. "OpTHyLiC: an Optimised Tool for Hybrid Limits Computation." In: *Comput. Phys. Commun.* 226 (2018), pp. 136–150. doi: 10.1016/j.cpc.2018.01.009. arXiv: 1502.02610 [hep-ex].

[85] M. Aaboud et al. "Search for resonances in diphoton events at $\sqrt{s}$=13 TeV with the ATLAS detector." In: *JHEP* 09 (2016), p. 001. doi: 10.1007/JHEP09(2016)001. arXiv: 1606.03833 [hep-ex].

[86] V. Khachatryan et al. "Search for Resonant Production of High-Mass Photon Pairs in Proton-Proton Collisions at $\sqrt{s}$ =8 and 13 TeV." In: *Phys. Rev. Lett.* 117.5 (2016), p. 051802. doi: 10.1103/PhysRevLett.117.051802. arXiv: 1606.04093 [hep-ex].

[87] L. Lista. "Practical Statistics for Particle Physicists." In: *2016 European School of High-Energy Physics*. Sept. 2016. doi: 10.23730/CYRSP-2017-005.213. arXiv: 1609.04150 [physics.data-an].

[88] G. Cowan, K. Cranmer, E. Gross, and O. Vitells. “Asymptotic formulae for likelihood-based tests of new physics.” In: *Eur. Phys. J. C* 71 (2011). [Erratum: Eur.Phys.J.C 73, 2501 (2013)], p. 1554. doi: 10.1140/epjc/s10052-011-1554-0. arXiv: 1007.1727 [physics.data-an].

[89] G. Cowan and E. Gross. “Discovery significance with statistical uncertainty in the background estimate.” In: *ATLAS Statistics Forum*. May 2008.

[90] S. Dimopoulos and J. Preskill. “Massless composites with massive constituents.” In: *Nuclear Physics B* 199.2 (1982), pp. 206–222. issn: 0550-3213. doi: https://doi.org/10.1016/0550-3213(82)90345-5. url: https://www.sciencedirect.com/science/article/pii/0550321382903455.

[91] D. B. Kaplan and H. Georgi. “SU(2) × U(1) breaking by vacuum misalignment.” In: *Physics Letters B* 136.3 (1984), pp. 183–186. issn: 0370-2693. doi: https://doi.org/10.1016/0370-2693(84)91177-8. url: https://www.sciencedirect.com/science/article/pii/0370269384911778.

[92] D. B. Kaplan, H. Georgi, and S. Dimopoulos. “Composite Higgs scalars.” In: *Physics Letters B* 136.3 (1984), pp. 187–190. issn: 0370-2693. doi: https://doi.org/10.1016/0370-2693(84)91178-X. url: https://www.sciencedirect.com/science/article/pii/037026938491178X.

[93] K. Agashe, R. Contino, and A. Pomarol. “The Minimal composite Higgs model.” In: *Nucl. Phys. B* 719 (2005), pp. 165–187. doi: 10.1016/j.nuclphysb.2005.04.035. arXiv: hep-ph/0412089.

[94] R. Contino, L. Da Rold, and A. Pomarol. “Light custodians in natural composite Higgs models.” In: *Phys. Rev. D* 75 (2007), p. 055014. doi: 10.1103/PhysRevD.75.055014. arXiv: hep-ph/0612048.

[95] R. Barbieri, B. Bellazzini, V. S. Rychkov, and A. Varagnolo. “The Higgs boson from an extended symmetry.” In: *Phys. Rev. D* 76 (2007), p. 115008. doi: 10.1103/PhysRevD.76.115008. arXiv: 0706.0432 [hep-ph].

[96] B. Gripaios, A. Pomarol, F. Riva, and J. Serra. “Beyond the Minimal Composite Higgs Model.” In: *JHEP* 04 (2009), p. 070. doi: 10.1088/1126-6708/2009/04/070. arXiv: 0902.1483 [hep-ph].

[97] C. Anastasiou, E. Furlan, and J. Santiago. “Realistic Composite Higgs Models.” In: *Phys. Rev. D* 79 (2009), p. 075003. doi: 10.1103/PhysRevD.79.075003. arXiv: 0901.2117 [hep-ph].

[98] J. R. Espinosa, B. Gripaios, T. Konstandin, and F. Riva. “Electroweak Baryogenesis in Non-minimal Composite Higgs Models.” In: *JCAP* 01 (2012), p. 012. doi: 10.1088/1475-7516/2012/01/012. arXiv: 1110.2876 [hep-ph].

[99] J. Mrazek, A. Pomarol, R. Rattazzi, M. Redi, J. Serra, and A. Wulzer. "The Other Natural Two Higgs Doublet Model." In: *Nucl. Phys. B* 853 (2011), pp. 1–48. doi: 10.1016/j.nuclphysb.2011.07.008. arXiv: 1105.5403 [hep-ph].

[100] E. Bertuzzo, T. S. Ray, H. de Sandes, and C. A. Savoy. "On Composite Two Higgs Doublet Models." In: *JHEP* 05 (2013), p. 153. doi: 10.1007/JHEP05(2013)153. arXiv: 1206.2623 [hep-ph].

[101] M. Chala. "$h \longrightarrow \gamma\gamma$ excess and Dark Matter from Composite Higgs Models." In: *JHEP* 01 (2013), p. 122. doi: 10.1007/JHEP01(2013)122. arXiv: 1210.6208 [hep-ph].

[102] L. Vecchi. "The Natural Composite Higgs." In: (2013). arXiv: 1304.4579 [hep-ph].

[103] B. Bellazzini, C. Csáki, and J. Serra. "Composite Higgses." In: *Eur. Phys. J.* C74.5 (2014), p. 2766. doi: 10.1140/epjc/s10052-014-2766-x. arXiv: 1401.2457 [hep-ph].

[104] N. Fonseca, R. Zukanovich Funchal, A. Lessa, and L. Lopez-Honorez. "Dark Matter Constraints on Composite Higgs Models." In: *JHEP* 06 (2015), p. 154. doi: 10.1007/JHEP06(2015)154. arXiv: 1501.05957 [hep-ph].

[105] M. Chala, G. Nardini, and I. Sobolev. "Unified explanation for dark matter and electroweak baryogenesis with direct detection and gravitational wave signatures." In: *Phys. Rev.* D94.5 (2016), p. 055006. doi: 10.1103/PhysRevD.94.055006. arXiv: 1605.08663 [hep-ph].

[106] M. Chala and M. Spannowsky. "Behavior of composite resonances breaking lepton flavor universality." In: *Phys. Rev. D* 98.3 (2018), p. 035010. doi: 10.1103/PhysRevD.98.035010. arXiv: 1803.02364 [hep-ph].

[107] G. Cacciapaglia, H. Cai, A. Deandrea, and A. Kushwaha. "Composite Higgs and Dark Matter Model in SU(6)/SO(6)." In: *JHEP* 10 (2019), p. 035. doi: 10.1007/JHEP10(2019)035. arXiv: 1904.09301 [hep-ph].

[108] L. Da Rold and A. N. Rossia. "The Minimal Simple Composite Higgs Model." In: (2019). arXiv: 1904.02560 [hep-ph].

[109] L. Di Luzio, M. Redi, A. Strumia, and D. Teresi. "Coset Cosmology." In: *JHEP* 06 (2019), p. 110. doi: 10.1007/JHEP06(2019)110. arXiv: 1902.05933 [hep-ph].

[110] M. Ruhdorfer, E. Salvioni, and A. Weiler. "A Global View of the Off-Shell Higgs Portal." In: (2019). arXiv: 1910.04170 [hep-ph].

[111] R. Contino. "The Higgs as a Composite Nambu-Goldstone Boson." In: *Theoretical Advanced Study Institute in Elementary Particle Physics: Physics of the Large and the Small*. May 2010. doi: 10.1142/9789814327183_0005. arXiv: 1005.4269 [hep-ph].

[112] G. Panico and A. Wulzer. "The Composite Nambu-Goldstone Higgs." In: *Lect. Notes Phys.* 913 (2016), pp.1–316. doi: 10.1007/978-3-319-22617-0. arXiv: 1506.01961 [hep-ph].

[113] S. Coleman, J. Wess, and B. Zumino. "Structure of Phenomenological Lagrangians. I." In: *Phys. Rev.* 177 (5 1969), pp. 2239–2247. doi: 10.1103/PhysRev.177.2239. url: https://link.aps.org/doi/10.1103/PhysRev.177.2239.

[114] C. G. Callan, S. Coleman, J. Wess, and B. Zumino. "Structure of Phenomenological Lagrangians. II." In: *Phys. Rev.* 177 (5 1969), pp. 2247–2250. doi: 10.1103/PhysRev.177.2247. url: https://link.aps.org/doi/10.1103/PhysRev.177.2247.

[115] G. F. Giudice, C. Grojean, A. Pomarol, and R. Rattazzi. "The Strongly-Interacting Light Higgs." In: *JHEP* 06 (2007), p. 045. doi: 10.1088/1126-6708/2007/06/045. arXiv: hep-ph/0703164 [hep-ph].

[116] D. B. Kaplan. "Flavor at SSC energies: A New mechanism for dynamically generated fermion masses." In: *Nucl. Phys. B* 365 (1991), pp. 259–278. doi: 10.1016/S0550-3213(05)80021-5.

[117] G. Cacciapaglia, C. Pica, and F. Sannino. "Fundamental Composite Dynamics: A Review." In: *Phys. Rept.* 877 (2020), pp. 1–70. doi: 10.1016/j.physrep.2020.07.002. arXiv: 2002.04914 [hep-ph].

[118] A. Lenz. "Constraints on a Fourth Generation of Fermions from Higgs Boson Searches." In: *Advances in High Energy Physics* 2013 (Feb. 2013). doi: 10.1155/2013/910275.

[119] J. Serra. "Beyond the Minimal Top Partner Decay." In: *JHEP* 09 (2015), p. 176. doi: 10.1007/JHEP09(2015)176. arXiv: 1506.05110 [hep-ph].

[120] M. S. Chanowitz and M. K. Gaillard. "The TeV Physics of Strongly Interacting W's and Z's." In: *Nucl. Phys. B* 261 (1985), pp. 379–431. doi: 10.1016/0550-3213(85)90580-2.

[121] A. De Simone, O. Matsedonskyi, R. Rattazzi, and A. Wulzer. "A First Top Partner Hunter's Guide." In: *JHEP* 04 (2013), p. 004. doi: 10.1007/JHEP04(2013)004. arXiv: 1211.5663 [hep-ph].

[122] E. Salvioni. "Phenomenology of Compositeness at the LHC." Doctoral dissertation. Padua U., July 2013.

[123] V. Sanz and J. Setford. "Composite Higgs Models after Run 2." In: *Adv. High Energy Phys.* 2018 (2018), p. 7168480. doi: 10.1155/2018/7168480. arXiv: 1703.10190 [hep-ph].

[124] A. M. Sirunyan et al. "A search for bottom-type, vector-like quark pair production in a fully hadronic final state in proton-proton collisions at $\sqrt{s} = 13$ TeV." In: *Phys. Rev. D* 102 (2020), p. 112004. doi: 10.1103/PhysRevD.102.112004. arXiv: 2008.09835 [hep-ex].

[125] M. Aaboud et al. "Search for pair production of up-type vector-like quarks and for four-top-quark events in final states with multiple b-jets with the ATLAS detector." In: *JHEP* 07 (2018), p. 089. doi: 10.1007/JHEP07(2018)089. arXiv: 1803.09678 [hep-ex].

[126] M. Aaboud et al. “Search for pair- and single-production of vector-like quarks in final states with at least one Z boson decaying into a pair of electrons or muons in pp collision data collected with the ATLAS detector at $\sqrt{s} = 13$ TeV.” In: *Phys. Rev. D* 98.11 (2018), p. 112010. doi: 10.1103/PhysRevD.98.112010. arXiv: 1806.10555 [hep-ex].

[127] A. M. Sirunyan et al. “Search for pair production of vector-like quarks in the bW$\bar{\text{b}}$W channel from proton-proton collisions at $\sqrt{s}$ = 13 TeV.” In: *Phys. Lett. B* 779 (2018), pp. 82–106. doi: 10.1016/j.physletb.2018.01.077. arXiv: 1710.01539 [hep-ex].

[128] M. Aaboud et al. “Search for pair production of heavy vector-like quarks decaying to high-p$_T$ W bosons and b quarks in the lepton-plus-jets final state in pp collisions at $\sqrt{s} = 13$ TeV with the ATLAS detector.” In: *JHEP* 10 (2017), p. 141. doi: 10.1007/JHEP10(2017)141. arXiv: 1707.03347 [hep-ex].

[129] M. Aaboud et al. “Combination of the searches for pair-produced vector-like partners of the third-generation quarks at $\sqrt{s} = 13$ TeV with the ATLAS detector.” In: *Phys. Rev. Lett.* 121.21 (2018), p. 211801. doi: 10.1103/PhysRevLett.121.211801. arXiv: 1808.02343 [hep-ex].

[130] “Search for a heavy resonance decaying to a top quark and a W boson at $\sqrt{s} = 13$ TeV in the fully hadronic final state.” In: (2021).

[131] “Search for single vector-like B quark production and decay via $B \to bH(b\bar{b})$ in pp collisions at $\sqrt{s} = 13$ TeV with the ATLAS detector.” In: (Apr. 2021).

[132] A. M. Sirunyan et al. “Search for electroweak production of a vector-like T quark using fully hadronic final states.” In: *JHEP* 01 (2020), p. 036. doi: 10.1007/JHEP01(2020)036. arXiv: 1909.04721 [hep-ex].

[133] M. Aaboud et al. “Search for large missing transverse momentum in association with one top-quark in proton-proton collisions at $\sqrt{s}$ = 13 TeV with the ATLAS detector.” In: *JHEP* 05 (2019), p. 041. doi: 10.1007/JHEP05(2019)041. arXiv: 1812.09743 [hep-ex].

[134] M. Aaboud et al. “Search for single production of vector-like quarks decaying into Wb in pp collisions at $\sqrt{s} = 13$ TeV with the ATLAS detector.” In: *JHEP* 05 (2019), p. 164. doi: 10.1007/JHEP05(2019)164. arXiv: 1812.07343 [hep-ex].

[135] A. M. Sirunyan et al. “Search for single production of vector-like quarks decaying to a b quark and a Higgs boson.” In: *JHEP* 06 (2018), p. 031. doi: 10.1007/JHEP06(2018)031. arXiv: 1802.01486 [hep-ex].

[136] A. M. Sirunyan et al. “Search for single production of a vector-like T quark decaying to a Z boson and a top quark in proton-proton collisions at $\sqrt{s}$ = 13 TeV.” In: *Phys. Lett. B* 781 (2018), pp. 574–600. doi: 10.1016/j.physletb.2018.04.036. arXiv: 1708.01062 [hep-ex].

[137] G. Aad et al. "Search for type-III Seesaw heavy leptons in pp collisions at $\sqrt{s} = 8$ TeV with the ATLAS Detector." In: *Phys. Rev. D* 92.3 (2015), p. 032001. doi: 10.1103/PhysRevD.92.032001. arXiv: 1506.01839 [hep-ex].

[138] V. Khachatryan et al. "Search for Excited Leptons in Proton-Proton Collisions at $\sqrt{s}$ = 8 TeV." In: *JHEP* 03 (2016), p. 125. doi: 10.1007/JHEP03(2016)125. arXiv: 1511.01407 [hep-ex].

[139] G. Aad et al. "Search for heavy lepton resonances decaying to a Z boson and a lepton in pp collisions at $\sqrt{s} = 8$ TeV with the ATLAS detector." In: *JHEP* 09 (2015), p. 108. doi: 10.1007/JHEP09(2015)108. arXiv: 1506.01291 [hep-ex].

[140] A. M. Sirunyan et al. "Search for vector-like leptons in multilepton final states in proton-proton collisions at $\sqrt{s}$ = 13 TeV." In: *Phys. Rev. D* 100.5 (2019), p. 052003. doi: 10.1103/PhysRevD.100.052003. arXiv: 1905.10853 [hep-ex].

[141] G. Aad et al. "Search for type-III seesaw heavy leptons in dilepton final states in pp collisions at $\sqrt{s}$ = 13 TeV with the ATLAS detector." In: *Eur. Phys. J. C* 81.3 (2021), p. 218. doi: 10.1140/epjc/s10052-021-08929-9. arXiv: 2008.07949 [hep-ex].

[142] G. Guedes and J. Santiago. "New leptons with exotic decays: collider limits and dark matter complementarity." In: (July 2021). arXiv: 2107.03429 [hep-ph].

[143] L. Di Luzio, M. Kirk, and A. Lenz. "Updated B_s-mixing constraints on new physics models for $b \to s\ell^+\ell^-$ anomalies." In: *Phys. Rev. D* 97.9 (2018), p. 095035. doi: 10.1103/PhysRevD.97.095035. arXiv: 1712.06572 [hep-ph].

[144] *Search for electroweak production of supersymmetric particles in the two and three lepton final state at $\sqrt{s} = 13$ TeV with the ATLAS detector*. Tech. rep. All figures including auxiliary figures are available at https://atlas.web.cern.ch/Atlas/GROUPS/PHYSICS/CONFNOTES/ATLAS-CONF-2017-039. Geneva: CERN, 2017. url: http://cds.cern.ch/record/2267406.

[145] A. M. Sirunyan et al. "Search for a heavy vector resonance decaying to a Z boson and a Higgs boson in proton-proton collisions at $\sqrt{s} = 13$ TeV." In: (Feb. 2021). arXiv: 2102.08198 [hep-ex].

[146] M. Petteni. "A Search for $t\bar{t}$ Resonances in the Dilepton Channel in 1.04 fb^{-1} of pp collisions at $\sqrt{s} = 7$ TeV with the ATLAS experiment." In: *31st International Symposium on Physics In Collision*. Nov. 2011. arXiv: 1111.6933 [hep-ex].

[147] G. Aad et al. "Search for resonances decaying into top-quark pairs using fully hadronic decays in pp collisions with ATLAS at $\sqrt{s} = 7$ TeV." In: *JHEP* 01 (2013), p. 116. doi: 10.1007/JHEP01(2013)116. arXiv: 1211.2202 [hep-ex].

[148] "Search for Anomalous Top Quark Pair Production in the Boosted All-Hadronic Final State using pp Collisions at sqrt(s) = 8 TeV." In: (2013).

[149] "Search for ttbar resonances in dilepton+jets final states in pp collisions at 8 TeV." In: (2014).

[150] "Search in two-dimensional mass space for T'T' to W'b W' b in the dilepton final state in proton-proton collisions at 8 TeV." In: (2015).

[151] G. Aad et al. "A search for $t\bar{t}$ resonances using lepton-plus-jets events in proton-proton collisions at $\sqrt{s} = 8$ TeV with the ATLAS detector." In: *JHEP* 08 (2015), p. 148. doi: 10.1007/JHEP08(2015)148. arXiv: 1505.07018 [hep-ex].

[152] M. Chala, J. Juknevich, G. Perez, and J. Santiago. "The Elusive Gluon." In: *JHEP* 01 (2015), p. 092. doi: 10.1007/JHEP01(2015)092. arXiv: 1411.1771 [hep-ph].

[153] A. Azatov, D. Chowdhury, D. Ghosh, and T. S. Ray. "Same sign di-lepton candles of the composite gluons." In: *JHEP* 08 (2015), p. 140. doi: 10.1007/JHEP08(2015)140. arXiv: 1505.01506 [hep-ph].

[154] J. P. Araque, N. F. Castro, and J. Santiago. "Interpretation of Vector-like Quark Searches: Heavy Gluons in Composite Higgs Models." In: *JHEP* 11 (2015), p. 120. doi: 10.1007/JHEP11(2015)120. arXiv: 1507.05628 [hep-ph].

[155] M. E. Peskin and T. Takeuchi. "New constraint on a strongly interacting Higgs sector." In: *Phys. Rev. Lett.* 65 (8 1990), pp. 964–967. doi: 10.1103/PhysRevLett.65.964. url: https://link.aps.org/doi/10.1103/PhysRevLett.65.964.

[156] J. A. Aguilar-Saavedra, R. Benbrik, S. Heinemeyer, and M. Pérez-Victoria. "Handbook of vectorlike quarks: Mixing and single production." In: *Phys. Rev. D* 88.9 (2013), p. 094010. doi: 10.1103/PhysRevD.88.094010. arXiv: 1306.0572 [hep-ph].

[157] K. Agashe, R. Contino, L. Da Rold, and A. Pomarol. "A Custodial symmetry for $Zb\bar{b}$." In: *Phys. Lett. B* 641 (2006), pp. 62–66. doi: 10.1016/j.physletb.2006.08.005. arXiv: hep-ph/0605341.

[158] A. M. Sirunyan et al. "Search for top quark partners with charge 5/3 in the same-sign dilepton and single-lepton final states in proton-proton collisions at $\sqrt{s} = 13$ TeV." In: *JHEP* 03 (2019), p. 082. doi: 10.1007/JHEP03(2019)082. arXiv: 1810.03188 [hep-ex].

[159] D. Ghosh, M. Salvarezza, and F. Senia. "Extending the Analysis of Electroweak Precision Constraints in Composite Higgs Models." In: *Nucl. Phys.* B914 (2017), pp. 346–387. doi: 10.1016/j.nuclphysb.2016.11.013. arXiv: 1511.08235 [hep-ph].

[160] G. Isidori. "Flavour Physics and Implication for New Phenomena." In: *Adv. Ser. Direct. High Energy Phys.* 26 (2016), pp. 339–355. doi: 10.1142/9789814733519_0017. arXiv: 1507.00867 [hep-ph].

[161] G. D'Ambrosio, G. F. Giudice, G. Isidori, and A. Strumia. "Minimal flavor violation: An Effective field theory approach." In: *Nucl. Phys. B* 645 (2002), pp. 155–187. doi: 10.1016/S0550-3213(02)00836-2. arXiv: hep-ph/0207036.

[162] R. Barbieri. "A view of flavour physics in 2021." In: (Mar. 2021). arXiv: 2103.15635 [hep-ph].

[163] M. Redi and A. Weiler. "Flavor and CP Invariant Composite Higgs Models." In: *JHEP* 11 (2011), p. 108. doi: 10.1007/JHEP11(2011)108. arXiv: 1106.6357 [hep-ph].

[164] V. Sanz and J. Setford. "Composite Higgses with seesaw EWSB." In: *JHEP* 12 (2015), p. 154. doi: 10.1007/JHEP12(2015)154. arXiv: 1508.06133 [hep-ph].

[165] G. Cacciapaglia, T. Flacke, M. Park, and M. Zhang. "Exotic decays of top partners: mind the search gap." In: *Phys. Lett.* B798 (2019), p. 135015. doi: 10.1016/j.physletb.2019.135015. arXiv: 1908.07524 [hep-ph].

[166] G. Ferretti and D. Karateev. "Fermionic UV completions of Composite Higgs models." In: *JHEP* 03 (2014), p. 077. doi: 10.1007/JHEP03(2014)077. arXiv: 1312.5330 [hep-ph].

[167] D. Marzocca and A. Urbano. "Composite Dark Matter and LHC Interplay." In: *JHEP* 07 (2014), p. 107. doi: 10.1007/JHEP07(2014)107. arXiv: 1404.7419 [hep-ph].

[168] A. Carmona and M. Chala. "Composite Dark Sectors." In: *JHEP* 06 (2015), p. 105. doi: 10.1007/JHEP06(2015)105. arXiv: 1504.00332 [hep-ph].

[169] T. Ma and G. Cacciapaglia. "Fundamental Composite 2HDM: SU(N) with 4 flavours." In: *JHEP* 03 (2016), p. 211. doi: 10.1007/JHEP03(2016)211. arXiv: 1508.07014 [hep-ph].

[170] S. Bruggisser, F. Riva, and A. Urbano. "Strongly Interacting Light Dark Matter." In: *SciPost Phys.* 3.3 (2017), p. 017. doi: 10.21468/SciPostPhys.3.3.017. arXiv: 1607.02474 [hep-ph].

[171] G. Ballesteros, A. Carmona, and M. Chala. "Exceptional Composite Dark Matter." In: *Eur. Phys. J.* C77.7 (2017), p. 468. doi: 10.1140/epjc/s10052-017-5040-1. arXiv: 1704.07388 [hep-ph].

[172] R. Balkin, M. Ruhdorfer, E. Salvioni, and A. Weiler. "Charged Composite Scalar Dark Matter." In: *JHEP* 11 (2017), p. 094. doi: 10.1007/JHEP11(2017)094. arXiv: 1707.07685 [hep-ph].

[173] Y. Wu, T. Ma, B. Zhang, and G. Cacciapaglia. "Composite Dark Matter and Higgs." In: *JHEP* 11 (2017), p. 058. doi: 10.1007/JHEP11(2017)058. arXiv: 1703.06903 [hep-ph].

[174] R. Balkin, G. Perez, and A. Weiler. "Little composite dark matter." In: *Eur. Phys. J.* C78.2 (2018), p. 104. doi: 10.1140/epjc/s10052-018-5552-3. arXiv: 1707.09980 [hep-ph].

[175] R. Balkin, M. Ruhdorfer, E. Salvioni, and A. Weiler. "Dark matter shifts away from direct detection." In: *JCAP* 1811.11 (2018), p. 050. doi: 10.1088/1475-7516/2018/11/050. arXiv: 1809.09106 [hep-ph].

[176] M. Chala, R. Gröber, and M. Spannowsky. “Searches for vector-like quarks at future colliders and implications for composite Higgs models with dark matter.” In: *JHEP* 03 (2018), p. 040. doi: 10.1007/JHEP03(2018)040. arXiv: 1801.06537 [hep-ph].

[177] T. Alanne, D. Buarque Franzosi, M. T. Frandsen, and M. Rosenlyst. “Dark matter in (partially) composite Higgs models.” In: *JHEP* 12 (2018), p. 088. doi: 10.1007/JHEP12(2018)088. arXiv: 1808.07515 [hep-ph].

[178] X.-M. Jiang, C. Cai, Z.-H. Yu, Y.-P. Zeng, and H.-H. Zhang. “Pseudo-Nambu-Goldstone dark matter and two-Higgs-doublet models.” In: *Phys. Rev.* D100.7 (2019), p. 075011. doi: 10.1103/PhysRevD.100.075011. arXiv: 1907.09684 [hep-ph].

[179] A. Davoli, A. De Simone, D. Marzocca, and A. Morandini. “Composite 2HDM with singlets: a viable dark matter scenario.” In: *JHEP* 10 (2019), p. 196. doi: 10.1007/JHEP10(2019)196. arXiv: 1905.13244 [hep-ph].

[180] C. A. Baker et al. “An Improved experimental limit on the electric dipole moment of the neutron.” In: *Phys. Rev. Lett.* 97 (2006), p. 131801. doi: 10.1103/PhysRevLett.97.131801. arXiv: hep-ex/0602020.

[181] V. Andreev et al. “Improved limit on the electric dipole moment of the electron.” In: *Nature* 562.7727 (2018), pp. 355–360. doi: 10.1038/s41586-018-0599-8.

[182] R. D. Peccei and H. R. Quinn. “CP Conservation in the Presence of Pseudoparticles.” In: *Phys. Rev. Lett.* 38 (25 1977), pp. 1440–1443. doi: 10.1103/PhysRevLett.38.1440. url: https://link.aps.org/doi/10.1103/PhysRevLett.38.1440.

[183] R. D. Peccei and H. R. Quinn. “Constraints imposed by CP conservation in the presence of pseudoparticles.” In: *Phys. Rev. D* 16 (6 1977), pp. 1791–1797. doi: 10.1103/PhysRevD.16.1791. url: https://link.aps.org/doi/10.1103/PhysRevD.16.1791.

[184] M. Bauer, M. Neubert, and A. Thamm. “Collider Probes of Axion-Like Particles.” In: *JHEP* 12 (2017), p. 044. doi: 10.1007/JHEP12(2017)044. arXiv: 1708.00443 [hep-ph].

[185] R. S. Gupta, Z. Komargodski, G. Perez, and L. Ubaldi. “Is the Relaxion an Axion?” In: *JHEP* 02 (2016), p. 166. doi: 10.1007/JHEP02(2016)166. arXiv: 1509.00047 [hep-ph].

[186] E. Ma, T. Ohata, and K. Tsumura. “Majoron as the QCD axion in a radiative seesaw model.” In: *Phys. Rev. D* 96.7 (2017), p. 075039. doi: 10.1103/PhysRevD.96.075039. arXiv: 1708.03076 [hep-ph].

[187] L. Calibbi, F. Goertz, D. Redigolo, R. Ziegler, and J. Zupan. “Minimal axion model from flavor.” In: *Phys. Rev. D* 95.9 (2017), p. 095009. doi: 10.1103/PhysRevD.95.095009. arXiv: 1612.08040 [hep-ph].

[188] Y. Nomura and J. Thaler. "Dark Matter through the Axion Portal." In: *Phys. Rev. D* 79 (2009), p. 075008. doi: 10.1103/PhysRevD.79.075008. arXiv: 0810.5397 [hep-ph].

[189] J. Liu, C. E. M. Wagner, and X.-P. Wang. "A light complex scalar for the electron and muon anomalous magnetic moments." In: *JHEP* 03 (2019), p. 008. doi: 10.1007/JHEP03(2019)008. arXiv: 1810.11028 [hep-ph].

[190] M. A. Buen-Abad, J. Fan, M. Reece, and C. Sun. "Challenges for an axion explanation of the muon $g-2$ measurement." In: (Apr. 2021). arXiv: 2104.03267 [hep-ph].

[191] B. Abi et al. "Measurement of the Positive Muon Anomalous Magnetic Moment to 0.46 ppm." In: *Phys. Rev. Lett.* 126.14 (2021), p. 141801. doi: 10.1103/PhysRevLett.126.141801. arXiv: 2104.03281 [hep-ex].

[192] N. Craig, H. K. Lou, M. McCullough, and A. Thalapillil. "The Higgs Portal Above Threshold." In: *JHEP* 02 (2016), p. 127. doi: 10.1007/JHEP02(2016)127. arXiv: 1412.0258 [hep-ph].

[193] S. Banerjee, M. Chala, and M. Spannowsky. "Top quark FCNCs in extended Higgs sectors." In: *Eur. Phys. J. C* 78.8 (2018), p. 683. doi: 10.1140/epjc/s10052-018-6150-0. arXiv: 1806.02836 [hep-ph].

[194] M. Chala, J. Santiago, and M. Spannowsky. "Constraining four-fermion operators using rare top decays." In: *JHEP* 04 (2019), p. 014. doi: 10.1007/JHEP04(2019)014. arXiv: 1809.09624 [hep-ph].

[195] V. Khachatryan et al. "Search for Higgs boson off-shell production in proton-proton collisions at 7 and 8 TeV and derivation of constraints on its total decay width." In: *JHEP* 09 (2016), p. 051. doi: 10.1007/JHEP09(2016)051. arXiv: 1605.02329 [hep-ex].

[196] R. Harnik, J. Kopp, and J. Zupan. "Flavor Violating Higgs Decays." In: *JHEP* 03 (2013), p. 026. doi: 10.1007/JHEP03(2013)026. arXiv: 1209.1397 [hep-ph].

[197] M. Aaboud et al. "Search for flavour-changing neutral current top-quark decays $t \longrightarrow qZ$ in proton-proton collisions at $\sqrt{s} = 13$ TeV with the ATLAS detector." In: *JHEP* 07 (2018), p. 176. doi: 10.1007/JHEP07(2018)176. arXiv: 1803.09923 [hep-ex].

[198] P. Fileviez Perez, H. H. Patel, M. J. Ramsey-Musolf, and K. Wang. "Triplet Scalars and Dark Matter at the LHC." In: *Phys. Rev. D* 79 (2009), p. 055024. doi: 10.1103/PhysRevD.79.055024. arXiv: 0811.3957 [hep-ph].

[199] D. Egana-Ugrinovic, M. Low, and J. T. Ruderman. "Charged Fermions Below 100 GeV." In: *JHEP* 05 (2018), p. 012. doi: 10.1007/JHEP05(2018)012. arXiv: 1801.05432 [hep-ph].

[200] A. M. Sirunyan et al. “Combined measurements of Higgs boson couplings in proton–proton collisions at $\sqrt{s} = 13\,\text{TeV}$.” In: *Eur. Phys. J. C* 79.5 (2019), p. 421. doi: 10.1140/epjc/s10052-019-6909-y. arXiv: 1809.10733 [hep-ex].

[201] R. Primulando and P. Uttayarat. “Probing Lepton Flavor Violation at the 13 TeV LHC.” In: *JHEP* 05 (2017), p. 055. doi: 10.1007/JHEP05(2017)055. arXiv: 1612.01644 [hep-ph].

[202] H. E. Logan. “TASI 2013 lectures on Higgs physics within and beyond the Standard Model.” In: (June 2014). arXiv: 1406.1786 [hep-ph].

[203] A. M. Sirunyan et al. “Search for low-mass resonances decaying into bottom quark-antiquark pairs in proton-proton collisions at $\sqrt{s} = 13$ TeV.” In: *Phys. Rev. D* 99.1 (2019), p. 012005. doi: 10.1103/PhysRevD.99.012005. arXiv: 1810.11822 [hep-ex].

[204] M. Aaboud et al. “Search for charged Higgs bosons decaying into top and bottom quarks at $\sqrt{s} =$ 13 TeV with the ATLAS detector.” In: *JHEP* 11 (2018), p. 085. doi: 10.1007/JHEP11(2018)085. arXiv: 1808.03599 [hep-ex].

[205] V. Khachatryan et al. “Search for a light charged Higgs boson decaying to $c\bar{s}$ in pp collisions at $\sqrt{s} = 8\,\text{TeV}$.” In: *JHEP* 12 (2015), p. 178. doi: 10.1007/JHEP12(2015)178. arXiv: 1510.04252 [hep-ex].

[206] A. M. Sirunyan et al. “Search for pair-produced resonances decaying to quark pairs in proton-proton collisions at $\sqrt{s} = 13$ TeV.” In: *Phys. Rev. D* 98.11 (2018), p. 112014. doi: 10.1103/PhysRevD.98.112014. arXiv: 1808.03124 [hep-ex].

[207] “Search for pair production of resonances decaying to a top quark plus a jet in final states with two leptons.” In: (2013).

[208] G. D. Kribs, A. Martin, B. Ostdiek, and T. Tong. “Dark Mesons at the LHC.” In: *JHEP* 07 (2019), p. 133. doi: 10.1007/JHEP07(2019)133. arXiv: 1809.10184 [hep-ph].

[209] M. Quiros. “Finite temperature field theory and phase transitions.” In: *ICTP Summer School in High-Energy Physics and Cosmology*. Jan. 1999. arXiv: hep-ph/9901312.

[210] *Projections for measurements of Higgs boson cross sections, branching ratios, coupling parameters and mass with the ATLAS detector at the HL-LHC*. Tech. rep. ATL-PHYS-PUB-2018-054. Geneva: CERN, 2018. url: https://cds.cern.ch/record/2652762.

[211] M. S. Turner, E. J. Weinberg, and L. M. Widrow. “Bubble nucleation in first-order inflation and other cosmological phase transitions.” In: *Phys. Rev. D* 46 (6 1992), pp. 2384–2403. doi: 10.1103/PhysRevD.46.2384. url: https://link.aps.org/doi/10.1103/PhysRevD.46.2384.

[212] A. Linde. "Decay of the false vacuum at finite temperature." In: *Nuclear Physics B* 216.2 (1983), pp. 421–445. issn: 0550-3213. doi: https://doi.org/10.1016/0550-3213(83)90293-6. url: https://www.sciencedirect.com/science/article/pii/0550321383902936.

[213] C. Caprini et al. "Detecting gravitational waves from cosmological phase transitions with LISA: an update." In: *JCAP* 03 (2020), p. 024. doi: 10.1088/1475-7516/2020/03/024. arXiv: 1910.13125 [astro-ph.CO].

[214] D. J. Weir. "Gravitational waves from a first order electroweak phase transition: a brief review." In: *Phil. Trans. Roy. Soc. Lond. A* 376.2114 (2018), p. 20170126. doi: 10.1098/rsta.2017.0126. arXiv: 1705.01783 [hep-ph].

[215] B. P. Abbott et al. "LIGO: The Laser interferometer gravitational-wave observatory." In: *Rept. Prog. Phys.* 72 (2009), p. 076901. doi: 10.1088/0034-4885/72/7/076901. arXiv: 0711.3041 [gr-qc].

[216] P. Amaro-Seoane et al. "Laser Interferometer Space Antenna." In: (Feb. 2017). arXiv: 1702.00786 [astro-ph.IM].

[217] C. Caprini et al. "Science with the space-based interferometer eLISA. II: Gravitational waves from cosmological phase transitions." In: *JCAP* 04 (2016), p. 001. doi: 10.1088/1475-7516/2016/04/001. arXiv: 1512.06239 [astro-ph.CO].

[218] A. M. et al. "LISA Pathfinder." In: (2019). arXiv: 1903.08924 [astro-ph.IM].

[219] C. L. Wainwright. "CosmoTransitions: Computing Cosmological Phase Transition Temperatures and Bubble Profiles with Multiple Fields." In: *Comput. Phys. Commun.* 183 (2012), pp. 2006–2013. doi: 10.1016/j.cpc.2012.04.004. arXiv: 1109.4189 [hep-ph].

[220] B. D. Fields, K. A. Olive, T.-H. Yeh, and C. Young. "Big-Bang Nucleosynthesis after Planck." In: *JCAP* 03 (2020). [Erratum: JCAP 11, E02 (2020)], p. 010. doi: 10.1088/1475-7516/2020/03/010. arXiv: 1912.01132 [astro-ph.CO].

[221] V. Keus, N. Koivunen, and K. Tuominen. "Singlet scalar and 2HDM extensions of the Standard Model: CP-violation and constraints from $(g-2)_\mu$ and eEDM." In: *JHEP* 09 (2018), p. 059. doi: 10.1007/JHEP09(2018)059. arXiv: 1712.09613 [hep-ph].

[222] K. Choi, S. H. Im, H. Kim, and D. Y. Mo. "750 GeV diphoton resonance and electric dipole moments." In: *Phys. Lett. B* 760 (2016), pp. 666–673. doi: 10.1016/j.physletb.2016.07.056. arXiv: 1605.00206 [hep-ph].

[223] L. Allwicher, G. Isidori, and A. E. Thomsen. "Stability of the Higgs Sector in a Flavor-Inspired Multi-Scale Model." In: *JHEP* 01 (2021), p. 191. doi: 10.1007/JHEP01(2021)191. arXiv: 2011.01946 [hep-ph].

[224] R. Aaij et al. “Test of lepton universality in beauty-quark decays.” In: (Mar. 2021). arXiv: 2103.11769 [hep-ex].

[225] C. Cornella, D. A. Faroughy, J. Fuentes-Martín, G. Isidori, and M. Neubert. “Reading the footprints of the B-meson flavor anomalies.” In: (Mar. 2021). arXiv: 2103.16558 [hep-ph].

[226] D. Buttazzo, A. Greljo, G. Isidori, and D. Marzocca. “B-physics anomalies: a guide to combined explanations.” In: *JHEP* 11 (2017), p. 044. doi: 10.1007/JHEP11(2017)044. arXiv: 1706.07808 [hep-ph].

[227] R. Aaij et al. “Search for decays of neutral beauty mesons into four muons.” In: *JHEP* 03 (2017), p. 001. doi: 10.1007/JHEP03(2017)001. arXiv: 1611.07704 [hep-ex].

[228] M. Chala, U. Egede, and M. Spannowsky. “Searching new physics in rare B-meson decays into multiple muons.” In: *Eur. Phys. J.* C79.5 (2019), p. 431. doi: 10.1140/epjc/s10052-019-6946-6. arXiv: 1902.10156 [hep-ph].

[229] M. Borsato et al. “Unleashing the full power of LHCb to probe Stealth New Physics.” In: (May 2021). arXiv: 2105.12668 [hep-ph].

[230] I. Brivio, M. B. Gavela, L. Merlo, K. Mimasu, J. M. No, R. del Rey, and V. Sanz. “ALPs Effective Field Theory and Collider Signatures.” In: *Eur. Phys. J. C* 77.8 (2017), p. 572. doi: 10.1140/epjc/s10052-017-5111-3. arXiv: 1701.05379 [hep-ph].

[231] K. Griest and D. Seckel. “Three exceptions in the calculation of relic abundances.” In: *Phys. Rev. D* 43 (10 1991), pp. 3191–3203. doi: 10.1103/PhysRevD.43.3191. url: https://link.aps.org/doi/10.1103/PhysRevD.43.3191.

[232] Y. Hochberg, E. Kuflik, H. Murayama, T. Volansky, and J. G. Wacker. “Model for Thermal Relic Dark Matter of Strongly Interacting Massive Particles.” In: *Phys. Rev. Lett.* 115.2 (2015), p. 021301. doi: 10.1103/PhysRevLett.115.021301. arXiv: 1411.3727 [hep-ph].

[233] N. Aghanim et al. “Planck 2018 results. VI. Cosmological parameters.” In: (2018). arXiv: 1807.06209 [astro-ph.CO].

[234] N. A. Bahcall, J. P. Ostriker, S. Perlmutter, and P. J. Steinhardt. “The Cosmic triangle: Assessing the state of the universe.” In: *Science* 284 (1999), pp. 1481–1488. doi: 10.1126/science.284.5419.1481. arXiv: astro-ph/9906463.

[235] S. Tulin and H.-B. Yu. “Dark Matter Self-interactions and Small Scale Structure.” In: *Phys. Rept.* 730 (2018), pp. 1–57. doi: 10.1016/j.physrep.2017.11.004. arXiv: 1705.02358 [hep-ph].

[236] F. Governato et al. “At the heart of the matter: the origin of bulgeless dwarf galaxies and Dark Matter cores.” In: *Nature* 463 (2010), pp. 203–206. doi: 10.1038/nature08640. arXiv: 0911.2237 [astro-ph.CO].

[237] E. Aprile et al. “First Dark Matter Search Results from the XENON1T Experiment.” In: *Phys. Rev. Lett.* 119.18 (2017), p. 181301. doi: 10.1103/PhysRevLett.119.181301. arXiv: 1705.06655 [astro-ph.CO].

[238] R. Essig, J. Mardon, and T. Volansky. “Direct Detection of Sub-GeV Dark Matter.” In: *Phys. Rev. D* 85 (2012), p. 076007. doi: 10.1103/PhysRevD.85.076007. arXiv: 1108.5383 [hep-ph].

[239] Y. Hochberg, Y. Kahn, N. Kurinsky, B. V. Lehmann, T. C. Yu, and K. K. Berggren. “Determining Dark Matter-Electron Scattering Rates from the Dielectric Function.” In: (Jan. 2021). arXiv: 2101.08263 [hep-ph].

[240] T. R. Slatyer. “Indirect Detection of Dark Matter.” In: *Theoretical Advanced Study Institute in Elementary Particle Physics: Anticipating the Next Discoveries in Particle Physics*. Oct. 2017. doi: 10.1142/9789813233348_0005. arXiv: 1710.05137 [hep-ph].

[241] G. Belanger, F. Boudjema, and A. Pukhov. “micrOMEGAs : a code for the calculation of Dark Matter properties in generic models of particle interaction.” In: *The Dark Secrets of the Terascale: Proceedings, TASI 2011, Boulder, Colorado, USA, Jun 6 - Jul 11, 2011*. 2013, pp. 739–790. doi: 10.1142/9789814390163_0012. arXiv: 1402.0787 [hep-ph].

[242] F. Ambrogi, C. Arina, M. Backovic, J. Heisig, F. Maltoni, L. Mantani, O. Mattelaer, and G. Mohlabeng. “MadDM v.3.0: a Comprehensive Tool for Dark Matter Studies.” In: *Phys. Dark Univ.* 24 (2019), p. 100249. doi: 10.1016/j.dark.2018.11.009. arXiv: 1804.00044 [hep-ph].

[243] E. Aprile et al. “First Dark Matter Search Results from the XENON1T Experiment.” In: *Phys. Rev. Lett.* 119.18 (2017), p. 181301. doi: 10.1103/PhysRevLett.119.181301. arXiv: 1705.06655 [astro-ph.CO].

[244] E. Aprile et al. “Dark Matter Search Results from a One Ton-Year Exposure of XENON1T.” In: *Phys. Rev. Lett.* 121.11 (2018), p. 111302. doi: 10.1103/PhysRevLett.121.111302. arXiv: 1805.12562 [astro-ph.CO].

[245] D. S. Akerib et al. “Projected WIMP sensitivity of the LUX-ZEPLIN dark matter experiment.” In: *Phys. Rev. D* 101.5 (2020), p. 052002. doi: 10.1103/PhysRevD.101.052002. arXiv: 1802.06039 [astro-ph.IM].

[246] A. Albert et al. “Searching for Dark Matter Annihilation in Recently Discovered Milky Way Satellites with Fermi-LAT.” In: *Astrophys. J.* 834.2 (2017), p. 110. doi: 10.3847/1538-4357/834/2/110. arXiv: 1611.03184 [astro-ph.HE].

[247] H. Abdallah et al. “Search for γ-Ray Line Signals from Dark Matter Annihilations in the Inner Galactic Halo from 10 Years of Observations with H.E.S.S.” In: *Phys. Rev. Lett.* 120.20 (2018), p. 201101. doi: 10.1103/PhysRevLett.120.201101. arXiv: 1805.05741 [astro-ph.HE].

[248] A. Hryczuk, K. Jodlowski, E. Moulin, L. Rinchiuso, L. Roszkowski, E. M. Sessolo, and S. Trojanowski. "Testing dark matter with Cherenkov light - prospects of H.E.S.S. and CTA for exploring minimal supersymmetry." In: (2019). arXiv: 1905.00315 [hep-ph].

[249] H. Abdallah et al. "Search for dark matter annihilations towards the inner Galactic halo from 10 years of observations with H.E.S.S." In: *Phys. Rev. Lett.* 117.11 (2016), p. 111301. doi: 10.1103/PhysRevLett.117.111301. arXiv: 1607.08142 [astro-ph.HE].

[250] B. S. Acharya et al. *Science with the Cherenkov Telescope Array*. WSP, 2018. isbn: 9789813270084. doi: 10.1142/10986. arXiv: 1709.07997 [astro-ph.IM].

[251] R. Allahverdi, B. Dutta, and K. Sinha. "Non-thermal Higgsino Dark Matter: Cosmological Motivations and Implications for a 125 GeV Higgs." In: *Phys. Rev.* D86 (2012), p. 095016. doi: 10.1103/PhysRevD.86.095016. arXiv: 1208.0115 [hep-ph].

[252] O. Matsedonskyi, G. Panico, and A. Wulzer. "Top Partners Searches and Composite Higgs Models." In: *JHEP* 04 (2016), p. 003. doi: 10.1007/JHEP04(2016)003. arXiv: 1512.04356 [hep-ph].

[253] T. Cohen, R. T. D'Agnolo, M. Hance, H. K. Lou, and J. G. Wacker. "Boosting Stop Searches with a 100 TeV Proton Collider." In: *JHEP* 11 (2014), p. 021. doi: 10.1007/JHEP11(2014)021. arXiv: 1406.4512 [hep-ph].

[254] A. Anandakrishnan, J. H. Collins, M. Farina, E. Kuflik, and M. Perelstein. "Odd Top Partners at the LHC." In: *Phys. Rev.* D93.7 (2016), p. 075009. doi: 10.1103/PhysRevD.93.075009. arXiv: 1506.05130 [hep-ph].

[255] S. Kraml, U. Laa, L. Panizzi, and H. Prager. "Scalar versus fermionic top partner interpretations of $t\bar{t}+E_T^{\mathrm{miss}}$ searches at the LHC." In: *JHEP* 11 (2016), p. 107. doi: 10.1007/JHEP11(2016)107. arXiv: 1607.02050 [hep-ph].

[256] S. Banerjee, D. Barducci, G. Bélanger, and C. Delaunay. "Implications of a High-Mass Diphoton Resonance for Heavy Quark Searches." In: *JHEP* 11 (2016), p. 154. doi: 10.1007/JHEP11(2016)154. arXiv: 1606.09013 [hep-ph].

[257] M. Chala. "Direct bounds on heavy toplike quarks with standard and exotic decays." In: *Phys. Rev.* D96.1 (2017), p. 015028. doi: 10.1103/PhysRevD.96.015028. arXiv: 1705.03013 [hep-ph].

[258] J. A. Aguilar-Saavedra, D. E. López-Fogliani, and C. Muñoz. "Novel signatures for vector-like quarks." In: *JHEP* 06 (2017), p. 095. doi: 10.1007/JHEP06(2017)095. arXiv: 1705.02526 [hep-ph].

[259] J. H. Kim and I. M. Lewis. "Loop Induced Single Top Partner Production and Decay at the LHC." In: *JHEP* 05 (2018), p. 095. doi: 10.1007/JHEP05(2018)095. arXiv: 1803.06351 [hep-ph].

[260] H. Alhazmi, J. H. Kim, K. Kong, and I. M. Lewis. "Shedding Light on Top Partner at the LHC." In: *JHEP* 01 (2019), p. 139. doi: 10.1007/JHEP01(2019)139. arXiv: 1808.03649 [hep-ph].

[261] J. H. Kim, S. D. Lane, H.-S. Lee, I. M. Lewis, and M. Sullivan. "Searching for Dark Photons with Maverick Top Partners." In: (2019). arXiv: 1904.05893 [hep-ph].

[262] R. Dermisek, E. Lunghi, and S. Shin. "Hunting for Vectorlike Quarks." In: *JHEP* 04 (2019), p. 019. doi: 10.1007/JHEP04(2019)019. arXiv: 1901.03709 [hep-ph].

[263] R. Benbrik et al. "Signatures of vector-like top partners decaying into new neutral scalar or pseudoscalar bosons." In: (2019). arXiv: 1907.05929 [hep-ph].

[264] *Prospects for measuring Higgs pair production in the channel $H(\to \gamma\gamma)H(\to b\bar{b})$ using the ATLAS detector at the HL-LHC*. Tech. rep. ATL-PHYS-PUB-2014-019. Geneva: CERN, 2014. url: https://cds.cern.ch/record/1956733.

[265] A. M. Sirunyan et al. "Search for Higgs boson pair production in the $\gamma\gamma\mathrm{b\bar{b}}$ final state in pp collisions at $\sqrt{s} = 13$ TeV." In: *Phys. Lett.* B788 (2019), pp. 7–36. doi: 10.1016/j.physletb.2018.10.056. arXiv: 1806.00408 [hep-ex].

[266] M. Cacciari, G. P. Salam, and G. Soyez. "FastJet User Manual." In: *Eur. Phys. J.* C72 (2012), p. 1896. doi: 10.1140/epjc/s10052-012-1896-2. arXiv: 1111.6097 [hep-ph].

[267] R. K. Leane, T. R. Slatyer, J. F. Beacom, and K. C. Y. Ng. "GeV-scale thermal WIMPs: Not even slightly ruled out." In: *Phys. Rev.* D98.2 (2018), p. 023016. doi: 10.1103/PhysRevD.98.023016. arXiv: 1805.10305 [hep-ph].

[268] J. de Blas. "Electroweak limits on physics beyond the Standard Model." In: *EPJ Web Conf.* 60 (2013). Ed. by M. Bosman, A. Juste, M. Martínez, and V. Sorin, p. 19008. doi: 10.1051/epjconf/20136019008. arXiv: 1307.6173 [hep-ph].

[269] A. M. Sirunyan et al. "Search for an excited lepton that decays via a contact interaction to a lepton and two jets in proton-proton collisions at $\sqrt{s} = 13$ TeV." In: (2020). arXiv: 2001.04521 [hep-ex].

[270] J. de Blas, M. Chala, M. Perez-Victoria, and J. Santiago. "Observable Effects of General New Scalar Particles." In: *JHEP* 04 (2015), p. 078. doi: 10.1007/JHEP04(2015)078. arXiv: 1412.8480 [hep-ph].

[271] J. Alcaide, S. Banerjee, M. Chala, and A. Titov. "Probes of the Standard Model effective field theory extended with a right-handed neutrino." In: *JHEP* 08 (2019), p. 031. doi: 10.1007/JHEP08(2019)031. arXiv: 1905.11375 [hep-ph].

[272] L. F. Abbott. "Introduction to the Background Field Method." In: *Acta Phys. Polon. B* 13 (1982), p. 33.

[273] P. Nogueira. “Automatic Feynman Graph Generation.” In: *Journal of Computational Physics* 105.2 (1993), pp. 279–289. issn: 0021-9991. doi: https://doi.org/10.1006/jcph.1993.1074. url: https://www.sciencedirect.com/science/article/pii/S0021999183710740.

[274] T. Hahn. “Generating Feynman diagrams and amplitudes with FeynArts 3.” In: *Comput. Phys. Commun.* 140 (2001), pp. 418–431. doi: 10.1016/S0010-4655(01)00290-9. arXiv: hep-ph/0012260.

[275] T. Hahn and M. Perez-Victoria. “Automatized one loop calculations in four-dimensions and D-dimensions.” In: *Comput. Phys. Commun.* 118 (1999), pp. 153–165. doi: 10.1016/S0010-4655(98)00173-8. arXiv: hep-ph/9807565.

[276] G. Buchalla, A. Celis, C. Krause, and J.-N. Toelstede. “Master Formula for One-Loop Renormalization of Bosonic SMEFT Operators.” In: (Apr. 2019). arXiv: 1904.07840 [hep-ph].

[277] C. Cheung and C.-H. Shen. “Nonrenormalization Theorems without Supersymmetry.” In: *Phys. Rev. Lett.* 115.7 (2015), p. 071601. doi: 10.1103/PhysRevLett.115.071601. arXiv: 1505.01844 [hep-ph].

[278] Z. Bern, J. Parra-Martinez, and E. Sawyer. “Nonrenormalization and Operator Mixing via On-Shell Methods.” In: *Phys. Rev. Lett.* 124.5 (2020), p. 051601. doi: 10.1103/PhysRevLett.124.051601. arXiv: 1910.05831 [hep-ph].

[279] E. E. Jenkins, A. V. Manohar, and P. Stoffer. “Low-Energy Effective Field Theory below the Electroweak Scale: Operators and Matching.” In: *JHEP* 03 (2018), p. 016. doi: 10.1007/JHEP03(2018)016. arXiv: 1709.04486 [hep-ph].

[280] F. Lyonnet and I. Schienbein. “PyR@TE 2: A Python tool for computing RGEs at two-loop.” In: *Comput. Phys. Commun.* 213 (2017), pp. 181–196. doi: 10.1016/j.cpc.2016.12.003. arXiv: 1608.07274 [hep-ph].

[281] E. E. Jenkins, A. V. Manohar, and P. Stoffer. “Low-Energy Effective Field Theory below the Electroweak Scale: Anomalous Dimensions.” In: *JHEP* 01 (2018), p. 084. doi: 10.1007/JHEP01(2018)084. arXiv: 1711.05270 [hep-ph].

[282] D. B. Kaplan and A. Manohar. “Strange Matrix Elements in the Proton from Neutral Current Experiments.” In: *Nucl. Phys. B* 310 (1988), pp. 527–547. doi: 10.1016/0550-3213(88)90090-9.

[283] C. Grojean, E. E. Jenkins, A. V. Manohar, and M. Trott. “Renormalization Group Scaling of Higgs Operators and \Gamma(h -> \gamma \gamma).” In: *JHEP* 04 (2013), p. 016. doi: 10.1007/JHEP04(2013)016. arXiv: 1301.2588 [hep-ph].

[284] K. Fraser and M. Reece. “Axion Periodicity and Coupling Quantization in the Presence of Mixing.” In: *JHEP* 05 (2020), p. 066. doi: 10.1007/JHEP05(2020)066. arXiv: 1910.11349 [hep-ph].

[285] G. G. Raffelt. "Astrophysical axion bounds." In: *Lect. Notes Phys.* 741 (2008). Ed. by M. Kuster, G. Raffelt, and B. Beltran, pp. 51–71. doi: 10.1007/978-3-540-73518-2_3. arXiv: hep-ph/0611350.

[286] J. Ebadi, S. Khatibi, and M. Mohammadi Najafabadi. "New probes for axionlike particles at hadron colliders." In: *Phys. Rev. D* 100.1 (2019), p. 015016. doi: 10.1103/PhysRevD.100.015016. arXiv: 1901.03061 [hep-ph].

[287] M. Bauer, C. Hörner, and M. Neubert. "Diphoton Resonance from a Warped Extra Dimension." In: *JHEP* 07 (2016), p. 094. doi: 10.1007/JHEP07(2016)094. arXiv: 1603.05978 [hep-ph].

[288] K. Choi, S. H. Im, C. B. Park, and S. Yun. "Minimal Flavor Violation with Axion-like Particles." In: *JHEP* 11 (2017), p. 070. doi: 10.1007/JHEP11(2017)070. arXiv: 1708.00021 [hep-ph].

[289] M. Bauer, M. Neubert, S. Renner, M. Schnubel, and A. Thamm. "The Low-Energy Effective Theory of Axions and ALPs." In: *JHEP* 04 (2021), p. 063. doi: 10.1007/JHEP04(2021)063. arXiv: 2012.12272 [hep-ph].

[290] J. Bonilla, I. Brivio, M. B. Gavela, and V. Sanz. "One-loop corrections to ALPs couplings." In: (July 2021). arXiv: 2107.11392 [hep-ph].

[291] M. Carena, I. Low, and C. E. M. Wagner. "Implications of a Modified Higgs to Diphoton Decay Width." In: *JHEP* 08 (2012), p. 060. doi: 10.1007/JHEP08(2012)060. arXiv: 1206.1082 [hep-ph].

[292] G. Passarino and M. J. G. Veltman. "One Loop Corrections for e+ e- Annihilation Into mu+ mu- in the Weinberg Model." In: *Nucl. Phys. B* 160 (1979), pp. 151–207. doi: 10.1016/0550-3213(79)90234-7.

[293] S. Coleman and E. Weinberg. "Radiative Corrections as the Origin of Spontaneous Symmetry Breaking." In: *Phys. Rev. D* 7 (6 1973), pp. 1888–1910. doi: 10.1103/PhysRevD.7.1888. url: https://link.aps.org/doi/10.1103/PhysRevD.7.1888.

[294] M. Laine and A. Vuorinen. *Basics of Thermal Field Theory*. Vol. 925. Springer, 2016. doi: 10.1007/978-3-319-31933-9. arXiv: 1701.01554 [hep-ph].

[295] A. Mazumdar and G. White. "Review of cosmic phase transitions: their significance and experimental signatures." In: *Rept. Prog. Phys.* 82.7 (2019), p. 076901. doi: 10.1088/1361-6633/ab1f55. arXiv: 1811.01948 [hep-ph].

[296] M. D'Onofrio and K. Rummukainen. "Standard model cross-over on the lattice." In: *Phys. Rev. D* 93.2 (2016), p. 025003. doi: 10.1103/PhysRevD.93.025003. arXiv: 1508.07161 [hep-ph].

[297] A. A. Belavin, A. M. Polyakov, A. S. Schwartz, and Y. S. Tyupkin. "Pseudoparticle Solutions of the Yang-Mills Equations." In: *Phys. Lett. B* 59 (1975). Ed. by J. C. Taylor, pp. 85–87. doi: 10.1016/0370-2693(75)90163-X.

[298] G. 't Hooft. "Symmetry Breaking Through Bell-Jackiw Anomalies." In: *Phys. Rev. Lett.* 37 (1976). Ed. by M. A. Shifman, pp. 8–11. doi: 10.1103/PhysRevLett.37.8.

[299] A. A. Anselm and A. A. Johansen. "Baryon nonconservation in standard model and Yukawa interaction." In: *Nucl. Phys. B* 407 (1993), pp. 313–330. doi: 10.1016/0550-3213(93)90060-3.

[300] M. D'Onofrio, K. Rummukainen, and A. Tranberg. "Sphaleron Rate in the Minimal Standard Model." In: *Phys. Rev. Lett.* 113.14 (2014), p. 141602. doi: 10.1103/PhysRevLett.113.141602. arXiv: 1404.3565 [hep-ph].

[301] O. Bertolami, D. Colladay, V. A. Kostelecky, and R. Potting. "CPT violation and baryogenesis." In: *Phys. Lett. B* 395 (1997), pp. 178–183. doi: 10.1016/S0370-2693(97)00062-2. arXiv: hep-ph/9612437.

[302] M. P. L. P. Ramos and J. Páramos. "Baryogenesis in Nonminimally Coupled $f(R)$ Theories." In: *Phys. Rev. D* 96.10 (2017), p. 104024. doi: 10.1103/PhysRevD.96.104024. arXiv: 1709.04442 [gr-qc].

[303] G. Arcadi, M. Dutra, P. Ghosh, M. Lindner, Y. Mambrini, M. Pierre, S. Profumo, and F. S. Queiroz. "The waning of the WIMP? A review of models, searches, and constraints." In: *Eur. Phys. J. C* 78.3 (2018), p. 203. doi: 10.1140/epjc/s10052-018-5662-y. arXiv: 1703.07364 [hep-ph].

[304] B. W. Lee and S. Weinberg. "Cosmological Lower Bound on Heavy-Neutrino Masses." In: *Phys. Rev. Lett.* 39 (4 1977), pp. 165–168. doi: 10.1103/PhysRevLett.39.165. url: https://link.aps.org/doi/10.1103/PhysRevLett.39.165.

[305] J. Rosa. "Introduction to Cosmology." In: 2012.

[306] Y. Hochberg, E. Kuflik, T. Volansky, and J. G. Wacker. "Mechanism for Thermal Relic Dark Matter of Strongly Interacting Massive Particles." In: *Phys. Rev. Lett.* 113 (2014), p. 171301. doi: 10.1103/PhysRevLett.113.171301. arXiv: 1402.5143 [hep-ph].

[307] K. Cheung, C.-W. Chiang, N. G. Deshpande, and J. Jiang. "Constraints on flavor-changing Z' models by B(s) mixing, Z' production, and B(s) —> mu+ mu-." In: *Phys. Lett. B* 652 (2007), pp. 285–291. doi: 10.1016/j.physletb.2007.07.032. arXiv: hep-ph/0604223.

[308] P. Ball and R. Zwicky. "New results on $B \to \pi, K, \eta$ decay formfactors from light-cone sum rules." In: *Phys. Rev. D* 71 (2005), p. 014015. doi: 10.1103/PhysRevD.71.014015. arXiv: hep-ph/0406232.

[309] A. Greljo and D. Marzocca. "High-p_T dilepton tails and flavor physics." In: *Eur. Phys. J. C* 77.8 (2017), p. 548. doi: 10.1140/epjc/s10052-017-5119-8. arXiv: 1704.09015 [hep-ph].

[310] O. Domenech, A. Pomarol, and J. Serra. "Probing the SM with Dijets at the LHC." In: *Phys. Rev. D* 85 (2012), p. 074030. doi: 10.1103/PhysRevD.85.074030. arXiv: 1201.6510 [hep-ph].

[311] J. C. Criado and M. Pérez-Victoria. "Field redefinitions in effective theories at higher orders." In: *JHEP* 03 (2019), p. 038. doi: 10.1007/JHEP03(2019)038. arXiv: 1811.09413 [hep-ph].

[312] J. Martin Camalich, M. Pospelov, P. N. H. Vuong, R. Ziegler, and J. Zupan. "Quark Flavor Phenomenology of the QCD Axion." In: *Phys. Rev. D* 102.1 (2020), p. 015023. doi: 10.1103/PhysRevD.102.015023. arXiv: 2002.04623 [hep-ph].

Appendix A

Mathematical relations

We use the following master integrals thoroughly in this work:

$$\int \frac{\mathrm{d}^{\mathrm{d}}k}{(2\pi)^{\mathrm{d}}} \frac{1}{\left(k^2 - M^2\right)^n} = \frac{(-1)^n \mathrm{i}}{(4\pi)^{\mathrm{d}/2}} \frac{\Gamma(n - \mathrm{d}/2)}{\Gamma(n)} \frac{1}{M^{2n-\mathrm{d}}} \equiv A_n \,, \tag{340}$$

$$\int \frac{\mathrm{d}^{\mathrm{d}}k}{(2\pi)^{\mathrm{d}}} \frac{k^\mu k^\nu}{\left(k^2 - M^2\right)^n} = \frac{1}{2} \frac{(-1)^{n-1} \mathrm{i}}{(4\pi)^{\mathrm{d}/2}} \frac{\Gamma(n - \mathrm{d}/2 - 1)}{\Gamma(n)} \frac{1}{M^{2n-\mathrm{d}-2}} g^{\mu\nu} \equiv B_n g^{\mu\nu} \,, \tag{341}$$

$$\begin{aligned} \int \frac{\mathrm{d}^{\mathrm{d}}k}{(2\pi)^{\mathrm{d}}} \frac{k^\mu k^\nu k^\rho k^\sigma}{\left(k^2 - M^2\right)^n} &= \frac{1}{4} \frac{(-1)^n \mathrm{i}}{(4\pi)^{\mathrm{d}/2}} \frac{\Gamma(n - \mathrm{d}/2 - 2)}{\Gamma(n)} \frac{1}{M^{2n-\mathrm{d}-4}} \left(g^{\mu\nu} g^{\rho\sigma} + g^{\mu\rho} g^{\nu\sigma} + g^{\mu\sigma} g^{\nu\rho}\right) \\ &\equiv C_n \left(g^{\mu\nu} g^{\rho\sigma} + g^{\mu\rho} g^{\nu\sigma} + g^{\mu\sigma} g^{\nu\rho}\right) \,, \end{aligned} \tag{342}$$

where $\mathrm{d} = 4 - 2\epsilon$ is the number of spacetime dimensions and we use the metric sign convention $g^{\mu\nu} = \mathrm{diag}\,(1, -1, -1, -1)$. At $\mathcal{O}(1/\epsilon)$, these integrals lead to:

$$A_2 = \frac{\mathrm{i}}{16\pi^2 \epsilon} + (\text{finite}) \,, \tag{343}$$

$$B_3 = \frac{\mathrm{i}}{64\pi^2 \epsilon} + (\text{finite}) \,, \tag{344}$$

$$C_4 = \frac{\mathrm{i}}{384\pi^2 \epsilon} + (\text{finite}) \,. \tag{345}$$

For expanding in external momentum, we use:

$$\frac{1}{(k+p)^2 - M^2} = \frac{1}{k^2 - M^2} \left[1 - \frac{2k \cdot p + p^2}{k^2 - M^2} + \frac{4(k \cdot p)^2}{(k^2 - M^2)^2}\right] + \mathcal{O}(p^3) \,. \tag{346}$$

The following relations involving the generators of $SU(N)$ are also employed in several results:

$$\mathrm{Tr}\left[T^a T^b\right] = T_F^{(N)} \delta_{ab}\,, \tag{347}$$

$$\sum_a \left(T^a T^a\right)_{ij} = C_F^{(N)} \delta_{ij}\,, \tag{348}$$

$$\sum_{c,d} f_{acd} f_{bcd} = C_A^{(N)} \delta_{ab}\,, \tag{349}$$

$$\sum_a T^a_{ij} T^a_{k\ell} = \frac{1}{2}\left(\delta_{i\ell}\delta_{jk} - \frac{1}{N}\delta_{ij}\delta_{k\ell}\right), \tag{350}$$

where $T_F^{(N)} = \frac{1}{2}$, $C_A^{(N)} = N$ and $C_F^{(N)} = \frac{N^2-1}{2N}$.

Finally, in identities involving the Levi-Civita tensor, we use the convention $\epsilon^{0123} = 1$. The following relations hold, in four dimensions[1]:

$$\mathrm{Tr}\left[\gamma^\alpha \gamma^\beta \gamma^\sigma \gamma^\delta \gamma^5\right] = -4\mathrm{i}\epsilon^{\alpha\beta\sigma\delta}\,, \tag{351}$$

$$\epsilon^{\alpha\beta\gamma\delta}\gamma_\beta\gamma_\gamma\gamma_\delta = 6\mathrm{i}\gamma^\alpha\gamma^5\,, \tag{352}$$

$$\epsilon^{\alpha\beta\gamma\delta}\epsilon^{\mu}_{\beta\gamma\delta} = -6\mathrm{i}g^{\alpha\mu}\,, \tag{353}$$

$$\epsilon^{\alpha\beta\gamma\delta}\gamma_\gamma\gamma_\delta = -\mathrm{i}[\gamma^\alpha, \gamma^\beta]\gamma^5\,. \tag{354}$$

The last of these relations furthermore implies:

$$\sigma^{\alpha\beta}\gamma^5 = \frac{\mathrm{i}}{2}\epsilon^{\alpha\beta\gamma\delta}\sigma_{\gamma\delta}\,, \tag{355}$$

where $\sigma^{\mu\nu} \equiv \mathrm{i}[\gamma^\mu, \gamma^\nu]/2 = \mathrm{i}(\gamma^\mu\gamma^\nu - g^{\mu\nu})$ and $\{\gamma^\mu, \gamma^\nu\} = 2g^{\mu\nu}$.

[1] Extensions to other dimensions can be found, for example, in Ref. [184].

Appendix B

One loop functions

The loop functions contributing to the Higgs to di-photon partial decay width, that we use in section 5.2 in the context of the triplet model, read [291]:

$$A_0(x) = -x^2\left[x^{-1} - f(x^{-1})\right], \tag{356}$$

$$A_{1/2}(x) = 2x^2\left[x^{-1} + (x^{-1} - 1)f(x^{-1})\right], \tag{357}$$

$$A_1(x) = -x^2\left[2x^{-2} + 3x^{-1} + 3(2x^{-1} - 1)f(x^{-1})\right], \tag{358}$$

for spin-0 (the EW triplet that we denote by Φ), spin-1 (the W boson) and spin-$1/2$ (the top quark) particles. In the case we are interested, where $m_H < 2m_i$ ($i = m_W,\ m_t,\ m_\Phi$),

$$f(x) = \arcsin^2\sqrt{x}\,. \tag{359}$$

In the remaining of this section, we compute explicitly the new physics contribution triggered by $\lambda_{H\Phi}$, defined in equation 123, to $h \longrightarrow \gamma\gamma$. There are two diagrams contributing to this process; see figure 38. The corresponding amplitude reads:

$$\begin{aligned} \mathrm{i}\mathcal{M} = \epsilon_\mu(p_1)\epsilon_\nu(p_2)(-\mathrm{i}\lambda_{H\Phi}v)\int \frac{d^4q}{(2\pi)^4}\Bigg\{ & \frac{\mathrm{i}^2\left(2\mathrm{i}e^2 g^{\mu\nu}\right)}{\left[(q+p_1+p_2)^2 - m_\Phi^2\right]\left[q^2 - m_\Phi^2\right]} \\ & +2\frac{\mathrm{i}^3\,(-\mathrm{i}e)^2\,(2q+p_1)^\mu\,(2q-p_2)^\nu}{\left[(q+p_1)^2 - m_\Phi^2\right]\left[(q-p_2)^2 - m_\Phi^2\right]\left[q^2 - m_\Phi^2\right]}\Bigg\}\,. \end{aligned} \tag{360}$$

This expression can be further simplified to

$$\mathrm{i}\mathcal{M} = 2\lambda_{H\Phi}ve^2\left[I_1 + I_2\right]\,, \tag{361}$$

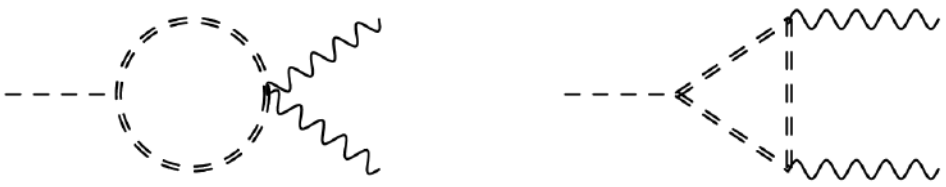

Figure 38: Scalar contributions to $h \to \gamma\gamma$. The momenta of the outgoing photons are labeled as p_1 and p_2. The double line denotes $\phi^\pm$.

where

$$I_2 \equiv \int \frac{d^4q}{(2\pi)^4} \frac{-g^{\mu\nu}}{\left[(q+p_1+p_2)^2 - m_\Phi^2\right]\left[q^2 - m_\Phi^2\right]}, \tag{362}$$

$$I_3 \equiv \int \frac{d^4q}{(2\pi)^4} \frac{4q^\mu q^\nu}{\left[(q+p_1)^2 - m_\Phi^2\right]\left[(q-p_2)^2 - m_\Phi^2\right]\left[q^2 - m_\Phi^2\right]}. \tag{363}$$

Next, we use the Passarino-Veltman Reduction [292] to simplify these tensor integrals, in particular to write I_3 (with $r = 2$ powers of the loop momentum in the numerator) as a linear combination of scalar functions (with $r = 0$). The former admits a generic expansion of the form:

$$C^{\mu\nu} = C^{00} g^{\mu\nu} + C^{11}(p_1^\mu p_1^\nu) + C^{12}(p_1^\mu p_2^\nu + p_1^\nu p_2^\mu) + C^{22}(p_2^\mu p_2^\nu). \tag{364}$$

A similar expansion exists for I_2, the scalar functions being denoted by B in this case. Using this reduction, we find:

$$I_2 = -g^{\mu\nu}\frac{\mathrm{i}B_0(\Delta_2)}{16\pi^2} \quad \text{and} \quad I_3 = 4\frac{\mathrm{i}\left[C_{00}(\Delta_3)g^{\mu\nu} + C_{12}(\Delta_3)p_2^\mu p_1^\nu\right]}{16\pi^2}, \tag{365}$$

using the same notation as in here[1]. The Δ-parameters are functions of the new variables of integration x and y: $\Delta_2 = (x^2 - x)m_H^2 + m_\Phi^2$, while $\Delta_3 \equiv -xym_H^2 + m_\Phi^2$. Note that all other components in equation 364 vanish due to the Ward identity. Plugging these expressions into the amplitude, we obtain:

$$\begin{aligned} \mathrm{i}\mathcal{M} &= \frac{2\mathrm{i}\lambda_{H\Phi}v e^2}{16\pi^2}\left[-g^{\mu\nu}B_0 + 4C_{00}g^{\mu\nu} + 4C_{12}p_1^\nu p_2^\mu\right] \\ &= \frac{2\mathrm{i}\lambda_{H\Phi}v e^2}{16\pi^2}\left[g^{\mu\nu}\left(\Delta_\epsilon - \int_0^1 dx \log\frac{\Delta_2}{\mu^2}\right) + g^{\mu\nu}\left(\Delta_\epsilon - 2\int_0^1\int_0^{1-x} dxdy \log\frac{\Delta_3}{\mu^2}\right)\right. \\ &\quad \left. + 4p_1^\nu p_2^\mu\left(-\int_0^1\int_0^{1-x} dxdy\frac{xy}{\Delta_3}\right)\right], \end{aligned} \tag{366}$$

[1] https://www.ugr.es/~jillana/SM/sm1.pdf.

where the divergences (parameterized by Δ_ϵ) and the μ-scale dependence cancel out. Therefore, we end up with

$$\mathrm{i}\mathcal{M} = \frac{2\mathrm{i}\lambda_{H\Phi}ve^2}{16\pi^2}\left[g^{\mu\nu}(X-2Y) + 4p_1^\nu p_2^\mu Z\right], \tag{367}$$

where

$$X \equiv \int dx \log\Delta_2\,, \quad Y \equiv \int\int dxdy \log\Delta_3 \quad \text{and} \quad Z \equiv \int\int dxdy\frac{xy}{\Delta_3}\,. \tag{368}$$

In turn, the squared amplitude reads:

$$\begin{aligned}
|\mathrm{i}\mathcal{M}|^2 &= \left(\frac{2\lambda_{H\Phi}ve^2}{16\pi^2}\right)^2\left[g^{\mu\nu}g_{\mu\nu}(X-2Y)^2 + 8p_1\cdot p_2(X-2Y)Z\right] \\
&= \left(\frac{2\lambda_{H\Phi}ve^2}{16\pi^2}\right)^2 4\left[(X-2Y)(X-2Y+m_H^2Z)\right] \\
&= \left(\frac{2\lambda_{H\Phi}ve^2}{16\pi^2}\right)^2 4\mathbf{A}_0^2(\tau)\,.
\end{aligned} \tag{369}$$

In the last line, we wrote the X, Y, Z integrals as a function of $\tau = 4m_\Phi^2/m_H^2$ and

$$\mathbf{A}_0(\tau) \equiv \frac{1}{\sqrt{2}}\left\{1 - \frac{\tau}{2}\left[\mathrm{Li}_2(z) + \mathrm{Li}_2(\bar{z})\right]\right\}\,, \quad \text{where} \quad z = \frac{2\left(1+\mathrm{i}\sqrt{\tau-1}\right)}{\tau}\,. \tag{370}$$

The decay width in the rest frame of the Higgs particle is given by

$$\Gamma(h\to\gamma\gamma) = \frac{1}{8\pi}\frac{|\overrightarrow{p_1}|}{m_H^2}\frac{1}{2}\left|\mathrm{i}\mathcal{M}\right|^2\,, \tag{371}$$

where $|\overrightarrow{p_1}| = m_H/2$. Plugging in equation 369, we finally obtain:

$$\Gamma\left(h\to\gamma\gamma\right) = \left(\lambda_{H\Phi}v\right)^2\frac{\alpha_{\mathrm{em}}^2}{32\pi^3 m_H}\mathbf{A}_0^2(\tau)\,, \tag{372}$$

which (although not apparently) agrees with the scalar contribution in equation 127.

Appendix C

Effective potential

C.1 At zero temperature

Let us consider a self-interacting $\mathbb{Z}_2$-symmetric scalar field theory, for simplicity. The effective potential at one-loop can be computed as

$$V = V_{\text{tree}} + \Delta V_{\text{CW}}\,, \tag{373}$$

where the first piece is the tree level potential

$$V_{\text{tree}} = \frac{1}{2}m^2\phi^2 + \frac{\lambda}{4!}\phi^4\,, \tag{374}$$

while the second one denotes the one-loop correction to V_{tree}, at zero temperature, as computed by Coleman and Weinberg [293]. The latter corresponds to an infinite series of 1PI diagrams evaluated at zero external momenta. An arbitrary diagram in this series contributes to ΔV_{CW} with

$$\underbrace{(-\mathrm{i}\lambda)^n}_{n\text{ vertices}} \times \underbrace{\mathrm{i}^n(p^2-m^2)^{-n}}_{n\text{ propagators}} \times \underbrace{\phi^{2n}}_{2n\text{ external legs}} \times \underbrace{(1/2)^n}_{\text{Bose statistics}} \times \underbrace{1/2n}_{\text{symmetry factor}}\,. \tag{375}$$

Above, the Bose-Einstein statistics factor takes into account that the exchange of two external lines in the same vertex does not produce a new graph; the symmetry factor comes from reflection and $\mathbb{Z}_n$ symmetries that act on the n-polygon in the 1PI expansion.

To study the form of the effective potential, we split the scalar field into a background plus a quantum fluctuation $\phi = \phi + \phi^q$, so that only the latter propagates internally. Making this replacement in equation 374, we obtain an effective mass for the quantum modes, $m^2_{\text{eff}} = m^2 + \lambda\phi^2/2$. Using the background

field and gathering the factors in equation 375, we find that

$$\begin{aligned}\Delta V_{\text{CW}} &= \mathrm{i}\sum_{n=1}^{\infty}\int\frac{d^4p}{(2\pi)^4}\frac{1}{2n}\left[\frac{\lambda\phi^2/2}{p^2-m^2}\right]^n \\ &= -\frac{\mathrm{i}}{2}\int\frac{d^4p}{(2\pi)^4}\log\left[1-\frac{\lambda\phi^2/2}{p^2-m^2}\right] \\ &= -\frac{\mathrm{i}}{2}\int\frac{d^4p}{(2\pi)^4}\log\left[p^2-m_{\text{eff}}^2\right],\end{aligned} \tag{376}$$

neglecting a field independent term (the second one in the expansion $\log x_1/x_2 = \log x_1 - \log x_2$).

Our final potential is however UV divergent [209]. To see this clearly, we can compute the first derivative of the potential with respect to the effective mass using dimensional regularization in $\mathrm{d} = 4-2\epsilon$ spacetime dimensions:

$$\begin{aligned}\frac{\partial\Delta V_{\text{CW}}}{\partial m_{\text{eff}}^2} &= \frac{\mathrm{i}}{2}\mu^{2\epsilon}\int\frac{d^{\mathrm{d}}p}{(2\pi)^{\mathrm{d}}}\frac{1}{p^2-m_{\text{eff}}^2} \\ &= -\frac{1}{32\pi^2}m^2(\phi)\left[\frac{1}{\epsilon}+1-\gamma_E+\log 4\pi+2\log\frac{m_{\text{eff}}}{\mu}\right]+O(\epsilon),\end{aligned} \tag{377}$$

where the μ-scale was introduced to make the effective coupling adimensional for any d, that is $\lambda \to \mu^{2\epsilon}\lambda$. In the last line, we have expanded equation 340 around $\epsilon \approx 0$, γ_E being the Euler-Mascheroni constant. Integrating equation 377 with respect to the mass, we obtain:

$$\Delta V_{\text{CW}} = \frac{m_{\text{eff}}^4}{64\pi^2}\left[-\left(\frac{1}{\epsilon}+\frac{3}{2}-\gamma_E+\log 4\pi\right)+\log\frac{m_{\text{eff}}^2}{\mu^2}\right]. \tag{378}$$

Finally, in the $\overline{\text{MS}}$ renormalization scheme, we can drop all the terms in parenthesis which are absorbed by the relevant counterterms. Therefore, the final expression for the full one-loop renormalized potential is

$$\Delta V_{\text{CW}} = \frac{m_{\text{eff}}^4}{64\pi^2}\left[-\frac{3}{2}+\log\frac{m_{\text{eff}}^2}{\mu^2}\right]. \tag{379}$$

C.2 At finite temperature

To derive the finite temperate corrections to the effective potential, let us start by considering the harmonic oscillator whose Hamiltonian is $\hat{H} = \epsilon(a^\dagger a + 1/2)$, with $\epsilon \equiv \hbar\omega$ being (twice) the ground state energy. To describe the statistics of this system in thermal equilibrium with a heat bath, the most fundamental quantity to compute is the partition function [294]

$$Z \equiv \text{Tr}\left[e^{-\beta\hat{H}}\right] = \sum_{n=0}^{\infty}\left\langle n|e^{-\beta\hat{H}}|n\right\rangle = \sum_{n=0}^{\infty}e^{-\beta\epsilon\left(n+\frac{1}{2}\right)} = \frac{e^{-\beta\epsilon/2}}{1-e^{-\beta\epsilon}}, \tag{380}$$

where $\beta \equiv \frac{1}{T}$. It follows that the free energy of the system is

$$F \equiv -T \log Z = \frac{\epsilon}{2} + T \log\left(1 - e^{-\beta\epsilon}\right). \tag{381}$$

To study the scalar field dynamics in a thermal bath, we can simply extend the previous analysis for a collection of harmonic oscillators, by replacing $\epsilon \longrightarrow \epsilon_k \equiv \sqrt{k^2 + m_{\text{eff}}^2}$. In this case, the partition function reads:

$$Z_\phi = \Pi_k Z^k = \Pi_k \exp\left\{-\frac{1}{T}\left[\frac{\epsilon_k}{2} + T \log\left(1 - e^{-\beta\epsilon_k}\right)\right]\right\}; \tag{382}$$

while the free energy density is

$$\begin{aligned} f_\phi = \lim_{V\to\infty} \frac{F_\phi}{V} &= \lim_{V\to\infty} \frac{1}{V} \sum_k \left[\frac{\epsilon_k}{2} + T \log\left(1 - e^{-\beta\epsilon_k}\right)\right] \\ &= \int \frac{d^{\mathrm{d}_s}\vec{k}}{(2\pi)^{\mathrm{d}_s}} \left[\frac{\epsilon_k}{2} + T \log\left(1 - e^{-\beta\epsilon_k}\right)\right]. \end{aligned} \tag{383}$$

The first term in the equation above is UV divergent and can be absorbed by a proper counterterm. The interesting phenomena are determined by the temperature-dependent term, that we denote by ΔV_T. Defining $y = k/T$, we can write it (in $d_s = 3$ spatial dimensions) as

$$\Delta V_T = \frac{T^4}{2\pi^2} \int_0^\infty \mathrm{d}y\, y^2 \log\left(1 - e^{-\sqrt{y^2 + \frac{m_{\text{eff}}^2}{T^2}}}\right), \tag{384}$$

which admits the following high-temperature expansion [294]:

$$\Delta V_T(m) = -\frac{\pi^2 T^4}{90} + \frac{m_{\text{eff}}^2 T^2}{24} - \frac{m_{\text{eff}}^3 T}{12\pi} + O(m_{\text{eff}}^4). \tag{385}$$

Using the expression for the effective mass, it becomes clear that at $T \gg m$, the zero-temperature masses get replaced by the thermal ones, $\sim \sqrt{\lambda} T$.

C.3 Phase transitions

Let us now study the implications of the evolution of the scalar potential in equation 374, which is invariant under a $\mathbb{Z}_2$ symmetry. At sufficiently high temperatures, the $O(T^2)$ corrections that we derived in the last section dominate, making the ϕ^2 term positive. In this case, the minima of the potential are all vanishing and therefore the potential is symmetric. As the temperature goes down, the main contribution to the potential arises instead from the Coleman-Weinberg corrections, which can make $m_{\text{eff}}^2 < 0$. Computing the minima for this case, we find that $\langle\phi\rangle \equiv v = \pm\sqrt{-6m_{\text{eff}}^2/\lambda}$. Therefore, the symmetry is spontaneously broken by the choice of the new vacuum.

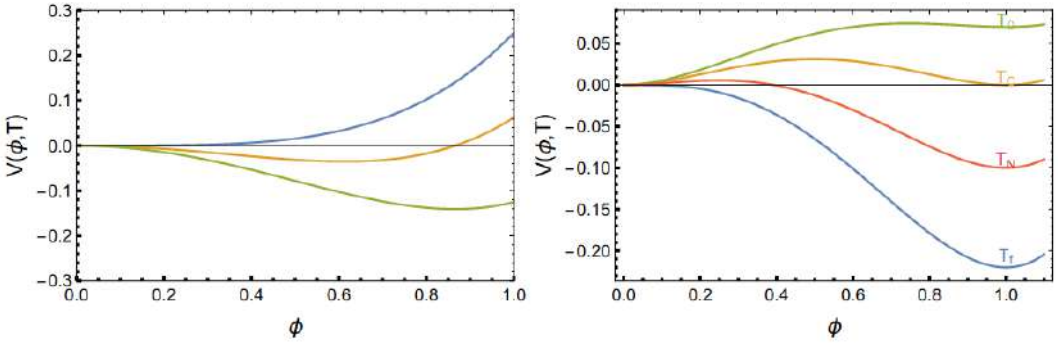

Figure 39: (Left) Example of a potential leading to a second order PT (taken from Ref. [295]). The evolution of the temperature should be read from the top to the bottom. (Right) The same for a first order PT. The second minimum is developed at $T \approx T_0$; it becomes degenerate with the origin at $T \approx T_c$. When the tunneling rate is larger than the Hubble rate, at $T \approx T_N$, the unbroken phase is effectively converted into the broken one. The PT is completed at T_f, when the volume fraction of the symmetric phase is negligible.

Whenever a new ground state becomes energetically favored, the Universe undergoes a PT. The corresponding properties are dependent on the details of the effective potential, in particular the interplay between each term in equation 385. The LO term in this equation (neglecting field-independent contributions) corrects the potential as follows:

$$V \sim \frac{1}{2}\left(m^2 + \frac{\lambda}{24}T^2\right)\phi^2 + \frac{\lambda}{4!}\phi^4 \,. \tag{386}$$

Therefore, the vacuum is symmetric only at temperatures above $T_c \sim \sqrt{-24m^2/\lambda}$. Below this critical value, the field changes the VEV smoothly: it rolls down continuously to the new minimum, maintaining thermal equilibrium. This scenario describes a second order PT; see the left panel of figure 39.

The NLO term in the high-temperature expansion, on the other hand, leads to:

$$V \sim \frac{T^2}{2}\frac{\lambda}{4!}\phi^2 - \frac{T}{6\pi}\left(\frac{\lambda}{2}\right)^{3/2}\phi^3 + \frac{\lambda}{4!}\phi^4 \,, \tag{387}$$

where we considered the limit $m \to 0$. Here, the cubic term produces a secondary minimum besides the one at $\phi = 0$, which induces a first order PT. This scenario is represented in the right panel of figure 39, where it can be seen that the evolution of the potential creates a barrier between the unbroken and broken phases. This PT is abrupt and happens out-of-equilibrium.

In this last case, the new minimum occurs when the cubic and quartic terms become comparable, that is for $\phi \sim \sqrt{\lambda}T/\pi$. It is, however, well known that the loop expansion parameter at finite temperature is [294]

$$\frac{\lambda T}{\pi m_{\text{eff}}} \sim \frac{\lambda T}{\pi\sqrt{\lambda}\phi} \sim \mathcal{O}(1) \,, \tag{388}$$

at this transition point. Therefore, perturbative methods are not reliable and we cannot trust that such first order PT had actually occurred. (To integrate light modes, non-perturbative methods are usually employed [209].)

Similarly, in the SM, the observed Higgs mass is such that a perturbative analysis is not reliable. From lattice calculations, we know that the EW PT is actually a crossover [296], leading to a radical but continuous change of the ground state of the theory.

Appendix D

Sakharov conditions for baryogenesis

In this section, we discuss the requirement of the three conditions, proposed by A.D. Sakharov [2], to generate a matter-antimatter asymmetry in the Universe.

D.1 Baryon number violation

Our Universe is assumed to have started as a neutral and symmetric system, free of any excess of charges. (Even if there were some unbalanced net, it would have been completely washout during inflation). Since we observe a baryon asymmetry, baryon number must have been violated at some point in the cosmological history.

In the SM, there are field configurations violating this B-number. They are called instantons (at temperature $T = 0$) and sphalerons (at $T \neq 0$). To see how they arise, let us explore the connection between the chiral anomaly and the topological nature of the EW vacua.

Consider a volume in $\mathrm{d} = 4$ euclidean dimensions, with the corresponding border $\partial V^4 \sim S^3$. A pure vacuum is $W^I_\mu = 0$ on the border and everywhere in V^4. However, taking a gauge-rotated vacuum as the boundary condition instead, it was found that there are non-trivial solutions inside the sphere [297]:

$$\frac{g_2^2}{32\pi^2}\int_{V^4} W^I_{\mu\nu}\widetilde{W}^{\mu\nu I}\mathrm{d}^4x = \Delta q\,; \tag{389}$$

with Δq being a topological quantum charge. Such charge characterizes the homotopic map between the gauge group $SU(2) \approx S^3$ and the coordinate space at the border which, in this case, is non-trivial; explicitly, $\pi^3(S_3) = \mathbb{Z}$. These integers cannot be deformed into one another, particularly a non-vanishing q cannot be set to zero. In this way, it was found that the EW ground state is infinitely degenerate and

made out of topologically distinct vacua, separated by potential barriers [25]. The instanton is the field configuration that connects two vacua differing by a unit of topological charge.

The connection to the chiral anomaly and the consequent impact on fermion interactions was discovered by Gerard 't Hooft [298]. It relies on the Bell-Jackiw anomaly equation [20],

$$\partial_\mu J^{\mu 5} = \frac{n_G g_2^2}{16\pi^2} W^I_{\mu\nu} \widetilde{W}^{\mu\nu I} \,. \tag{390}$$

Note that the baryon current can be expanded in terms of LH and RH currents, $J^\mu_B \sim J^\mu_L + J^\mu_R$, each including a vector and an axial part. Since the W interacts only with the LH fermions, the axial divergence in J_L is not canceled, which implies that the baryon current is anomalous as well; in fact, $\Delta Q^5 = \Delta B$ [299]. This argument, together with equations 389 and 390, shows that the instanton mediates processes leading to $\Delta B \propto n_G$. We cannot calculate such processes perturbatively, as signaled by the presence of the gauge coupling in the numerator of equation 389, which appears in the instanton action as $S = -8\pi^2/g_2^2$ [25]. The (tunneling) probability to evolve between adjacent vacua is correspondingly $\sim e^{-8\pi^2/g_2^2}$. Therefore, the $\Delta B \neq 0$ processes are extremely suppressed. This is compatible with the non-observation of proton decay.

At finite temperature, however, the field can surpass the high-energy barrier even classically, due to thermal fluctuations. The field configuration at the top of the barrier is the so-called sphaleron. The rate of B-violation per unit time per unit volume is given by [209]:

$$\Gamma_0 \sim (\alpha_2 T)^4 \,, \qquad \text{at } T > T_c \,; \tag{391}$$

$$\Gamma \sim \Gamma_0 e^{-E_{\text{sph}}(T)/T} \,, \qquad \text{at } T < T_c \,, \tag{392}$$

where the sphaleron energy, corresponding to the height of the barrier between the degenerate minima, is $E_{\text{sph}}/T_c \sim v_c/T_c$. (We adopt the same nomenclature used in the previous chapter, namely T_c is the critical temperature for the EW PT.) Detailed calculations comparing the Boltzmann suppression rate with the expansion rate of the Universe show that sphaleron processes switch off after the EW PT, at $T \sim 100$ GeV [300].

D.2 C and CP violation

These discrete symmetries interchange matter with antimatter. Therefore, their violation is also a requirement to generate a baryon asymmetry in the early Universe.

Assume baryon number violation and that there is, for example, an exotic particle X decaying into the SM fermions in the following processes:

$$X \to qq \quad \text{and} \quad X \to ql \,; \tag{393}$$

and that such particle exists in equal number as the corresponding antiparticle ($n_X = n_{\overline{X}}$). The fact that the final states in equation 393 have different baryon charges makes it clear that X violates baryon number. If charge conjugation (C) is a symmetry of the theory, the rates of these and the conjugated processes are equal, namely

$$\Gamma(X \to q_L q_L) = \Gamma(\overline{X} \to \overline{q_L q_L}) \,. \tag{394}$$

So, baryon number is being created at the same rate it is destroyed and the Universe remains baryon symmetric.

Suppose now C is no longer a symmetry, but CP is. Then, although equation 394 no longer holds, the following

$$\Gamma(X \to q_L q_L) + \Gamma(X \to q_R q_R) = \Gamma(\overline{X} \to \overline{q_L q_L}) + \Gamma(\overline{X} \to \overline{q_R q_R}) \tag{395}$$

does. While a left-right asymmetry might be created, we will end up with the same number of quarks and antiquarks, with no possibility to generate a baryon excess.

This shows that breaking one of these discrete symmetries is not enough. Both C and CP must be violated together in any successful model for baryogenesis.

D.3 Departure from thermal equilibrium

Finally, a departure from thermal equilibrium is also necessary. This can be seen by acting with the charge conjugation, parity and time reversal (CPT) symmetries on the thermal average net of baryon number produced (assuming that the two conditions D.1 and D.2 hold):

$$\begin{aligned} \langle B \rangle_T &= \mathrm{Tr}\left[e^{-\beta H} B\right] \\ &= \mathrm{Tr}\left[(CPT)(CPT)^{-1} e^{-\beta H} B\right] \\ &= \mathrm{Tr}\left[e^{-\beta H} (CPT)^{-1} B (CPT)\right] \\ &= -\langle B \rangle_T \,, \end{aligned} \tag{396}$$

where we used the fact that any CPT transformation commutes with the Hamiltonian H describing our Universe. Therefore, any excess of baryons that survives must have been generated out-of-equilibrium.

(We remark that this requirement can be evaded in string theories leading to the spontaneous breaking of CPT in the very primordial Universe [301] or non-standard cosmologies where gravity is coupled to a CPT-violating baryon current [302].)

Appendix E

The WIMP and other miracles

In this section, we briefly review the WIMP paradigm [303], the most common mechanism of DM production explored in the literature and in the present work.

The relic abundance of WIMPs is set thermally by $2 \longrightarrow 2$ annihilations, which, at some point in the Universe history, freeze out [304], making the DM decouple from the thermal bath. The onset condition for this decoupling is:

$$\Gamma_{2\to 2} \sim n_{\mathrm{DM}} \langle \sigma v \rangle \sim H \approx \sqrt{g_*} \frac{T^2}{M_P}, \tag{397}$$

during the radiation era. At the temperature of the matter-radiation equality, T_{eq}, the thermal energy density of matter is $\rho_{\mathrm{matter}} \approx \rho_{\mathrm{DM}} = \rho_\gamma \sim T_{\mathrm{eq}}^4$, where ρ_γ is the energy density of photons in thermal equilibrium and we neglected that of baryons, since $\rho_b \equiv \rho_{\mathrm{DM}}/\zeta \approx \rho_{\mathrm{DM}}/5$. Using this relation, we can obtain the particle number density of DM at the freeze out temperature, T_{F}, as

$$n_{\mathrm{DM}}(T_{\mathrm{F}}) \sim n_{\mathrm{DM}}(T_{\mathrm{eq}}) \left(\frac{T_{\mathrm{F}}}{T_{\mathrm{eq}}}\right)^3 \sim \frac{\rho_{\mathrm{DM}}(T_{\mathrm{eq}})}{m_{\mathrm{DM}}} \left(\frac{T_{\mathrm{F}}}{T_{\mathrm{eq}}}\right)^3 \sim \frac{m_{\mathrm{DM}}^2}{x_F^3} T_{\mathrm{eq}}, \tag{398}$$

where we assumed, in the first (second) equality, that the DM behaves as radiation (matter) [305]. We have furthermore defined $x \equiv m_{\mathrm{DM}}/T$. Plugging this expression into equation 397 and parameterizing the annihilation cross section as $\langle \sigma v \rangle \equiv \lambda_{\mathrm{ann}}^2/m_{\mathrm{DM}}^2$, we find:

$$m_{\mathrm{DM}} \sim \lambda_{\mathrm{ann}} \sqrt{T_{\mathrm{eq}} M_P} \sim \lambda_{\mathrm{ann}} (30\ \mathrm{TeV}), \tag{399}$$

using that $T_{\mathrm{eq}} = \zeta m_p \eta / c \approx 0.8$ eV [306], with $c \equiv (\zeta/1+\zeta)\,\frac{3}{4}(g_{*,\mathrm{eq}}/g_{*S,\mathrm{eq}}) \approx 5/8$. Here, m_p is the proton mass, η is the baryon-to-entropy ratio, and $g_{*(S)}$ is the energy (entropy) effective number of relativistic $d.o.f.$. The emergence of the weak scale in the DM problem, taking the effective coupling to be

of order weak, $\lambda_{\text{ann}} \sim 1/30$, is the so-called "WIMP miracle". It is an alternative motivation, besides the HP, for new physics around the TeV scale.

We should remark that other "miracles" also occur for different DM candidates: for example, if they scatter via $2 \longrightarrow 3$ processes, the strong rather than the weak scale emerges; in this case, strongly-interacting massive particles (SIMPs) with $\lambda_{\text{ann}} \lesssim 1$ and $m_{\text{DM}} \sim m_p$ are expected instead [306]. The value of x_F — which can be obtained by inserting the particle density distribution of a cold species, $n^2 \propto \left(m_{\text{DM}}\right)^3 e^{-2x_F}$, in equation 397 — depends logarithmically on the model parameters, so it typically takes similar values for several models including this and the WIMP case, $x_F \sim 20$.

Appendix F

B-meson decay widths

In the present section, we compute the full decay widths of the B-meson relevant for the discussion in section 5.3; we follow the notation therein.

The process $B_s^0 \to a_1 a_2$ is depicted in the left panel of figure 18. Using the partial decay rate formula for two-body decays in Ref. [13], assuming that the B is in its rest frame, we obtain:

$$\Gamma = \frac{f_B^2}{16\pi m_V^4} \left(g_{sb} g_{12}\right)^2 \frac{\left(m_1^2 - m_2^2\right)^2}{m_B} \mathcal{K}\left(\frac{m_1}{m_B}, \frac{m_2}{m_B}\right), \tag{400}$$

with

$$\mathcal{K}(x,y) = \left[x^4 + (1-y^2)^2 - 2x^2(1+y^2)\right]^{1/2} \tag{401}$$

and $f_B \sim 0.23$ GeV [307]. All other parameters are defined in equation 165 and in the text that follows it.

On the other hand, the amplitude for $B_s^0 \to a_1 a_1 a_1$ reads:

$$\mathcal{M} = 2 g_{sb} g_{12} \frac{f_B m_{12}}{m_V^2} \left[\frac{q_{12}^2 - m_1^2}{q_{12}^2 - m_2^2} + \frac{q_{23}^2 - m_1^2}{q_{23}^2 - m_2^2} + \frac{q_{13}^2 - m_1^2}{q_{13}^2 - m_2^2}\right], \tag{402}$$

where $q_{12}^2 = (p_1 + p_2)^2$, $q_{23}^2 = (p_2 + p_3)^2$ and $q_{13}^2 = (p_1 + p_3)^2 = 3m_1^2 + m_B^2 - q_{12}^2 - q_{23}^2$. Here, p_1 and p_2 are the momenta of the two a_1 particles connected to a_2, which is assumed to be off-shell, and p_3 is the momentum of the remaining a_1. Using the partial decay rate formula for three-body decays in Ref. [13] and integrating over q_{23}^2, we obtain:

$$\frac{d\Gamma}{dq_{12}^2} = \frac{\left(g_{sb} g_{12}\right)^2 m_2^2}{384\pi^3 m_B^3} \left(\frac{f_B m_{12}}{m_V^2}\right)^2 F\left[\frac{m_1}{m_2}, \frac{m_B}{m_2}, \frac{q_{12}}{m_2}, \frac{q_{23}}{m_2}\right]_{(q_{23}^2)^{\min}}^{(q_{23}^2)^{\max}}; \tag{403}$$

with

$$
\begin{aligned}
F(x,y,w,v) = &\left(1-x^2\right)^2\left[\frac{1}{1-v^2}+\frac{1}{3x^2+y^2-w^2-v^2-1}\right]+\frac{v^2\left(2+x^2-3w^2\right)^2}{(w^2-1)^2} \\
&+2(x^2-1)\left\{\frac{3x^4+x^2(3+y^2-9w^2)+y^2(2-3w^2)+3(w^4+w^2-1)}{(w^2-1)(3x^2+y^2-w^2-2)}\right\} \\
&\times\left[\log\left(v^2-1\right)-\log\left(1+w^2+v^2-3x^2-y^2\right)\right],
\end{aligned}
\tag{404}
$$

which should be evaluated at

$$
\begin{aligned}
\left(q_{23}^2\right)^{\max} &= \left(E_2^*+E_3^*\right)^2-\left(\sqrt{E_2^{*2}-m_1^2}-\sqrt{E_3^{*2}-m_1^2}\right)^2, \\
\left(q_{23}^2\right)^{\min} &= \left(E_2^*+E_3^*\right)^2-\left(\sqrt{E_2^{*2}-m_1^2}+\sqrt{E_3^{*2}-m_1^2}\right)^2,
\end{aligned}
\tag{405}
$$

where $E_2^* \equiv q_{12}/2$ and $E_3^* \equiv \left(m_B^2-q_{12}^2-m_1^2\right)/(2q_{12})$. The final decay width is obtained after integrating over q_{12}^2, between $4m_1^2$ and $(m_B-m_1)^2$. The result is lengthy and it poses no advantage to present it in here.

In the limit $m_1, m_2 \longrightarrow 0$, the integrated width is much simpler and given by:

$$
\Gamma \sim \frac{3\left(g_{sb}g_{12}\right)^2}{256\pi^3}\frac{f_B^2 m_{12}^2}{m_V^4}m_B\,. \tag{406}
$$

Finally, the process $B^+ \longrightarrow K^+a_1a_2$ is depicted in the right panel of figure 18. The corresponding amplitude reads:

$$
\mathcal{M} = -\frac{g_{sb}g_{12}}{m_V^2}\left\langle K(p_3)|\bar{s}\gamma_\mu b|B(p)\right\rangle(p_2-p_1)^\mu, \tag{407}
$$

where

$$
\left\langle K(p_3)|\bar{s}\gamma_\mu b|B(p)\right\rangle = f_+(q^2)\left[(p+p_3)_\mu-\frac{m_B^2-m_K^2}{q^2}q_\mu\right]+f_0(q^2)\frac{m_B^2-m_K^2}{q^2}q_\mu, \tag{408}
$$

and $q^2=(p-p_3)^2=(p_1+p_2)^2$ is the transferred momentum, ranging from $(m_1+m_2)^2$ to $(m_B-m_K)^2$. In this case, p_1 and p_2 refer to the momenta of the a_1 and a_2 particles; while p_3 is the momentum of the additional kaon. The initial momentum of the B-meson is labeled as p. The contraction of this matrix element with (p_2-p_1) in equation 407 leads to

$$
\begin{aligned}
\mathcal{M} = -\frac{g_{sb}g_{12}}{m_V^2}\Bigg\{&\frac{\left(m_B^2-m_K^2\right)\left(m_2^2-m_1^2\right)}{q^2}\left[f_0(q^2)-f_+(q^2)\right] \\
&+\left[2\left(p_2+p_3\right)^2+q^2-m_1^2-m_2^2-m_B^2-m_K^2\right]f_+(q^2)\Bigg\}.
\end{aligned}
\tag{409}
$$

For convenience, we trade these variables for $M_{12}^2 \equiv m_2^2 - m_1^2$ and $M_{BK}^2 \equiv m_B^2 - m_K^2$, obtaining

$$\frac{d\Gamma}{dq^2} = \frac{\left(g_{sb} g_{12}\right)^2}{768\pi^3 m_V^4 m_B^3} F(q^2)\,, \tag{410}$$

with

$$F(q^2) = \frac{1}{q^2}\left[\frac{(M_{BK}^2 + q^2)^2}{q^4} - 4\frac{m_B^2}{q^2}\right]^{1/2}\left[\frac{(M_{12}^2 + q^2)^2}{q^4} - 4\frac{m_2^2}{q^2}\right]^{1/2}\left\{3M_{BK}^4 M_{12}^4 |f_0(q^2)|^2 + \left[q^4 + 2q^2\left(M_{BK}^2 - 2m_B^2\right) + M_{BK}^4\right]\left[q^4 + 2q^2\left(M_{12}^2 - 2m_2^2\right) + M_{12}^4\right]|f_+(q^2)|^2\right\}. \tag{411}$$

Following Ref. [308], we parameterize the form factor f_+ as

$$f_+(q^2) = \frac{r_1}{(1 - q^2/m^2)} + \frac{r_2}{(1 - q^2/m^2)^2}\,, \tag{412}$$

with $r_1 = 0.162$, $r_2 = 0.173$ and $m^2 = 5.41^2$ GeV^2. Similarly,

$$f_0(q^2) = \frac{r_2}{(1 - q^2/m_{\text{fit}}^2)} \tag{413}$$

with $r_2 = 0.330$ and $m_{\text{fit}}^2 = 37.46$ GeV^2.

Again, in the approximation $m_1, m_2, m_K \to 0$ and $f_0, f_+(q^2) \to 1$, we obtain:

$$\Gamma \sim \frac{\left(g_{sb} g_{12}\right)^2}{3072\pi^3 m_V^4} m_B^5\,. \tag{414}$$

Appendix G

Composite completion of the SM+E EFT

The purpose of this appendix is to show that there exists a (composite) completion of the SM+E EFT, described in section 6.1, where purely SMEFT operators are generated but can be suppressed relatively to those involving the heavy lepton E. With this aim, we consider the MCHM and assume MFV. In turn, the LH fermions are required to be mostly elementary.

For the mediator of the effective interactions, we consider a heavy vector V that couples to the RH fermions according to equation 105. After rewriting the renormalizable Lagrangian in the mass basis and integrating V out, we obtain the operators in the EFT basis, with Wilson coefficients

$$f_{(\bar{q}q)(\bar{E}e)} \sim \frac{g_1^2}{m_V^2} \frac{\sin^2\phi_{q_R} \sin\phi_{q_R} \cos\phi_{e_R}}{\sin^2\theta}\,, \tag{415}$$

not referring to any Lorentz structure in particular. Note that the renormalizable interaction $y\overline{l_L}HE$ is automatically turned off due to the MFV requirement, since $y \sim \sin\phi_{qL} \ll 1$. On top of these operators, the purely SMEFT ones that also arise are:

$$f_{(\bar{q}q)(\bar{e}e)} \sim \frac{g_1^2}{m_V^2} \sin^2\phi_{qR} \sin^2\phi_{eR} \cot^2\theta\,; \tag{416}$$

$$f_{(\bar{q}q)(\bar{q}q)} \sim \frac{g_1^2}{m_V^2} \sin^4\phi_{qR} \cot^2\theta\,; \tag{417}$$

$$f_{(\bar{u}u)(\bar{d}d)} \sim \frac{g_1^2}{m_V^2} \sin^2\phi_{uR} \sin^2\phi_{dR} \cot^2\theta\,; \tag{418}$$

$$f_{(\bar{e}e)(\bar{e}e)} \sim \frac{g_1^2}{m_V^2} \sin^4\phi_{eR} \cot^2\theta\,. \tag{419}$$

The experimental bounds on the $(\bar{q}q)(\bar{e}e)$ operators [309] allow values of $f_{(\bar{q}q)(\bar{E}e)} \gtrsim \mathcal{O}(0.1)$ TeV^{-2}, assuming that $\sin\phi_{eR} \sim \mathcal{O}(0.1)$. Bounds on the $(\bar{q}q)(\bar{q}q)$ operators [310] are compatible with even larger values, $f_{(\bar{q}q)(\bar{E}e)} \sim \mathcal{O}(1)$, taking the light quarks composite fractions to be $\sin\phi_{qR} \sim \sin\phi_{eR}$. We therefore conclude that the effective operators relevant for the production and decay of the VLL can be sizable while compatible with other data.

In the previous discussion, we neglected operators involving the Higgs boson, *e.g.* $(H \overleftrightarrow{D}^{\mu} H)(\bar{e}\gamma_{\mu}e)$, which might also arise from the UV model. This operator contributes to the $Ze\bar{e}$ effective vertex and could therefore enhance $\Gamma(E \longrightarrow \ell Z)$. Such corrections are however negligible if, for example, V is associated with the $U(1)_X$ symmetry of the MCHM.

Appendix H

Computations in the ALP SMEFT

H.1 Divergences at one-loop

In this section, we enumerate the different processes and amplitudes we computed to match the UV divergences onto the CP-even Green basis given by the operators in table 8. We work consistently up to dimension five, therefore considering a single insertion of an effective operator per loop. (All diagrams which are depicted in the figures below but not explicitly mentioned are either finite or do not contribute to the counterterms of interest.)

H.1.1 $S(p_1)H_i^\dagger(p_3) \to q_{Lj}^\alpha(p_2)\overline{u_R}^\beta(p_4)$

The one-loop diagrams which contribute to this process are depicted in figure 40. The amplitudes corresponding to diagrams with insertions of the Yukawa-like operators read:

$$\mathrm{i}\mathcal{M}_1^Y = \frac{1}{(4\pi)^2\epsilon}\lambda_{SH}(a_{SHu})_{\alpha\beta}\epsilon_{ji}\overline{u_2}P_R v_4\,; \tag{420}$$

$$\mathrm{i}\mathcal{M}_4^Y = \frac{1}{(4\pi)^2\epsilon}\left[y^d_{\alpha\rho}(y^d)^*_{\sigma\rho}(a_{SHu})_{\sigma\beta}\right]\epsilon_{ij}\overline{u_2}P_R v_4\,, \tag{421}$$

$$\mathrm{i}\mathcal{M}_6^Y = \frac{1}{(4\pi)^2\epsilon}\left[(a_{SHd})_{\alpha\rho}(y^d)^*_{\sigma\rho}y^u_{\sigma\beta}\right]\epsilon_{ij}\overline{u_2}P_R v_4\,, \tag{422}$$

$$\mathrm{i}\mathcal{M}_9^Y = \frac{-1}{(4\pi)^2\epsilon}\left[y^d_{\alpha\rho}(a_{SHd})^*_{\sigma\rho}y^u_{\sigma\beta}\right]\epsilon_{ij}\overline{u_2}P_R v_4\,. \tag{423}$$

The diagrams where the gauge bosons run in the loop contribute with

$$\mathrm{i}\mathcal{M}^V = \frac{-(a_{SHu})_{\alpha\beta}}{(4\pi)^2\epsilon}\left[g_1^2\frac{25}{36}+g_2^2\frac{3}{4}+g_3^2\frac{16}{3}\right]\epsilon_{ji}\overline{u_2}P_R v_4\,. \tag{424}$$

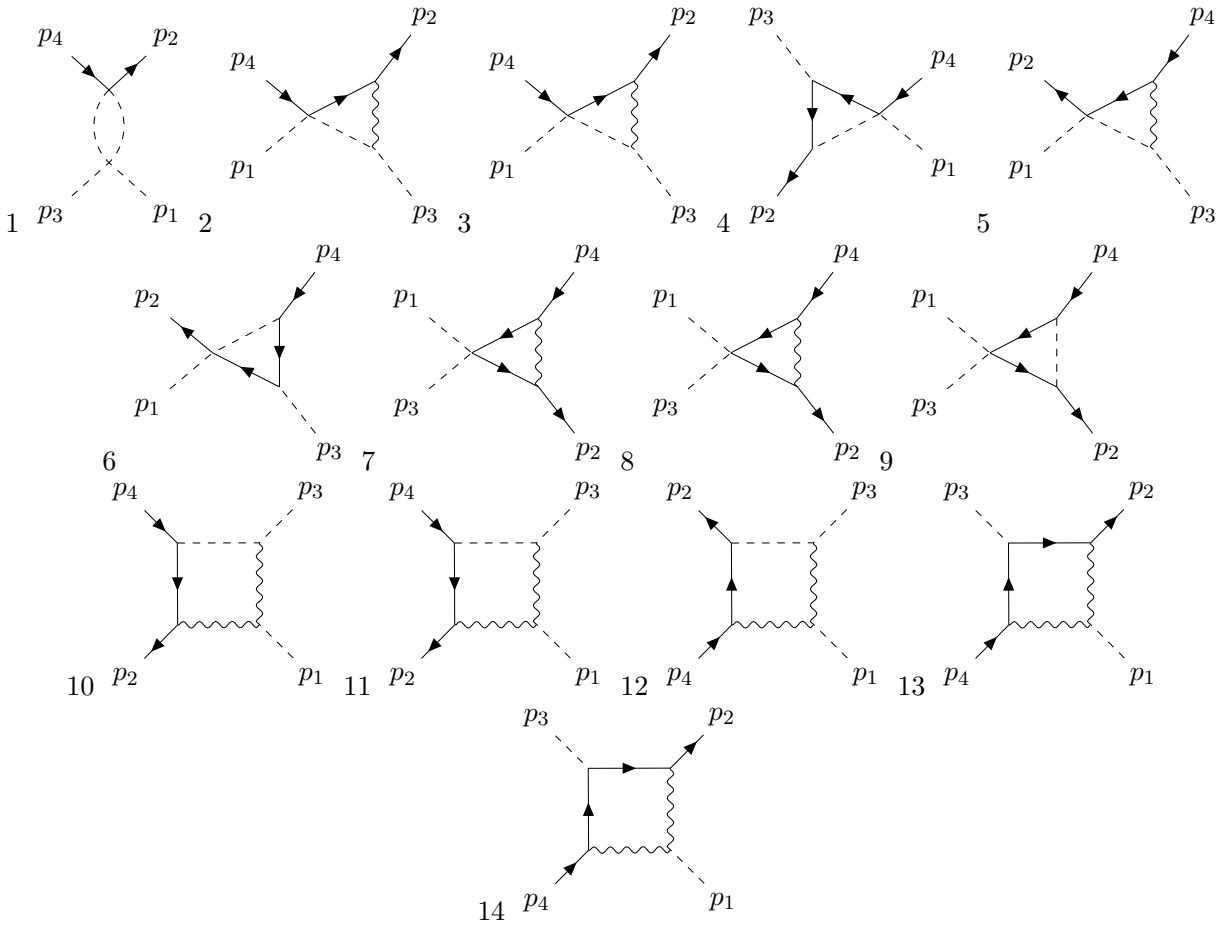

Figure 40: Diagrams contributing to the renormalization of 2 scalar–2 quark interactions.

In turn, the following counterterm a'_{SHu} in the tree level EFT amplitude,

$$i\mathcal{M}_{\text{EFT}} = -(a_{SHu})'_{\alpha\beta}\epsilon_{ji}\overline{u_2}P_R v_4\,, \tag{425}$$

is used to cancel the sum of the divergent UV amplitudes calculated above.

H.1.2 $S(p_1)H_i(p_3) \to q^{\alpha}_{Lj}(p_2)\overline{d_R}^{\beta}(p_4)$

The same topologies as before are generated. The corresponding one-loop amplitudes read:

$$\mathrm{i}\mathcal{M}^Y_1 = \frac{1}{(4\pi)^2\epsilon}\lambda_{SH}(a_{SHd})_{\alpha\beta}\delta_{ij}\overline{u_2}P_R v_4\,; \tag{426}$$

$$\mathrm{i}\mathcal{M}^Y_4 = \frac{-1}{(4\pi)^2\epsilon}\left[y^u_{\alpha\rho}(y^u)^*_{\sigma\rho}(a_{SHd})_{\sigma\beta}\right]\delta_{ij}\overline{u_2}P_R v_4\,, \tag{427}$$

$$\mathrm{i}\mathcal{M}^Y_6 = \frac{-1}{(4\pi)^2\epsilon}\left[(a_{SHu})_{\alpha\rho}(y^u)^*_{\sigma\rho}y^d_{\sigma\beta}\right]\delta_{ij}\overline{u_2}P_R v_4\,, \tag{428}$$

$$\mathrm{i}\mathcal{M}^Y_9 = \frac{1}{(4\pi)^2\epsilon}\left[y^u_{\alpha\rho}(a_{SHu})^*_{\sigma\rho}y^d_{\sigma\beta}\right]\delta_{ij}\overline{u_2}P_R v_4\,, \tag{429}$$

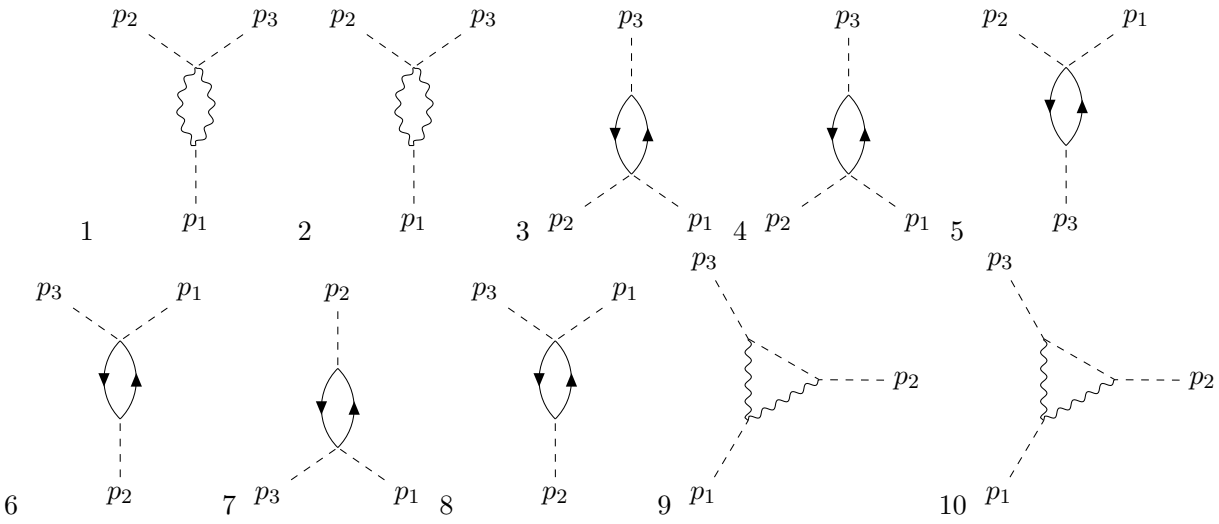

Figure 41: Diagrams contributing to the renormalization of 3 scalar interactions.

and

$$\mathrm{i}\mathcal{M}^V = \frac{-(a_{SHd})_{\alpha\beta}}{(4\pi)^2\epsilon}\left[g_1^2\frac{1}{36} + g_2^2\frac{3}{4} + g_3^2\frac{16}{3}\right]\delta_{ij}\overline{u_2}P_R v_4\,. \tag{430}$$

On the other hand, the tree level one is given by

$$\mathrm{i}\mathcal{M}_{\mathrm{EFT}} = -(a_{SHd})'_{\alpha\beta}\delta_{ij}\overline{u_2}P_R v_4\,. \tag{431}$$

H.1.3 $S(p_1)H_i(p_3) \to l^\alpha_{Lj}(p_2)\overline{e_R}^\beta(p_4)$

Considering the leptons case and turning off gauge interactions, only the first diagram in figure 40 exists (the triangle diagrams are absent because they do not conserve internally the hypercharge):

$$\mathrm{i}\mathcal{M}_1^Y = \frac{1}{(4\pi)^2\epsilon}\lambda_{SH}(a_{SHe})_{\alpha\beta}\delta_{ij}\overline{u_2}P_R v_4\,, \tag{432}$$

while

$$\mathrm{i}\mathcal{M}^V = \frac{-(a_{SHe})_{\alpha\beta}}{(4\pi)^2\epsilon}\left[\frac{9g_1^2}{4} + \frac{3g_2^2}{4}\right]\delta_{ij}\overline{u_2}P_R v_4\,. \tag{433}$$

At tree level in the EFT, we get:

$$\mathrm{i}\mathcal{M}_{\mathrm{EFT}} = -(a_{SHe})'_{\alpha\beta}\delta_{ij}\overline{u_2}P_R v_4\,. \tag{434}$$

H.1.4 $S(p_1) \to H_i(p_2)H_j^\dagger(p_3)$

The one-loop diagrams contributing to this process are depicted in figure 41. Starting by the amplitudes involving the Yukawa-like operators, the leptonic loop labeled by the number 6 gives:

$$\mathrm{i}\mathcal{M}_6^\ell = -\mathrm{i}(a_{SHe})^*_{\alpha\beta}y^e_{\alpha\beta}\delta_{ij}I\,, \tag{435}$$

where a (-1) factor comes from the closed fermionic loop and

$$I = \int \frac{d^{\mathrm{d}}k}{(2\pi)^{\mathrm{d}}} \mathrm{Tr}\left[\frac{\not{k}}{k^2} P_L \frac{\not{k}+\not{p}_2}{(k+p_2)^2} P_R\right] = \frac{1}{2}\int \frac{d^{\mathrm{d}}k}{(2\pi)^{\mathrm{d}}} \mathrm{Tr}\left[\frac{\not{k}}{k^2}\frac{\not{k}+\not{p}_2}{(k+p_2)^2}\right]$$
$$= \frac{\mathrm{d}}{2}\int \frac{d^{\mathrm{d}}k}{(2\pi)^{\mathrm{d}}} \frac{k^2 + k\cdot p_2}{k^2(k^2+p_2^2)} \equiv \frac{\mathrm{d}}{2}(I_1 + I_2)\,. \tag{436}$$

The two integrals above read:

$$I_1 = \int \frac{d^{\mathrm{d}}k}{(2\pi)^{\mathrm{d}}} \frac{1}{k^2}\left\{1 - \frac{p_2^2}{k^2} + 4\frac{(k\cdot p_2)^2}{k^4}\right\} = A_1 - p_2^2 A_2 + 4p_2^2 B_3\,, \tag{437}$$

where the master integrals are defined in appendix A; and

$$I_2 = \int \frac{d^{\mathrm{d}}k}{(2\pi)^{\mathrm{d}}} \frac{k\cdot p_2}{k^4}\left(\frac{-2k\cdot p_2}{k^2}\right) = -2p_2^\mu p_2^\nu \int \frac{d^{\mathrm{d}}k}{(2\pi)^{\mathrm{d}}} \frac{k_\mu k_\nu}{k^6} = -2p_2^2 B_3\,, \tag{438}$$

up to second order in external momenta (and dropping from the beginning the k-odd contributions). Therefore, we obtain:

$$I = 2p_2^2\left(-A_2 + 2B_3\right) = 2p_2^2\left(\frac{-\mathrm{i}}{16\pi^2\epsilon} + \frac{\mathrm{i}}{32\pi^2\epsilon}\right) = \frac{-\mathrm{i}}{16\pi^2\epsilon}p_2^2\,, \tag{439}$$

using the mathematical relations in appendix A. Consequently,

$$\mathrm{i}\mathcal{M}_6^\ell = \frac{-1}{16\pi^2\epsilon}(a_{SHe})^*_{\alpha\beta} y^e_{\alpha\beta}\delta_{ij}p_2^2\,. \tag{440}$$

The integral in equation 439 is the same for all fermionic loops in figure 41. The evaluation of the second type of diagram, namely the number 3, is hence straightforward:

$$\mathrm{i}\mathcal{M}_3^\ell = \mathrm{i}(a_{SHe})_{\alpha\beta}(y^e)^*_{\alpha\beta}\delta_{ij} I(p_2 \to -p_3) = \frac{1}{16\pi^2\epsilon}(a_{SHe})_{\alpha\beta}(y^e)^*_{\alpha\beta}\delta_{ij}p_3^2\,. \tag{441}$$

When the up-quark runs in the loops, the amplitudes of the two conjugated diagrams read instead:

$$\mathrm{i}\mathcal{M}_6^u = \frac{3}{16\pi^2\epsilon}(a_{SHu})_{\alpha\beta}(y^u)^*_{\alpha\beta}\delta_{ij}p_2^2\,, \tag{442}$$

$$\mathrm{i}\mathcal{M}_3^u = \frac{-3}{16\pi^2\epsilon}(a_{SHu})^*_{\alpha\beta} y^u_{\alpha\beta}\delta_{ij}p_3^2\,, \tag{443}$$

where we have summed over colors and contracted $\epsilon_{mi}\epsilon_{mj} = \delta_{ij}$, with $\epsilon_{mi} = -\epsilon_{im}$.

For the down-quark case, we have:

$$\mathrm{i}\mathcal{M}_6^d = \frac{-3}{16\pi^2\epsilon}(a_{SHd})^*_{\alpha\beta} y^d_{\alpha\beta}\delta_{ij}p_2^2\,, \tag{444}$$

$$\mathrm{i}\mathcal{M}_3^d = \frac{3}{16\pi^2\epsilon}(a_{SHd})_{\alpha\beta}(y^d)^*_{\alpha\beta}\delta_{ij}p_3^2\,. \tag{445}$$

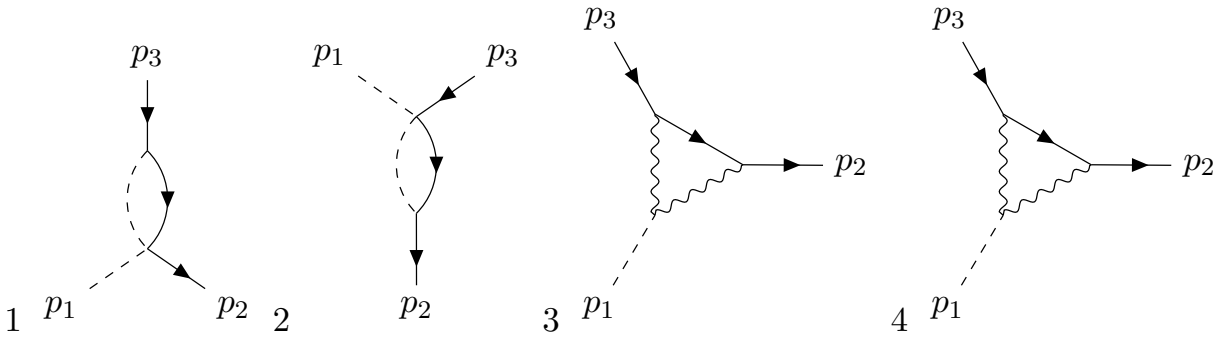

Figure 42: Diagrams contributing to the renormalization of 1 scalar–2 fermion interactions.

On the other front, the EFT amplitude is

$$\mathrm{i}\mathcal{M}_{\text{EFT}} = \delta_{ij}\left[-\mathrm{i}r_{HS\Box}p_1^2 + r_{SH\Box}(p_2^2 - p_3^2)\right], \tag{446}$$

from which we obtain that $r_{HS\Box} = 0$ by matching.

All the amplitudes involving gauge bosons vanish. Considering, for instance, the first diagram in figure 41,

$$\mathrm{i}\mathcal{M}_1^V \propto \left[a_{S\widetilde{B}}\epsilon_{\mu\rho\eta\lambda}p_1^\eta p_2^\lambda\right] g^{\mu\nu}g^{\rho\sigma}\left[g_1^2 g_{\nu\sigma}\right] = 0\,. \tag{447}$$

Finally, note that there are two different flavour structures arising in the amplitudes, $\text{Tr}\left[a_{SHu}y_u^\dagger\right] \neq \text{Tr}\left[y_u a_{SHu}^\dagger\right]$. These are only equivalent in the CP conserving limit, which is the one we take. (The imaginary part in these structures gives divergent contributions to the CP-odd operator with the same field content as $\mathcal{R}_{SH\Box}$; check the original Ref. [8].)

H.1.5 $S(p_1) \to \psi_i^\alpha(p_2)\overline{\psi}_j^\beta(p_3)$

The first two diagrams in figure 42 exist for each fermion in the theory that runs within the loop. Starting by computing the amplitude for $\psi = e_R$, we get:

$$\mathrm{i}\mathcal{M}_1^{e_R} = -\mathrm{i}(a_{SHe})_{\rho\beta}(y^e)^*_{\rho\alpha}\delta_{mm}\overline{u_2}I'P_R v_3\,, \tag{448}$$

where

$$I' = \int \frac{d^{\mathrm{d}}k}{(2\pi)^{\mathrm{d}}}\frac{\not{k}}{k^2}\frac{1}{(k-p_2)^2} = \int \frac{d^{\mathrm{d}}k}{(2\pi)^{\mathrm{d}}}\frac{\not{k}}{k^4}\left(\frac{2k\cdot p_2}{k^2}\right) = 2\not{p}_2 B_3 = \frac{\mathrm{i}}{32\pi^2\epsilon}\not{p}_2\,. \tag{449}$$

Therefore:

$$\mathrm{i}\mathcal{M}_1^{e_R} = \frac{1}{16\pi^2\epsilon}(a_{SHe})_{\rho\beta}(y^e)^*_{\rho\alpha}\overline{u_2}\not{p}_2 P_R v_3\,. \tag{450}$$

Regarding the second diagram, the same integral appears with $p_2 \to -p_3$; therefore:

$$\mathrm{i}\mathcal{M}_2^{e_R} = \frac{1}{16\pi^2\epsilon}y^e_{\rho\beta}(a_{SHe})^*_{\rho\alpha}\overline{u_2}\not{p}_3 P_R v_3\,. \tag{451}$$

On the other hand, the amplitude from the diagrams involving the gauge bosons (in this case, B_μ) read:

$$\begin{aligned}
\mathrm{i}\mathcal{M}_V^{e_R} &= (2\mathrm{i}a_{S\widetilde{B}})\int \frac{d^{\mathrm{d}}k}{(2\pi)^{\mathrm{d}}}\epsilon_{\mu\nu\sigma\rho}\left[k^\rho\left(k-p_1\right)^\sigma - k^\sigma\left(k-p_1\right)^\rho\right]\frac{(-\mathrm{i})^2}{k^2(k-p_1)^2} \\
&\times\left[\overline{u_2}\left(-\mathrm{i}g_1\gamma^\nu P_R\right)\frac{\mathrm{i}\left(\not{k}-\not{p_2}\right)}{\left(k-p_2\right)^2}\left(-\mathrm{i}g_1\gamma^\mu P_R\right)v_3\right]\delta_{\beta\alpha} \\
&= -4a_{S\widetilde{B}}g_1^2\delta_{\beta\alpha}\epsilon_{\mu\nu\sigma\rho}\left[\overline{u_2}P_L\gamma^\nu\gamma_\chi\gamma^\mu v_3\right]I^{\rho\sigma\chi}\,,
\end{aligned} \tag{452}$$

where

$$I^{\rho\sigma\chi} \equiv \int \frac{d^{\mathrm{d}}k}{(2\pi)^{\mathrm{d}}}\frac{k^\rho\left(k-p_1\right)^\sigma\left(k-p_2\right)^\chi}{k^2(k-p_1)^2(k-p_2)^2} \to -p_1^\sigma g^{\rho\chi}B_3\,. \tag{453}$$

In the above integral, we neglected the symmetric contributions under the interchange $\sigma \leftrightarrow \rho$ (to be contracted with the Levi-Civita tensor) and the ones with more than one power of external momentum (since we are matching to an operator of the form $\overline{\psi}\not{D}\psi$). After these simplifications[1],

$$\begin{aligned}
\mathrm{i}\mathcal{M}_V^{e_R} &= \frac{\mathrm{i}}{(4\pi)^2\epsilon}a_{S\widetilde{B}}g_1^2\delta_{\beta\alpha}\epsilon_{\mu\nu\sigma\rho}\left[\overline{u_2}P_L\gamma^\nu\gamma^\rho\gamma^\mu v_3\right]p_1^\sigma \\
&= \frac{-\mathrm{i}}{(4\pi)^2\epsilon}a_{S\widetilde{B}}g_1^2\delta_{\beta\alpha}\epsilon_{\mu\nu\rho\sigma}\left[\overline{u_2}P_L\gamma^\mu\gamma^\nu\gamma^\rho v_3\right]p_1^\sigma \\
&= \frac{\delta_{\beta\alpha}}{(4\pi)^2\epsilon}a_{S\widetilde{B}}g_1^2\left(-\mathrm{i}\epsilon_{\mu\nu\rho\sigma}\right)\left(-\mathrm{i}\epsilon^{\chi\mu\nu\rho}\right)\left[\overline{u_2}P_L\gamma_\chi\gamma^5 v_3\right]p_1^\sigma \\
&= \frac{\delta_{\beta\alpha}}{(4\pi)^2\epsilon}a_{S\widetilde{B}}g_1^2\left(-6\delta_\sigma^\chi\right)\left[\overline{u_2}P_L\gamma_\chi\gamma^5 v_3\right]p_1^\sigma \\
&= -\frac{3}{8\pi^2\epsilon}\delta_{\beta\alpha}a_{S\widetilde{B}}g_1^2\left[\overline{u_2}P_L\not{p}_1\gamma^5 v_3\right] \\
&= -\frac{3}{8\pi^2\epsilon}\delta_{\beta\alpha}a_{S\widetilde{B}}g_1^2\left[\overline{u_2}\not{p}_1 P_R v_3\right]\,.
\end{aligned} \tag{454}$$

The contraction of the Levi-Civita tensor with the Dirac matrices (in the third line) is computed according to appendix A, with $\epsilon^{0123} = 1$ (the same convention is used in `FormCalc`).

The amplitudes for the $S \to l_L\overline{l_L}$, $S \to u_R\overline{u_R}$ and $S \to d_R\overline{d_R}$ processes are obtained analogously:

$$\mathrm{i}\mathcal{M}_1^{l_L} = \frac{-1}{32\pi^2\epsilon}(a_{SHe})^*_{\beta\rho}y^e_{\alpha\rho}\delta_{ij}\overline{u_2}\not{p}_2 P_L v_3\,, \tag{455}$$

$$\mathrm{i}\mathcal{M}_2^{l_L} = \frac{-1}{32\pi^2\epsilon}(y^e)^*_{\beta\rho}(a_{SHe})_{\alpha\rho}\delta_{ij}\overline{u_2}\not{p}_3 P_L v_3\,, \tag{456}$$

$$\mathrm{i}\mathcal{M}_V^{l_L} = \frac{3}{32\pi^2\epsilon}\delta_{\beta\alpha}\delta_{ij}\left(a_{S\widetilde{B}}g_1^2 + 3a_{S\widetilde{W}}g_2^2\right)\overline{u_2}\not{p}_1 P_L v_3\,, \tag{457}$$

[1] We remark that the `FormCalc` one-loop amplitude agrees exactly with the result in equation 454. This should *not* be the case, given the information in the manual that the "`Eps`" definition carries a factor of $(-\mathrm{i})$. This seems to be a problem only when the Levi-Civita tensor appears directly in the vertex, such that — when converting the `FeynRules` model into a `FeynArts` output — this replacement is not done. Computing at tree level $S \to VV$, we confirm that this is indeed the case.

where the minus sign, in comparison to the last line in equation 454, comes from the interchange $P_L \leftrightarrow P_R$. In addition,

$$\mathrm{i}\mathcal{M}_1^{u_R} = \frac{1}{16\pi^2\epsilon}(a_{SHu})_{\rho\beta}(y^u)^*_{\rho\alpha}\overline{u_2}\not{p}_2 P_R v_3\,, \tag{458}$$

$$\mathrm{i}\mathcal{M}_2^{u_R} = \frac{1}{16\pi^2\epsilon}y^u_{\rho\beta}(a_{SHu})^*_{\rho\alpha}\overline{u_2}\not{p}_4 P_R v_3\,, \tag{459}$$

$$\mathrm{i}\mathcal{M}_V^{u_R} = \frac{1}{6\pi^2\epsilon}\delta_{\beta\alpha}\left(a_{s\widetilde{B}}g_1^2 + 3a_{s\widetilde{G}}g_3^2\right)\overline{u_2}\not{p}_1 P_R v_3\,. \tag{460}$$

$$\mathrm{i}\mathcal{M}_1^{d_R} = \frac{1}{16\pi^2\epsilon}(a_{SHd})_{\rho\beta}(y^d)^*_{\rho\alpha}\overline{u_2}\not{p}_2 P_R v_3\,, \tag{461}$$

$$\mathrm{i}\mathcal{M}_2^{d_R} = \frac{1}{16\pi^2\epsilon}y^d_{\rho\beta}(a_{SHd})^*_{\rho\alpha}\overline{u_2}\not{p}_3 P_R v_4\,, \tag{462}$$

$$\mathrm{i}\mathcal{M}_V^{d_R} = \frac{-1}{24\pi^2\epsilon}\delta_{\beta\alpha}\left(a_{s\widetilde{B}}g_1^2 + 12a_{s\widetilde{G}}g_3^2\right)\overline{u_2}\not{p}_1 P_R v_3\,. \tag{463}$$

Finally, for $S \to q_L\overline{q_L}$, there are two additional diagrams with Yukawa insertions, from having both u and d quarks running in the loop:

$$\mathrm{i}\mathcal{M}_{1,u}^{q_L} = \frac{-1}{32\pi^2\epsilon}(a_{SHu})^*_{\beta\rho}y^u_{\alpha\rho}\delta_{ij}\overline{u_2}\not{p}_2 P_L v_3\,, \tag{464}$$

$$\mathrm{i}\mathcal{M}_{2,u}^{q_L} = \frac{-1}{32\pi^2\epsilon}(y^u)^*_{\beta\rho}(a_{SHu})_{\alpha\rho}\delta_{ij}\overline{u_2}\not{p}_4 P_L v_3\,, \tag{465}$$

$$\mathrm{i}\mathcal{M}_{1,d}^{q_L} = \frac{-1}{32\pi^2\epsilon}(a_{SHd})^*_{\beta\rho}y^d_{\alpha\rho}\delta_{ij}\overline{u_2}\not{p}_2 P_L v_3\,, \tag{466}$$

$$\mathrm{i}\mathcal{M}_{2,d}^{q_L} = \frac{-1}{32\pi^2\epsilon}(y^d)^*_{\beta\rho}(a_{SHd})_{\alpha\rho}\delta_{ij}\overline{u_2}\not{p}_4 P_L v_3\,. \tag{467}$$

Regarding the contributions with gauge bosons, we have:

$$\mathrm{i}\mathcal{M}_V^{q_L} = \frac{3}{8\pi^2\epsilon}\delta_{\beta\alpha}\delta_{ij}\left(a_{s\widetilde{B}}\frac{g_1^2}{36} + a_{s\widetilde{W}}\frac{3g_2^2}{4} + a_{s\widetilde{G}}\frac{4g_3^2}{3}\right)\overline{u_2}\not{p}_1 P_L v_3\,. \tag{468}$$

The EFT amplitudes, with the counterterms required to absorb the previous divergences, are:

$$\mathrm{i}\mathcal{M}_{\mathrm{EFT}}(S \to e_R\overline{e_R}) = \overline{u_2}\left[(r_{Se})^*_{\beta\alpha}\not{p}_2 + (r_{Se})_{\alpha\beta}\not{p}_4\right]P_R v_3\,, \tag{469}$$

$$\mathrm{i}\mathcal{M}_{\mathrm{EFT}}(S \to l_L\overline{l_L}) = \delta_{ij}\overline{u_2}\left[(r_{Sl})^*_{\beta\alpha}\not{p}_2 + (r_{Sl})_{\alpha\beta}\not{p}_4\right]P_L v_3\,, \tag{470}$$

$$\mathrm{i}\mathcal{M}_{\mathrm{EFT}}(S \to u_R\overline{u_R}) = \overline{u_2}\left[(r_{Su})^*_{\beta\alpha}\not{p}_2 + (r_{Su})_{\alpha\beta}\not{p}_4\right]P_R v_3\,, \tag{471}$$

$$\mathrm{i}\mathcal{M}_{\mathrm{EFT}}(S \to d_R\overline{d_R}) = \overline{u_2}\left[(r_{Sd})^*_{\beta\alpha}\not{p}_2 + (r_{Sd})_{\alpha\beta}\not{p}_4\right]P_R v_3\,, \tag{472}$$

$$\mathrm{i}\mathcal{M}_{\mathrm{EFT}}(S \to q_L\overline{q_L}) = \delta_{ij}\overline{u_2}\left[(r_{Sq})^*_{\beta\alpha}\not{p}_2 + (r_{Sq})_{\alpha\beta}\not{p}_4\right]P_L v_3\,. \tag{473}$$

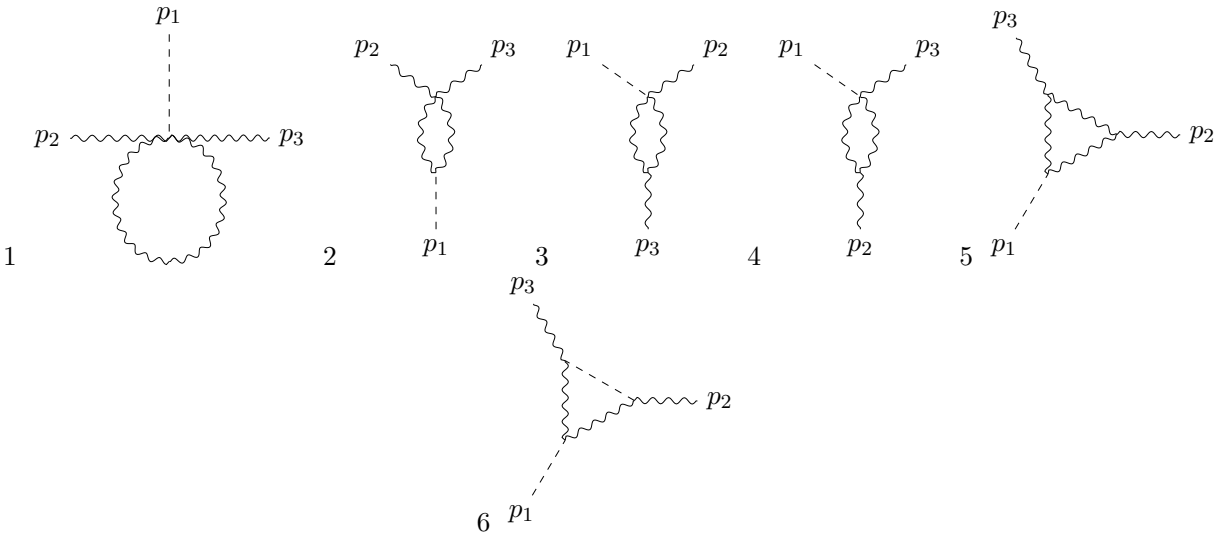

Figure 43: Diagrams contributing to the renormalization of 1 scalar–2 gluon interactions.

H.1.6 $S(p_1) \to V^a_\mu(p_2)V^b_\nu(p_3)$

Let us consider in detail the case with gluons, to understand why the divergent amplitudes in these processes cancel exactly. To start, we can easily verify that the contributions from the diagrams 1 and 2 in figure 43 are zero (we leave the external polarization vectors implicit):

$$\mathrm{i}\mathcal{M}_1 = 4\mathrm{i}a_{s\widetilde{G}}g_3^2\epsilon_{\mu\nu\rho\sigma}\left(f_{ade}f_{bce} - f_{ace}f_{bde} + f_{abe}f_{cde}\right)\int \frac{d^{\mathrm{d}}k}{(2\pi)^{\mathrm{d}}}\frac{-\mathrm{i}g^{\rho\sigma}}{k^2}\delta_{cd} = 0\,; \tag{474}$$

while

$$\begin{aligned}\mathrm{i}\mathcal{M}_2 = -2\mathrm{i}a_{s\widetilde{G}}\delta_{cd}\epsilon_{\rho\sigma\gamma\eta}\int \frac{d^{\mathrm{d}}k}{(2\pi)^{\mathrm{d}}}\Bigg\{\Big[(-k)^\eta(k-p_1)^\gamma + (-k)^\gamma(k-p_1)^\eta\Big]\frac{-\mathrm{i}}{k^2} \\ \times(-\mathrm{i}g_3^2)\Big[(f_{ade}f_{bce} - f_{ace}f_{bde} + f_{abe}f_{cde})g^{\mu\rho}g^{\nu\sigma} + (-f_{ade}f_{bce} + f_{ace}f_{bde} + f_{abe}f_{cde})g^{\mu\sigma}g^{\nu\rho} \\ + (f_{ade}f_{bce} + f_{ace}f_{bde})g^{\mu\nu}g^{\rho\sigma}\Big]\frac{-\mathrm{i}}{(k-p_1)^2}\Bigg\} = 0\,,\end{aligned} \tag{475}$$

due to the contraction of the group structure constants in the second line with δ_{cd}, and the contraction of the Levi-Civita with the metric tensor in the third line of the equation above.

Regarding the non-vanishing diagrams, we have:

$$\begin{aligned}\mathrm{i}\mathcal{M}_3 &= 2a_{s\widetilde{G}}g_3\epsilon_{\sigma\mu\rho\chi}p_1^\chi f_{cad}\int \frac{d^{\mathrm{d}}k}{(2\pi)^{\mathrm{d}}}\frac{-2g_3 f_{cbd}}{k^2(k-p_3)^2}\left[p_3^\rho g^{\nu\sigma} - p_3^\sigma g^{\nu\rho} - k^\nu g^{\sigma\rho} + \frac{p_3^\nu}{2}g^{\sigma\rho}\right] \\ &= 8a_{s\widetilde{G}}g_3^2 C_A^{(3)}\delta_{ab}\epsilon_{\sigma\mu\rho\chi}p_1^\chi p_3^\sigma g^{\nu\rho}\int \frac{d^{\mathrm{d}}k}{(2\pi)^{\mathrm{d}}}\frac{1}{k^4} \\ &= -\frac{2\mathrm{i}}{\pi\epsilon}a_{s\widetilde{G}}\alpha_3 C_A^{(3)}\delta_{ab}\epsilon_{\mu\nu\chi\sigma}p_2^\chi p_3^\sigma\,,\end{aligned} \tag{476}$$

where we have kept only the LO term in the expansion of the denominator in the first line, according to equation 346, because we are interested in two powers of momenta only (to match onto the EFT). Furthermore,

$$\mathcal{M}_4 = \mathcal{M}_3\,; \tag{477}$$

and

$$\begin{aligned}
\mathrm{i}\mathcal{M}_5 = -2\mathrm{i}a_{s\widetilde{B}}\epsilon_{\rho\chi\gamma\eta}\delta_{ce}\int\frac{d^{\mathrm{d}}k}{(2\pi)^{\mathrm{d}}}\Bigg\{\Bigg[-k^\eta(k-p_1)^\gamma+k^\gamma(k-p_1)^\eta\Bigg]\frac{-\mathrm{i}}{k^2}g_3 f_{cad} \\
\times\left[2p_2^\sigma g^{\mu\rho}-2p_2^\rho g^{\mu\sigma}-2k^\mu g^{\rho\sigma}+p_2^\mu g^{\rho\sigma}\right]\frac{(-\mathrm{i})^2}{(k-p_2)^2(k-p_3)^2}g_3 f_{dbe} \\
\times\left[2p_3^\chi g^{\nu\sigma}-2p_3^\sigma g^{\nu\chi}-2k^\nu g^{\sigma\chi}+(p_2+p_1)^\nu g^{\sigma\chi}\right]\Bigg\} \\
= 32a_{s\widetilde{G}}g_3^2\epsilon_{\rho\chi\gamma\eta}C_A^{(3)}\delta_{ab}B_3 p_1^\gamma\left[p_2^\sigma g^{\eta\nu}g^{\mu\rho}g^{\sigma\chi}+p_3^\chi g^{\eta\mu}g^{\rho\sigma}g^{\nu\sigma}\right] \\
= \frac{2\mathrm{i}}{\pi\epsilon}a_{s\widetilde{G}}\alpha_3 C_A^{(3)}\delta_{ab}\left[\epsilon_{\mu\sigma\gamma\nu}p_3^\gamma p_2^\sigma+\epsilon_{\nu\chi\gamma\mu}p_2^\gamma p_3^\chi\right] \\
= \frac{4\mathrm{i}}{\pi\epsilon}a_{s\widetilde{G}}\alpha_3 C_A^{(3)}\delta_{ab}\epsilon_{\mu\nu\gamma\sigma}p_2^\gamma p_3^\sigma\,,
\end{aligned} \tag{478}$$

where the C_A constants are defined in appendix A.

We conclude that $\mathcal{M}_3+\mathcal{M}_4+\mathcal{M}_5=0$. Note that the diagram with number 6 in figure 43 involves two powers of the new physics scale and therefore does not contribute to the EFT of interest. Similar cancellations are obtained for processes involving the gauge boson of $SU(2)$.

H.2 Wave function renormalization factors

In this section, we compute the WFR factors of each field present in the ALP EFT. All the loop integrals involved, as well as $SU(N)$ constants, are defined in appendix A.

H.2.1 Fermions

The diagrams contributing to the LH lepton kinetic term are depicted in figure 44. (Similar ones are obtained for the other fermions, with the exceptions that no diagram involving the $SU(2)$ gauge boson exists for RH fields. In the case of quarks, there is an additional diagram where the gluon runs in the loop; and the scalar contribution to q_L involves two diagrams where either u_R or d_R runs in the loop.)

We calculate the corresponding divergent amplitudes below, with the subscript (superscript) denoting the field being integrated out (external field). In all amplitudes, p denotes the external momentum and α (i) is the flavour (weak) index of the external field.

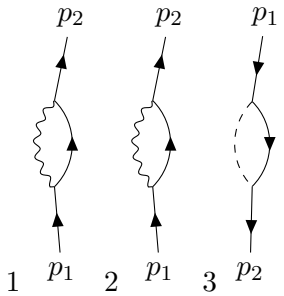

Figure 44: Diagrams contributing to the renormalization of the kinetic term of the LH lepton.

$$\mathrm{i}\mathcal{M}_H^{\ell_L} = (y^e_{\alpha\rho})^* y^e_{\alpha\rho} \frac{\mathrm{i}}{32\pi^2\epsilon} \overline{u}_L \not{p} u_L \,; \tag{479}$$

$$\begin{aligned}\mathrm{i}\mathcal{M}_B^{\ell_L} &= -\left(\frac{g_1}{2}\right)^2 \left[\overline{u}\gamma_\mu P_L \gamma^\alpha \gamma^\mu P_L u\right] I_\alpha = -\left(\frac{g_1}{2}\right)^2 \left[\overline{u}\gamma_\mu \left(2g^{\alpha\mu} - \gamma^\mu\gamma^\alpha\right) P_L u\right] I_\alpha \\ &= -\left(\frac{g_1}{2}\right)^2 (2-\mathrm{d})(2B_3)\overline{u_L}\not{p} u_L = \left(\frac{g_1}{2}\right)^2 \frac{\mathrm{i}}{(4\pi)^2\epsilon} \overline{u_L}\not{p} u_L \,,\end{aligned} \tag{480}$$

with

$$I_\alpha \equiv \int \frac{d^{\mathrm{d}}k}{(2\pi)^{\mathrm{d}}} \frac{k_\alpha}{k^2(k-p)^2} = 2B_3 p_\alpha \,; \tag{481}$$

$$\mathrm{i}\mathcal{M}_W^{\ell_L} = (-g_2^2) T^a_{im} T^a_{mi} \left[\overline{u}\gamma_\mu P_L \gamma^\alpha \gamma^\mu P_L u\right] I_\alpha = g_2^2 \frac{\mathrm{i}}{(4\pi)^2\epsilon} C_F^{(2)} \overline{u_L}\not{p} u_L \,. \tag{482}$$

From here, we derive a generic expression for the fermionic $1 \longrightarrow 1$ amplitude from one-loop diagrams with gauge fields, which we apply in the following cases:

$$\mathrm{i}\mathcal{M}_{B,W,G} = \frac{\mathrm{i}}{(4\pi)^2\epsilon} \left[g_1^2 Y^2 + g_2^2 C_F^{(2)} + g_3^2 C_F^{(3)}\right] \overline{u_{L,R}}\not{p} u_{L,R} \,. \tag{483}$$

We therefore obtain:

$$\mathrm{i}\mathcal{M}_H^{e_R} = y^e_{\rho\alpha} (y^e_{\rho\alpha})^* \frac{\mathrm{i}}{16\pi^2\epsilon} \overline{u_R}\not{p} u_R \,, \tag{484}$$

$$\mathrm{i}\mathcal{M}_B^{e_R} = \frac{\mathrm{i}}{(4\pi)^2\epsilon} g_1^2 \overline{u_R}\not{p} u_R \,. \tag{485}$$

$$\mathrm{i}\mathcal{M}_H^{d_R} = y^d_{\rho\alpha} (y^d_{\rho\alpha})^* \frac{\mathrm{i}}{16\pi^2\epsilon} \overline{u_R}\not{p} u_R \,, \tag{486}$$

$$\mathrm{i}\mathcal{M}_{B,G}^{d_R} = \frac{\mathrm{i}}{(4\pi)^2\epsilon} \left[g_1^2 \left(\frac{1}{3}\right)^2 + g_3^2 C_F^{(3)}\right] \overline{u_R}\not{p} u_R \,. \tag{487}$$

$$\mathrm{i}\mathcal{M}_H^{u_R} = y^u_{\rho\alpha} (y^u_{\rho\alpha})^* \frac{\mathrm{i}}{16\pi^2\epsilon} \overline{u_R}\not{p} u_R \,, \tag{488}$$

$$\mathrm{i}\mathcal{M}_{B,G}^{u_R} = \frac{\mathrm{i}}{(4\pi)^2\epsilon} \left[g_1^2 \left(\frac{2}{3}\right)^2 + g_3^2 C_F^{(3)}\right] \overline{u_R}\not{p} u_R \,. \tag{489}$$

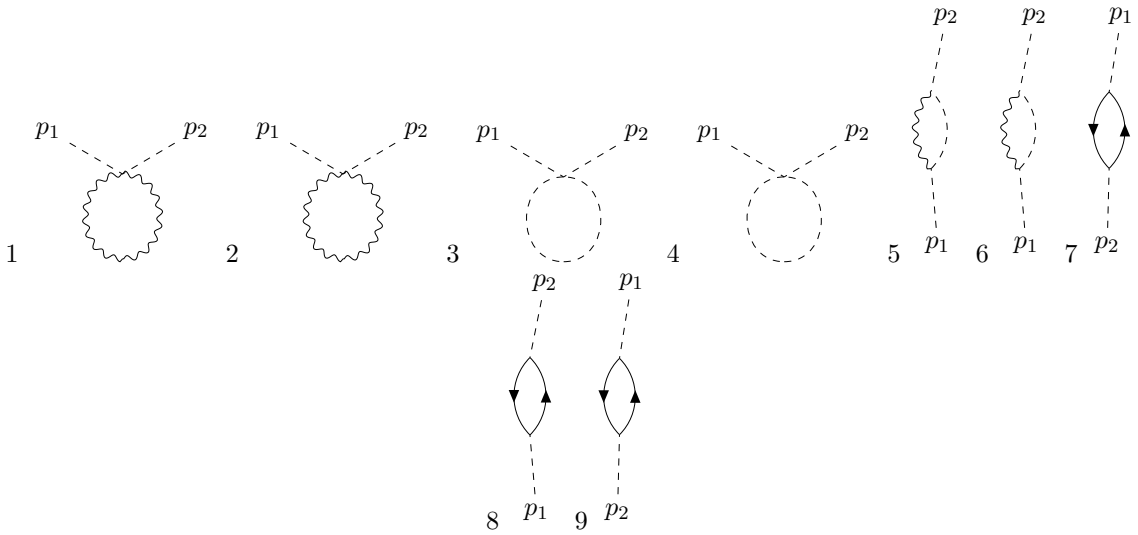

Figure 45: Diagrams contributing to the renormalization of the Higgs doublet kinetic term.

$$\mathrm{i}\mathcal{M}_H^{q_L} = \left[(y_{\alpha\rho}^u)^* y_{\alpha\rho}^u + (y_{\alpha\rho}^d)^* y_{\alpha\rho}^d\right] \frac{\mathrm{i}}{32\pi^2\epsilon} \overline{u_L} \not{p} u_L \,, \tag{490}$$

$$\mathrm{i}\mathcal{M}_{B,W,G}^{q_L} = \frac{\mathrm{i}}{(4\pi)^2\epsilon} \left[g_1^2 \left(\frac{1}{6}\right)^2 + g_2^2 C_F^{(2)} + g_3^2 C_F^{(3)}\right] \overline{u_L} \not{p} u_L \,. \tag{491}$$

H.2.2 Scalars

The diagrams contributing to the Higgs boson kinetic term are depicted in figure 45. The corresponding divergent amplitudes read:

$$\mathrm{i}\mathcal{M}_\psi^H = \left[y_{\sigma\rho}^e (y_{\sigma\rho}^e)^* + 3 y_{\sigma\rho}^d (y_{\sigma\rho}^d)^* + 3 y_{\sigma\rho}^u (y_{\sigma\rho}^u)^*\right] \frac{\mathrm{i}}{16\pi^2\epsilon} p^2 \,; \tag{492}$$

$$\mathrm{i}\mathcal{M}_B^H = (-g_1^2) \left(\frac{1}{2}\right)^2 I = \frac{\mathrm{i}}{(4\pi)^2\epsilon} \left(\frac{-g_1^2}{2}\right) p^2 \,, \tag{493}$$

where

$$I \equiv \int \frac{d^{\mathrm{d}}k}{(2\pi)^{\mathrm{d}}} \frac{1}{k^2 (k-p)^2} (2p-k)\cdot(2p-k) = (3A_2 - 4B_3) p^2 = \frac{\mathrm{i}}{(4\pi)^2\epsilon} 2p^2 \,; \tag{494}$$

$$\mathrm{i}\mathcal{M}_W^H = (-g_2^2) T_{ik}^a T_{ki}^a I = \frac{-2\mathrm{i}}{(4\pi)^2\epsilon} g_2^2 C_F^{(2)} p^2 \,. \tag{495}$$

Regarding the ALP, there are no divergent contributions to the kinetic term up to $\mathcal{O}(1/\Lambda)$.

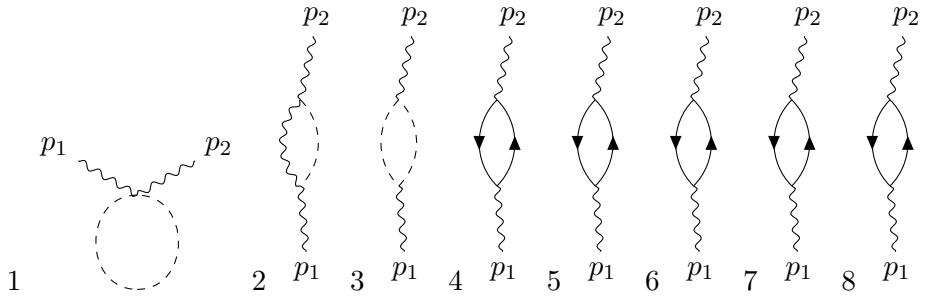

Figure 46: Diagrams contributing to the renormalization of the kinetic term of the abelian gauge boson.

H.2.3 Gauge fields

The diagrams contributing to the kinetic term of the U(1) gauge bosons are represented in figure 46. The corresponding divergent amplitudes are given by (with the external polarization vectors implicit):

$$\mathrm{i}\mathcal{M}_H^B = \frac{g_1^2}{4}\sum_i \delta_{ii} I' = \frac{\mathrm{i}}{(4\pi)^2\epsilon}\frac{g_1^2}{6}\left[p^\mu p^\nu - p^2 g^{\mu\nu}\right], \tag{496}$$

where

$$\begin{aligned} I' &\equiv \int \frac{d^{\mathrm{d}}k}{(2\pi)^{\mathrm{d}}}\frac{(2k-p)^\mu (2k-p)^\nu}{k^2(k-p)^2} = p^2 g^{\mu\nu}\left(-4B_3 + 16C_4\right) + p^\mu p^\nu\left(32C_4 - 8B_3 + A_2\right) \\ &= \frac{\mathrm{i}}{(4\pi)^2\epsilon}\frac{1}{3}\left[p^\mu p^\nu - p^2 g^{\mu\nu}\right]. \end{aligned} \tag{497}$$

Considering the fermionic loops (in particular the one associated to e_R), we have:

$$\mathrm{i}\mathcal{M}_{e_R}^B = (-1)\sum_\alpha \delta_{\alpha\alpha} g_1^2 I'' = \frac{\mathrm{i}}{(4\pi)^2\epsilon}\frac{2g_1^2}{3} n_G\left[p^\mu p^\nu - p^2 g^{\mu\nu}\right], \tag{498}$$

where $n_G = 3$ denotes the number of fermion generations and

$$\begin{aligned} I'' &\equiv \int \frac{d^{\mathrm{d}}k}{(2\pi)^{\mathrm{d}}}\frac{1}{k^2(k-p)^2}\left\{\mathrm{Tr}\left[\gamma^\mu P_R \not{k}\gamma^\nu P_R\left(\not{k}-\not{p}\right)\right] = \frac{1}{2}\mathrm{Tr}\left[\gamma^\mu \not{k}\gamma^\nu\left(\not{k}-\not{p}\right)\right]\right\} \\ &= \frac{\mathrm{d}}{2}\left[p^2 g^{\mu\nu}\left(A_2 - 4B_3 + 8C_4\right) + p^\mu p^\nu\left(16C_4 - 4B_3\right)\right] \\ &= \frac{\mathrm{i}}{(4\pi)^2\epsilon}\frac{2}{3}\left[p^2 g^{\mu\nu} - p^\mu p^\nu\right]. \end{aligned} \tag{499}$$

In the first line of the integral above, we omitted a second part of the trace originating from the projector, $\mathrm{Tr}\left[\gamma^5\gamma^\mu \not{k}\gamma^\nu\left(\not{k}-\not{p}\right)\right] = -\mathrm{i}k_\alpha(k-p)_\beta\epsilon^{\mu\nu\alpha\beta}\mathrm{d}/2$, which cannot contribute since the only structures allowed by gauge invariance are symmetric upon permutation of the indices $\mu \leftrightarrow \nu$.

In this way, all the other (LH or RH) fermionic loops can be easily computed by including the hypercharge factor Y^2 and the sum over colors and particles in the doublet. Altogether, they contribute with

$$\mathrm{i}\mathcal{M}_\psi^B = \frac{\mathrm{i}}{32\pi^2\epsilon} g_1^2\left[p^\mu p^\nu - p^2 g^{\mu\nu}\right] n_G\left(2 + \frac{22N_C}{27}\right). \tag{500}$$

In the case of non-abelian gauge theories (where we use a, b to denote the group indices), we have to take into account additional contributions from gauge boson self-interactions and ghost fields. The first of these contributions gives:

$$\mathrm{i}\mathcal{M}_W^W = \frac{-g_2^2}{2}\epsilon_{cad}\epsilon_{cbd}I''' = g_2^2\frac{\mathrm{i}\delta_{ab}}{(4\pi)^{2}\epsilon}\frac{10C_A^{(2)}}{3}\left[p^2 g^{\mu\nu} - p^\mu p^\nu\right], \tag{501}$$

where

$$\begin{aligned} I''' &\equiv \int \frac{d^{\mathrm{d}}k}{(2\pi)^{\mathrm{d}}}\Big[-8g^{\mu\nu}p^2 + (8-\mathrm{d})p^\mu p^\nu + 2\mathrm{d}(p^\mu k^\nu + p^\nu k^\mu) - 4\mathrm{d}k^\mu k^\nu\Big] \\ &= p^2 g^{\mu\nu}\Big[-8A_2 + 4\mathrm{d}(B_3 - 4A_4)\Big] + p^\mu p^\nu\Big[(8-\mathrm{d})A_2 + 8\mathrm{d}B_3 - 32\mathrm{d}C_4\Big] \\ &= \frac{\mathrm{i}}{(4\pi)^{2}\epsilon}\frac{20}{3}\left[p^\mu p^\nu - p^2 g^{\mu\nu}\right]; \end{aligned} \tag{502}$$

while the contribution from ghost fields reads:

$$\mathrm{i}\mathcal{M}_{\text{ghost}}^W = (-1)\mathrm{i}^2 g_2^2\epsilon_{amn}\epsilon_{bnm}I' = g_2^2\frac{\mathrm{i}\delta_{ab}}{(4\pi)^{2}\epsilon}\frac{C_A^{(2)}}{3}\left[p^2 g^{\mu\nu} - p^\mu p^\nu\right]. \tag{503}$$

On the other hand, the contribution from fermions is given by

$$\mathrm{i}\mathcal{M}_\psi^W = (-1)g_2^2 T_{ij}^a T_{ji}^b\sum_\alpha \delta_{\alpha\alpha}I'' = g_2^2\frac{\mathrm{i}\delta_{ab}}{(4\pi)^{2}\epsilon}\frac{2T_F^{(2)}}{3}n_G\left(1+N_C\right)\left[p^\mu p^\nu - p^2 g^{\mu\nu}\right]. \tag{504}$$

Finally, the diagram where the Higgs boson runs in the loop contributes with

$$\mathrm{i}\mathcal{M}_H^W = g_2^2 T_{ij}^a T_{ji}^b I' = g_2^2\frac{\mathrm{i}\delta_{ab}}{(4\pi)^{2}\epsilon}\frac{T_F^{(2)}}{3}\left[p^2 g^{\mu\nu} - p^\mu p^\nu\right]. \tag{505}$$

These results can be straightforwardly recast for the case of $SU(3)$:

$$\mathrm{i}\mathcal{M}_{G+\text{ghost}}^G = g_3^2\frac{\mathrm{i}\delta_{ab}}{(4\pi)^{2}\epsilon}\frac{11C_A^{(3)}}{3}\left[p^2 g^{\mu\nu} - p^\mu p^\nu\right]. \tag{506}$$

Regarding the fermions, all quarks u_R, d_R and q_L couple to the gluon and transform in the same (fundamental) representation of $SU(3)$. Their contribution can be therefore obtained from equation 504 with the replacement of $(1+N_C) \longrightarrow (1+1+2)$, leading to:

$$\mathrm{i}\mathcal{M}_\psi^G = g_3^2\frac{\mathrm{i}\delta_{ab}}{(4\pi)^{2}\epsilon}\frac{8T_F^{(3)}}{3}n_G\left[p^\mu p^\nu - p^2 g^{\mu\nu}\right]. \tag{507}$$

To obtain the final WFR factors, all previous amplitudes should be matched with the tree level amplitudes computed with the kinetic counterterm Lagrangian:

$$\mathrm{i}\mathcal{M}_{\text{EFT}}^\psi = \mathrm{i}(Z_\psi - 1)\bar{u}\not{p}u, \tag{508}$$

$$\mathrm{i}\mathcal{M}_{\text{EFT}}^H = \mathrm{i}(Z_H - 1)p^2, \tag{509}$$

$$\mathrm{i}\mathcal{M}_{\text{EFT}}^V = -\mathrm{i}(Z_V - 1)\left[p^2 g^{\mu\nu} - p^\mu p^\nu\right]\delta_{ab}. \tag{510}$$

H.3 Removing redundancies

The $\mathcal{R}$-operators generated in the process of renormalization can be removed upon field redefinitions, such as $S \longrightarrow S + \mathcal{O}'/\Lambda$. To linear order in $1/\Lambda$, the latter can be implemented via the EOMs [311] of the SM+ALP:

$$\partial^2 S = -m_S^2 S - \frac{\kappa_S}{2} S^2 - \frac{\lambda_S S^3}{3!} - \kappa_{SH}|H|^2 - \lambda_{SH} S|H|^2 \,; \tag{511}$$

$$\begin{aligned} D^2 H_k = &-\mu_H^2 H_k - 2\lambda_H |H|^2 H_k - (y^u)_{\alpha\beta} \overline{q^\alpha_{Lj}} \epsilon_{jk} u^\beta_R - (y^d)^\dagger_{\beta\alpha} \overline{d^\beta_R} q^\alpha_{Lk} \\ &- (y^e)^\dagger_{\beta\alpha} \overline{e^\beta_R} l^\alpha_{Lk} - \kappa_{SH} S H_k - \frac{\lambda_{SH}}{2} S^2 H_k \end{aligned} \tag{512}$$

$$i\not{D} q^\alpha_{Lk} = (y^d)_{\alpha\beta} H_k d^\beta_R + (y^u)_{\alpha\beta} \widetilde{H}_k u^\beta_R \tag{513}$$

$$i\not{D} l^\alpha_{Lk} = (y^e)_{\alpha\beta} H_k e^\beta_R \,; \tag{514}$$

$$i\not{D} d^\alpha_R = (y^d_{\alpha\beta})^\dagger H^\dagger_k q^\beta_{Lk} \,; \tag{515}$$

$$i\not{D} u^\alpha_R = (y^u_{\alpha\beta})^\dagger \widetilde{H}^\dagger_k q^\beta_{Lk} \,; \tag{516}$$

$$i\not{D} e^\alpha_R = (y^e_{\alpha\beta})^\dagger H^\dagger_k l^\beta_{Lk} \,, \tag{517}$$

where we again used latin (greek) indices for $SU(2)$ (flavour). Using these equations, we arrive at the following relations, valid on-shell[2]:

$$\mathcal{R}_{S\Box} = -m_S^2 S^3 - \frac{\kappa_S}{2} S^4 - \frac{\lambda_S}{3!} \mathcal{O}_5 - \kappa_{SH} S^2 |H|^2 - \lambda_{SH} \mathcal{O}_{S^3} \,, \tag{518}$$

$$\begin{aligned} \mathcal{R}_{SH\Box} = &-\mu_H^2 S|H|^2 - 2\lambda_H \mathcal{O}_S - y^u_{\alpha\beta} \mathcal{O}^{\alpha\beta}_{SHu} - (y^d)^*_{\alpha\beta} (\mathcal{O}^{\alpha\beta}_{SHd})^\dagger \\ &- (y^e)^*_{\alpha\beta} (\mathcal{O}^{\alpha\beta}_{SHe})^\dagger - \kappa_{SH} S^2 |H|^2 - \frac{\lambda_{SH}}{2} \mathcal{O}_{S^3} \,, \end{aligned} \tag{519}$$

$$\mathcal{R}_{HS\Box} = -m_S^2 S|H|^2 - \frac{\kappa_S}{2} S^2 |H|^2 - \frac{\lambda_S}{3!} \mathcal{O}_{S^3} - \kappa_{SH} |H|^4 - \lambda_{SH} \mathcal{O}_S \,, \tag{520}$$

$$\mathcal{R}^{\alpha\beta}_{Sq} = y^u_{\beta\sigma} \mathcal{O}^{\alpha\sigma}_{SHu} + y^d_{\beta\sigma} \mathcal{O}^{\alpha\sigma}_{SHd} \,, \tag{521}$$

$$\mathcal{R}^{\alpha\beta}_{Sl} = y^e_{\beta\sigma} \mathcal{O}^{\alpha\sigma}_{SHe} \,, \tag{522}$$

$$\mathcal{R}^{\alpha\beta}_{Su} = (y^u)^*_{\sigma\beta} (\mathcal{O}^{\sigma\alpha}_{SHu})^\dagger \,, \tag{523}$$

$$\mathcal{R}^{\alpha\beta}_{Sd} = (y^d)^*_{\sigma\beta} (\mathcal{O}^{\sigma\alpha}_{SHd})^\dagger \,, \tag{524}$$

$$\mathcal{R}^{\alpha\beta}_{Se} = (y^e)^*_{\sigma\beta} (\mathcal{O}^{\sigma\alpha}_{SHe})^\dagger \,. \tag{525}$$

[2] To clarify the notation, the conjugated operator of $\mathcal{O}^{\alpha\beta}_{SHd} = S\overline{q^\alpha_L} \phi d^\beta_R$ is $(\mathcal{O}^{\alpha\beta}_{SHd})^\dagger = \overline{d^\beta_R} \phi^\dagger q^\alpha_L S$.

Altogether, these equations lead to the following replacements:

$$a'_{SHu} \to a'_{SHu} - r_{SH\Box} y^u + r_{Sq} y^u - y^u r_{Su}^T , \tag{526}$$
$$a'_{SHd} \to a'_{SHd} + r_{SH\Box} y^d + r_{Sq} y^d - y^d r_{Sd}^T , \tag{527}$$
$$a'_{SHe} \to a'_{SHe} + r_{SH\Box} y^e + r_{Sl} y^e - y^e r_{Se}^T . \tag{528}$$

H.4 Chirality-preserving basis and comparison with the literature

Commonly, the ALP Lagrangian is written in a different basis than the one used in this work [184, 230, 287, 288, 312], favoring operators with derivative terms on the ALP so that its shift-symmetry is explicit:

$$\mathcal{L}_{\text{shift}} = (\partial_\mu S) \sum_\psi \bar{\psi} C_\psi \gamma^\mu \psi + g_3^2 C_G S G^A_{\mu\nu} \widetilde{G}^{\mu\nu,A} + g_2^2 C_W S W^A_{\mu\nu} \widetilde{W}^{\mu\nu,A} + g_1^2 C_B S B_{\mu\nu} \widetilde{B}^{\mu\nu} , \tag{529}$$

with ψ summing over all the chiral fermions in the theory. In the leptonic sector alone, we count $9+9 = 18$ parameters in this basis, assuming both CP-preserving and CP-breaking interactions; while in our basis there also are 18 parameters in a_{SHe}. However, ours describes both shift-breaking and shift-symmetric operators, while the basis in equation 529 preserves the ALP shift-symmetry. Hence, some of the $d.o.f.$ in $C_e + C_l$ must be redundant.

Under certain assumptions, it is even possible to trade completely the LH operators by the RH ones, since

$$\begin{aligned}
&\partial_\mu S \overline{e}_R \left[\frac{y^{e-1} C_l y^e + y^{e\dagger} C_l (y^{e-1})^\dagger}{2} \right] e_R \\
&= -S \overline{e_R} \frac{y^{e-1} C_e y^e}{2} \left[\overleftarrow{\not{D}} + \not{D} \right] e_R - S \overline{e_R} \frac{y^{e\dagger} C (y^{e-1})^\dagger}{2} \left[\overleftarrow{\not{D}} + \not{D} \right] e_R \\
&= -S \overline{e_R} y^{e-1} C_l y^e \overleftarrow{\not{D}} e_R - S \overline{e_R} \frac{-y^{e-1} C_l y^e + y^{e\dagger} C_l (y^{e-1})^\dagger}{2} \overleftarrow{\not{D}} e_R \\
&\qquad - S \overline{e_R} y^{e\dagger} C_l (y^{e-1})^\dagger \not{D} e_R - S \overline{e_R} \frac{y^{e-1} C_l y_e - y^{e\dagger} C_l (y^{e-1})^\dagger}{2} \not{D} e_R \\
&= -S \left[\mathrm{i} \overline{l_L} H C_l y^e e_R + \text{h.c.} \right] - S \overline{e_R} \left[\frac{y^{e-1} C_l y^e - y^{e\dagger} C_l (y^{e-1})^\dagger}{2} \right] \left[-\overleftarrow{\not{D}} + \not{D} \right] e_R \\
&= -\partial_\mu S \overline{l_L} C_l \gamma^\mu l_L - S \overline{e_R} \left[\frac{y^{e-1} C_l y^e - y^{e\dagger} C_l (y^{e-1})^\dagger}{2} \right] \left[-\overleftarrow{\not{D}} + \not{D} \right] e_R ,
\end{aligned}$$

where we used IBP, together with the EOMs of leptons. (We ignored corrections to the anomalous gauge operators that arise due to the anomaly equation [290].) A sufficient condition for the LH↔RH equivalence is therefore to make the last term vanish, which is the case, for example, if $[C_l, y^e] = 0$.

In this case, the minimal chirality-preserving basis can be constructed out of the three RH fermionic operators solely. Furthermore, in this limit, the Wilson coefficients in the chirality-preserving and chirality-flipping bases become unambiguously related and we can obtain the RGEs in the former. Indeed, upon the use of IBP and the EOMs,

$$(\partial_\mu S)\overline{e_R}C_e\gamma^\mu e_R = \mathrm{i}S\overline{e_R}C_e\left[\mathrm{i}\not{D} + \mathrm{i}\overleftarrow{\not{D}}\right]e_R = \mathrm{i}S\left[\overline{e_R}C_e(y^e)^\dagger H^\dagger l_L - \overline{l_L}Hy^eC_e e_R\right], \tag{530}$$

allowing us to identify

$$a_{SHe} = -\mathrm{Re}\left[y^eC_e\right], \qquad \text{in the } CP\text{-preserving limit.} \tag{531}$$

Similarly for the other fermions. Note that the presence of the Yukawa matrix is necessary to make some of the $d.o.f.$ in a_{SHe} inactive, otherwise such identification would be impossible (because the CP-even matrix a_{SHe} contains 9 real parameters, whereas C_e is made of only 6). To see that this is indeed the case, consider the limit of $y^e \longrightarrow 0$ which makes a_{SHe} vanish, in contrast with the result from our original basis where these two parameters are independent. Furthermore, equation 531 gives a sufficient condition to make the Wilson coefficients shift-symmetric in the chirality-flipping basis, for any arbitrary hermitian matrix C_e; see Ref. [8].

From equation 531, it follows that the evolution of the C-matrices is given by $\dot{C} = y^{-1}\dot{y}y^{-1}a - y^{-1}\dot{a}$. After replacing $\dot{a}_{SH\psi}$ by equations 249, 250 and 251, and using equations 208-210 in Ref. [8] to account for the running of the SM Yukawa matrices, we obtain:

$$\begin{aligned}\beta_{C_u} =& y^{u\dagger}y^uC_u + 2C_uy^{u\dagger}y^u + 2\lambda_{SH}C_u + (y^u)^{-1}y^dC_dy^{d\dagger}y^u \\ &+ \frac{17}{3}g_1^4C_B + 9g_2^4C_W + 32C_Gg_3^4C_G - 2\gamma',\end{aligned} \tag{532}$$

$$\begin{aligned}\beta_{C_d} =& y^{d\dagger}y^dC_d + 2C_dy^{d\dagger}y^d + 2\lambda_{SH}C_d + (y^d)^{-1}y^uC_uy^\dagger y^d \\ &+ \frac{5}{3}g_1^4C_B + 9g_2^4C_W + 32g_3^4C_G + 2\gamma',\end{aligned} \tag{533}$$

$$\beta_{C_e} = y^{e\dagger}y^eC_e + 2C_ey^{e\dagger}y^e + 2\lambda_{SH}C_e + 15g_1^4C_B + 9g_2^4C_W + 2\gamma', \tag{534}$$

with

$$\gamma' \equiv \mathrm{Tr}\left[y^eC_ey^{e\dagger} + 3y^dC_dy^{d\dagger} - 3y^uC_uy^{u\dagger}\right]. \tag{535}$$

Note that no gauge corrections arise in the renormalization group evolution of the parameters in the new basis. Although these corrections are present in the original RGEs of the $\mathcal{O}_{SHu}$, $\mathcal{O}_{SHd}$ and $\mathcal{O}_{SHe}$ operators, such contributions are exactly canceled by the running of the Yukawa matrices in the SM. The argument goes as follows: since $J^\mu \equiv \overline{\psi}\gamma^\mu\psi$ is a conserved $U(1)$ current, it cannot be renormalized *directly*. Indeed, the difference δJ^μ between the renormalized (J_R) and non-renormalized (J_0) currents, which is a sum of ϵ pole terms, must itself satisfy the Ward identity. Hence, $\partial_\mu\delta J^\mu = 0$ and $J_0^\mu = J_R^\mu$. This does not hold if there are redundant operators involving gauge fields which can give corrections to $(\partial_\mu S)J^\mu$ upon the

use of the EOMs. However, no redundant operators involving the ALP and the gauge bosons exist (up to dimension five) in our Green basis. The argument is completed once we note that the non-abelian structure of the weak and strong interactions are not manifest in the renormalization of the ALP-fermion operators at one-loop.

In Ref. [312], the ALP Lagrangian in equation 529 is supplemented by the following interaction:

$$\mathcal{L}'_{\text{shift}} \supset c_H \left(\partial_\mu S\right) \mathrm{i} \left[H^\dagger D^\mu H - \left(D_\mu H\right)^\dagger H\right] . \tag{536}$$

Such operator can be removed by redefining $H \longrightarrow e^{\mathrm{i}c_H S} H$ and $\psi \longrightarrow e^{-\mathrm{i}2c_H Y_\psi S}\psi$. This leads to a shift in the ALP–fermion couplings of the form $C_\psi \longrightarrow C_\psi + 2c_H Y_\psi$, so that the RGEs in the basis without the operator above are given by $\dot{C}'_\psi = \dot{C}_\psi + 2\dot{c}_H Y_\psi$. In this case, the analogous of equation 530, with the inclusion of all fermions, leads to:

$$a_{SHu} = \frac{y^u}{2f}\left(C'_q - C'_u\right) , \tag{537}$$

$$a_{SHd} = \frac{y^d}{2f}\left(C'_q - C'_d\right) , \tag{538}$$

$$a_{SHe} = \frac{y^e}{2f}\left(C'_l - C'_e\right) , \tag{539}$$

in the one-family limit with real Yukawa couplings[3]. Using the RGEs in appendix A of Ref. [312], together with the evolution equations of the Yukawa matrices provided in Ref. [8], we can translate the results in that Ref. into our original basis and compare the final RGEs with the ones obtained in section 6.2.2. We find a single mismatch in the sign of the last term in equations 249–251. We do not find enough information to track the origin of this discrepancy though.

Additionally, we can compare directly the one-loop ALP-fermion couplings induced by the ALP-gauge boson operators in equations 532–534 with the results obtained in Ref. [184]. We find exact agreement.

Finally, let us comment on the factorization of the gauge couplings in the bosonic ALP Lagrangian which is often adopted to make C_G, C_W and C_B scale-invariant, that is $dC_V/d\mu = 0$, at one-loop order [287]. To check that this is the case, we focus on the gluonic operator. The relation between the Wilson coefficients in the this and our bases implies, under the previous hypothesis, that

$$\beta_{s\widetilde{G}} = 64\pi^3 C_G \mu \frac{d(\alpha_3)}{d\mu} . \tag{540}$$

Employing the running of the strong gauge coupling at one-loop [8],

$$\mu\frac{d\alpha_3}{d\mu} = \frac{\alpha_3^2}{\pi}\left(-\frac{11}{2} + \frac{2n_G}{3}\right) = -\frac{\alpha_3^2}{\pi}\frac{7}{2} , \tag{541}$$

[3]The $1/2$ factor comes from the different normalization of the ALP–fermion couplings in the basis of Ref. [312].

the previous RGE becomes

$$\beta_{s\widetilde{G}} = 16\pi^2(-14)\alpha_s^2 C_G = -14 g_3^4 C_G\,, \tag{542}$$

which matches exactly our equation 252, upon the identification $a_{s\widetilde{G}} = g_3^2 C_G$. The scale-invariance of the remaining $C_{W,B}$ couplings can be checked analogously.

Appendix I

Computations in the ALP LEFT

I.1 Divergences at one-loop

Analogously to section H.1, here we enumerate the different processes and amplitudes we have obtained in order to fix the counterterms in the ALP LEFT. In this case, we do not compute the one-loop diagrams by hand, but depict all the diagrams involved, pointing out the relations we used to simplify the results from `FormCalc` to match onto the LEFT.

I.1.1 $V(p_1) \to \psi^\alpha(p_2)\overline{\psi}^\beta(p_3)$

The diagrams contributing to this process are represented in figure 47, for $V = A$ and $\psi = e$. The corresponding divergent amplitudes read:

$$\begin{aligned} \mathrm{i}\mathcal{M}_{1+2+4} = \frac{Q_e\tilde{e}}{32\pi^2\epsilon}\Big[& 4\tilde{a}_{s\widetilde{A}}(\tilde{c}_e)_{\alpha\beta}\,\epsilon_{\mu\nu\sigma\rho}\epsilon_*^\sigma p_1^\rho \overline{u}_2 P_R \gamma^\mu\gamma^\nu v_3 \\ & + \mathrm{i}(\tilde{c}_e\tilde{c}_e^\dagger)_{\alpha\beta}\epsilon_*^\mu \overline{u}_2 P_R\gamma_\mu v_3\Big] + \dots, \end{aligned} \tag{543}$$

$$\begin{aligned} \mathrm{i}\mathcal{M}_3 = \frac{\mathrm{i}}{4\pi\epsilon}Q_e^2\tilde{\alpha}_{\mathrm{em}}\Big\{ & (-3\tilde{a}_{eA}\tilde{m}_e^\dagger - 3\tilde{m}_e\tilde{a}_{eA}^\dagger + Q_e\tilde{e}\delta)_{\alpha\beta}\epsilon_*^\mu\overline{u}_2 P_R\gamma_\mu v_3 \\ & + 2\left(\tilde{a}_{eA}\right)_{\alpha\beta}\Big[\epsilon_*^\mu p_1^\nu \overline{u}_2 P_R\gamma_\mu\gamma_\nu v_3 + 2\left(-2\epsilon_*\cdot p_3 + \epsilon_*\cdot p_2\right)u_2 P_R v_3\Big]\Big\} + \dots, \end{aligned} \tag{544}$$

where we wrote only the LH or RH parts of the amplitudes which are sufficient to fix univocally the counterterms (the dots encode the remaining chiral part of the amplitudes that we do not show).

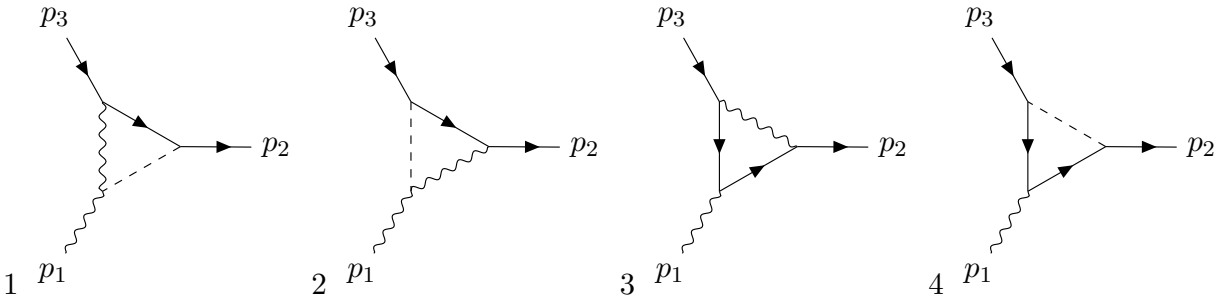

Figure 47: Diagrams contributing to the renormalization of 1 photon–2 fermion interactions.

On the other hand, the tree level amplitude is given by:

$$\begin{aligned} \mathrm{i}\mathcal{M}_{\mathrm{EFT}} = {} & \mathrm{i}Q_e\tilde{e}\left(Z_{\alpha\beta}-1\right)\epsilon_*^{\mu}\overline{u}_2 P_R\gamma_\mu v_3 - 2\mathrm{i}\left(\tilde{a}_{eA}\right)_{\alpha\beta}\epsilon_*^{\mu}p_1^{\nu}\overline{u}_2 P_R\left(\gamma_\mu\gamma_\nu - g_{\mu\nu}\right)v_3 \\ & + \mathrm{i}Q_e\tilde{e}\left(\tilde{r}_{e\Box}\right)_{\alpha\beta}\left(\epsilon_*\cdot p_3 - \epsilon_*\cdot p_2\right)\overline{u}_2 P_R v_3\,. \end{aligned} \tag{545}$$

In particular, this process allows us to cross-check the WFR of the electron:

$$\left(Z_{e_L}-1\right) = -\frac{1}{32\pi^2\epsilon}\tilde{c}_e\tilde{c}_e^{\dagger} - \frac{1}{16\pi^2\epsilon}Q_{\tilde{e}}^2\tilde{e}^2 + \frac{3}{16\pi^2\epsilon}Q_e\tilde{e}\left(\tilde{a}_{eA}\tilde{m}_e^{\dagger} + \tilde{m}_e\tilde{a}_{eA}^{\dagger}\right), \tag{546}$$

in matrix form. Similarly, by extracting the RH elements in the one-loop amplitude, we fix $\left(Z_{e_R}-1\right)$.

The term with the Levi-Civita tensor in equation 543 can be reduced using the identity 355:

$$\epsilon_{\mu\nu\sigma\rho}P_R\gamma^{\mu}\gamma^{\nu} = -\mathrm{i}\epsilon_{\mu\nu\sigma\rho}P_R\sigma^{\mu\nu} = -2P_R\gamma_5\sigma_{\sigma\rho} = 2\mathrm{i}P_R\left(g_{\sigma\rho}-\gamma_\rho\gamma_\sigma\right), \tag{547}$$

so that it can be directly matched to $\mathcal{M}_{\mathrm{EFT}}$.

To obtain easily the results for processes involving quarks, we did not replace the electric charge Q_e in the previous results.

I.1.2 $S(p_1) \longrightarrow \psi^{\alpha}(p_2)\overline{\psi}^{\beta}(p_3)$

The diagrams contributing to this process are represented in figure 48, for $\psi = u$. The corresponding amplitudes read:

$$\begin{aligned} \mathrm{i}\mathcal{M}_{1+2} = \frac{1}{16\pi^2\epsilon}\Bigg[& -2\left\{(\tilde{a}_u)_{\alpha\sigma}(\tilde{c}_u)_{\rho\beta}\tilde{m}_u^{*\rho\sigma} + (\tilde{a}_u)_{\sigma\beta}(\tilde{c}_u)_{\alpha\rho}\tilde{m}_u^{*\sigma\rho}\right\}\overline{u}_2 P_R v_3 \\ & - (\tilde{a}_u)_{\alpha\sigma}(\tilde{c}_u)^*_{\beta\sigma}\overline{u_2}P_R\not{p}_3 v_3 - (\tilde{a}_u)^*_{\beta\sigma}(\tilde{c}_u)_{\alpha\sigma}\overline{u_2}P_R\not{p}_2 v_3\Bigg] + \dots\,, \end{aligned} \tag{548}$$

(549)

$$\begin{aligned} \mathrm{i}\mathcal{M}_{3+4} &= -\mathrm{i}\frac{\delta_{\alpha\beta}}{\pi\epsilon}\left(\tilde{\alpha}_{\mathrm{em}}\frac{Q_u^2}{4}\tilde{a}_{s\widetilde{A}} + \tilde{\alpha}_3\frac{1}{3}\tilde{a}_{s\widetilde{G}}\right)\left[\epsilon_{\mu\nu\rho\sigma}p_3^{\sigma}\overline{u}_2 P_L\gamma^{\mu}\gamma^{\nu}\gamma^{\rho}v_3 + \dots\right] \\ &= \frac{\delta_{\alpha\beta}}{\pi\epsilon}\left(\tilde{\alpha}_{\mathrm{em}}\frac{Q_u^2}{4}\tilde{a}_{s\widetilde{A}} + \tilde{\alpha}_3\frac{1}{3}\tilde{a}_{s\widetilde{G}}\right)\left[-6\overline{u}\not{p}_2 P_R v + \dots\right], \end{aligned} \tag{550}$$

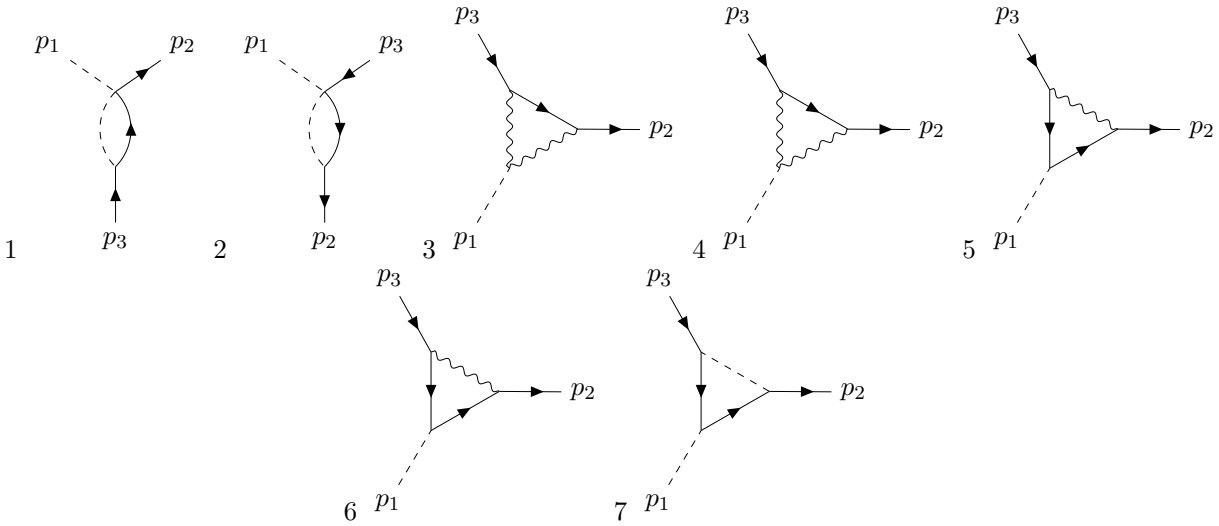

Figure 48: Diagrams contributing to the renormalization of 1 scalar–2 fermion interactions.

where we used the identity 352. Furthermore,

$$\mathrm{i}\mathcal{M}_{5+6} = -\frac{4}{9\pi\epsilon}\left(\tilde{\alpha}_{\mathrm{em}} + 3\tilde{\alpha}_3\right)(\tilde{c}_u)_{\alpha\beta}\overline{u_2}P_R v_3 + \dots\,, \tag{551}$$

$$\mathrm{i}\mathcal{M}_7 = \frac{1}{16\pi^2\epsilon}(\tilde{c}_u)_{\alpha\sigma}(\tilde{c}_u)^*_{\rho\sigma}(\tilde{c}_u)_{\rho\beta}\overline{u_2}P_R v_3 + \dots \tag{552}$$

On the other hand, the tree level EFT amplitude is given by:

$$\begin{aligned}\mathrm{i}\mathcal{M}_{\mathrm{EFT}} = &-(\tilde{c}_u)_{\alpha\beta}\overline{u}_2 P_R v_3 + (\tilde{c}_u)^*_{\beta\alpha}\overline{u}_2 P_L v_3 + (\tilde{r}_{Su_L})^*_{\beta\alpha}\overline{u}_2 P_R \not{p}_2 v_3 \\ &+ (\tilde{r}_{Su_R})^*_{\beta\alpha}\overline{u}_2 P_L \not{p}_2 v_3 + (\tilde{r}_{Su_L})_{\alpha\beta}\overline{u}_2 P_R \not{p}_3 v_3 + (\tilde{r}_{Su_R})_{\alpha\beta}\overline{u}_2 P_L \not{p}_3 v_3\,.\end{aligned} \tag{553}$$

The amplitudes involving other fermions are again trivially obtained from these results (replacing the corresponding indices and charges).

I.1.3 $S(p_1)S(p_2) \to \psi^\alpha(p_3)\overline{\psi}^\beta(p_4)$

The diagrams contributing to this process are represented in figure 49, for $\psi = u$. The corresponding amplitudes are very similar to the previous case and no additional identity is required to reduce them.

I.1.4 $S(p_1) \longrightarrow V^\mu(p_2)V^\nu(p_3)$

The diagrams depicted in figure 50, contributing to the process $S \longrightarrow AA$, lead to the following divergent amplitude[1]:

$$\begin{aligned}
\mathrm{i}\mathcal{M}_{2\text{–}7} = \frac{\tilde{e}}{2\pi^2\epsilon}\epsilon_2^{*\mu}\epsilon_3^{*\nu}p_2^\sigma p_3^\rho\Big[&Q_e\left\{\mathrm{Tr}\left[\tilde{c}_e\tilde{a}_{eA}^\dagger + \tilde{c}_e^\dagger\tilde{a}_{eA}\right]\mathrm{i}\epsilon_{\mu\nu\sigma\rho} - \mathrm{Tr}\left[\tilde{c}_e\tilde{c}_{eA}^\dagger - \tilde{c}_e^\dagger\tilde{c}_{eA}\right]\left(g_{\mu\rho}g_{\nu\sigma} - g_{\mu\nu}g_{\sigma\rho}\right)\right\}\\
&+ 3Q_d\left\{\mathrm{Tr}\left[\tilde{c}_d\tilde{a}_{dA}^\dagger + \tilde{c}_d^\dagger\tilde{a}_{dA}\right]\mathrm{i}\epsilon_{\mu\nu\sigma\rho} - \mathrm{Tr}\left[\tilde{c}_d\tilde{a}_{dA}^\dagger - \tilde{c}_d^\dagger\tilde{a}_{dA}\right]\left(g_{\mu\rho}g_{\nu\sigma} - g_{\mu\nu}g_{\sigma\rho}\right)\right\}\\
&+ 3Q_u\left\{\mathrm{Tr}\left[\tilde{c}_u\tilde{a}_{uA}^\dagger + \tilde{c}_u^\dagger\tilde{a}_{uA}\right]\mathrm{i}\epsilon_{\mu\nu\sigma\rho} - \mathrm{Tr}\left[\tilde{a}_u\tilde{a}_{uA}^\dagger - \tilde{c}_u^\dagger\tilde{a}_{uA}\right]\left(g_{\mu\rho}g_{\nu\sigma} - g_{\mu\nu}g_{\sigma\rho}\right)\right\}\Big]\,.
\end{aligned} \tag{554}$$

The component of the trace proportional to the metric terms, which is matched to the CP-odd operator $SA^{\mu\nu}A_{\mu\nu}$, can be decomposed as

$$\mathrm{Tr}\left[\tilde{c}_\psi\tilde{a}_{\psi A}^\dagger - \tilde{c}_\psi^\dagger\tilde{a}_{\psi A}\right] = 2\mathrm{i}\mathrm{Tr}\left[\mathrm{Im}(\tilde{c}_\psi)\mathrm{Re}(\tilde{a}_{\psi A}) - \mathrm{Re}(\tilde{c}_\psi)\mathrm{Im}(\tilde{a}_{\psi A})\right]. \tag{555}$$

As expected, by considering only the CP-even part of the singlet Yukawa and dipole operators (that is, by taking their coefficients to be real), the contribution above vanishes.

The tree level amplitude for this process reads[2]:

$$\mathrm{i}\mathcal{M}_{\mathrm{EFT}} = 4\mathrm{i}\tilde{a}_{SA}\epsilon_{\mu\nu\sigma\rho}\epsilon_2^{*\mu}\epsilon_3^{*\nu}p_2^\sigma p_3^\rho\,. \tag{556}$$

This and the one-loop amplitude can be therefore matched straightforwardly. The same conclusion holds for the gluon case.

I.1.5 $S(p_1)S(p_2) \longrightarrow S(p_3)S(p_4)$

There are 72 diagrams contributing to this process; those not involving the quarks are represented in figure 51. The corresponding one-loop amplitudes are trivially matched to the tree level EFT.

I.1.6 $S(p_1) \longrightarrow S(p_2)$

The diagrams contributing to this process are represented in figure 52. We focus on the insertion of effective operators, which can only contribute to the singlet mass along with three insertions of $\tilde{m}_\psi$. Therefore, using the BF in equation 268, we compute the amplitude associated to $S \longrightarrow S\varphi\varphi\varphi$:

$$\begin{aligned}
\mathrm{i}\mathcal{M}_{7+8+9} =& \frac{9\mathrm{i}}{2\pi^2\epsilon}\mathrm{Tr}\left[\tilde{m}_d^\dagger\tilde{a}_d\tilde{m}_d^\dagger\tilde{m}_d + \tilde{m}_d^\dagger\tilde{m}_d\tilde{a}_d^\dagger\tilde{m}_d + \tilde{m}_u^\dagger\tilde{a}_u\tilde{m}_u^\dagger\tilde{m}_u + \tilde{m}_u^\dagger\tilde{m}_u\tilde{a}_u^\dagger\tilde{m}_u\right]\\
&+ \frac{3\mathrm{i}}{2\pi^2\epsilon}\mathrm{Tr}\left[\tilde{m}_e^\dagger\tilde{a}_e\tilde{m}_e^\dagger\tilde{m}_e + \tilde{m}_e^\dagger\tilde{m}_e\tilde{a}_e^\dagger\tilde{m}_e\right]\,.
\end{aligned} \tag{557}$$

[1] We ignore the first diagram in figure 50, which is of higher order.

[2] Check footnote 1.

This should be matched to the tree level amplitude from the spurion interaction

$$\mathcal{L}_{S^2\varphi^3} = -\frac{a_{S^2\varphi^3}}{2} S^2\varphi^3\,, \quad \text{where} \quad a_{S^2\varphi^3}\langle\varphi\rangle^3 \equiv \tilde{m}^2\,, \tag{558}$$

given by:

$$\mathrm{i}\mathcal{M}_{\text{EFT}} = -\mathrm{i}3!a_{S^2\varphi^3}\,. \tag{559}$$

We cross checked the counterterm resulting from this procedure with that obtained in the limit of real and diagonal fermion masses, with no insertion of the BF. The results match.

I.1.7 $\psi^\alpha(p_1) \longrightarrow \psi^\beta(p_2)$

The diagrams contributing to this process are represented in figure 53, for $\psi = e$. Similarly to the previous case, the effective operators can only contribute with two insertions of the fermion mass. We therefore compute the process $\psi \longrightarrow \psi\varphi\varphi$, to fix the mass counterterm. For the case of the electron, the corresponding one-loop amplitude is:

$$\mathrm{i}\mathcal{M}_{2+3} = -\frac{3}{4\pi^2\epsilon}\mathrm{i}\tilde{e}Q_e\left(\tilde{m}_e\tilde{m}_e^\dagger\tilde{a}_{eA} + \tilde{a}_{eA}\tilde{m}_e^\dagger\tilde{m}_e\right)_{\beta\alpha}\overline{u}_2 P_R u_1 + \dots \tag{560}$$

There is also a contribution proportional to the scalar mass:

$$\mathrm{i}\mathcal{M}_4 = -\mathrm{i}\frac{1}{16\pi^2}\tilde{m}_S^2\,(\tilde{a}_e)_{\beta\alpha}\,\overline{u}_2 P_R u_1 + \dots \tag{561}$$

The sum of these amplitudes is finally matched to tree level one,

$$\mathrm{i}\mathcal{M}_{\text{EFT}} = -\mathrm{i}2!\tilde{m}_e^{\beta\alpha}\overline{u}_2 P_R u_1 + \dots \tag{562}$$

Similar considerations hold for quarks, with extra contributions from the chromomagnetic operators.

I.2 Removing redundancies

The purely SMEFT operators in equation 267 can be redefined away using the relation[3]

$$D^2 = \not{D}^2 + \frac{\sigma_{\mu\nu}}{2}\left(\tilde{e}QA^{\mu\nu} + \tilde{g}_3 G^{A\mu\nu}T^A\right)\,, \tag{563}$$

and the following EOM of the ALP LEFT:

$$\mathrm{i}\not{D}\psi = \tilde{m}_\psi\psi_R + \tilde{m}_\psi^\dagger\psi_L - \mathrm{i}\tilde{c}_\psi S\psi_R + \mathrm{i}\tilde{c}_\psi^\dagger S\psi_L\,. \tag{564}$$

[3]Note that $D^2 = g_{\mu\nu}D^\mu D^\nu = \left(\gamma_\mu\gamma_\nu + \mathrm{i}\sigma_{\mu\nu}\right)D^\mu D^\nu$. Since the σ-matrix is anti-symmetric, $D^2 = \not{D}^2 + \mathrm{i}\sigma_{\mu\nu}[D^\mu, D^\nu]/2$. Using that $A_{\mu\nu} = \mathrm{i}[D_\mu, D_\nu]/2$ (in the minus sign convention), we obtain equation 563.

To correctly use the EOM, we must start with a Lagrangian that is explicitly hermitian,

$$\mathcal{L}_R \supset \overline{\psi}_L^{\alpha}(\tilde{r}_{\psi\square})_{\alpha\beta}\not{D}^2\overline{\psi}_R^{\beta} + \overline{\psi}^{\beta}\overleftarrow{\not{D}}^2(\tilde{r}^{\dagger}_{\psi\square})_{\beta\alpha}\psi_L^{\alpha}\,; \tag{565}$$

alternatively, using IBP, we can consider

$$\mathcal{L}'_R \supset \frac{1}{2}\left[\overline{\psi}_L^{\alpha}(\tilde{r}_{\psi\square})_{\alpha\beta}\not{D}^2\psi_R^{\beta} + \overline{\psi}^{\beta}\overleftarrow{\not{D}}^2(\tilde{r}^{\dagger}_{\psi\square})_{\beta\alpha}\psi_L^{\alpha} + \overline{\psi}_L^{\alpha}(\tilde{r}_{\psi\square})_{\alpha\beta}\overleftarrow{\not{D}}^2\psi_R^{\beta} + \overline{\psi}^{\beta}(\tilde{r}^{\dagger}_{\psi\square})_{\beta\alpha}\not{D}^2\psi_L^{\alpha}\right], \tag{566}$$

which we take from now on. Applying the EOM in the first two terms, we obtain:

$$\mathcal{L}'_R \supset -\frac{1}{2}\left[\overline{\psi}_L\tilde{r}_{\psi\square}\,(\mathrm{i}\not{D})\left[\tilde{m}^{\dagger}_{\psi} + \mathrm{i}\tilde{c}^{\dagger}_{\psi}S\right]\psi_L - \overline{\psi}_L\left[\tilde{m}_{\psi} - \mathrm{i}S\tilde{c}_{\psi}\right](\mathrm{i}\overleftarrow{\not{D}})\tilde{r}^{\dagger}_{\psi\square}\psi_L + \dots\right]. \tag{567}$$

The two terms, in this equation, proportional to the mass contribute to the WFR of the LH fermions. Matching to

$$\left(Z_{\psi L} - 1\right)\overline{\psi}_L\mathrm{i}\not{D}\psi_L\,, \tag{568}$$

we obtain the following counterterm:

$$Z_{\psi L} - 1 = -\frac{1}{2}\left(\tilde{r}_{\psi\square}\tilde{m}^{\dagger}_{\psi} + \tilde{m}_{\psi}\tilde{r}^{\dagger}_{\psi\square}\right). \tag{569}$$

In the same way, applying the EOM to the last two operators in equation 566, we find:

$$Z_{\psi R} - 1 = -\frac{1}{2}\left(\tilde{m}^{\dagger}_{\psi}\tilde{r}_{\psi\square} + \tilde{r}^{\dagger}_{\psi\square}\tilde{m}_{\psi}\right). \tag{570}$$

We remark that, in case we had worked with equation 565, the results for the WFR factors would have been *apparently* different. We have checked explicitly that this difference can be removed by performing suitable chiral rotations and therefore has no physical meaning [8, 281].

In equation 567, there are still redundant operators which can be further reduced. With that aim, we apply again IBP+EOM in these operators, obtaining:

$$\begin{aligned}\frac{1}{2}\Big\{\overline{\psi}_L(\mathrm{i}\overleftarrow{\not{D}})\tilde{r}_{\psi\square}\left[\mathrm{i}\tilde{c}^{\dagger}_{\psi}S\right]\psi_L + \overline{\psi}_L\left[\mathrm{i}S\tilde{c}_{\psi}\right]\tilde{r}^{\dagger}_{\psi\square}(\mathrm{i}\not{D})\psi_L\Big\} \\ = \frac{1}{2}\mathrm{i}S\overline{\psi}_L\tilde{c}_{\psi}\tilde{r}^{\dagger}_{\psi\square}\left[\tilde{m}_{\psi} - \mathrm{i}S\tilde{c}_{\psi}\right]\overline{\psi}_R + \text{h.c.}\end{aligned} \tag{571}$$

Repeating this procedure for the two last operators in equation 566, we obtain the following relations:

$$\tilde{c}_{\psi} = \frac{1}{2}\left(\tilde{c}_{\psi}\tilde{r}^{\dagger}_{\psi\square}\tilde{m}_{\psi} + \tilde{m}_{\psi}\tilde{r}^{\dagger}_{\psi\square}\tilde{c}_{\psi}\right), \tag{572}$$

$$\tilde{a}_{\psi} = \tilde{c}_{\psi}\tilde{r}^{\dagger}_{\square}\tilde{c}_{\psi}\,. \tag{573}$$

The contributions to the dipole operators are directly read from the identity 563:

$$\tilde{a}_{\psi A} = \frac{\tilde{e}Q_{\psi}}{2}\tilde{r}_{\psi\square}\,, \tag{574}$$

$$\tilde{a}_{\psi G} = \frac{\tilde{g}_3}{2}\tilde{r}_{\psi\square}\,. \tag{575}$$

Finally, the redundant operators involving the ALP can be removed by applying the EOM. For example, for those involving the up-quark,

$$S\overline{u_L^\alpha}\mathrm{i}\not{D}u_L^\beta = (\tilde{m}_u)_{\beta\rho}S\overline{u}_L^\alpha u_R^\rho - \mathrm{i}(\tilde{c}_u)_{\beta\rho}S^2\overline{u}_L^\alpha u_R^\rho\,, \tag{576}$$

$$S\overline{u_R^\alpha}\mathrm{i}\not{D}u_R^\beta = (m_u)^*_{\rho\beta}S\overline{u}_R^\alpha u_L^\rho + \mathrm{i}(\tilde{c}_u)^*_{\rho\beta}S^2\overline{u}_R^\alpha u_L^\rho\,. \tag{577}$$

This reduction adds the following contributions to the ALP–fermion couplings:

$$\tilde{c}_\psi = \tilde{r}_{S\psi_L}\tilde{m}_\psi - \tilde{m}_\psi\tilde{r}^\dagger_{S\psi_R}\,, \tag{578}$$

$$\tilde{a}_\psi = \tilde{r}_{S\psi_L}\tilde{c}_\psi - \tilde{c}_\psi\tilde{r}^\dagger_{S\psi_R}\,. \tag{579}$$

Altogether, the redundant operators in the SM+ALP LEFT lead to the following replacements:

$$\left(Z_{\psi L}-1\right) \to (Z_L-1) - \frac{1}{2}\left(\tilde{r}_{\psi\Box}\tilde{m}^\dagger_\psi + \tilde{m}_\psi\tilde{r}^\dagger_{\psi\Box}\right)\,, \tag{580}$$

$$\left(Z_{\psi R}-1\right) \to (Z_R-1) - \frac{1}{2}\left(\tilde{m}^\dagger_\psi\tilde{r}_{\psi\Box} + \tilde{r}^\dagger_{\psi\Box}\tilde{m}_\psi\right)\,, \tag{581}$$

$$\tilde{c}_\psi \to \tilde{c}_\psi + \frac{1}{2}\left(\tilde{c}_\psi\tilde{r}^\dagger_{\psi\Box}\tilde{m}_\psi + \tilde{m}_\psi\tilde{r}^\dagger_{\psi\Box}\tilde{c}_\psi\right) + \tilde{r}_{S\psi_L}\tilde{m}_\psi - \tilde{m}_\psi\tilde{r}^\dagger_{S\psi_R}\,, \tag{582}$$

$$\tilde{a}_\psi \to \tilde{a}_\psi + \tilde{c}_\psi\tilde{r}^\dagger_\Box\tilde{c}_\psi + \tilde{r}_{S\psi_L}\tilde{c}_\psi - \tilde{c}_\psi\tilde{r}^\dagger_{S\psi_R}\,, \tag{583}$$

$$\tilde{a}_{\psi A} \to \tilde{a}_{\psi A} + \frac{\tilde{e}Q_\psi}{2}\tilde{r}_{\psi\Box}\,, \tag{584}$$

$$\tilde{a}_{\psi G} \to \tilde{a}_{\psi G} + \frac{\tilde{g}_3}{2}\tilde{r}_{\psi\Box}\,. \tag{585}$$

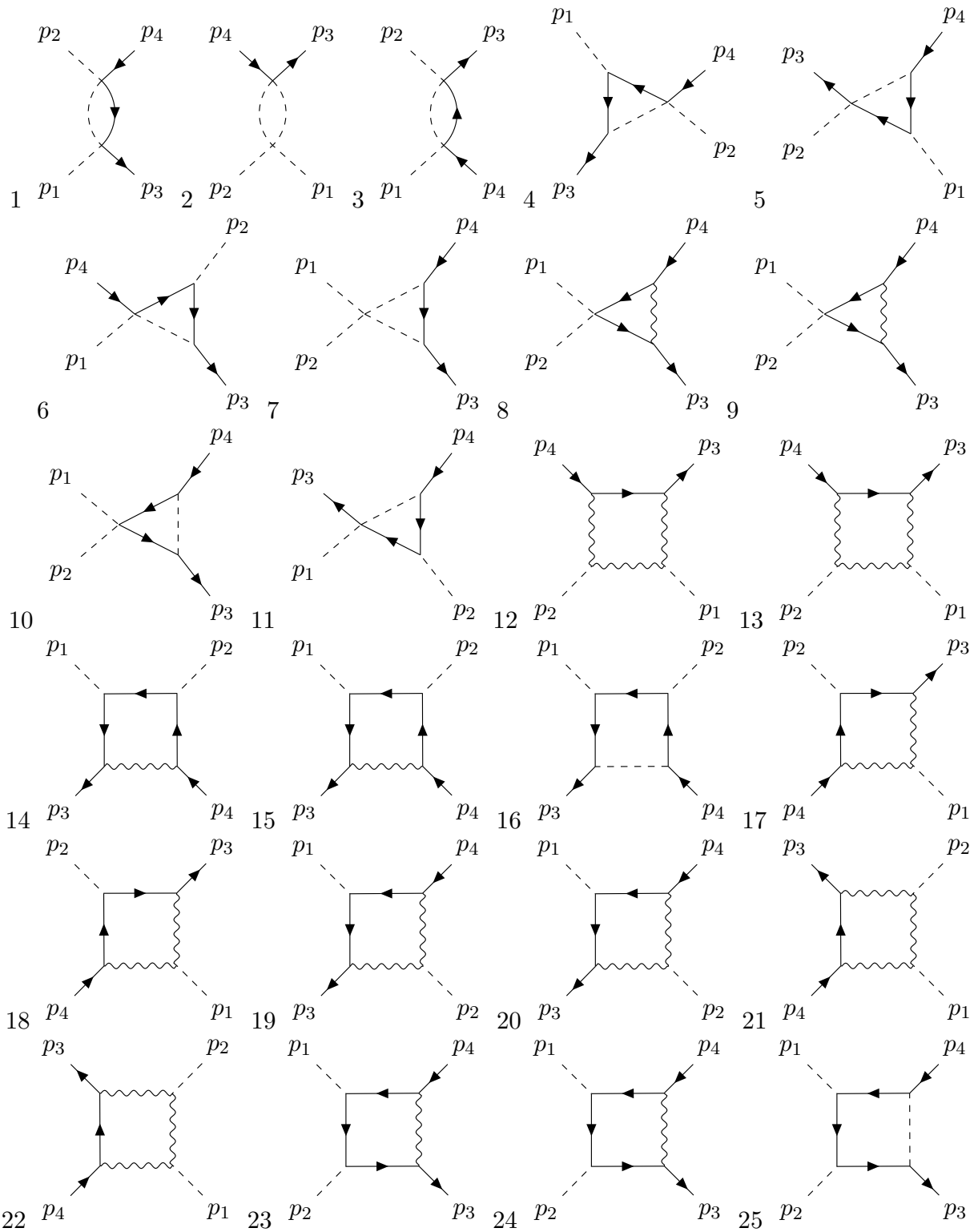

Figure 49: Diagrams contributing to the renormalization of 2 scalar–2 fermion interactions.

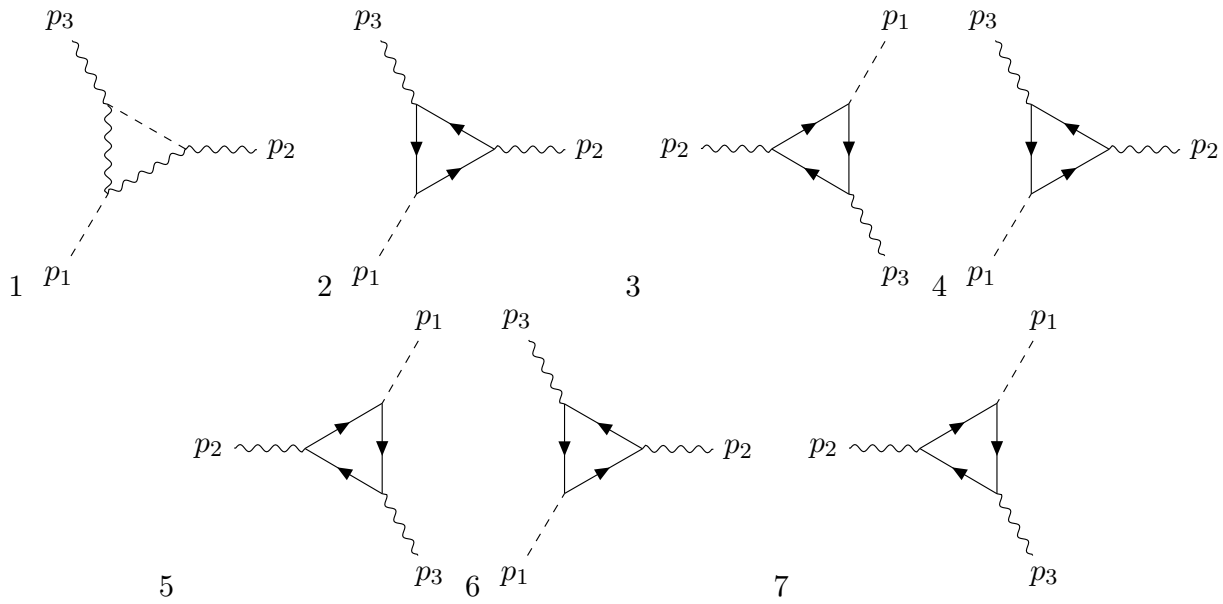

Figure 50: Diagrams contributing to the renormalization of 1 scalar–2 gauge boson interactions.

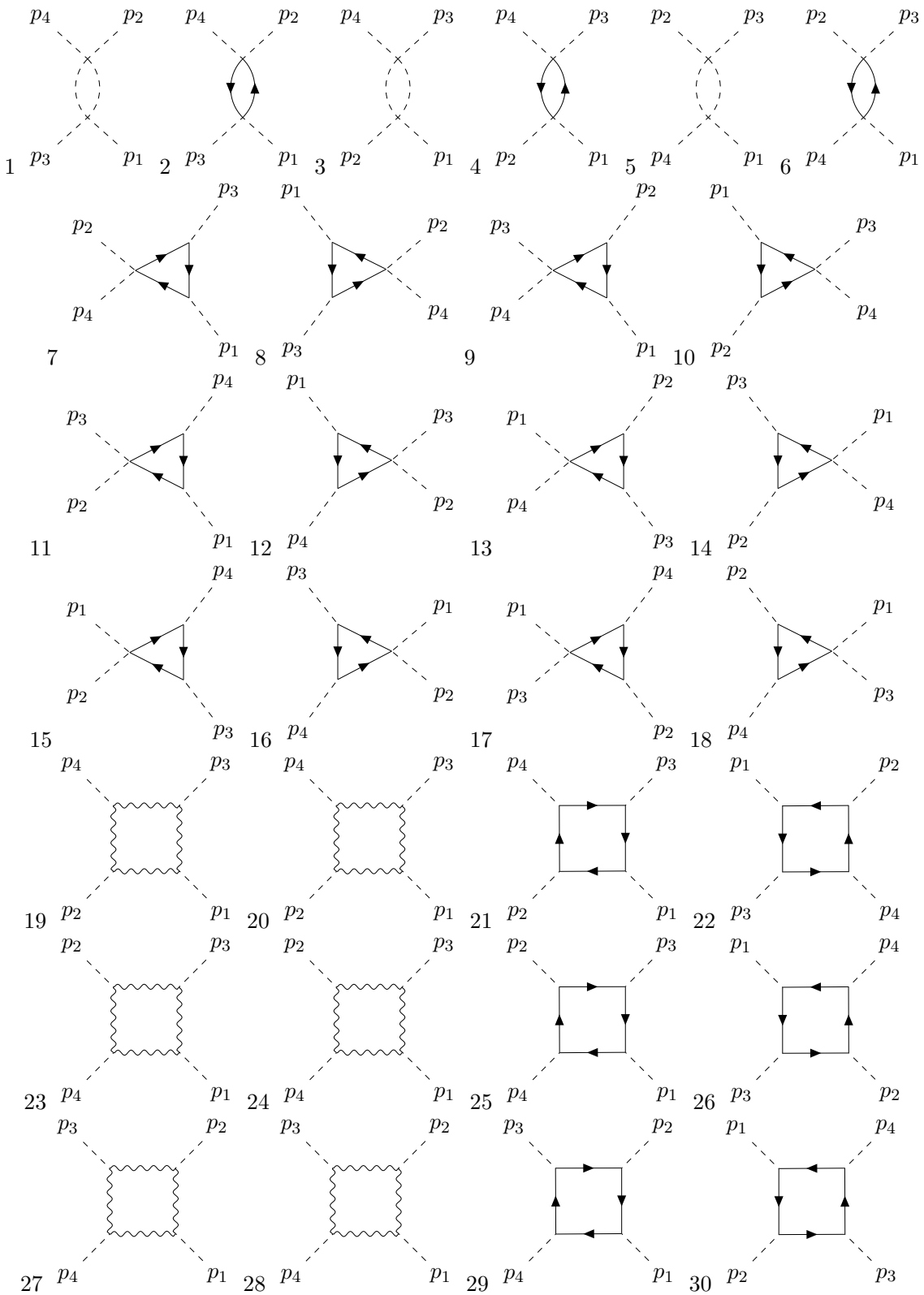

Figure 51: Diagrams contributing to the renormalization of 4 scalar interactions (ignoring the contributions from quarks).

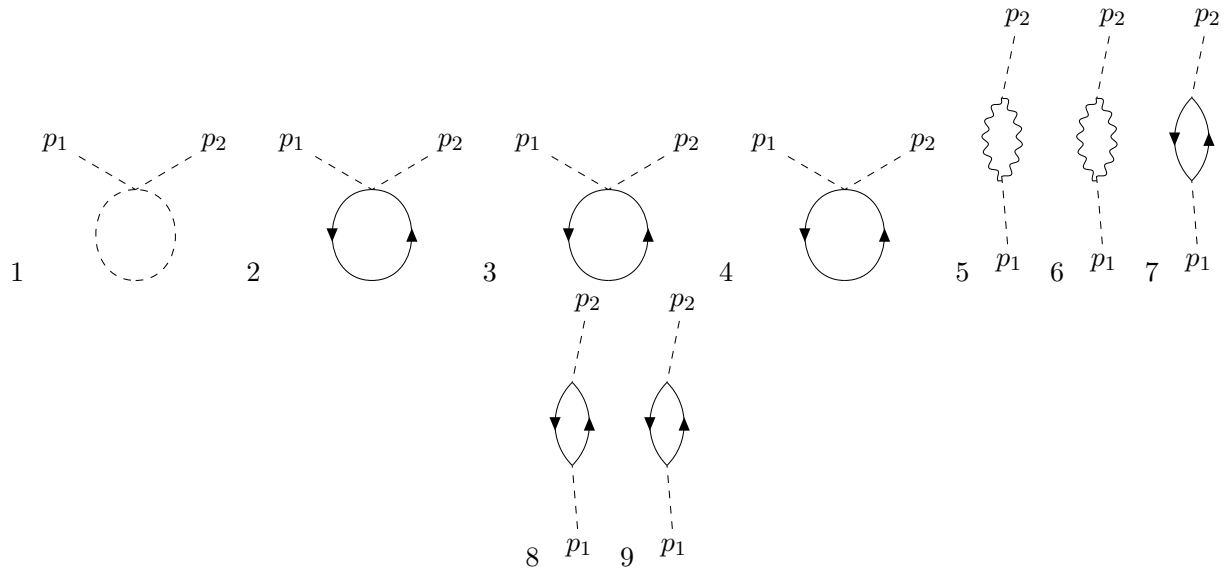

Figure 52: Diagrams contributing to the renormalization of the scalar mass.

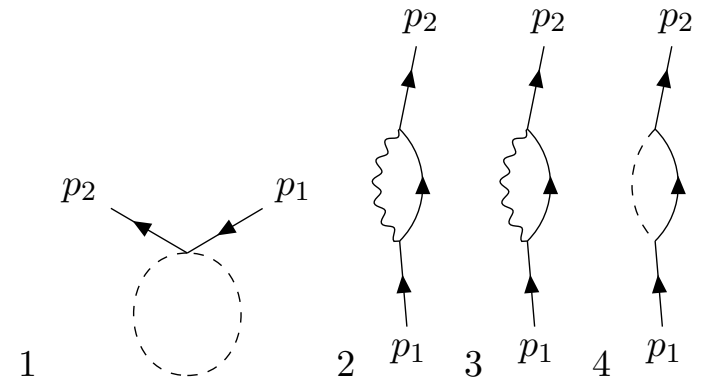

Figure 53: Diagrams contributing to the renormalization of of the electron mass.